Flux switching machines using segmental rotors

Ackim Zulu

A thesis submitted for the degree of
Doctor of Philosophy

Newcastle University
School of Electrical, Electronic and Computer Engineering

Abstract

Flux switching machines (FSM) employing a segmental rotor have field and armature systems on the stator and a presentation of an unexcited rotor with isolated segments. The single-tooth winding arrangement on the stator provides a potential for material and energy savings. The principle for producing bipolar flux in the armature stator teeth relies on the natural switching of the armature tooth flux, accomplished by the moving segments of the rotor. Three phase configurations have been studied, from conception and design to construction and testing, with field excitation provided by either a field winding or permanent magnets (PM).

Flux switching machines have shown characteristics that are peculiar when employing a segmental rotor, significantly affecting the symmetry of the induced armature EMF waveform and parity of magnitudes of the positive and negative torques. For three phase operation, six topologies are feasible when employing a 12-tooth stator and two other topologies may be produced on a 24-tooth stator. An optimum topology on the 12/8-configuration and another proof-of-principle topology on the 12/5-configuration, using field-windings and permanent-magnets, have been designed and constructed, while applying modern practices and considerations for manufacture.

The characteristics of FSMs employing a segmental rotor, initially predicted by finite-element (FE) modelling, have been verified by measurements. The FSM employing a field-winding is found to have a specific torque output which is similar to the conventional switched reluctance motor and still substantially higher than that of the synchronous reluctance motor. Although the PM adaptation of the FSM produces specific torque output which is nearly twice that of the wound-field FSM and about 64% that of an equivalent permanent-magnet synchronous motor (PMSM) with surface or insert magnets, accounting for the usage of the magnets reflects its specific torque output to be about 1.48 times higher than the PMSM.

Although the FSM is operated as an AC machine with sinusoidal three-phase currents, its *dq*-equivalent representation shows significant differences from that of the conventional AC machine. In the prediction of the performance, it is found, in both the wound-field and PM configurations, that the *dq* model is more dependable if the coupling *dq* inductance is taken into account.

Acknowledgments

Foremost, my utmost thanks to Prof. Barrie Mecrow who not only introduced me to this line of enquiry and the fantastic world of curious inventions but also provided first-rate supervision on my research project. I have appreciated the guidance of Dr Mathew Armstrong, the co-supervisor of my research project, particularly his direction in unravelling the moods of packaged electric drives and the treachery of feedback devices.

Mr Chris Manning, of the mechanical workshop, is deserving of special thanks for building all my prototypes. At times, Chris's work on my prototype machines required more than one pair of hands, and I laud the assistance and support in the mechanical workshop of Messrs Jack Noble, Allan Wheatley, and Stuart Baker. All pieces of my experiments in the power lab including instrumentation and cabling were adeptly arranged for by Mr James Richardson.

I benefited from the advice of Prof. Alan Jack during assembly of the machines, Dr Glynn Atkinson and Dr Bogi Jenson while performing no-load tests, and Mr John Bennet at the initial set-up of the electric drives, all whom I sincerely thank.

I value the friendship of Dr Lemba Nyirenda and his family, whose encouragement and support at the start of my studies, made the difference in deciding the worth of this venture. Dr Joseph Mutale and Prof. Barry Williams deserve mention in supporting me on the scholarship application.

The Commonwealth Scholarship Commission of UK provided the scholarship for my studies, and I gratefully acknowledge their support. In the same breath, I thank the University of Zambia for leave to undertake further studies.

In all this, my children Nkonde and Mubanga, and my wife Ndawa, have endured the vagaries of a student whose role as a dad and hubby has been fleeting. For them, 'thank you' is, in some way, not propitious enough.

To the memory of my father

Who departed at the start of my studies

Contents

List of figures

List of tables

Acronyms and symbols

Acronyms

abc	symmetrical *a*, *b* and *c* three phase
AFM	Axial flux machine or motor
dq	orthogonal direct and quadrature axes two phase
EDM	Electrical discharge machining
EMF	electromotive force
FE	finite element
FEA	finite element analysis
FSM	flux switching machine or motor
MEC	magnetic equivalent circuit
MMF	magnetomotive force
PM	permanent magnet
PMFSM	permanent-magnet flux switching machine or motor
PMSM	permanent-magnet synchronous machine or motor
PWM	pulse width modulation
RFM	Radial flux machine or motor
RMS	root mean square
SMC	Soft magnetic composite
SRM	switched reluctance machine or motor
SyRM	synchronous reluctance machine or motor
TEFC	Totally-enclosed fan-cooled
TFM	Transverse flux machine or motor
THD	total harmonic distortion
UMF	unbalanced magnetic force
UMP	unbalanced magnetic pull

Symbols for variables and constants

	Description	*units*
B	flux density	[T]
e	electromotive force, voltage	[V]
f	frequency	[Hz], [rad/s]
i	current	[A]
I	current	[A]
J	current density	[A/m^2]
k	general constant	
l	length	[m]
L	inductance	[H]
M	mutual inductance	[H]
m	number of phases	
N	Number of	
p	number of pole pairs	
r	radius	[m]
R	resistance	[W]
t	time	[s]
T	torque	[Nm]
u	translational speed	[m/s]
v	voltage	[V]
V	voltage	[V]
W	stored energy	[J]
x	dispalcement, one of 3D orthorgonal axes	[m]
y	3D orthorgonal axis	[m]
z	3D orthorgonal axis	[m]
α	span	Rad]
ϕ	current phase angle from voltage	[rad]
β	current phase angle from q-axis	[rad]
δ	voltage phase angle from q-axis	[rad]
$\mathcal{F}$	Magnetomotive force	[A]

ψ	Flux linkage	[Wb]
Λ	permeance	[Wb/A]
$\mathfrak{R}$	reluctance	[A/Wb]
θ	angular position, span	[rad]
μ	permeability	[H/m]
ω	angular speed	[rad/s]

Subscripts' symbols

a	armature; axial; of phase *a*
b	of phase *b*
c	of phase *c*
e	electromagnetic
d	of direct axis
g	airgap
f	field
i	input; instantaneous
m	amplitude
max	magnet; maximum
n	normal
o	output
p	peak
q	of quadrature axis
r	rotor
rv	rotor volume
s	stator
seg	segment
sep	separation
t	tangential; tooth
tp	tooth pitch
ts	tooth span

Chapter 1

Introduction

The incentives that have led to the development of innovative types of electrical machines in the past half-century have mainly been driven by economical and environmental imperatives. The combined requirements of economy and consideration for the environment demands a sensible application of materials resource and processes of manufacturing for electrical machines, whilst standardisation and global regulations for electric motors [1]-[4] puts a premium on efficient machines [5]-[8]. In the past two decades, an additional requirement of fault tolerance is sought in electrical machines particularly for applications of safety-critical designation [9]. While recognising the influence of these pressures and requirements, it is also acknowledged that the notable developments shown in the appearance of innovative electrical machines during this period are due to the corresponding rapid developments in power semiconductor and integrated circuit devices, micro computing technology, including facilities for numerical analysis, and discoveries of new electromagnetic materials. Before this period, the configurations that define the DC commutator machine, AC induction and AC synchronous machine were the dominant types, and have now been augmented by the entry of the AC synchronous reluctance machine (SyRM), the switched reluctance machine (SRM) and various types of brushless AC and DC permanent-magnet machines.

The emergence of the flux switching machine is as recent as just over a decade ago, exploiting the advances in drives technology for feasibility of operation and exhibiting high specific output and economy of construction. Employing a segmental rotor in flux switching machines, which is the direction followed by the work in this thesis, enhances efficiency and reduces usage of copper, both situations accomplished by having shorter

end-turns of the winding, regardless of whether field excitation is by coils or permanent magnets. Specific study of the use of a segmental rotor in flux switching machines has only been under consideration in the last five years and has culminated in this thesis on three phase flux switching machines employing segmental rotors.

1.1 Background

Flux switching machines in general are typified by having all excitation sources on the stator, providing simpler cooling options in principle, leaving the rotor to carry neither windings nor magnets and essentially dispensing with the brush gear and slip rings. Another obvious advantage of this arrangement is the simplicity of the rotor, which allows for easy manufacture and attainment of relatively high speeds in operation. The shape of the rotor is designed to present a variable reluctance to the windings on the stator as it rotates, modulating the flux in defined sections of the stator to produce bipolar AC flux linkages of the armature windings. Whilst there is a requirement to have at least one type of unidirectional primary excitation, which can be by a DC field winding or permanent magnets, it is known that use of a toothed-rotor configuration, as applied in the conventional switched reluctance machines and adopted in the earlier types of flux switching machines, enables a configuration of shorter single-tooth windings only if field excitation is by permanent magnets. On the other hand, employing a segmental rotor in the flux switching machine, while significantly presenting a different mechanism of the flux switching to that perceived with toothed-rotors, ensures implementation of single-tooth windings on the stator without regard for the type of primary excitation. This proves useful as an obvious direction to increase efficiency and save materials.

As an introductory overview, it can be said that the flux switching machine, employing segmental rotors in three phase configuration, combines already well-known configurations of stator and rotor topologies to produce a yet unconsidered configuration of a rotating electrical machine. In this configuration, there are potential beneficial attributes in the main consideration but, like in most inventions, there are some forms of sacrifice, which may be mitigated to a degree by imaginative designs.

1.2 Perspectives and Trends in Electrical Machines Development

Although the term electrical machine includes generators and motors, it is the class operating as motors on the utilisation side of energy conversion that gives the greater variety of configurations and sizes. Much of the insights in the proceeding discussion is applicable to the motoring class of electrical machines which, as of publications of 2008 [10], [11], is estimated to account for 60-70% of the electrical energy utilisation in the developed world. In the following sub-sections, the global trends and influence of new technologies on the development of the electrical machines, in response to economical and environmental pressures, are briefly recounted with a reference to the position of developing flux switching machines.

1.2.1 Power electronics and control

Advances in power electronics (PE) in the recent past [12]-[16] have facilitated the emergence of high power variable frequency power converters and innovative control strategies, in some cases extending and in other cases enabling operation of a variety of electrical machines. The flux switching machine, requiring a power converter and controls, owes this technology the essence of operation as a motor. As the capabilities of semiconductor devices and power converters grow [17]-[20], it is expected that there are to be improvements in the performance of the flux switching machines and considerations of new configurations.

1.2.2 Computing and computer-aided design

The continuous development of the micro computing technology of the desktop [21]-[23], together with tools for computer-aided design (CAD), has enabled rapid design and prototyping of electrical machines. The desktop workstation of present date has high processing power and speed and handles repetitive design problems with an ease not experienced before. Taking advantage of this power, CAD tools with numeral analysis functions for electrical machine designs, typically those using FEA with parameterisation and 2D or 3D capabilities, are now routinely applied in design, analysis and optimisation of machine dimensions [24]-[26]. Additionally, control algorithms for power processing in the operation of the electrical machine are now more easily and cheaply handled with inexpensive microcomputer technology. In the design

and analysis of FSMs of this study, extensive use of 2D FE modelling with parameterisation and time-stepping function has been applied.

1.2.3 Efficiency

While the level of efficiency of an electrical machine depends on the power rating and operating load condition, five approaches, gathered from recent literature, may be applied to affect the efficiency of the motor. One approach is to target favourable classes of machines, as certain kinds of machines are generally more efficient than others [27]. Since efficiency is tightly allied to losses in the machine, a choice of low-loss materials or materials that mitigate generation of losses [28]-[30] serves to increase the efficiency of the machine and may be another valid approach. Certain specified configurations of machines [31], [32], even within a class of machines, may be applied and are found to affect the efficiency. The indirect approach to improve efficiency, when there are constraints of materials and configurations, is to optimise the dimensional design of the machines [33]-[39] for high efficiency. Although this approach is indirect, it is still likely to significantly affect other performance parameters. If an application is known and well-understood, it may be specifically targeted for improved efficiency of the machine [40]-[43].

In considering the flux switching machine employing a segmental rotor, even though its initial development is not specifically targeted at optimum efficiency, there is a natural inclination to a lower winding loss due to a presentation of shorter end-windings than in machines with configurations of overlapping or long-pitched windings. This benefit is a by-product of the required presentation of the winding for the principle of operation.

1.2.4 New materials

There has been a notable impact of the discovery of new and varied materials for electrical machines [44], ranging from soft magnet materials for cores [45], [46], hard magnetic materials for primary excitation [47]-[52] and insulating and conductor materials, including exploitation of superconductivity [53], [54]. Although the levels of saturation flux densities in soft magnetic materials have not significantly increased, core loss in these materials has been substantially addressed by use of amorphous steels, high silicon steels and powder metallurgy. Improvements in hard magnetic materials is allied to the discoveries or development of rare-earth materials, notably Neodymium-Iron-

Boron (NdFeB) and Samarium Cobalt (SmCo), where both the residual flux density and temperature grade are exceptionally raised. Improvements of insulation properties of electrical materials are being embodied in the new manufacturing techniques, so that thicker insulations may be applied to withstand both thermal degradation and steep-fronted impulse voltages. The new frontier for conductors is in superconductors. At present, superconducting is possible only with some means of special refrigeration systems and the mass-market industry is justifiably wary of this technology. However, there is noteworthy development of high-temperature superconductivity for applications in marine propulsion machines [55], [56], where gains in efficiency are worthwhile as mission equipment is mostly operating at part load.

1.2.5 Fault tolerance

From the 1990's, as application of electric motors and actuators started to permeate the safety-critical industries, fault tolerance grew in prominence as an aspect required of electric machines destined for such industry. Presently, fault-tolerance is required and applied to motors in application for aerospace [57]-[61], automotive [62]-[66] and traction industries [67], where the drive is towards the more- or all-electric aircraft and automobile. Alongside these industries, application in wind generation [68] has also gained a sizeable share of the demand for machines with attributes of fault tolerance.

The property of fault-tolerance is generally exhibited in machines having means of redundancy, typically applied by multiphase configurations. It is enhanced by having a separation or decoupling of the phases. Switched reluctance machines [69]-[71] and flux switching machines [72], [73] have these properties inherently. Due to the inability to de-excite during a fault, extraneous effort is required to make PM machines achieve a degree of fault tolerance. To this end, PM synchronous machines for fault tolerant applications are reported in [74]-[79].

In the class of PM machines, the interior permanent-magnet motor (IPM) configuration [80] presents inherent fault tolerance due facility of reluctance torque. The fault tolerance capability in IPM motors may be improved by employing a favourable slot-to-pole number combination [81], using factional slot-winding configuration [82]-[84] or employing a dual-winding configuration [85].

For various types of electrical machines, converter control techniques may be employed [86], including techniques for connection of the converter to the motor [87], [88], for fault tolerance capability. In [89], [90], special topologies have been suggested with the aim of improving fault-tolerance. While it is not necessarily being advocated that the poly-phase FSM is a candidate for safety critical applications, its inherent fault tolerance capability is overtly suggested by the degree of redundancy and a presentation of decoupled phases.

1.3 General Configurations of Electrical Machines

The general configuration of an electrical machine is fundamentally based on the 3D-orthogonal axes orientation of the three quantities u, l, and B, of Faraday's law of voltage induction, defined as the speed, u, of a current-carrying conductor of length l, in a magnetic field of density, B . The well-known expression

$$e = Blu \tag{1.1}$$

gives the induced voltage, e across the ends of the conductor, and is the basis of electrical machines based on magnetic field excitation. The relative orientation of the three quantities on the orthogonal axes, illustrated in figure 1.1, is exploited for defining fundamental configurations and gives rise to three major classes of electrical machines, namely the radial flux machine (RFM) [91], the axial flux machine (AFM) [92]-[95] and the transverse flux machine (TFM) [96]-[99]. In the common cylindrical arrangement of the electrical machine, the z-axis in figure 1.1 depicts the longitudinal or cylindrical axis of the machine.

The commonest and widely-applied configuration for electrical machine is the RFM, where the structures for magnetic field production (primary excitation) and current-carrying conductors (secondary excitation) are arrayed in the same plane. If the relative positioning of the structures for magnetic field production and current-carrying conductor is interchanged, the AFM configuration is the result and is usually implemented where there is a restriction in the axial dimension, such as in wheel-motor applications [100]-[102]. The TFM configuration is produced by having the structures for magnetic field production and current-carrying conductor in different planes. As the planes for both magnetic field production and current-carrying conductor are subject to greater freedom of independent variation, higher specific torque than in either AFM or RFM is possible [103], [104].

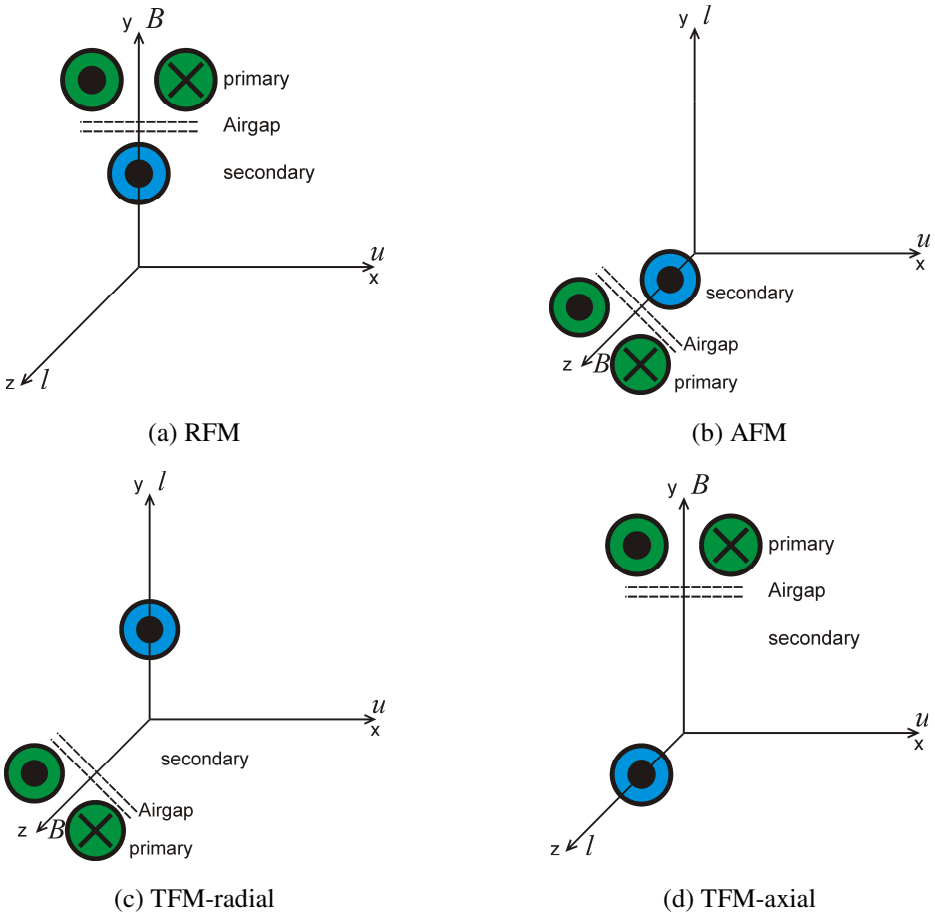

Fig. 1.1. Principal spatial orientation of excitation structures in electrical machines

Apart from applications in situations of restricted axial dimension, AFM may surpass RFM in selected aspects of performance, particularly as presented by the rotor active volume advantage at high number of poles [105]-[106]. However, TFM are known to suffer a poor power factor [107], a deficiency which is being addressed in recent research [108], [109]. The flux switching machines developed in this study are of the RFM configuration, such that any design optimisation must be considered as a competition of space between the structures for magnetic field production and current-carrying conductors in the same plane.

Windings or coils are a source of primary and secondary excitation in electrical machines. The winding configurations in electrical machines take varied forms, but are invariably classified as either single-layer or double layer arrangements. Depending on the machine type and its topology, there is further differentiation of winding types into distributed or concentrated windings, which may be fully-pitched or short-pitched [110], [111]. Concentrated winding arrangements appear easier to realise and are well-suited to radial flux machines for maximising output and efficiency. In configuring three-phase

machines with a high number of poles, a fractional number of the slots per pole presents a difficulty in ordering the phases, but a systematic approach proposed in [112], [113] appears to overcome this. The single-tooth form of concentrated windings, however, displays more simplicity and the associated short end-windings are key to improving machine efficiency. This type of winding, dictated by function, is followed for flux switching machines employing a segmental rotor.

1.4 Objectives and General Methodology

The principal objective of the work reported in this thesis is to develop three-phase flux switching machines implemented with a segmental rotor. There are four specific objectives which are outlined below, and also constitute the general chronological methodology followed to pursue the principal objective.

- ***Concept.*** As a first object of the project, the intention is to characterise the mechanism of flux switching implemented by means of a segmental rotor and propose configurations that produce three-phase configurations. Finite element modelling and linear magnetic equivalent circuits are to be used for this objective.
- ***Design and Evaluation.*** The proposed feasible configurations are to be evaluated for a selection of the configuration with favourable performance attributes; the favoured configuration is to be subjected to a design process for optimisation with defined aspects of performance. FE modelling is to be the method by which to obtain prediction results.
- ***Construction.*** Construction of the prototype machine is to be done using the current practices of manufacture and assembly.
- ***Testing.*** The final part of the objectives, considers testing and verification of performance of the constructed prototype machine; standard laboratory testing processes at no-load and loaded conditions are to be followed.

1.5 Contribution to Knowledge and Publications

The work in this thesis can claim to have provided new insight or products in the following aspects.

- Characterisation of the principle of flux switching implemented by means of segmental rotors
- Cause and origin of the asymmetry of induced EMF waveform in segmental-rotor FSM
- Feasible topologies for three phase configurations of segmental-rotor FSM
- A wound-field three-phase segmental-rotor FSM
- A permanent-magnet three-phase segmental-rotor FSM
- Inductance profile of the three-phase segmental-rotor FSM
- An improved dq model of the segmental-rotor FSM for steady-state performance prediction

In the pursuit of research for this thesis, the following publications in journal and proceedings at international conferences, all peer-reviewed, have been produced.

[1] Zulu, A., Mecrow, B.C., and Armstrong, M., 'A Wound-Field Three-Phase Flux-Switching Synchronous Motor with All Excitation Sources on the Stator,' IEEE Transactions on Industry Applications, vol. 46, no. 6, November/December 2010, pp. 2363-2371.

[2] Zulu, A., Mecrow, B.C., and Armstrong, M., 'Prediction of Performance of a Wound-field Segmented-Rotor Flux-Switching Synchronous Motor Using a *dq*-Equivalent Model,' 19th International Conference on Electrical Machines, ICEM 2010, Rome, Italy, 6-8 September, 2010, pp. 1-6.

[3] Zulu, A., Mecrow, B.C., and Armstrong, M., 'Topologies for Wound-Field Three-Phase Flux-Switching Machines using Segmented Rotors,' IET 5th International Conference on Power Electronics, Machines and Drives, PEMD 2010, Brighton, UK,18-21 April 2010, pp. 1-6.

[4] Zulu, A., Mecrow, B.C., and Armstrong, M., 'A Wound-Field Three-Phase Flux-Switching Synchronous Motor with All Excitation Sources on the Stator,' IEEE 1st Energy Conversion Congress and Exposition, ECCE'09, San José, California, USA, 20-23 September 2009, pp. 1502-1509.

1.6 Thesis Structure Overview

The thesis is structured into nine chapters and an appendix, to recount the substantive work from concepts to testing of the prototype machines. Citation of the literature reviewed is provided through all chapters, except the conclusions, and arranged to appear within the themes under consideration.

Chapter 1 is an introduction and provides the general context in which the motivation and surrounding issues for this work are embedded. The major contributions of this

work are also outlined together with a set of general objectives and a list of publications arising from this work.

In **chapter 2**, the topic of flux switching machines is explored, charting its evolution from old treatments to modern interest and capabilities. A uniform and consistent definition of the flux switching term is introduced and associated with the evolutionary development.

The principle of flux switching by means of a segmental rotor is scrutinised with the help of elementary cell structures in **chapter 3**. The characterisation of the principle by this mechanism is the highlight of this chapter.

The topological configurations for three phase arrangements of flux switching machines by means of a segmental rotor are in **chapter 4**. This chapter also includes an evaluation of the predicted performance of each of the proposed topologies.

Further design evaluations for the favoured topologies are presented in **chapter 5**, with considerations for construction. It is also in this chapter that the construction process and details, as built, are provided.

Chapters 6 and **7,** give accounts of the testing and performance results of the wound-field and permanent-magnet prototype machines, respectively. The performance of the prototype machines are compared with their nearest affinitive counterparts in the established classes of machines.

The conclusion is presented in **chapter 9**, giving a summary of the major results of the previous chapters, but is preceded, in **chapter 8**, by an exploration of the machine inductances and the suitability of using the classical *dq* modelling in predicting performance of the flux switching motor with a segmental rotor.

Chapter 2

Flux switching machines

This chapter surveys the types of rotating electrical machines operating on the principle of switching flux. Firstly, the working definition of the term is presented with a mention of the attributes of the principle. Several types of flux switching concepts are described, from the early schemes to the modern concepts, before introducing the flux switching concept by means of a segmented rotor. As the thesis is on flux switching machines which employ segmented rotors, more detail and emphasis is supplied to these types of machines in the final sections.

2.1 Background and Definition

The induced voltage e, in the armature system of a rotating electrical machine is predicted by Faraday's law at a specified mechanical angular speed ω_r, as the change of flux linkages ψ_a, with position θ,

$$e = -\omega_r \frac{d\psi_a}{d\theta} \tag{2.1}$$

It is a standard presentation in electrical machines configurations to have coils in the armature system linking the flux from the field system. Through motion, with respect to the armature system, the flux linking the armature coil system from the field system is made to change with time. A cycle of the change of flux linkage comprises a part for building up the flux to a maximum value and another part for reducing flux to a minimum value. It may be useful to see the situation as the flux changing between a low and a high state. In the conventional configuration of machines, the change of state of the armature flux between low and high states is aided by the relative motion of the polarised field system, either a pair of single N and S poles, or a consequent-pole configuration. The position of either the N or S pole relative to the armature system influences the amount of flux that links the armature system.

In other configurations, the flux may be made to change between the low and high state without using the change of the relative position of the N and S polarisation of the field system with the armature system. One way to do this is to modulate the flux linking the armature system from a field system with a constant or fixed excitation by changing the permeance seen by the armature. The permeance seen by the armature is then controlled by the position of the rotor. For the rotor position to influence the permeance seen by the armature system in a considerable way, the rotor must have saliency on circumferential geometry, such as achieved by slotting or tooth structures. The change of the armature flux between the high and low states as caused by variation of the permeance seen by the armature has come to be called 'flux switching'. Machines that work on this principle are thus called 'flux switching machines' or 'switching flux machines'. They are characterised by having both the field and the armature system on the stationary stator, with the rotor design having a structure that provides significantly varying permeance of the armature coils as the rotor rotates.

The principle of flux switching has been known from as early as the 1940's when Walker [114] codified the theoretical design of the inductor alternator based on this principle, but the terminology appears to have come into use a decade later as Rauch and Johnson [115] presented the analytical approach to the design of the inductor alternator. More work on such types of machines followed [116]-[121] on this principle even though the publications avoided using the term flux switching. It is not until in the recent interest of the implementation of the principle in electrical machines, in the late the 1990's, spurred by the developments in power electronics technology, which stimulated the inventions of new topologies and configurations, that the term has been overtly used [122]-[125].

2.2 Modes of Flux Switching

A tenet of the flux switching principle is that armature flux linkage changes with position principally due to the change in the permeance seen by the armature coils with position. Although the permeance varies between the maximum (high state) and minimum (low state) values with rotor position due to saliency or slotting of the rotor, the cycles of variation between maximum and minimum values for the armature flux linkages are distinguished by two modes: unipolar and bipolar flux linkages. The variable flux linkages for unipolar mode are of one polarity whereas variable flux linkages for bipolar are between positive maximum and negative maximum values. The two modes of flux linkages are depicted in Fig 2.1, for the idealised variation of permeance with position.

The implementation of the flux switching in unipolar mode may be seen to be entirely influenced by the variation of the permeance. However, for the bipolar mode, in addition to the influence of the variation of permeance, there is another effect that aids the flux switching and defines this mode in a unique way. The armature coils link the flux from both the N and S south polarisation of the field system, and the amount of flux linkages from each pole is determined by the position of the salient or slotted rotor. With this presentation, it is obvious that the net flux linkage in the armature coils may vary between two polarities. The nature of the variation of the net flux linkages to the extent described, combined with the influence of the variable permeance, is more complex for the bipolar mode than depicted in figure. 2.1, even with an idealised view.

As the field flux in the flux switching arrangement is invariably of fixed polarity, the magnetic circuits associated with the armature coils are correspondingly deemed to operate with unipolar or bipolar flux, if the flux linkages are unipolar or bipolar, respectively. There is an advantage for operating with bipolar flux, stemming from a better utilisation of the armature magnetic circuit or less material usage, with benefits of higher power densities and less copper loss [115], [125]-[128].

In both the unipolar and bipolar mode, if current i_a is applied in the armature coil, the electromagnetic torque T_e, developed is

$$T_e = i_a \frac{d\psi_a}{d\theta} \tag{2.2}$$

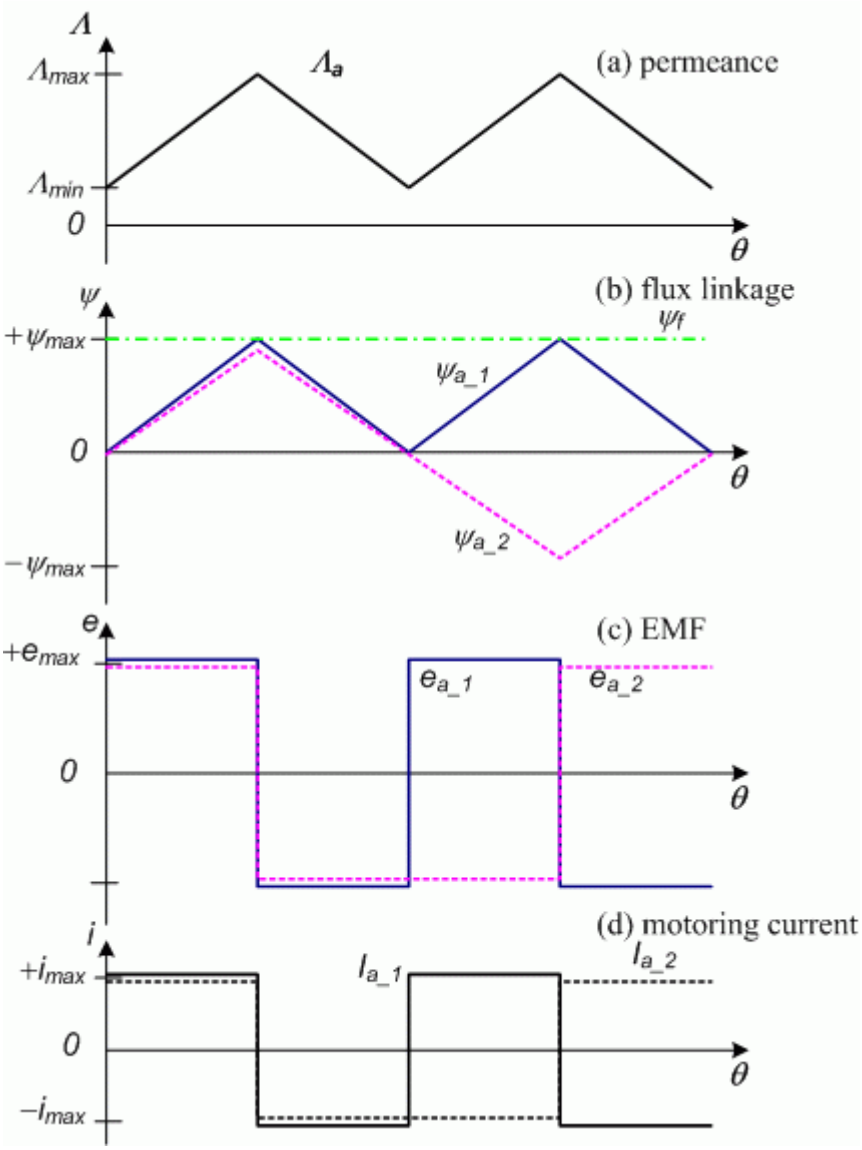

Figure 2.1. Unipolar and bipolar flux linkage with variation of permeance.

2.3 Evolution of Flux Switching Machines

It is apparent from the definition of flux switching adopted in this thesis that there can be classes of flux switching machines broadly defined and differentiated by:

(a) the source of the field flux, i.e. field winding or permanent magnet
(b) the orientation of the source of field flux
(c) the operating mode of the armature flux, i.e. unipolar or bipolar
(d) the form of the armature current.

The oldest and early forms of flux switching machines employed wound-field excitation. As materials development advanced, the high-energy magnets, which can also operate at reasonably high temperatures (> 100°C), became available. This presented the possibility to replace wound-field excitation systems with PM excitation in many types of high power applications. Configurations with PM excitation generally tend to have higher torque densities than the wound-field excitation configurations, as magnets provide loss-free excitation, generally occupy less space, and in many cases the space freed by the field winding increases the allotment for the armature system.

Whether the excitation system is by wound-field or PM, the orientation of the source of field flux spawns variations of configurations of flux switching machines. The main configurations have the source of the field excitation oriented either in the radial direction, (i.e. across the width of stator tooth body), in the circumferential direction (along the back-iron body) or in the longitudinal (axial) direction. Configurations with the source of field flux orientated in the radial direction are the subject of competition of the stator slot space between the field and armature systems, if the excitation is wound-field. On the other hand, the source of field flux oriented in the circumferential direction is preferably deployed with a PM excitation system, especially if the source is oriented across the width of stator tooth body. The deployment of the source field excitation in the oldest types of flux switching machine has been in the axial direction, and characterises the so-called homopolar machine. This configuration also gives the possibility to dedicate all the slot space on the stator to the armature system, and has been exploited in the development of the transverse flux machine, but leads to having unipolar armature flux linkages.

The distinction between unipolar and bipolar armature flux linkages has been made in the definition of flux switching and can be used as a basis for classifying flux switching

machines. The early types of flux switching machines, including heteropolar configurations, were typically arranged to produce unipolar flux linkages but nearly all types of flux switching machines developed in the last two decades are arranged to produce bipolar flux linkage because of the premium placed on performance. Arrangements producing bipolar armature flux linkages in general can be designed to produce higher torque density because the magnetic circuit can ideally undergo twice the flux change.

In the following sections the main types and variations of flux switching machines arising from the differentiation listed above are described. This thesis is on the type of flux switching machines with either a field winding or permanent magnet excitation, in which the armature coil permeance is made variable by use of a segmented rotor.

2.3.1 The inductor alternator

The inductor alternator appears to be oldest form of machine in the class of flux switching machines. References in early literature [114] indicate that it dominated in electrical power generation until the advent of the excited-rotor and revolving-field machine at the turn of the 20th century. As its dominance waned in the subsequent later period, its application became limited and specialised. It maintained its attraction where generation of high frequency currents was needed and this proved suitable in high frequency electric furnaces and wireless telegraphy.

In the principle of operation, there are two major presentations of the inductor alternator, both invariably operating with unipolar armature flux linkages: the homopolar machine and the heteropolar machine. As much as there are operational differences in the application of the flux switching principle, there are also major structural differences in the construction of the homopolar and heteropolar inductor alternator, as will be shown below.

The basic presentation of the homopolar machine is shown in figure 2.2. It consists of a slotted and laminated armature core in two parts, **a1** and **a2**, joined on a common frame **b** and housing an armature coil A (or A1 and A2). A field coil F (or F1 and F2) is wound concentric with the longitudinal axis of the machine. A slotted rotor core **r** completes the path for the flux, shown in the longitudinal view of the figure. Motion of the rotor is accompanied by the variation of the permeance seen by the armature coils

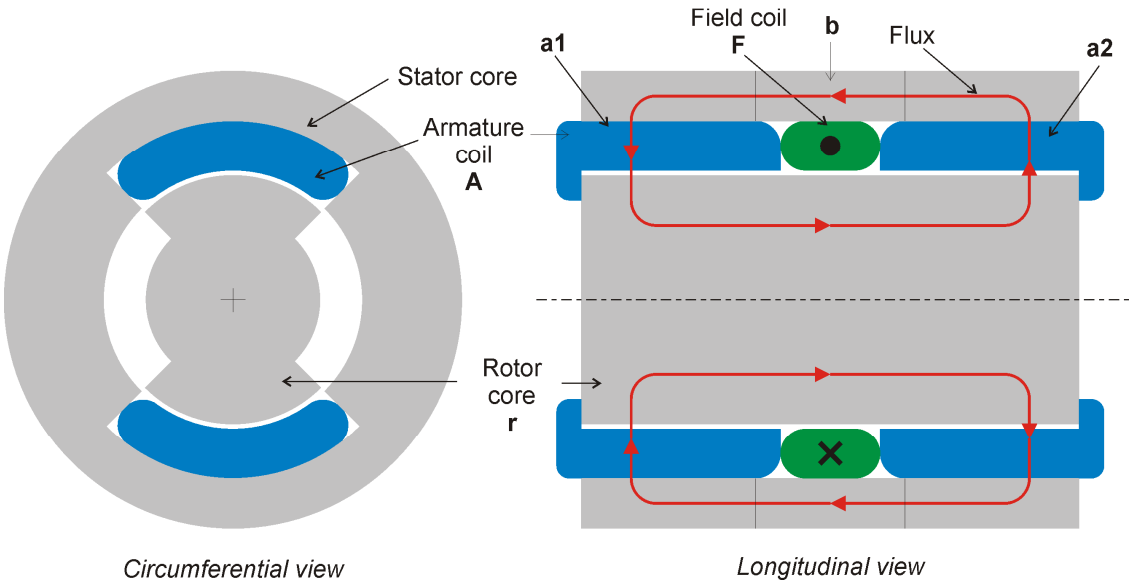

Figure 2.2. Basic structure of the homopolar machine.

due to changes in the airgap length and produces unidirectional flux linkage changes in the armature coils. As the armature coil links with unidirectional flux only, the flux linkage is characteristically unipolar.

It is apparent, even from the sketch of figure 2.2, that the homopolar configuration presents a complex magnetic geometry, whose analysis requires 3-D capability. Despite being a relatively old idea, the concept has been revived in recent years [131], [132], with allusions to SRM control concepts, and an accompanying modern-day drive has been proposed. It is not surprising that the prototypes report significantly lower flux linkages than expected when laminated steel is used, suggestive of substantial eddy currents due to cross flux in the laminations. A solution to this appears to employ powdered-iron cores, as in transverse flux machines, which minimises eddy current effects in all directions.

In the early development of the inductor alternators, the homopolar machine was the only configuration used for high frequency generation, till the emergence of the heteropolar machine. In dynamic operation, the heteropolar machine is typified by a significantly smaller time constant than the homopolar machine, making it superior in applications requiring close and rapid control of alternator terminal voltage [116].

In structural presentation, shown in figure 2.3, the heteropolar machine appears to be simpler than the homopolar machine, and its basic configuration consists of slotted stator core laminations carrying both the armature and field coils. The armature and field coils may be in the same slots, one on top and the other at the bottom or side by side, as in (a), or they may be in alternate slots, as in (b), The number of rotor slots may

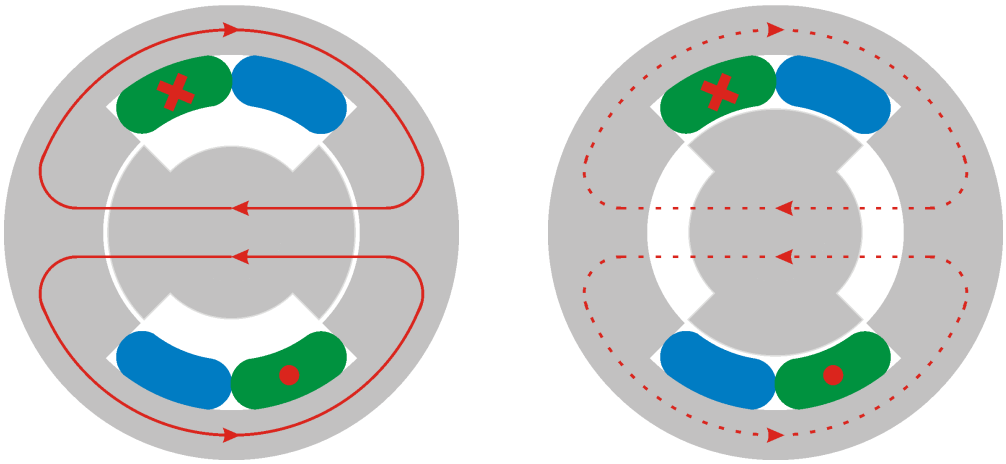

aligned, maximum flux linkage unaligned, minimum flux linkage

(a) 2/2 configuration-shared slots, unipolar flux linkage

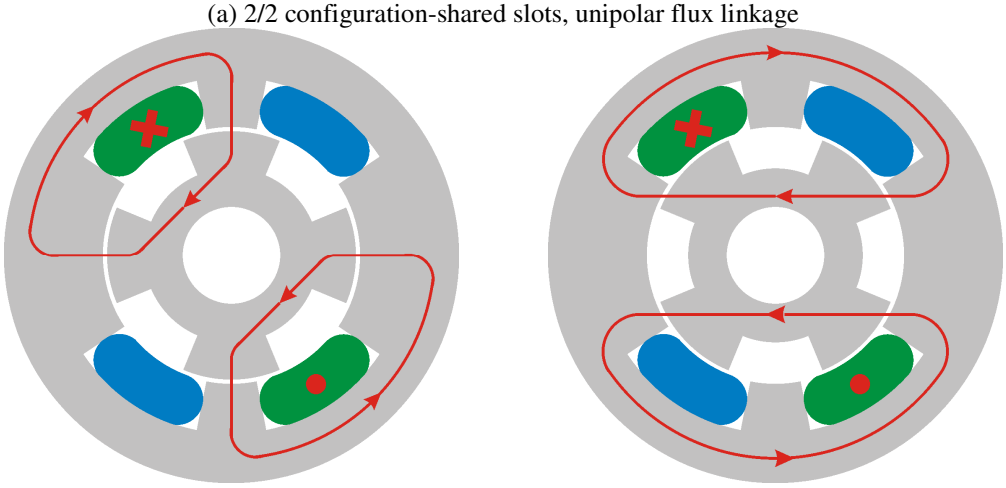

aligned, minimum flux linkage unaligned, maximum flux linkage

(b) 4/4 configuration-alternate slots, unipolar flux linkage

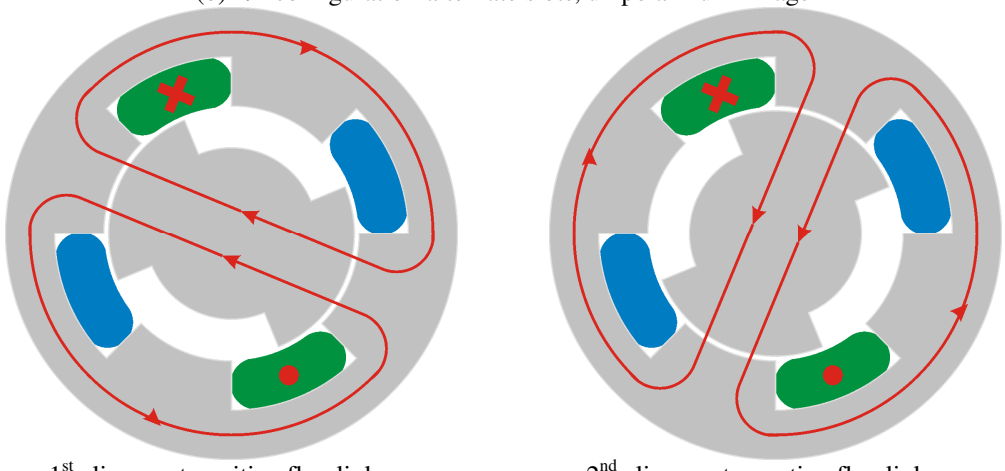

1st alignment-positive flux linkage 2nd alignment-negative flux linkage

(c) 4/2 configuration-alternate slots, bipolar flux linkage

Figure 2.3. Basic topologies of the heteropolar machine; field coils in green, armature coils in blue.

be designed to be an integer multiple of the number of stator slots. A slotted laminated rotor core carries no windings, and its motion causes the flux linkage of the armature coil to vary with rotor position, with flux excitation provided by the field coil. As in the homopolar machine, the slotting of the rotor and stator causes a change in permeance when the rotor moves, which influences the flux linkages of the armature coil. The arrangement with alternate slots has been applied in modern schemes to produce bipolar armature flux linkages by simply ensuring that the number of stator slots is less than the number of rotor teeth [122].

Starting with the basic concepts shown in the illustrations in figure 2.2 and figure 2.3, the number of slots on the stator and rotor may be increased for optimisation. In one effect this improves the performance of the design, by grouping several pole pairs for optimal flux densities in the cores, and in another effect it produces poly-phase machines by an appropriate choice of the number and size of slots on the rotor and stator. The topologies described in [116], [117], [120], [121] are three phase configurations appropriated by the second effect, but an ingenious configuration proposed by Subbiah and Krishnamurthy [118], [119] may use a single winding for both field excitation and armature output to produce a scheme for either single phase or polyphase output.

2.3.2 The flux-switching alternator

The basic configuration of the heteropolar inductor alternator of figure 2.3 functions just as well in principle if, in the production of the field excitation, a field winding is replaced by permanent magnets. In [115], Rauch and Johnson describe such an arrangement and it appears to be the earliest point in history that the term 'flux-switching' is overtly used to describe an inductor alternator with bipolar armature flux linkages. The concept presented at the time is shown in figure 2.4, and it is clear to see the similarities with the concept presented in figure 2.3 for heteropolar inductor alternator. In practice the concept with permanent magnets evolved to implementation in the form shown in figure 2.5. In figure 2.4, a pair of magnets with the orientation indicated is mounted on a stack of stator iron laminations, which in turn are wound with armature coils. The rotor is a simple stack of laminations with two salient poles. The flux shown in part A completely changes direction when the rotor has moved through

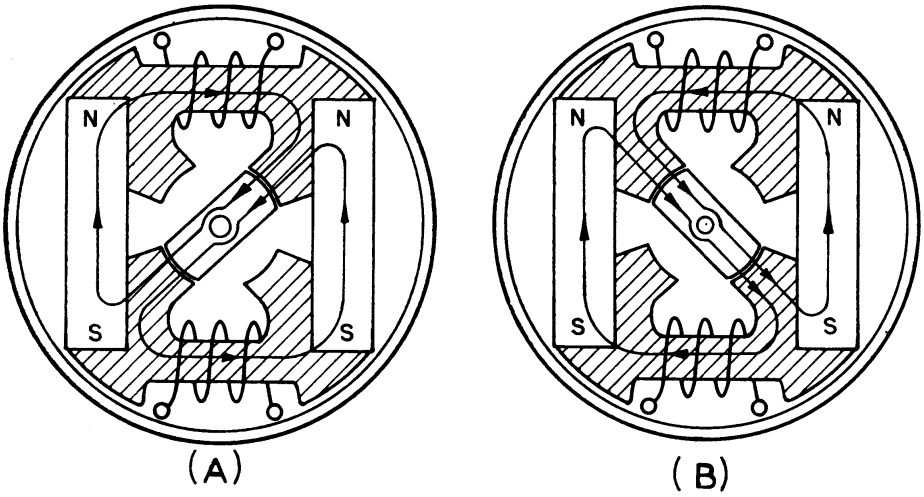

Figure 2.4. A simplified flux-switch alternator scheme [115].

half the electrical cycle in the position shown in part B. The rotor completes two electrical cycles in one revolution.

The capacity of the available magnets, in terms of the energy and coercive force, posed a challenge on the use of the space for practical designs during that period. The practical design shown in figure 2.5, for a design with three strokes in one revolution, attempted to balance the competing requirements by having a short-circuited coil **b** around the magnets that would prevent demagnetisation and having an arrangement of the armature winding **f** that suited the existing manufacturing methods.

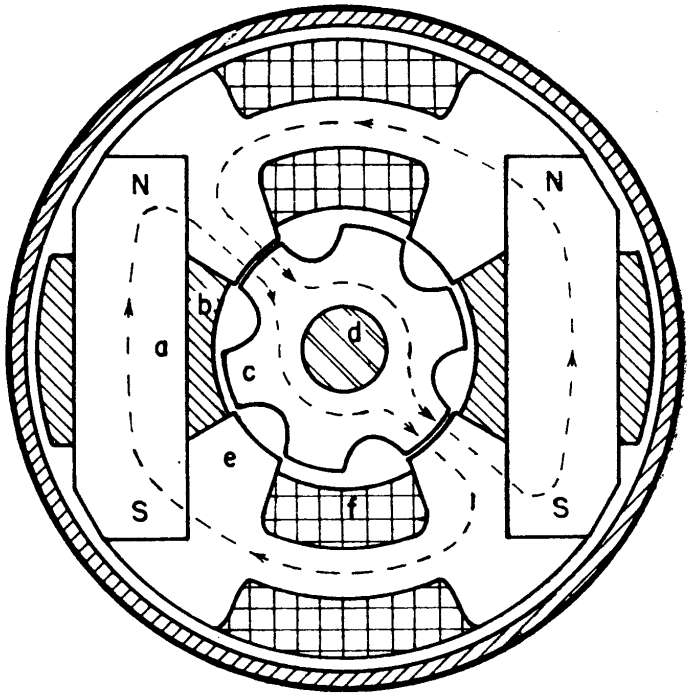

Figure 2.5. A flux-switch alternator concept with 4 stator and 6 rotor poles [115].

2.3.3 The flux-reversal machine

The flux reversal machine (FRM) [126] is another form of switching flux machine operating with bipolar armature flux linkages and bipolar flux in the armature poles and appeared in literature a little more than a decade ago. It has the structure of the SRM but with a pair of high energy permanent magnets with opposing polarity in the stator poles. It possesses a naturally low electrical time constant and low mechanical inertia and appears suitable in applications which require fast response, such as electric vehicle generators.

Figure 2.6 shows the basic configuration of the FRM, with two stator poles and three salient rotor poles. On the stator pole face are placed two magnets of opposing polarity. The structure of the rotor presents varying permeance with position seen by the coils wound round the stator poles.

Both the permeance and armature flux linkages change with position in the manner shown previously in figure 2.1. Figure 2.7 illustrates the operating principle, where parts (b) and (d) identify the two positions in the electrical cycle with maximum permeance and also maximum armature flux linkages, corresponding to the maximum positive and maximum negative flux linkage or vice-versa. The positions represented by parts (a) and (c) identify the minimum permeance and zero flux linkages flux linkages. The complete electrical sequence from (a) to (d) cycles the armature flux linkages and the flux in the stator pole from zero to positive maximum, then back to zero before going to negative maximum.

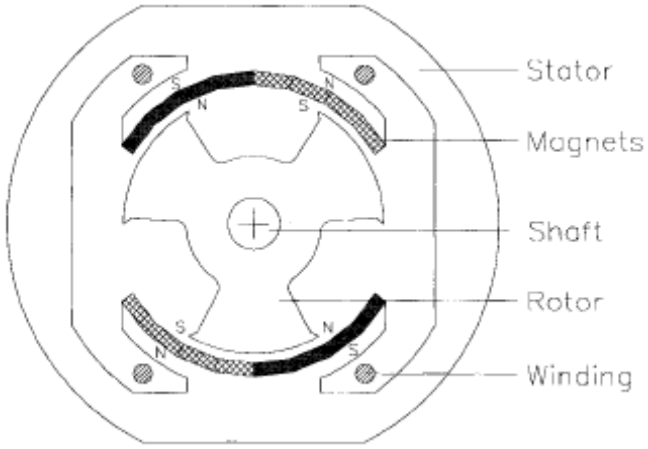

Figure 2.6. Basic configuration of a 2/3 flux reversal concept [126].

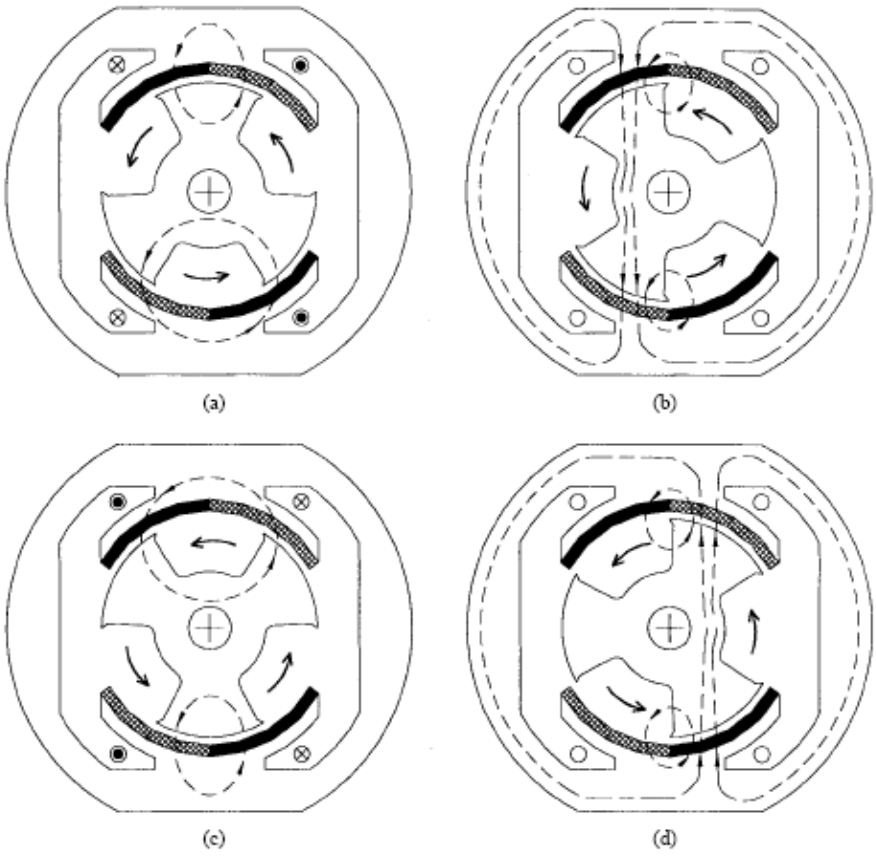

Figure 2.7. Operating principle of the flux reversal machine [126].

Although the depiction in the basic concept is on a 2/3 topology, it is easy to understand how variations in the number of stator and rotor poles can be applied to produce different configurations, including multiphase machines [129], [130].

2.3.4 Modern flux switching machines using a toothed-rotor

In the last decades, machines with flux switching attributes based on the original concepts of the inductor alternator and the flux-switch alternator described in the previous sections have appeared in novel configurations. They have been facilitated by discoveries of new magnetic materials, advanced developments in manufacturing methods, and most importantly, advances in semiconductor technology. The new developments in power electronics alone have meant that machine configurations requiring power conditioning interfaces are now being considered and are encouraged due to the availability of low-cost and more efficient drives. In the usage of the term flux switching for modern concepts, it is exclusively meant to apply to those types that produced bipolar armature flux linkages.

The basic and common presentation of the modern flux switching machine using a toothed-rotor is based on the principle of Rauch's flux switch alternator shown in figure 2.4. At the close of the last century, Hoang et al [125] presented a new stator structure using U-shaped magnetic core modules, which allowed an efficient accommodation of both the permanent magnets and the armature coil. The fundamental principle is illustrated in rectilinear representation in figure 2.8, showing an elementary cell which contains a permanent magnet sandwiched between two U-shaped magnetic stator cores, an armature winding and a toothed-rotor. At the first alignment position shown in part (a), the flux linkage of the armature coil due to the permanent magnet excitation is of one polarity and at the second alignment position in part (b), the flux linkage of the armature coil is of the other polarity, depicting bipolar flux linkage with rotor motion.

In practice, a concatenation of a series of the elementary cells in rotary arrangement is used to get an optimum design, and an appropriate choice of the combination of the number of stator teeth and rotor teeth may be used to create multiphase topologies. Based on this concept, a rotary elementary single-phase concept has been discussed in [133], while a practical single phase concept of four U-stator cores, four magnets and a 4-tooth rotor has been credited with industrial application [124]. More extensive developments and applications on these structures have been, however, on multiphase arrangements [125], [127], [134]-[140]. Figure 2.9 illustrates the main line of evolution of the modern flux switching structures, from the basic rotary principle to a polyphase concept.

A major modification to the polyphase structure involves having a further split in the tooth structure of the stator, effectively presenting two stator teeth on each side of the

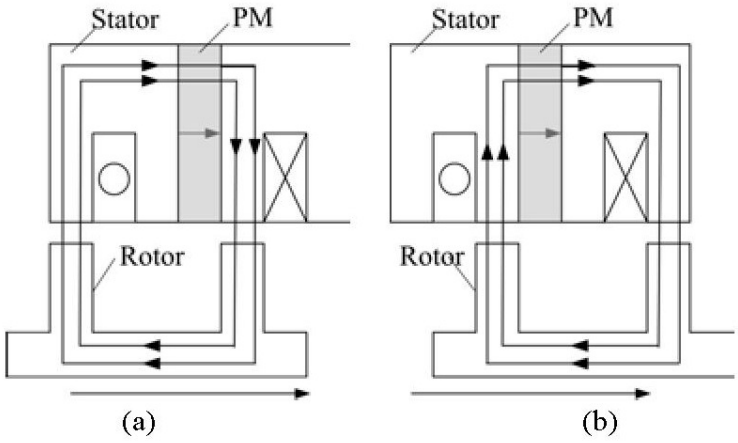

Figure 2.8. Elementary scheme of modern flux switching concept [125].

stator-mounted permanent magnets. At the expense of torque capability at high electric loading, multi-tooth structures presented in [141], [142] require only half the number of permanent magnets used in a standard three phase arrangements. A multi-tooth structure, with the form shown in figure 2.9 (d), presents lower torque ripple and higher torque density at low armature currents.

Whilst the modern flux switching concept discussed above and the schemes presented in figure 2.9 employ permanent magnet excitation, the arrangements can be implemented using field winding excitation, in configurations similar in many respects to the concept of the heteropolar inductor alternator shown earlier in figure 2.3. With a field winding in the place of permanent magnets, it is easier to control field flux using the field current.

In a basic deployment derived from the form of the basic heteropolar topology of figure 2.3, if the field and armature coils are deployed in separate and alternate slots as shown, the armature coil experiences bipolar flux linkages with the motion of the rotor. This is

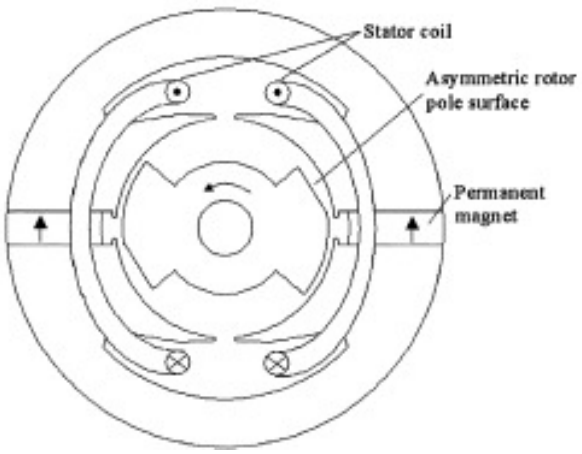

(a) basic concept [134]

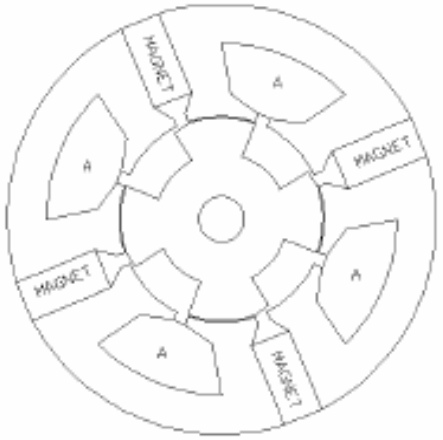

(b) practical one-phase concept [124]

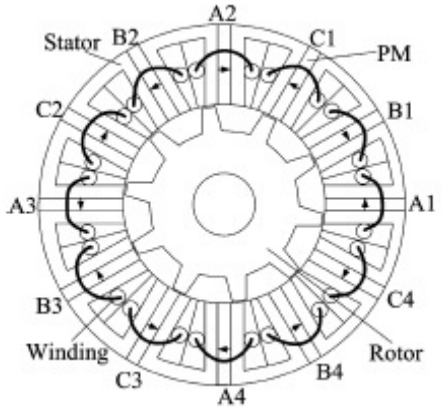

(c) three-phase concept [142]

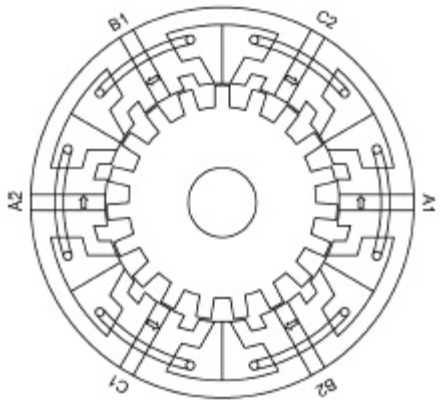

(c) multi-tooth three-phase concept [143]

Figure 2.9. Modern structures of flux switching machines.

illustrated in figure 2.10. For single phase topologies, this requires that the number of stator slots is twice the number of rotor slots. If this rule is not followed through, there is a possibility for the topology to degenerate to the inductor alternator topology with unipolar armature flux linkage, even when the field and armature coils are in alternate slots.

Pollock and Wallace [122] appear to be the first to apply a field winding excitation on this concept in a motor application, and developed a form of DC motor having neither brushes nor magnets. The scheme evolves from the basic concept of the inductor alternator with bipolar flux linkages shown in figure 2.3 (c), where the number of stator teeth is purposefully chosen to be twice the number of rotor teeth.

Instead of the basic 4/2 topology, practical topologies for single phase motors are favoured on 8/4 and 12/6 topologies, illustrated in figure 2.11, to reduce the end-winding conductor material. These configurations have been demonstrated for industrial applications requiring high power densities and a good level of durability [143], [144].

It would appear that a topology with hybrid excitation, i.e. having both permanent magnets and a field winding, would pose a more serious challenge in practical implementation than in concept. However, a decade following the appearance of the U-shaped stator structures with permanent magnets, used as elements to develop modern flux switching machines, Hoang et al [145], [146] proposed an elementary presentation of a hybrid excitation and an accompanying three phase topology, shown in figure 2.12. In this concept, the permanent magnets provide the primary field flux whilst a field

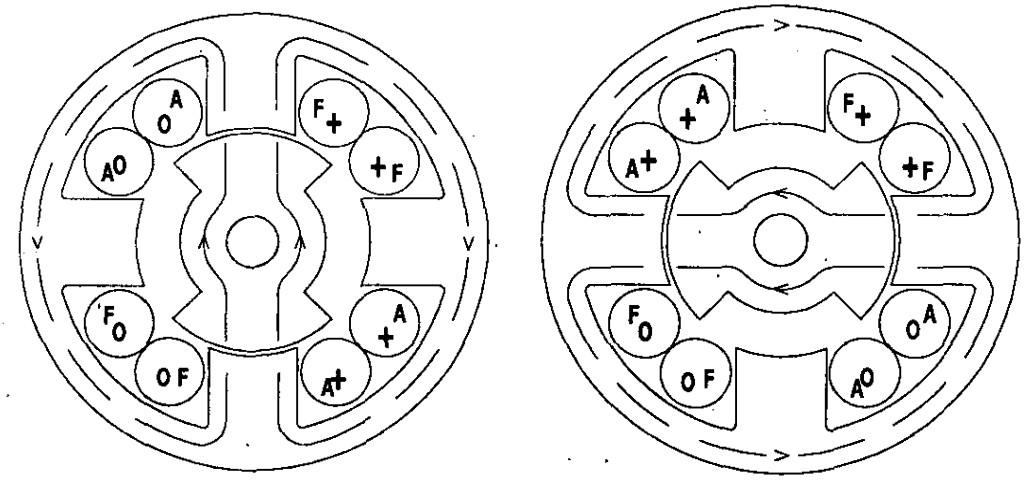

(a) positive armature flux linkage (b) negative armature flux linkage

Figure 2.10. Basic principle with field winding excitation [122].

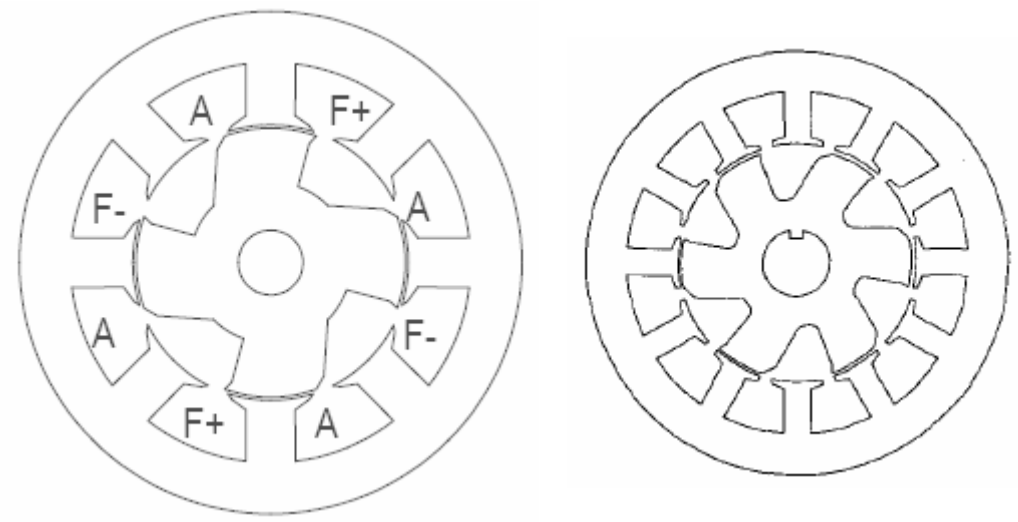

(a) 8/4 structure [145] 12/6 structure [146]

Figure 2.11. Motor topologies using field-winding excitation.

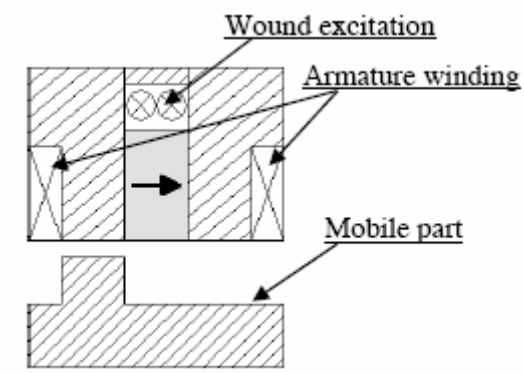

Figure 2.12. Elementary cell-representation for hybrid excitation [146].

winding with variable DC current provides the additional secondary field flux, which may be cumulative or differential. In the practical evaluation, whilst the addition of the DC source adds to complexity and cost, the useful outcome seems to be the facility availed for field weakening and influencing the iron losses by changing the field current, which can be beneficial in gearless drive applications with a large range of operating speeds. In the most recent work exploiting hybrid excitation [147], the effect of the position of iron flux bridges are investigated, in which it is found that the position at the outer radius of the rotor aids the excitation from the field winding.

2.3.5 Flux switching machines using a segmented-rotor

The discussion of flux switching machine in the previous sections was with rotors with toothed or slotted structure. With a complete loop coil-turn arrangement, a standard configuration in electrical machines with multi-turn windings, the windings are long-pitched, if not fully-pitched, and invariably overlap. In [148], Mecrow et al suggested a scheme of producing mutual coupling of single-tooth coils using a segmental rotor for

switched reluctance motor configurations. This configuration maintains the production of higher torque densities by the principle of the changing mutual inductance [149], [150], but has a further advantage of reduced copper usage and power loss due to resulting shorter end-windings. Use of a segmental rotor as applied to flux switching machines [123], turns the scheme for field-winding excitation proposed by Pollock et al [122] and presented in the previous section, into one with single-tooth windings. Thus, for flux switching machines employing a segmental rotor, there is, firstly, the attraction of achieving higher torque densities due to operating with bipolar flux and secondly, a reduction of copper losses and material due to shorter end-windings.

The basic scheme employing a segmented rotor is shown in figure 2.13 and is modelled from the basic principle illustrated in figures 2.3 (c) and 2.10. For the two rotor positions shown in the figure, while the field flux F1 and F2 are unchanged, there is a change of polarity of the armature flux linkages on A1 and A2 as the rotor segments S1 as S2 rotate. It is easy to follow that the scheme can be implemented with PM excitation by replacing the field winding on F1 and F2 with radially acting PMs on the field teeth structures, as shown in figure 2.14. In practice, significant benefits of short-endings appear with the 8/4-configuration if a single-phase topology is sought, whilst the 12/6 is another possible configuration with significantly shorter end-windings.

2.4 Conclusion

By embracing a clear yet broad definition of the term ‘flux switching’, it has been shown how machines operating on the principle of flux switching have evolved through

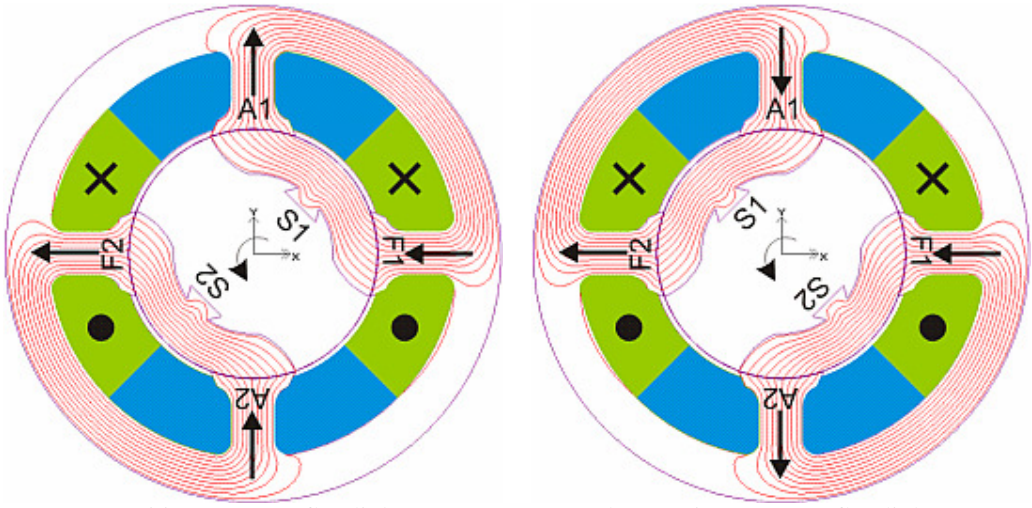

(a) positive armature flux linkage (b) negative armature flux linkage

Figure 2.13. Basic segmental rotor scheme with field winding excitation.

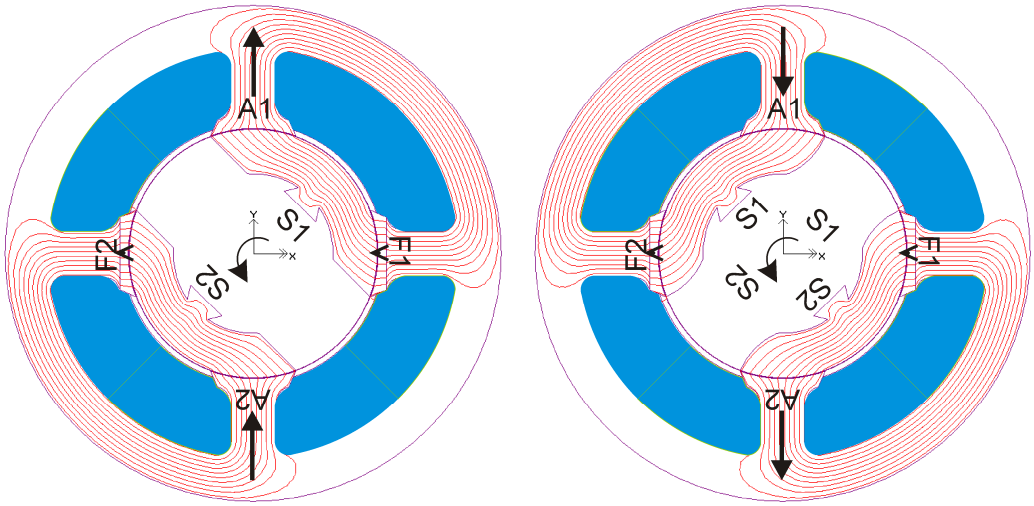

(a) positive armature flux linkage (b) negative armature flux linkage

Figure 2.14. Basic segmental rotor scheme with PM excitation.

the last century, culminating in the modern configurations of the last two decades. With the adopted definition, configurations producing unipolar and bipolar flux linkages are embraced, and are characterised by a change of state of the flux linkage due to a variable reluctance. The classification of the configurations follows this main distinction between unipolar and bipolar armature flux linkages, but is further differentiated by the types of the source of the field excitations and their location and orientation on the stator. The configurations have been described from the point of view of the basic concepts, as a form of chronological development, chiefly because it is an evolution which has profited from both the development of new magnetic materials and advances in semiconductor technology and computing techniques.

Due to a premium on performance and pressing considerations for conservation of resources which favour simplicity of manufacture, the dominant configurations in the last two decades employ bipolar armature flux linkages. Apart from the differences in the principle of operation between the arrangements with toothed-rotor and segmented-rotor, other differences in their stator winding arrangement may point to an opportunity to exploit savings in materials and reduction in copper loss.

Chapter 3

Flux switching using a segmental rotor

The principle of flux switching using a segmental rotor is described and examined in detail. Using elementary rectilinear cell representation, the principle is described and features are compared or contrasted with the precursor scheme using a toothed rotor. Although the elementary cell unit is rectilinear and lacks the complexity and detail normally applied in the design of practical rotary machines, the features which are elucidated are intrinsic and pertinent to the arrangements producing switching flux by means of a segmental rotor.

3.1 Background

The invention of the schemes, about a decade ago, that effectively place the field excitation and armature systems in the stator structure for flux switching machines [122], [125], presented credible options in the class of brushless machines. For primary field excitation, the schemes employ either a field winding with variable DC current, permitting control characteristics as of a DC motor, or circumferentially acting magnets placed between U-shaped stator structures, with prospects for high power and torque densities. Regardless of the type of the source of field excitation, the rotors are invariably of a toothed-structure. In this section, the use of a segmental rotor to implement flux switching principle is introduced. The major advantages in the flexible control characteristics with field winding excitation and high power and torque densities with PM excitation, are maintained, but there are also additional benefits presented by this scheme. Firstly, the armature stator teeth experience bipolar flux, effectively increasing the magnetic loading capability in the magnetic structure as the flux undergoes twice the flux change compared to a design for unipolar flux. Secondly, the implementation of the scheme employs single-tooth windings, which are associated with shorter end-windings, potentially reducing the use of copper and also the copper loss.

Use of magnetically conducting segments in rotor configurations has been applied previously, since the 1960s, to conventional machines such as synchronous reluctance machines to enhance performance characteristics. For instance, the saliency ratio of the synchronous reluctance motor with solid iron rotor segments can be significantly increased compared to the topologies using toothed-rotors [151]-[154], in a similar effect to the application of flux barriers. In the 1990s, switched reluctance motor concepts were implemented using laminated-iron segments, in which performance is reportedly increased for both the cases employing the principle of changing mutual inductance [155] and the principle of changing self-inductance [148], [156]. Whilst rotor segments are applied only to enhance a desired machine parameter in the synchronous reluctance machines, specifically the saliency ratio, their use in switched reluctance and flux switching machines involves an alteration to the mechanism of operation, including the switching sequences and winding arrangements.

3.2 Flux Switching Scheme

The basic scheme of flux switching by means of a segmental rotor can be seen as an extended idea of the switching flux scheme by means of a toothed rotor. By using elementary rectilinear cell structures with wound-field excitation, it is shown how the flux switching concept implemented by a segmental rotor is developed from the well-known toothed-rotor arrangement scheme. It is a matter of course that both schemes can be extended to be implemented with PM excitation.

3.2.1 Elementary rectilinear cell structures with a field winding

The stator structure incorporating elementary rectilinear cells for both the schemes with a segmental rotor and toothed rotor consists of a core with four identical teeth and four identical slots, as shown in figure 3.1. The stator slots accommodate field windings F1 and F2, or F for the toothed rotor scheme, and armature windings A1 and A2, or A for the toothed rotor scheme. For the purpose of comparison, the stator core structure for the scheme with a toothed rotor and the segmental rotor are made identical, although the winding connections are different. On the rotor, there are two teeth (and two slots) for

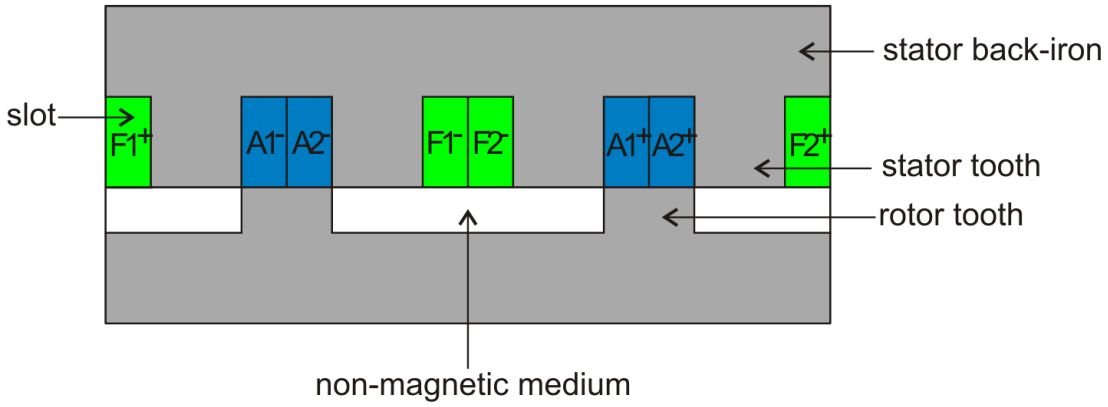

(a) toothed-rotor scheme

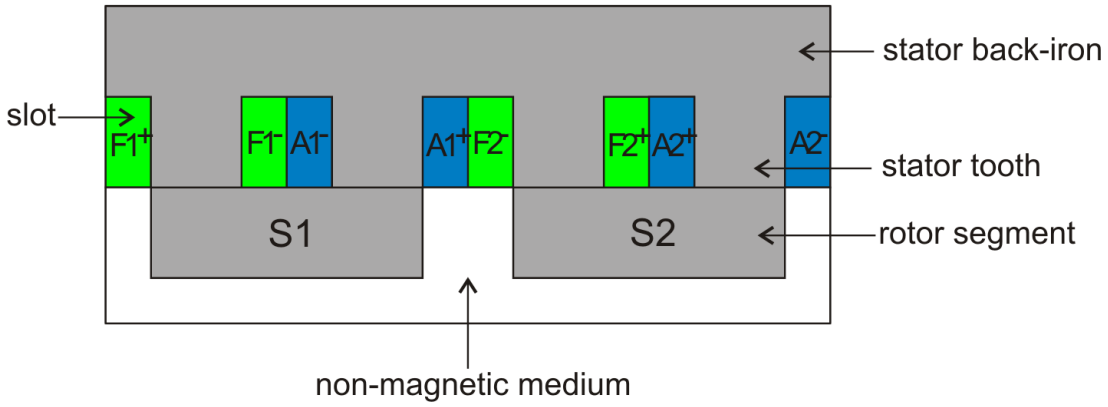

(b) segmental-rotor scheme

Figure 3.1. Elementary rectilinear structures with field winding; green = field, blue = armature.

the toothed-rotor scheme and two segments, S1 and S2, (and two non-magnetic slot spaces) for the segmental-rotor scheme.

In the toothed-rotor arrangement, each of the coils comprising the field coil F and armature coil A, spans two stator teeth, or a full pitch, whilst in the segmental-rotor arrangement each of the coils comprising the field coils F1 and F2, and armature coils A1 and A2, is around a single tooth. As each coil is around a single-tooth in the segmental-rotor configuration, a stator tooth may be identified as either a field tooth, if encircled by a field coil, or an armature tooth, if encircled by an armature coil. A special condition is required for the polarity of the field coils around the field teeth in the segmental rotor scheme. For this arrangement to produce a change of polarity of the armature coil flux linkage, the field coils are arranged such that when flux in one field tooth is designated as N pole the flux in the next field tooth has to be of S polarity, or vice-versa. In both cases, the polarity of the DC field coil is invariant.

3.2.2 Mechanism of flux switching

Starting with a situation when the rotor teeth are aligned with the stator teeth, the toothed-rotor scheme is considered as the first case. Over a full cycle of motion and with constant DC current in the field winding F, the armature conductors A link the flux in the back-iron which changes with rotor position, as shown in the flux plots of figure 3.2 (a). At one alignment position of the rotor and stator teeth, the flux in the back-iron over the armature slots, indicated by the arrows, have one polarity and at the next alignment position the flux has the other polarity. At the two intermediate positions, when there is no overlap between the rotor and stator teeth, there is zero flux linkage in armature coils and also zero net flux in the back-iron core over the armature slots. This is a basic illustration of the bipolar flux switching principle, implemented by a purposely designed rotor structure. The structure of the rotor also imparts a variable reluctance to the armature winding. Whilst the armature winding has bipolar flux linkages, this arrangement harbours bipolar flux only in the parts of the back-iron associated with the armature slots, with the rest of the stator core structure experiencing unipolar, though variable, flux.

In the second case, where the flux switching scheme is implemented by a segmental rotor, the armature coils A1 and A2 link the flux around the teeth encircled by the respective coils. The sequence of flux plots as the position of the segments changes is

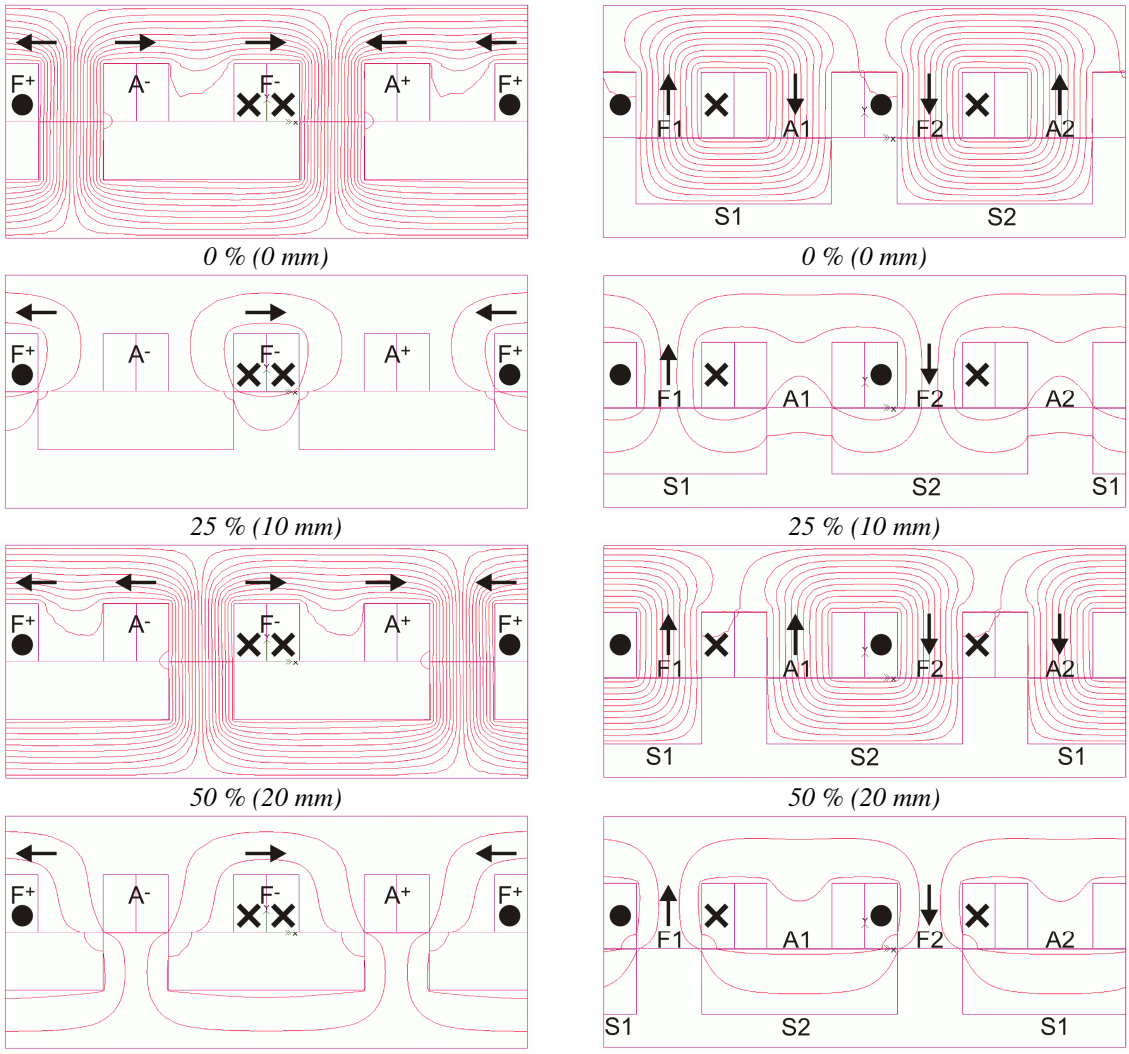

Figure 3.2. Flux plots in elementary structures with field winding at various rotor positions in steps of 25% of a cycle. Field coils only are excited.

shown in figure 3.2 (b). With constant DC current in the field coils F1 and F2, the encircled armature tooth flux changes with the position of the rotor segments. At the first alignment position in the initial position, when each of the segments is aligned with two adjacent stator teeth, the tooth flux linking an armature coil is of one polarity, and at the next alignment position, when the rotor has moved through half the cycle, the polarity of the tooth flux is reversed. Equally in this scheme, bipolar flux switching principle is achieved by the purposeful design of the rotor, and the resulting structure of the rotor gives a variable reluctance to the armature winding.

However, in the segmental rotor scheme, the two intermediate positions which give rise to zero flux linkages in the armature coils are of special interest. One position of zero armature flux linkage results from the segments being centred with the stator teeth, while the other position of zero armature flux linkage arises from the non-magnetic

space between rotor segments being centred with stator teeth. Though both situations have the overall effect of presenting zero armature flux linkages, the magnetic flux distribution in the armature teeth is different and may have notable consequences in advanced designs, such as the polyphase implementation. This arrangement also produces bipolar armature flux linkages but, in contrast to the scheme with a toothed rotor arrangement, it is the teeth encircled by the armature coils that experience bipolar flux, while the stator core-back structure experiences variable unipolar flux.

It should also be noted that, with the segmental rotor arrangement, only half the field MMF is available to drive the flux round the magnetic circuit. The flux in the core-back for the segmental rotor scheme may rise as high as in the field tooth, whilst for the toothed-rotor scheme it may rise only to half the value of the flux in the field teeth. This gives the possibility to design a core back depth for the toothed-rotor arrangement which is significantly less than the width of the stator teeth.

3.3 Magnetisation of the Stator Armature Teeth

The magnetisation of the armature tooth through one electrical cycle for the scheme with a segmental rotor when only field excitation is applied is of particular interest due the incongruence between the armature flux linkage and the geometrical presentation of the core arrangement with position. Whilst the two situations for peak armature flux linkages correspond to the geometric arrangement when the segments are aligned with the stator teeth, the two situations for zero armature flux linkages correspond to two different geometric arrangements of the core elements. The sequence of magnetisation of the armature teeth through one electrical cycle is summarised in Table 3.1.

For the this rotor design, in which the segment span exactly overlaps two stator teeth for the case of a segmental-rotor scheme, or the rotor tooth exactly overlaps the stator tooth in the case of the toothed-rotor scheme, the armature flux linkage is expected to vary in a quasi-sinusoidal manner with rotor position. The polarity of the armature flux linkage is determined by the orientation of the armature tooth flux, whilst its magnitude depends on the combined effects of the level of field excitation and the resultant reluctance seen by the armature coil.

Ideally, the magnetisation of the stator core during the build-up of armature flux linkage towards positive and towards negative maximums when only field excitation is applied

would be similar. This is the case in the toothed rotor arrangement, but is not so in the segmental-rotor scheme. In the segmental-rotor scheme, the trajectories for building armature flux linkage to positive maximum and for building flux linkage to negative maximum on the rotor position scale tend to be different to the extent given by the disparity in effect of a segment and a rotor's non-magnetic slot being centred with the armature tooth. The discrepancy in the magnetisation patterns of the stator tooth core at these two positions may be indicative of the deviation of the two trajectories, and appears to be influenced largely by the segment span or the span of the non-magnetic space between the segments and to some extent by the level of the constant field excitation.

Table 3.1. Armature flux linkage in relation to core geometry

Rotor position (cycle)	**Armature flux linkage, ψ**	**Core's geometrical presentation**
0	$-\psi_m$	Segment alignment
¼	0	Rotor slot centred with tooth
½	$+\psi_m$	Segment alignment
¾	0	Segment centred with tooth
1	$-\psi_m$	Segment alignment

Whilst the disparity in the magnetisation patterns at these two positions with field excitation only can be inferred from the difference in the geometric presentation, figure 3.3 clearly shows representative flux density plots in the field and armature tooth at these two positions, underlining the distinction in magnetisation of the stator teeth. The

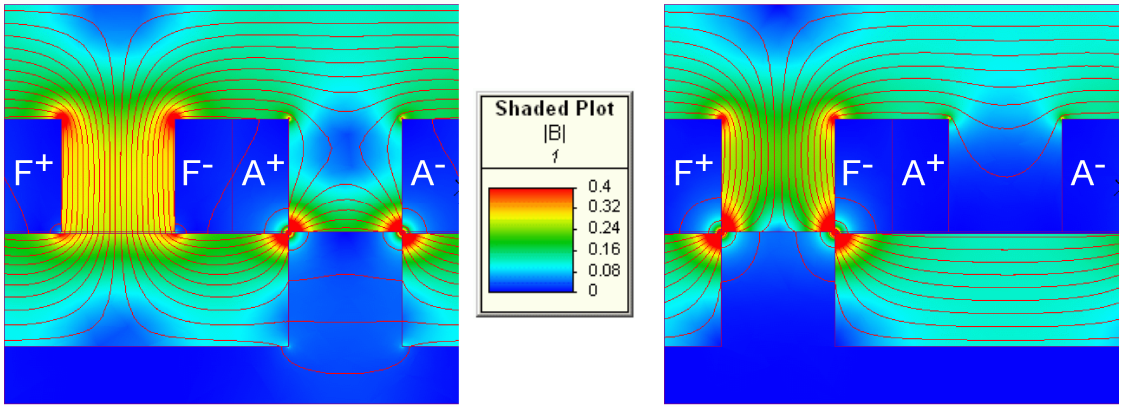

(a) slot centred with armature tooth (b) segment centred with armature tooth

Figure 3.3. Magnetisation of stator teeth at zero flux linkages position, with field excitation only.

stator teeth are magnetised at a higher flux density when the armature tooth is centred with rotor slot than when it is centred with the rotor segment. This may have the effect that, as the rotor is displaced, the stator core reaches saturation flux density more quickly in the magnetisation trajectory associated with the armature tooth being centred with the slot than one with the armature tooth being centred with the segment.

3.4 Coil Flux Linkages

This sections deals with the flux linkages of the coils when only field coils are excited. The exact dimensions of the rectilinear model and the excitation applied are fully supplied in appendix E.

The flux linkage in the coils designated as armature coils can be discerned, as from the description of the mechanism of flux switching given above, to be changing between a definite positive maximum and negative maximum, and may be implemented by a toothed rotor or a segmental rotor. Figure 3.4 shows the variation of the field and armature flux linkages with the position of the rotor on the elementary rectilinear cell arrangement, predicted from finite element modelling. The design applied in this comparison is such that the segment span exactly overlaps two stator teeth in the segmental rotor scheme and the rotor tooth width is equal to the stator teeth in the toothed-rotor scheme.

Despite employing a constant DC field current in both the segmental and toothed-rotor

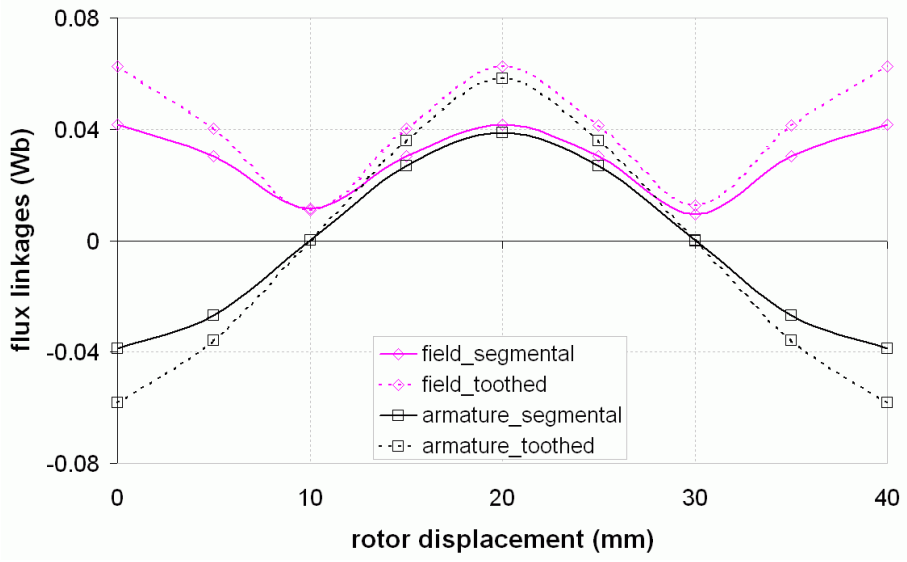

Fig. 3.4. Field and armature flux linkages with rotor position at nominal segment span and rotor tooth width.

schemes, the field flux linkage is unipolar but executes two cycles of fluctuation in one electrical cycle. The armature flux linkage is characteristically quasi-sinusoidal and is closely identical in both the types of flux switching schemes.

The fluctuation of field flux linkage due to rotor position, whilst constant DC current is applied, underpins the influence of the reluctance seen by the coils, which is predicted to change with rotor position. If the source is constant, the flux linkage of the field coil is inversely proportional to the reluctance and therefore the initial inference is that the positions for which the field flux linkages fall to minimum values are the positions of maximum reluctance. On the other hand, the armature flux linkage is seen to be zero at the inferred positions of maximum reluctance. The coincidence of the positions of minimum coil reluctance with the positions at which there is maximum flux linking the armature coils and the coincidence of maximum coil reluctance with the positions at which flux changes polarity in the armature coils are desirable conditions as they enhance coil flux linkages, but are not a necessary condition for the implementation of the flux switching scheme.

When the rotor segments are displaced through one electrical cycle the armature flux linkages on the armature coils may be described as traversing two magnetisation trajectories, one with a positive gradient and the other with a negative gradient, with respect to the rotor position. Although there is a hardly perceptible difference in the gradients of the two trajectories for armature flux linkage at the chosen level of field current and design of segment span for the segmental-rotor scheme, the field flux linkage minima provides the initial glimpse of the difference that may exist in the two magnetisation trajectories. The field flux linkage is perceptibly lower at the zero armature flux linkage position when the armature tooth is centred with the segment than when it is centred with the slot. These disparities constitute part of the investigation in the next subsection, where the parameters of segment span and field excitation are varied.

The mismatch between the field flux linkage minima may be quantified as the difference between the two minima values expressed as a percentage of the mean value of the field flux linkage. The disparity between positive and negative armature flux linkage gradients may be expressed as a percentage of, for instance, the positive gradient. As the gradient of the armature flux linkage continuously changes with

position, two pairs of symmetrically located positions may be chosen for the comparisons. One pair of points may represent the points at zero flux linkage and is called 'gradient through zero', while the other pair of points are each at an equal short distance (5 mm) from the location of the peak flux linkage and is called 'gradient towards peak'. Disparity between positive and negative armature flux linkage, as defined, may act as a measure of the asymmetry of the prospective induced EMF in the coil.

3.4.1 Influence of segment span and separation

An examination of the effect of changing the segment span, interpreted as the segment width in the rectilinear representation, below and above the span of exact overlap over two stator teeth by 50% of the stator tooth width (i.e. 5 mm) for the scheme employing a segmental rotor is shown in figure 3.5. This designation produces three study cases as follows: a nominal segment width denoted as 'nominal' at 30 mm, a reduced segment width denoted as 'reduce' at 25 mm and an increased segment width denoted as 'increase' at 35 mm. For all cases of segment span considered, the field excitation is kept constant.

The shape of the waveform of the armature flux linkage is markedly affected by the change in the segment span, departing significantly from the quasi-sinusoidal shape (part (a)). A reduction in segment span inclines the armature flux linkage waveform to have a triangular shape, whilst an increase in segment span makes it tend towards the trapezoidal shape. The impression is that a design which produces a trapezoidal shape of armature flux linkage is undesirable as it leads to instances of zero induced EMF, in the bands when the flux linkage is constant with motion. As an alternative index (part (c)), the peak value of armature flux linkage barely changes with segment span until the nominal span is exceeded, when it is observed to fall. The index for quantifying the disparity between the positive and negative gradients of the armature flux linkages (part (e)) suggests that although the disparity increases with segment span, its magnitude is so small as to be insignificant (less than 1.2 percentage points).

The form of the waveforms of the field flux linkages appears to be greatly affected by the segment span. For the case of increased segment span, the positions of zero armature flux linkages (at 10 and 30 mm of displacement) have substantially different and opposing effects. At 10 mm displacement, the field flux linkage is at its minimum, as in

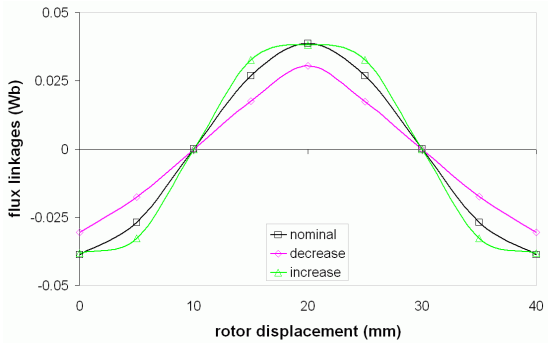

(a) armature flux linkage waveforms

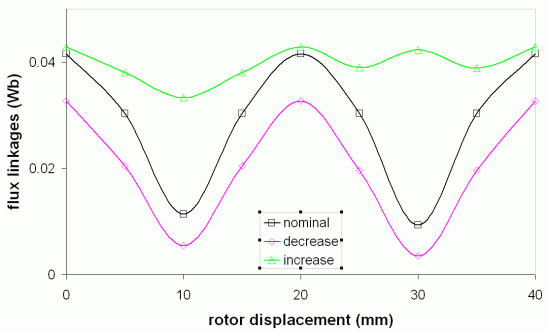

(b) field flux linkage waveforms

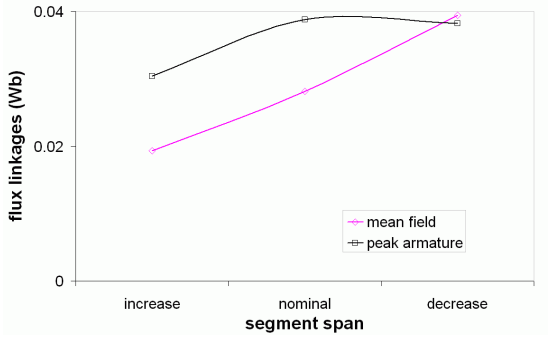

(c) flux linkages

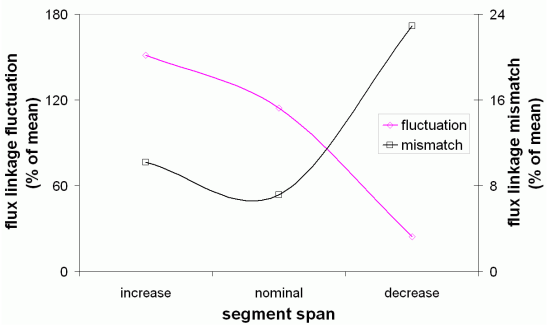

(d) field flux linkage fluctuation and deviation from symmetry

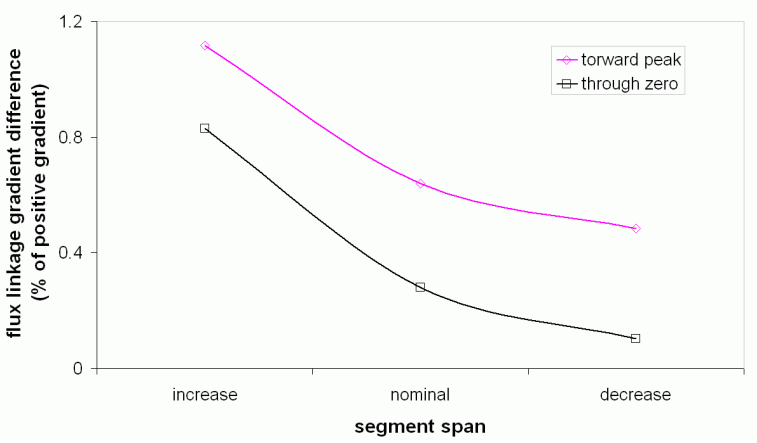

(e) deviation of armature flux linkage waveform from symmetry

Figure 3.5. Effect of varying segment span in the segmental-rotor scheme. The segment span is inversely related to the rotor slot width.

the case of the nominal and decreased segment span, but at 30 mm displacement, instead of assuming a comparable minimum value, the field flux linkage recoils to a higher value which is comparable to that of the peak value. An examination of the flux paths at these two positions, as shown in figure 3.6, explains this fascinating outcome.

Apparently, when the segment span is increased such that the span of the non-magnet rotor slot space is less than the stator tooth width, substantial flux subsists in the field teeth (F1 and F2), coupling through the tips of intermediate armature teeth (A1 and A2),

at one of the zero-armature flux linkage positions (at 30 mm displacement). At the other zero-armature flux linkage position (at 10 mm displacement), a different amount of flux subsists in the field teeth, coupling through the rotor segments. The extended edges of the segments tend to provide bridges for flux path to include more than two stator teeth in the magnet circuit but circumvent the middle tooth. It is thought that the effective coil permeance is increased due the additional parallel paths for flux when more than two stator teeth are involved. The difference in the magnetic circuit constitution, as seen by the field coils when the segment span is extended at these positions, accounts for the difference in the field flux linkages.

Changing the segment span has an equally remarkable effect on the magnitude of the field flux linkages. Over this range of segment span, the mean field flux linkage (figure 3.5 (c)) increases with segment span and is accompanied, in figure 3.5 (d), by a reduction in the field flux linkage fluctuation and a reduction in the mismatch of field flux linkages at the positions of zero-armature flux linkages.

The general outcome of this examination is that changing the segment span below and above the span of exact overlap over two stator teeth produces potentially competing outcomes on the field and armature flux linkages, which are summarised in the following outline:

- the shape of the armature flux linkage waveform is significantly affected by segment span, causing the waveform to be triangular when span is reduced and to be trapezoidal when span is increased.
- the shape of the field flux linkage waveform is affected by the segment span, presenting two different constitutions at the two positions of zero-armature flux

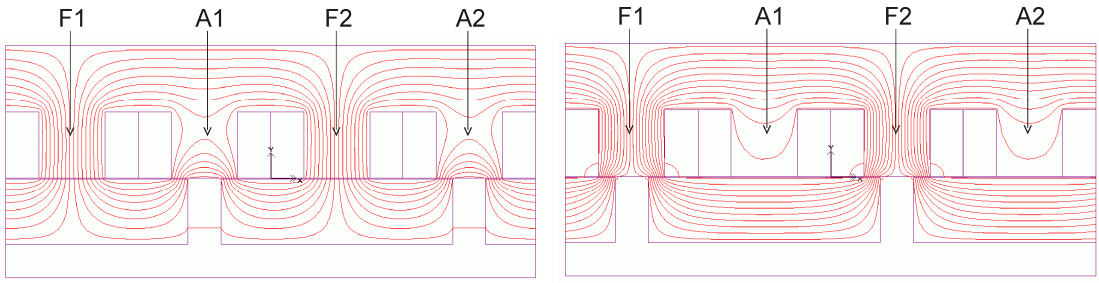

(a) rotor slot centred with armature tooth (10 mm) (b) segment centred with armature tooth (30 mm)

Figure 3.6. Coupling between field teeth and between armature teeth due to increased segment span.

linkages when span is increased, although there is no significant difference when span is reduced.

- the peak armature flux linkage is not perceptibly affected by an increase of segment span from the nominal span, but the value tends to fall with a decrease of segment span.
- the mean value of the field flux linkage increases proportionally with increase of segment span.

3.4.2 Effect of field MMF

In this part of investigation, the field excitation is varied while the segment span is fixed at the nominal dimension. The effect of changing the excitation field MMF, from the nominal value of 160 A down to 25 % (40 A) and up 3 times the nominal value (480 A), on the field and armature flux linkages, is shown in figure 3.7. The characteristic shape of the flux linkage waveform with rotor position for the both the armature and field coil appears to be unaffected by the field excitation (part (a) and (b)). However, both the mean field flux linkage and peak armature flux linkage (part (c)) appear to increase proportionally with field excitation, with signs of saturation at high excitation. Increasing the field current tends to slightly reduce the fluctuation of the field flux linkage but has a substantial effect of raising the mismatch between the two minima of the field flux linkage (part (d)). At this specification of segment span, the disparity between the positive and negative gradients of the armature flux linkage attains prominence when field excitation is increased beyond the nominal level (part (e)).

As established in the investigation of the effect of segment span, changing the field excitation has a notable affect on not just the magnitude but the characteristics the field and armature flux linkages.

3.5 Magnetic Circuit Presentation of Segmental-Rotor Elementary Structures

The magnetic equivalent circuit (MEC) representation of the elementary rectilinear structures elucidates the flux switching principle employing a segmental rotor in a different light and may be applied to track the mechanism of flux switching with the variation of the permeance.

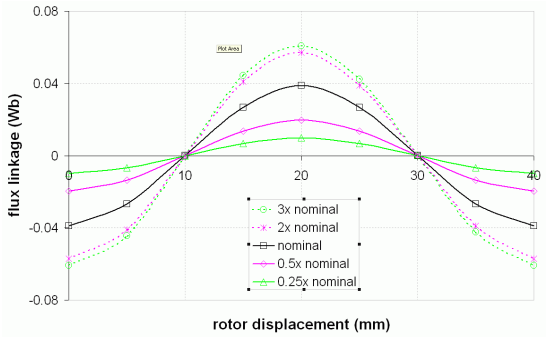

(a) armature flux linkage waveforms

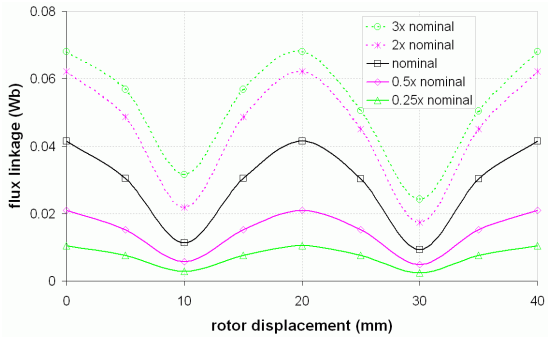

(b) field flux linkage waveforms

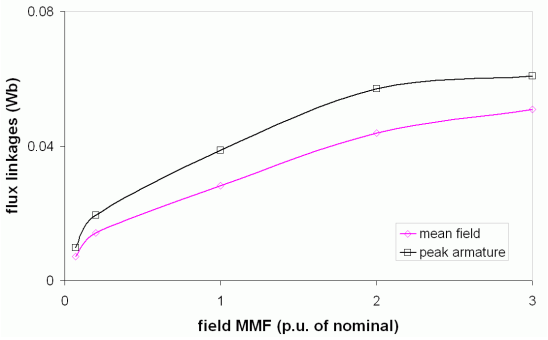

(c) flux linkages against field excitation

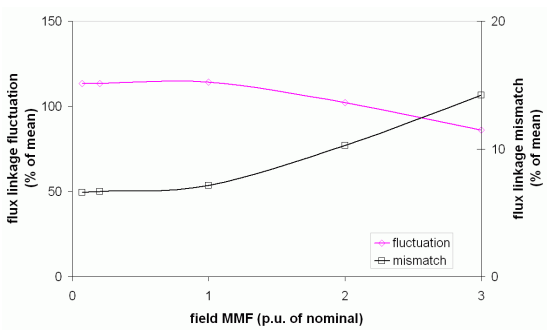

(d) field flux linkage ripple against field excitation

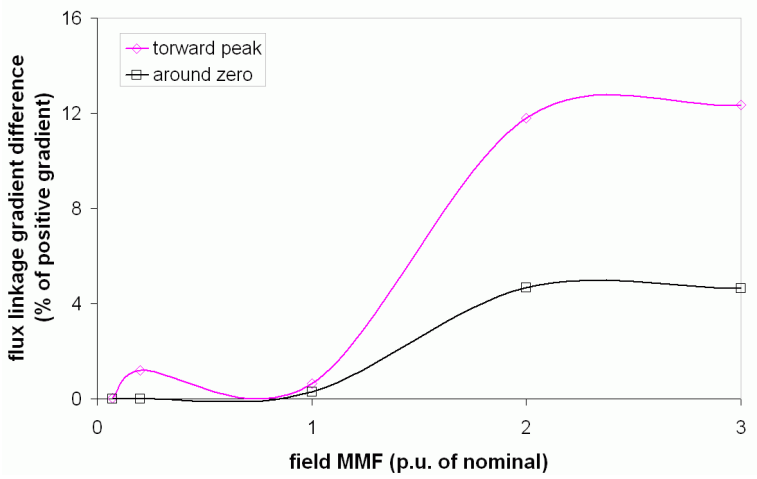

(d)

Figure 3.7. Effect of varying field excitation

3.5.1 Background

Since the seminal works of Laithwaite [157] and Carpenter [158] in the later part of the 1960's, the magnetic equivalent circuit methods have been progressively improved and applied in the design and analysis of various forms of electrical machines, ranging from the conventional machines of the types of induction and permanent magnet synchronous machines [159], [160] to the new forms of machines typified by the switched reluctance and flux switching machines 127], [161]. In [159], it was demonstrated how MEC can be seen as a form of FEA, and can be made as accurate as necessary. Recently [162], it

has been argued, with the support of evidence of extensive comparisons of literature, that the magnetic circuit equivalent models may be as good as the FE analysis models, if not better, when constructed to account for non-linear and eddy current effects. However, in the rectilinear representation of the cell elementary structures studied here, the MEC representation has been applied in a simplified linear form to study the basic characteristics of the permeance seen by coils with rotor position.

A MEC representation of the segmental-rotor rectilinear elementary structure, with the level of detail and complexity to give it the accuracy comparable 2D FEA, requires formulation of a reluctance network that incorporates permeances that account for the various effects as follows.

a. ***Overlap airgap permeance***: the permeance which occurs directly between the overlap of the rotor segment and the stator tooth. It is therefore dependent on the position of the rotor relative to the stator and is at its maximum when the segment completely overlaps the stator tooth. The accuracy of this permeance can be improved by including a permeance in series, to account for fringing effects.
b. ***Core permeance***: the permeance of the stator and segment core structures. This permeance is dependant on the flux in the core structure but not on the rotor position and is nonlinear in character.
c. ***Permeance due to leakage flux***: permeance of the non-magnetic medium other than the airgap. There are two major routes for leakage flux. In the first case, the flux may pass between two adjacent stator teeth and comes to be called the slot leakage. In the second case, the stator tooth and rotor segment are in a non-overlapping position, but may be close enough for flux to pass between them, and the effect may be called tooth-to-segment leakage. The rotor position and the amount of flux have no influence on this type of permeance.

Since the rectilinear elementary structure used here is a conceptual representation, this investigation benefits from considerable simplification by assuming the core permeance to be very high (infinity) and the permeance due to leakage flux to be negligible (zero). The resulting model, incorporating only overlap airgap permeances and without considering fringing effects, is deemed sufficient to capture the essential characteristics of flux switching by means of a segmental rotor.

3.5.2 Linear magnetic equivalent circuit model

The simplified MEC model for the rectilinear structure with a segmental rotor is shown in figure 3.8. The field MMF, $\mathcal{F}_{F1}$ and $\mathcal{F}_{F2,}$ are the only magnetic sources in the representation, while the flux passing through the unexcited armature coils is denoted by ϕ_{A1} and ϕ_{A1} in the short-circuit branches. The reluctances, denoted by $\Re$, are constructed as functions of the overlap length between the segment and the stator tooth, $x_{over}(x,b)$, which in turn is determined by the rotor position, x and the state b of the applicable circuit branch, whether connected or isolated by the switch, so that the reluctance of a branch is given by

$$\Re(b) = \frac{1}{\Lambda(b)} = \frac{l_g}{\mu_0 l_a} . \frac{1}{x_{over}(x,b)} \tag{3.1}$$

where l_g and l_a are the gap and axial lengths, respectively, μ_0 is the permeability of free space and Λ is the permeance.

At any particular rotor position, depending on whether the stator tooth is overlapped by a segment or not, the links between branches may be closed or open, the effect which is represented by the state of switches T1 to T4. Due to vertical symmetry presented by the elementary structure, whereby a unit comprising a field and armature tooth and one rotor segment repeats itself through horizontal distance, the operation of the switches is ganged in pairs as T1 with T3 and T2 with T4. The physical interpretation of the operation of the magnetic circuit switches, from the point of view of an armature branch, can be seen as admitting flux from the adjacent N or S pole source when either of the adjoining edges of the armature tooth are overlapped by a segment (switches are closed), and shutting out the flux from the adjacent sources when there is no overlap (switches are open). The operation of the magnetic switches leads, inevitably, to a presentation of different circuit configurations determined by the states of the switches. Thus, for any design of the flux switching configuration employing a segmental rotor, there is more than one circuit configuration of operation through one electrical cycle.

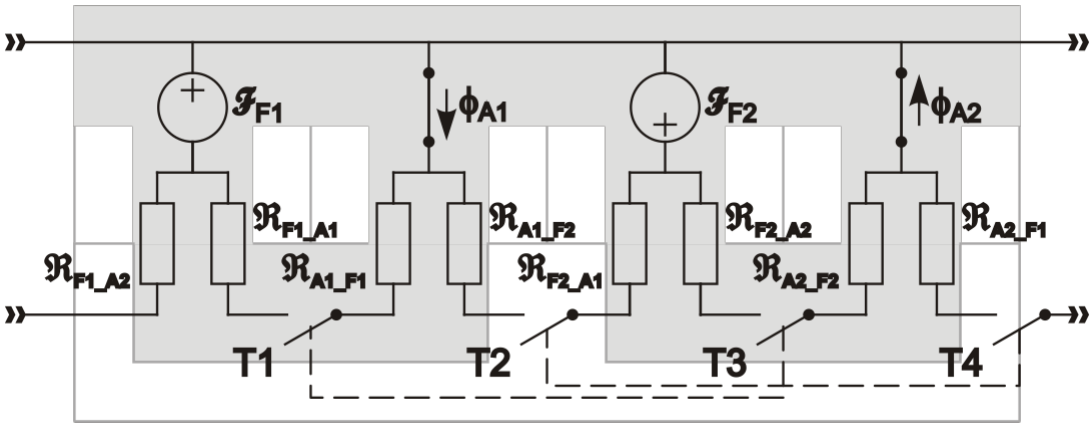

Figure 3.8. Magnetic equivalent circuit model of the elementary segmental-rotor rectilinear structure.

3.5.3 Magnetic circuit operating stages and their configurations

Three designs, broadly typifying the ranges of classification of the manner the segment may overlap the stator tooth, are considered. The first design, considered as the nominal design, has a segment span that exactly overlaps the stator tooth at the alignment position, or conversely the span of the non-magnet space between segments is equivalent to the stator tooth width. The second design has the segment span which is less than that in the nominal design, or conversely, the span of the non-magnetic medium between the segments is greater than in the nominal design. To balance the investigation, the third design has the segment span which is greater than that in the nominal design, conversely expressed as having the span of the non-magnetic medium which is less that in the nominal design. The chosen change in the segment span for the second and third design is a value which is 25% of the stator tooth width.

With field excitation only, and starting at the position of segment alignment, the operating stages in each design, controlled by the states of the switches, are as shown in Table 3.2. Each of the operating stages assumes one of the circuit configurations shown in figure 3.9, designated as configurations A, B, C and D.

It is sufficient to examine only the operation of switches T1 and T2 and their associated loops, as the operation of T3 and T4 and their associated loops is a reflection of T1 and T2.

In one electrical cycle, the three broad designs generally have two major operating stages, coinciding with the states when armature flux linkage is negative and positive, and assumes the magnetic circuit configurations A and B in figure 3.9, respectively. In particular, the nominal design strictly fits this description, but the designs with reduced and increased segment span each have two additional and intermediate operating stages, occurring around the transitional change from negative to positive armature flux linkages, and vice versa, so that there are four operating stages. The dwell of these transition stages is seen to be proportional to the extent of the departure from the nominal design. For the design with reduced segment span, the intermediate transitional stages assume a circuit configuration without any closed path, whilst in the design with increased segment span they assume the magnetic circuit configurations C and D.

Table 3.2. Magnetic circuit stages and switch states.
switch state 1 = closed; switch state 0 = open

Design	**Operating Stage**	**Switch State**				**Circuit Configuration**
		T1	T2	T3	T4	
Nominal	I	1	0	1	0	A
	II	0	1	0	1	B
Reduced Segment Span	I	1	0	1	0	A
	II	0	0	0	0	No connected network
	III	0	1	0	1	B
	IV	0	0	0	0	No connected network
Increased Segment Span	I	1	0	1	0	A
	II	1	1	1	1	C
	III	0	1	0	1	B
	IV	1	1	1	1	D

Although it can be discerned from the FE modelling that the segment span has significant influence on the armature flux linkages, through the permeance presented to the coils, it cannot be as easily shown through this method what is inherently happening to the electromagnetic system around the instances when flux switching occurs as with the simplified magnetic circuit method. The MEC approach has shown that the magnetic circuit configurations, apart from the variation of values of the model reluctances or permeance with rotor, change with the change of the polarity of the

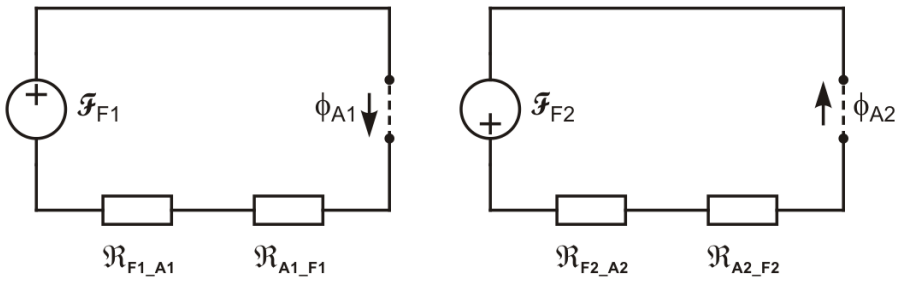

(a) configuration A

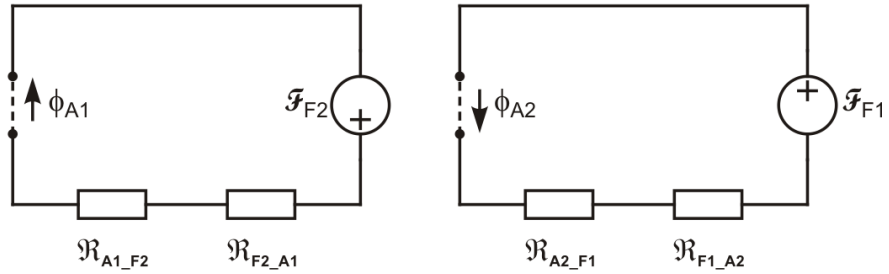

(b) configuration B

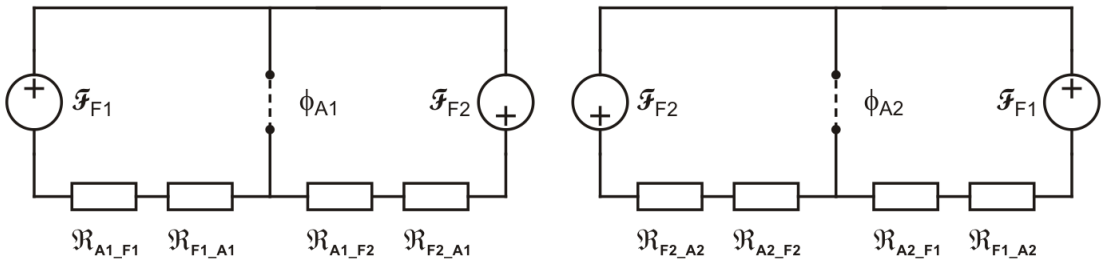

(c) configuration C

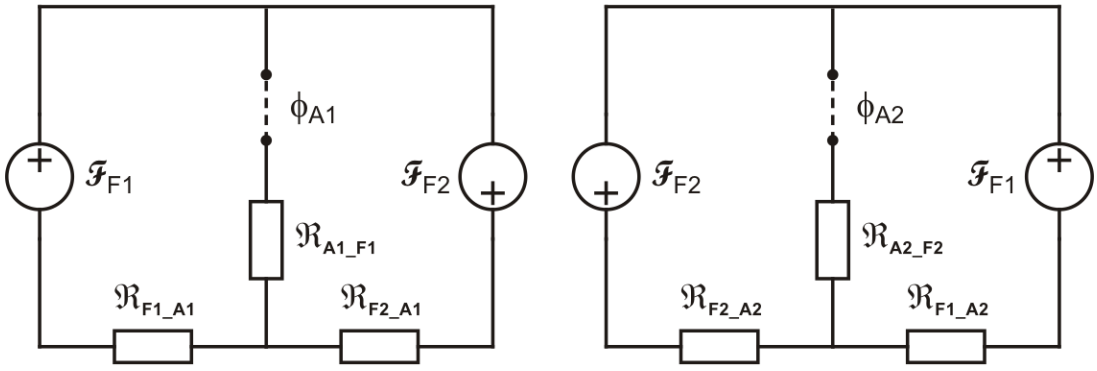

(d) configuration D

Figure 3.9. Magnetic circuit configurations as determined by switch states

armature flux linkages. Further more, transitional periods connected with the extent of the departure of the segment span from the nominal design, have been identified by additional configurations of the magnetic circuit, whose form depends on the direction of departure of the segment span from the nominal design.

3.5.4 Stator coil permeance

The stator coil terminals are the access points for the electric circuit model of the elementary rectilinear structure. Apart from the sources, an electric circuit model may consist of passive elements of resistances, inductances and capacitances. If resistance and capacitance are neglected, as in the simplified MEC model, the simplified electric circuit model consists of the inductances, which are derived from the permeance network. The MEC model, naturally affords the chance to directly view the permeance of the coils.

Figure 3.10 shows the variation of the armature coil permeance with rotor position, derived from the permeance network of the MEC model. As the elementary rectilinear structure is a relatively simple topology, a more accurate armature coil permeance may be as easily extracted from the FE results as the approximate results can be obtained from the simplified MEC model, and the results from the two approaches are shown side by side.

The form of the variation of permeance with rotor position is in agreement with the theoretical expectation presented, for the ideal variation, in figure 3.1. As expected, the simplified MEC model predictions are discernibly different from the prediction from the

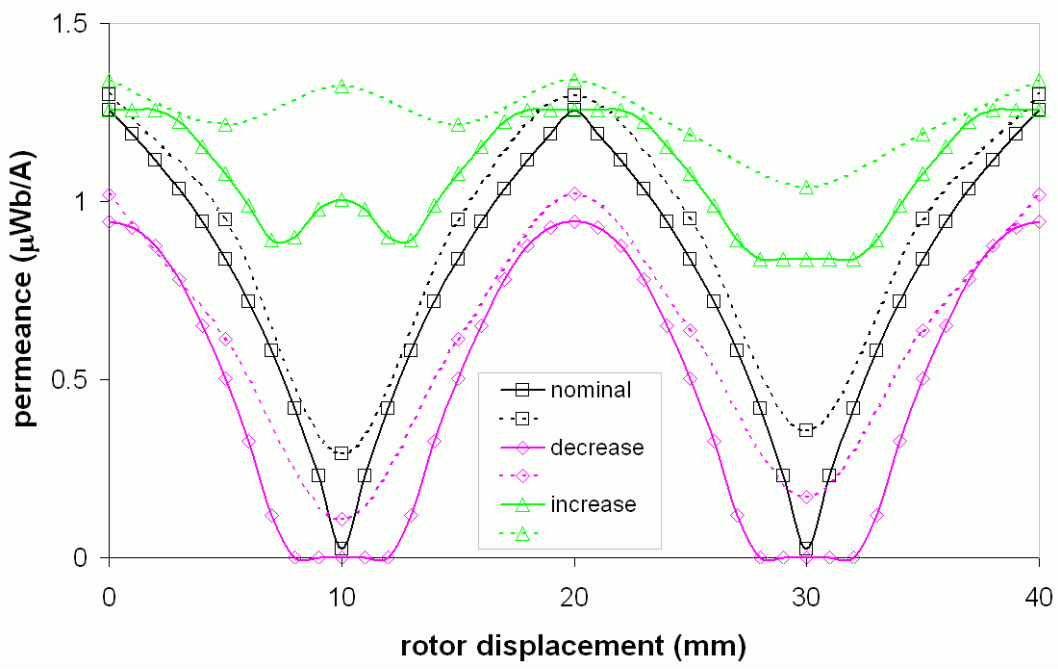

Figure 3.10. Variation of armature permeance with rotor position for three designs of segment span. solid = MEC model; dashed = 2D FE model

more accurate FE models and underestimate the magnitudes of the peaks and the troughs, mainly as a result of neglecting the core permeance, leakage flux and saturation. However, the MEC model, in predicting the variation of the permeance with position, captures the essential characteristic nearly as well the FE model. From the point of view of armature permeance, the effect of reducing or increasing the segment span appears to be to accentuate or diminish the fluctuation of the permeance with rotor position. From these results, following geometric correspondence with the graphs for armature flux linkage, there is a strong suggestion that the position at which armature flux linkage switches polarity coincides with the position for minimum armature permeance. This is particularly well collaborated for rotor designs where the span of the non-magnetic space between rotor segments does not exceed the stator tooth width.

3.6 Use of Permanent Magnet Excitation

Having described, earlier in this chapter, how flux switching is realised with field winding excitation for schemes with toothed and segmental rotors using illustrations on elementary rectilinear cell structures, it is reasonable to consider that field windings may be replaced by permanent magnets. In this conversion, the elementary rectilinear cell structures are also applied to illustrate the implementation for both the toothed and segmental rotor scheme. It appears that the conversion to permanent excitation may be more straightforward in the segmental rotor arrangement, where a field is around a single tooth, than in the toothed rotor arrangement where a field coil spans at least two teeth.

With the same constraint of restricting the location of all excitation systems to the stator structure, an approach to the conversion is to identify the stator core parts on the wound-field schemes that convey unipolar flux throughout the cycle as probable locations for magnets. For the scheme employing a segmental rotor, the stator teeth encircled by a field winding convey unipolar flux and are the likely locations for permanent magnets to act in the radial direction. Some parts of the core back, the sections subtended on the slots harbouring field coil, convey unipolar flux in the toothed rotor scheme and are the likely locations for permanent magnets to act in the circumferential direction. While it is clear that any point on the length of the field tooth may house a magnet acting in a radial direction to implement flux switching in the

segmental rotor scheme, more careful thought is required for the correct location of the magnets in the core-back of the toothed-rotor scheme.

3.6.1 Elementary rectilinear structures with permanent magnets

The feasible structures for flux switching schemes implemented with permanent magnets, represented by elementary rectilinear cell structures, for the toothed and segmental-rotor arrangements are shown in figure 3.11. The structure for the toothed rotor scheme appears to be first reported by Hoang et al [125] around 1997 and is now the standard structure for permanent magnet flux switching machines. The structure for the segmental rotor scheme, conceived at Newcastle University in 2008 in the course of this work, is the subject of the quest for high torque density machine configurations.

In part (b) of figure 3.11, showing the segmental rotor scheme arrangement, the structure of the stator core is similar to the one for the wound-field scheme in figure 3.1, except for accommodating the permanent magnets, M1 and M2, at the tips of the field

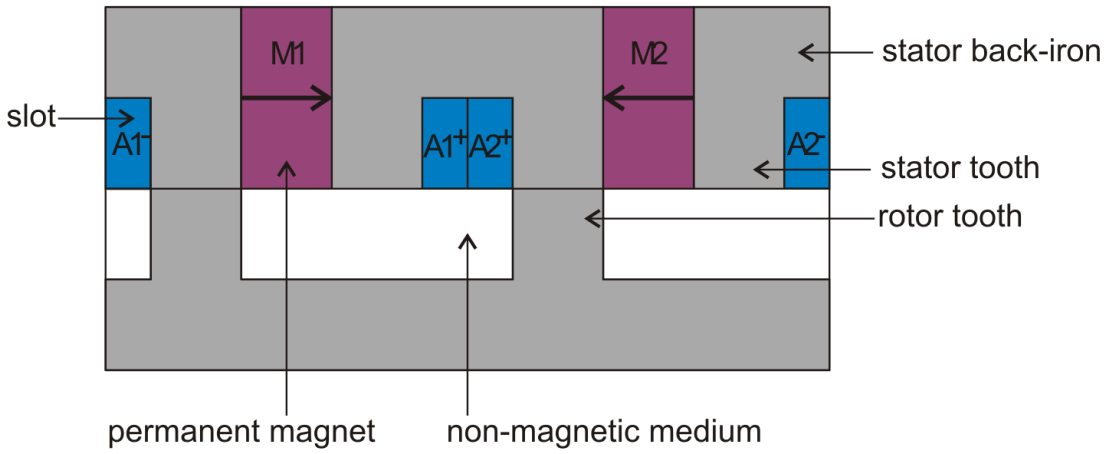

(a) toothed-rotor scheme

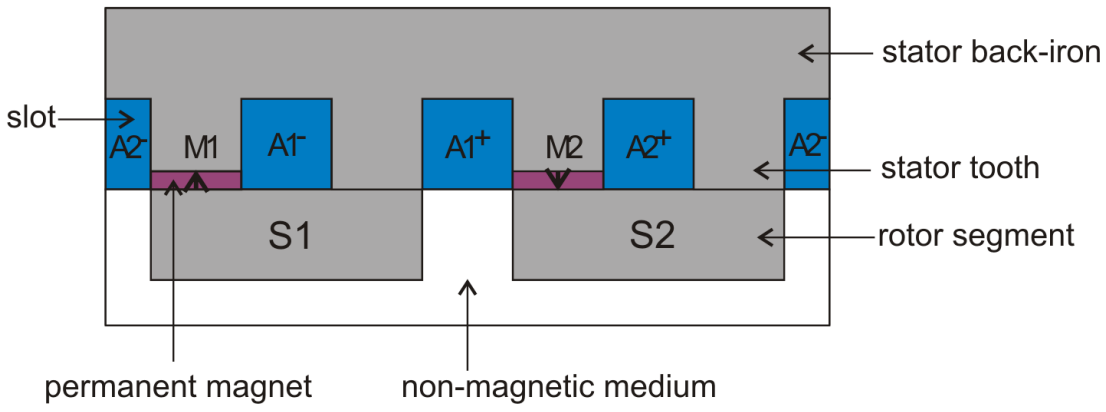

(b) segmental-rotor scheme

Figure 3.11. Elementary rectilinear structures with PM excitation.

teeth. The setting of the magnets at the tips of the teeth is particularly advantageous for easy access and assembly. The polarisation of the magnets is in opposing polarity, in sequence, and the available slot space is used to accommodate entirely the armature tooth windings, A1 and A2 round the armature teeth. There is no requirement for any change to the structure of the rotor from the one depicted for the wound-field configuration.

The structure of the stator core for the toothed rotor arrangement, depicted in part (a) of figure 3.11, is drastically different from that depicted for the wound-field configuration in figure 3.1 (a). In comparison with the stator core structure for the wound-field configuration, the one with permanent magnet excitation appears to have sections of the core-back replaced by magnets, M1 and M2, which extend in the radial direction inwards but act in the circumferential direction and in opposing polarity. The modularised stator core structure has the appearance of having two identical U-shaped sections, sandwiched by magnets. Each of the armature coils, A1 and A2, spans the adjoined adjacent legs of the two U-shaped stator cores. The structure of the rotor requires no fundamental change, but the rotor tooth width may be adjusted to comply with the alignment requirements with the leg of the U-shaped stator core. As a representative design for the flux switching principle, the dimensions are chosen as suggested in an preliminary design considered in [163], [164], where the stator tooth width, rotor tooth width, magnet width in the magnetisation direction and core back depth have the same dimension. The toothed rotor designs discussed in [125], [140] also have an identical dimension for the stator tooth and the magnet thickness, at the least. Accommodating a magnet between the U-shaped cores, whilst maintaining the dimension of the stator tooth width as found in the wound-field configuration, results in noticeable concession of slot space for the armature conductors.

One notable distinction between the toothed and segmental rotor schemes in the implementation of the flux switching schemes using PM excitation is the application of rather larger amounts of magnets in the toothed rotor scheme. This gives an advantage to the segmental rotor scheme in terms of the cost of the applied magnets, although there is an associated reduction in its performance. There is also a susceptibility of the magnets to demagnetise in the segmental rotor scheme, as the magnets are located next to the airgap, a problem also well-known in the flux-reversal machine.

3.6.2 Mechanism of flux switching

With the conversion to permanent magnet excitation described above, the mechanisms of flux switching ascribed to configurations employing a field winding for both the toothed rotor and segmental rotor schemes are maintained. The conversion ensures that sections of the back-iron connecting the two legs of the U-shaped stator core modules of the toothed rotor scheme experience bipolar flux with change of the rotor position, and so do those stator teeth without magnets for the segmental rotor scheme, as shown in figure 3.12. Thus, there is bipolar flux linkage for the armature conductors in slots formed by the U-shaped core in the toothed rotor scheme, and for the armature

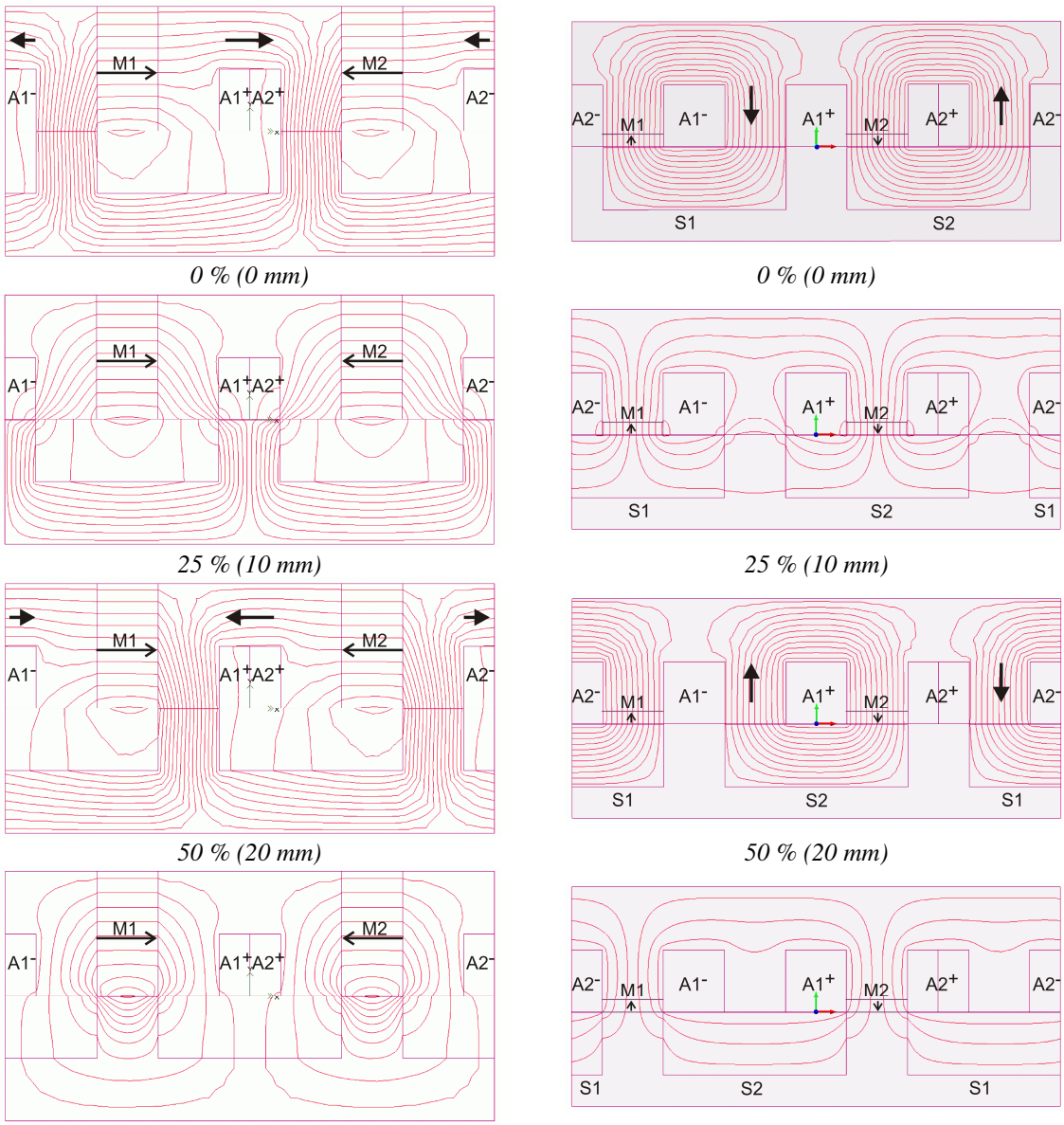

Figure 3.12. Flux plots in elementary structures with permanent magnets at various rotor positions in steps of 25% of a cycle. Armature coils are unexcited.

conductors in slots forming coils to encircle the stator teeth without magnets in the segmental rotor scheme. A replication of the flux switching mechanism, as with a field winding, is completed by harbouring only unipolar flux in the legs sections of the U-core stator modules for the toothed rotor scheme and in the back-iron section of the stator core for the segmental rotor scheme.

3.6.3 Armature coil flux linkages

The investigation of coil flux linkages with PM excitation only, like that for wound-field excitation in the previous sections, uses the design dimensions for rectilinear cell structures supplied in appendix E. A linear approach, such as shown in the illustration of appendix B, is applied to determine the number of turns on the coils.

The armature flux linkage waveform with respect to rotor position for this design, as expected from the above description, is quasi-sinusoidal in shape for both the toothed and segmental rotor schemes, as depicted in figure 3.13. However, the disparity between the positive and negative gradients of the armature flux linkage is more apparent than in the case with field winding excitation. The gradient difference is about 14% and 24% of the positive gradient for the toothed and segmental rotor schemes, respectively when examined around the zero-flux linkage position. Within a little displacement (or a few degrees) either side of the position of peak flux linkage, the gradient difference is about 34% and 168% of the positive gradient for the toothed and segmental rotor schemes,

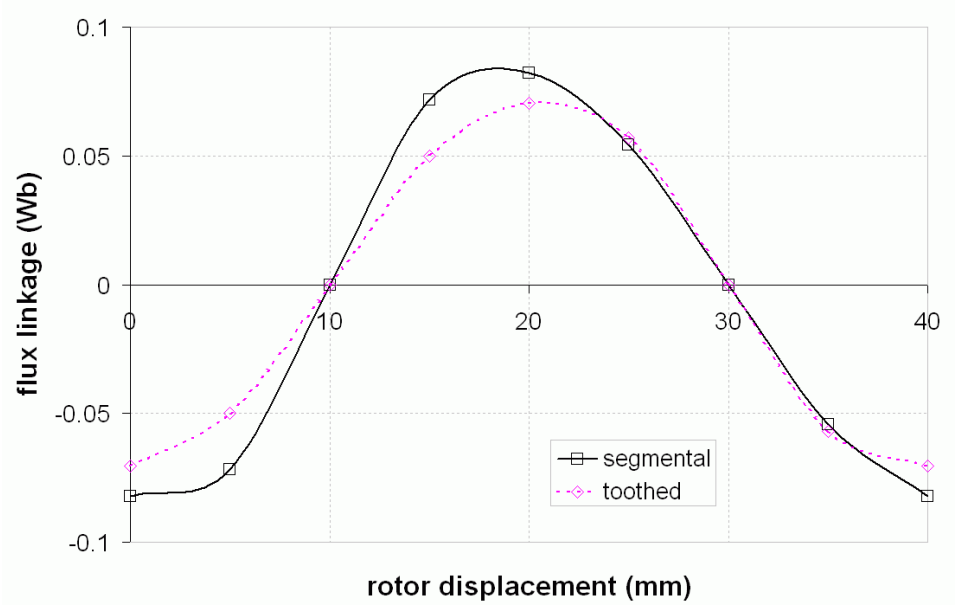

Figure 3.13. Armature coil flux linkages.

respectively. This result is suggestive of substantial asymmetry in the alternations of the prospective induced EMF waveform, and appears to be more pronounced in the segmental than the toothed rotor scheme. The effect is attributed to the additional reluctance presented by the space occupied by magnets and may be explained with the aid of the flux plots in figure 3.14 in the following way.

The flux and flux density plots in figure 3.14 show the transition of these quantities around the position of peak flux linkage, comparing the patterns at the positions which are 1/8 of a cycle way on both sides of the position for peak flux linkage. Scrutiny of the patterns reveals that the difference in the flux linkages at these two positions for the toothed rotor scheme is due to more leakage of the flux in the conductor slot when the rotor tooth is approaching than when it is leaving the alignment position.

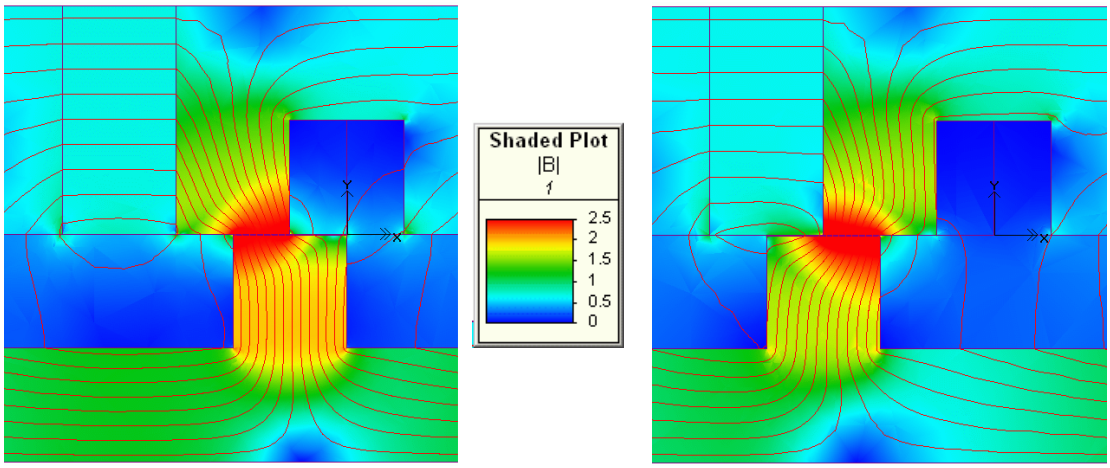

approaching alignment leaving alignment

(a) toothed rotor scheme

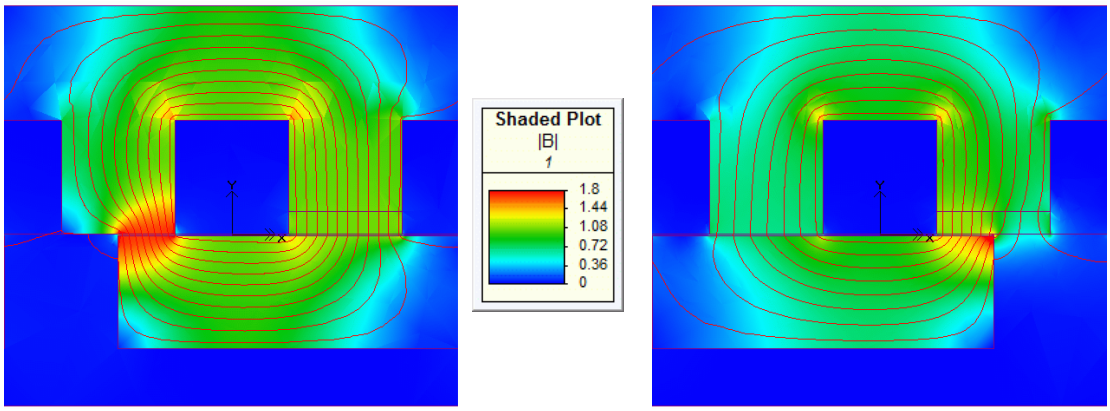

approaching alignment leaving alignment

(b) segmental rotor scheme

Figure 3.14. Magnetisation patterns at positions of approaching and leaving alignment.

For the case of the segmental rotor scheme, two effects combine to produce the difference in the flux linkages. Firstly, the magnet is fully overlapped by the segment at the approaching position to link more flux to the armature tooth than at the leaving position when it is partially overlapped by the segment. Secondly, since the magnet thickness is larger than the airgap length ($\frac{l_m}{l_g} = 20$, in this case), the reluctance presented by the magnet space is dominant, so that the reluctance seen by armature coil is lower at the approaching position than at the leaving position. In both the toothed and segmental rotor schemes, the differences are fundamentally due to the incongruence in the geometries for magnetisation introduced by accommodating the magnets.

3.7 Comparison of the Toothed and Segmental Rotor Schemes

It is shown in the above sections how a segmental rotor can be applied to implement the principle of flux switching, developed as an extension of the scheme employing a toothed rotor. A comparison of some salient features inherent in the two schemes serves to suggest areas which may be exploited for optimisation and specific performance.

The approach to this comparison is to firstly reiterate the features which are common to both schemes. The second part compares the differences that subsist in the two schemes.

3.7.1 Common features

It is worth repeating that both the schemes produce bipolar armature flux linkages with constant application of field excitation and involve a similar mode of variation of reluctance with rotor position. The field and armature systems are stationary and are both located on the stator, allowing the rotor to be of a simple structure without carrying any winding or magnets. The excitation systems on the stator may benefit from easy access to a variety of cooling methods making high loading possible. The simplicity of the rotor may aid construction and the resulting robustness may permit increased speeds to be attained. As a drawback in both the schemes, the location of the primary excitation system together with the secondary excitation system on the same structure, i.e. the stator, is indicative of a competition for space traditionally designated for only one of the excitation systems, and may affect performance.

3.7.2 Differences

There are a number of pertinent differences between the schemes with a toothed and segmental rotor, both in structure and operation, and are tabulated in Table 3.3.

As there is bipolar flux operation through each electrical cycle in the pertinent magnetic sections (back-iron for toothed scheme and armature tooth for segmental rotor scheme), the utilisation of the magnetic structure is superior to that for arrangements with unipolar flux in all sections, such as DC and switched reluctance machines. However, it appears that the segmental rotor scheme potentially may have gains for applying coils with shorter end-windings than the toothed rotor scheme. This may mean savings both in materials and in copper loss. It also appears that the segmental rotor scheme, when implemented with permanent magnet excitation, concedes less useful space for the magnets than the toothed rotor scheme, with prospects for improved performance.

Table 3.3. Differences between toothed and segmental rotor schemes

	Toothed Rotor Scheme	**Segmental Rotor Scheme**
1.	Bipolar flux in back-iron	Bipolar flux in armature teeth
2.	Unipolar flux in all teeth	Unipolar flux in back-iron and field teeth
3.	Magnets located in back-iron structure	Magnets located in teeth structure
4.	Magnets acting circumferentially	Magnets acting in radial direction
5.	Magnet position displaces slot (and tooth) space on stator	Magnet position is recessed into stator tooth.
6.	Reduced space for conductor slots with PM excitation	Increased space for conductor slot with PM excitation
7.	Coil spans more than one tooth	Coil around one tooth
8.	Long end-windings	Short end-windings
9.	Large amounts of magnets	Small amounts magnets

3.8 Conclusion

The elementary rectilinear cell structures have been applied to describe and investigate the principle of flux switching as implemented by toothed and segmental rotor schemes on arrangements with all excitation sources on the stator. Although either field coils or

permanent magnets may be applied to provide primary excitation, there are some important distinctions which arise in the arrangements and in performance.

As part of the investigation of the salient features of segmental rotor scheme compared to toothed rotor scheme, the field and armature flux linkages reveal remarkable effects underlined by the magnetisation trajectories with respect to rotor position. The difference in the trajectories for magnetisation and demagnetisation, presented by the peculiar method for implementing flux switching in the segmental rotor scheme, appears to be responsible for the inequality in the alternations of the prospective induced EMF waveform. However there are other factors, such as the segment span and the level of field excitation or the type of excitation (wound-field or PM) which seem to affect the symmetry of the alternations in the EMF waveform. A linear magnet circuit model has helped to identify and synchronise the variation of reluctance with the armature flux linkage.

A comparison of the segmental and toothed rotor structure affirms some subtle differences in operation, but the perceived difference in the structure of winding arrangements points to savings in materials and reduced copper loss that arises for the segmental rotor scheme in employing single-tooth windings, which gives shorter end-windings.

Chapter 4

Three phase topologies using segmental rotors

This chapter describes the development of three phase topologies for flux switching machines using segmental rotors and single-tooth windings on the stator. In the previous chapter it has been shown how a segmented rotor can be applied to realise switching flux in the armature teeth, with the description of the development of the wound-field and PM implementation. The basic principle of flux switching by means of a segmental rotor is now extended to apply for three phase AC working. At the outset, a set of performance indices to be used in the assessment of the designs is prescribed and defined. Several possible designs are proposed, examined and compared for merits and drawbacks. The schemes reported in this chapter are based primarily on the wound-field configurations, but the principal conclusions are deemed to be the same as for PM-excited configurations.

4.1 Introduction

There are advantages for employing machine arrangements with more than one phase, some of them known since inception of polyphase AC machines and other asserted during the development of modern torque control techniques for AC machines and new requirements of attributes of machines. Below is a listing of the some of the known advantages.

- ***Utilisation of airgap periphery***. It has been known since the development of early polyphase AC machines [165], [166] that utilisation of the airgap periphery is enhanced with increase of the number of phases employed in the machine, even though there is a limit, set by the trend of diminishing returns. On this aspect, polyphase arrangements on three phases appear to be widely applied.

- ***Torque pulsations***. An increased number of phases in an arrangement has the effect of reducing the torque pulsations [167]-[170]. This is easily evident in machines where torque is produced in strokes, such as the SRM. As such, it justifies the consideration of configurations starting from the 6/4 topology in SRMs, if the application is known to be sensitive to torque ripple [171].

- ***Converter rating***. The rating of the power converter per phase is lower for poly-phase than single-phase arrangements. As with utilisation of the airgap periphery, the law of diminishing returns is prominently applicable with power converters, as a high number of phases is associated with increased number of switches and complexity of control.

- ***Fault tolerance***. The redundancy afforded by a presentation of more than one phase is an attribute of fault tolerance. Polyphase arrangements are routinely employed to enhance fault tolerance, as introduced in chapter 1.

- ***Direct torque control***. In AC machine control, direct torque control is known to be improved due to an increase of the number voltage vectors to be applied for arrangements with number of phases exceeding three, in so-called multiphase machines [172], [173].

The wound-field single-phase FSM employing a segmental rotor in [123] presents substantial fluctuation of DC field current, reported at twice the electrical frequency and interfering with DC current control. This result is consistent with the effect of the coupling of the armature circuits carrying sinusoidal currents with the field circuit carrying DC current. Three phase AC armature circuits are, in principle, expected to produce a null coupling effect in the field circuit. Three phase arrangements of FSM with a segmental rotor may therefore give a presentation that eliminates the fluctuation of the DC field current in wound-field configurations.

4.2 Performance Indices

In order to make a performance evaluation and comparisons, a set of quantifiable parameters is introduced. The approach followed is to examine combinations of the number of stator teeth and rotor segments for producing three phase armature flux linkages. A stator in standard presentation [174] for holding concentrated single tooth windings is considered. This allows the segment span to be the main variable parameter across the segment pitch in the design process. The merits of the designs are appraised on the basis of the following parameters:

- torque capability
- peak armature flux linkage
- RMS value of the phase induced EMF
- level of distortion of the induced phase EMF
- torque ripple

These parameters influence performance in ways described below.

Torque Capability

For a general electrical machine, torque capability is derived from the torque output equation [175], the torque produced at specified dimensions of a machine's physical dimensions and loading conditions. The torque per unit rotor volume T_{rv} is controlled in a direct manner by the functional electrical loading A and magnetic loading $B_{g\max}$ as given by

$$T_{rv} = k_m A B_{g\max} \tag{4.1}$$

where k_m is a machine constant and embodies the physical dimensions of the machines and the excitation pattern. If the dimensions of the machine are fixed, the torque capability can be evaluated at different magnetic and electric loading conditions, alongside their susceptibility to machine topology and design parameters.

Peak Armature Flux Linkage

The armature flux linkage is directly affected by the magnetic loading. It has already been mentioned that the magnetic loading affects the torque per unit volume in direct proportion, and therefore the peak armature flux linkages, a parameter which can be predicted from simulations, forms a reliable part of the performance assessment indices. If the slot space and winding turns are defined and specified, the armature flux linkage can be a functional measure of performance.

Induced EMF

At specified speed, the power output of an electrical machine is proportional to the EMF in the armature winding. The induced EMF in the armature winding at specified speed and magnetic loading can thus be reliably be used as a performance index.

Waveform Distortion

For AC machines, the sinusoidal waveform is the ideal shape. Drive schemes implementing sinusoidal current control are presently pervasive. When supplied with an AC sinusoidal current, an AC machine develops power with the fundamental of the AC EMF. In this arrangement, the harmonic components of the EMF are associated with undesirable effects. Total harmonic distortion (THD) is a standard measure of the distortion of the waveform from the ideal sinusoidal waveform. The definition adopted in this investigation is given by [176]

$$THD = 100\% \times \frac{\sqrt{E_a^2 - E_{a\_1}^2}}{E_{a\_1}} \tag{4.2}$$

where E_a is the rms value of the EMF and E_{a_1} is the rms value of the fundamental component of the EMF.

Torque Ripple

By adopting concentrated single-tooth winding arrangements, there is a likelihood of torque pulsations. This is generally an undesirable outcome as it produces vibrations

and acoustic noise. It is commonly quantified as torque ripple, T_{ripple}. There are several definitions of torque ripple but in this evaluation the computationally efficient form, described in [177], is generally adopted, and is defined as

$$T_{ripple} = 100\% \times \frac{T_{\max} - T_{\min}}{T_{\max}} \tag{4.3}$$

where $T_{\max}$ and $T_{\min}$ are the maximum and minimum torques, respectively. It is sometimes desirable to apply the other definition of torque ripple expressed as

$$T_{ripple} = 100\% \times \frac{T_{\max} - T_{\min}}{T_{mean}} \tag{4.4}$$

where T_{mean}, is the average torque. Where this is done, it is explicitly stated.

In choosing the desirable attributes, the optimisation function is to maximise the torque capability, peak flux linkage, and induced EMF, whilst minimising the EMF waveform distortion and torque ripple.

4.3 Feasible Topologies

The fundamental principle of the flux switching scheme using rotor segments has been explained in the previous chapter. For its implementation, there is a requirement for the positions of the armature teeth to alternate in series with the position of the field teeth. A further requirement is for the polarity of one field tooth to be opposite that of the next field tooth. Following these tenets, it is seen that the minimum number of teeth on the stator for single-phase arrangements is 4. It might appear that 6 is the minimum number of teeth for basic three-phase arrangements, but this is not the case. Three of the six teeth are to be deployed as armature teeth for the three phases, leaving three teeth which can not form alternate pairs of field teeth. Therefore, under this restriction, the plausible minimum number of teeth for three phase AC arrangements is 12, and other configurations may be built in multiples of 12, as in 24, 36, etc. The primary investigation therefore considers a 12-tooth stator which may allow for two sets of three phase windings.

The deployment of the field and armature teeth on a 12-tooth stator, implementing the flux switching principle by means of a segmental rotor, is shown in figure 4.1. Six of

the twelve stator teeth, F1 to F6, are wound as field coils and excited with DC current. These field coils produce three N poles interspersed between three S poles. The remaining six stator teeth, A1, A2, B1, B2, C1, and C2, contain six armature coils. As the rotor rotates the displacement of segments causes a switch of the armature tooth flux so that flux alternates up and down these six teeth. Each time the rotor rotates through one segment pitch, the flux linking the armature coils goes through a complete cycle. If N_{seg} is the number of segments on the rotor, the frequency ω of the AC EMF induced in the armature is

$$\omega = N_{seg}\omega_r \tag{4.5}$$

where ω_r is the angular speed of rotation.

Adjacent armature coils are displaced 60 mechanical degrees apart, corresponding to $60N_{seg}$ electrical degrees, and so the flux linkages or induced EMF in the stator armature adopt this angle of separation in electrical degrees.

For effective implementation of the flux switching principle using rotor segments as

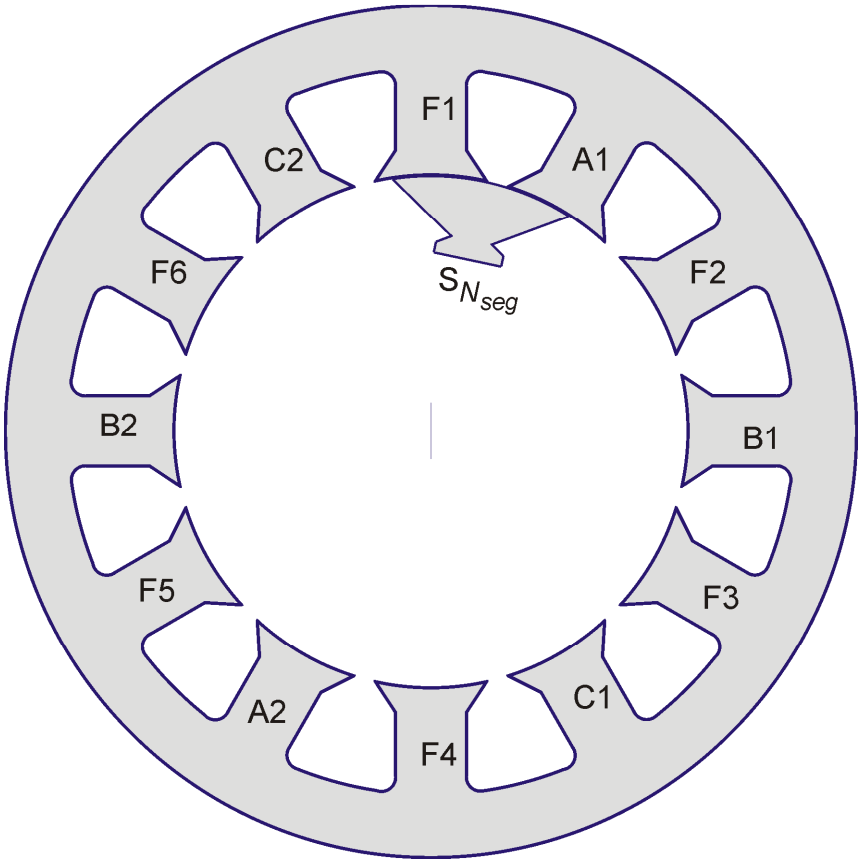

Fig.4.1. Deployment of field and armature teeth.

described in the previous chapter, it is desirable to limit the number of segments on the rotor to less than the number of stator teeth. With a 12-tooth stator, it is apparent that any number of rotor segments from 1 to 11 may produce three phase AC working, except for 3, 6 and 9, which result in single phase AC working. Table 4.1 presents the results for all segments.

Topologies of apparent practical significance on a 12-tooth stator start from 4 segments. Although there is an anticipated unbalanced magnetic force (UMF) for topologies with an odd number of segments, topologies with 5, 7 and 11 segments warrant an examination as they may naturally transpose into even-number segments on a 24-tooth stator, as in 24/10 for 12/5 and 24/14 for 12/7 configurations.

Table 4.1. Segment and phase relations

No. of segments, N_{seg}	**Phase separation, $60°\times N_{seg}$ [° electrical]**	**Equivalent phase separation [° electrical]**	**No. of phases**	**3-phase sequence**
1	60	60	6	A, C, B
2	120	120	3	A, B, C
3	180	180	1	—
4	240	120	3	A, -B, C
5	300	60	6	A, C, B
6	360	0	2	—
7	420	-60	6	A, B, C
8	480	-120	3	A, C, -B
9	540	-180	1	—
10	600	120	3	A, -B, C
11	660	60	6	A, C, B
12	720	0	2	—

4.4 Design Parameters

The basic dimensions for the designs are sized within the capacity of the in-house manufacturing equipment which can produce stator laminations up to an outside diameter of 200 mm. The philosophy for a fair comparison of the topologies is to keep the similar dimensions on all topologies the same, except those which may define and differentiate the topology. As the number of rotor segments is used to characterise a topology, dimensions of the segment on the rotor are deemed variable while all other dimensions are fixed and are common to all topologies.

4.4.1 Common parameters

Starting with a choice of a stator with a prescribed outside diameter, the common dimensions are chosen and derived by the approximation using linear magnetic circuit approach and exemplified as in appendix A3. In this investigation, the terms and parameters, constructed from the denotations of the more detailed scheme in figure 4.2, are defined as follows.

a) ***stator tooth pitch, θ_{tp} and rotor segment pitch, θ_{sp}***. The pitch of the rotor segment and the stator tooth, respectively.

b) ***stator tooth span, θ_{ts} and rotor segment span, θ_{seg}***. The span of the stator tooth and the rotor segment, respectively.

c) ***number of stator teeth, N_{st} and number of rotor segments, N_{seg}***. The number of stator teeth and rotor segments, respectively.

d) ***angle of full segment alignment, θ_{align}***. The angle measured for a segment to exactly overlap two stator segments. It is equivalent to the span of two stator teeth and one slot span, thus

$$\theta_{align} = 2\theta_{ts} + \theta_{slot} \tag{4.6}$$

e) ***angle of segment separation, θ_{sep}***. The angular span of the space between two adjacent rotor segments. It is also known as the span of the rotor slot, if the rotor segment separation is considered as a slot, and is expressed as

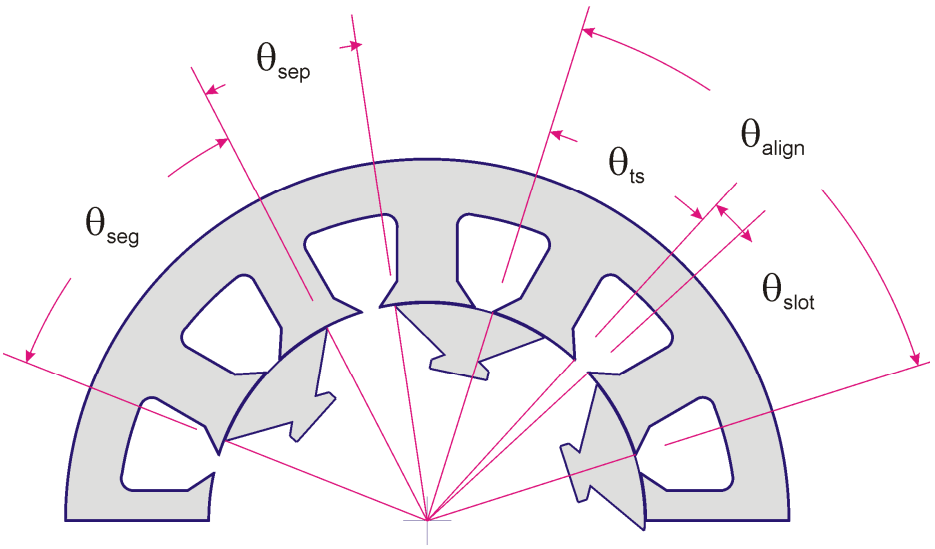

Figure 4.2. Definition of stator and rotor parameters.

$$\theta_{sep} = \frac{360^\circ - N_{seg}\theta_{seg}}{N_{seg}} = \frac{360^\circ}{N_{seg}} - \theta_{seg} = \theta_{sp} - \theta_{seg} \tag{4.7}$$

A summary of the common dimensions applied for modelling is shown in Table 4.2.

Table 4.2. Common dimensions for modelling

Stator outside diameter	150 mm
Stator yoke depth	11 mm
Stator tooth width	12.5 mm
Span of stator tooth tip	25^o
Span of slot opening	5^o
Rotor diameter	90 mm
Core axial length	150 mm
Air-gap length	0.3 mm
Number of turns per field tooth coil	44
Number of turns per armature tooth coil	44

4.4.2 Variable parameters

Of the possible dimensions on the rotor segment, the segment span is the principal variable in the optimisation of the rotor design for each topology. The segment depth for a particular topology may be adjusted only as deep as it is required to avoid magnetic saturation of the segment, but matched to the saturation level of the stator field teeth. A particular topology is defined by the number of segments, which in turn prescribes the segment pitch. For that topology, the maximum segment span is limited by the segment pitch.

Since there are as many presentations of segment pitches as there are topologies, a preliminary study of the predisposed ability of a topology to be influenced by the segment span is necessary. Two new parameters, which are the utilisation factors of the rotor space, peculiar to the principle of switching flux by means of rotor segments, may be defined as follows.

a) ***segment pitch utilisation factor, k_p***. The ratio of the segment pitch to the angle of full segment alignment, expressed as

$$k_p = \frac{\theta_{sp}}{\theta_{align}} \tag{4.8}$$

It is a factor to measure how a choice of the number of segments affects the relative ability to vary the segment span, both below and above the full segment alignment span. This factor returns a value less than 1 for segment spans which are below the angle of full segment alignment and returns a value greater than 1 for those above this angle, thus defining the range of segment spans which exceed the angle of full segment alignment.

b) ***segment span utilisation factor, k_s***. This is the ratio of the maximum permitted segment span to the angle of full segment alignment. It is expressed as

$$k_s = \frac{\theta_{seg-\max}}{\theta_{align}} \tag{4.9}$$

When the segment span matches the angle of full segment alignment, a value of 1 is returned, indicating 100% compliance with the principle of flux switching by means of a segmental rotor, and may therefore be viewed as a compliance factor. To have meaningful use of the compliance factor, the numerator $\theta_{seg\text{-max}}$ is set to the value of θ_{align} if the topology has the ability to exceed θ_{align}.

Figure 4.3 shows the values of k_p and k_s for the 12-tooth and 24-tooth stator, as the number of rotor segments is changed for a specified θ_{sep} of 4° (mechanical). The

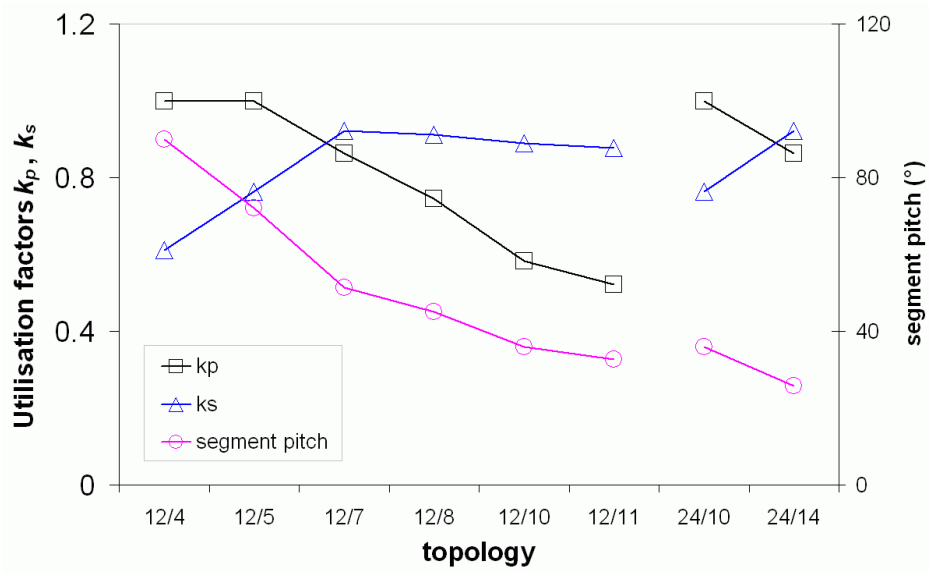

Figure 4.3. Rotor utilisation factors on various topologies.

segment pitch utilisation factor, k_p varies inversely with the number of segments on both the 12-tooth and 24-tooth stator, closely following the trend presented by the segment pitch against the number of segments. The trend is broken with the 4-segment and 5-segment rotor on the 12-tooth stator, because these configurations have the capacity for the segment pitch to exceed the angle of full segment alignment. The 12/4-configuration has the highest segment pitch utilisation factor on the 12-tooth stator while the 24/14-configuration has the highest segment pitch utilisation factor on the 24-tooth stator. The 12/11-configuration presents the lowest segment pitch utilisation factor on the 12-tooth stator. On the 24-tooth stator, the segment pitch utilisation factor is better for the 10-segment rotor than for the 14-segment rotor.

On a 12-tooth stator, the segment span utilisation factor k_s is lowest with the 4-segment rotor at 0.61 and highest with 7-segment rotor at 0.92. As a general trend the 12-tooth stator presents relatively low values of k_s if the number of segments is less than 7, but k_s hovers at relatively high values for configurations from 7 segments. On the 24-tooth stator the 14-segment rotor has a higher value of k_s than the 10-segment rotor and definitely higher than all rotor configurations on the 12-tooth stator.

Based on this preliminary investigation of applying utilisation factors k_p and k_s, it appears that the 12/7 topology gives the best mix of attributes for a three phase flux switching scheme employing a segmental rotor on a 12-tooth stator. For the 24-tooth stator, the 24/14 topology is a better configuration than the 24/10 topology, combining relatively high values of both k_p and k_s.

4.5 Modelling and Simulation

The electromagnetic behaviour of the machines of different topologies and various design specifications is predicted from machine models and simulations performed using a commercial finite element analysis package.

4.5.1 Modelling

2D models of the machines are prepared and extruded in the axial direction. The adoption of this method obviously neglects the end-winding effects, including the actual conductor material presented by the end-windings. Additionally the model ignores the effects in the casing and external airspace by limiting the external airspace boundary to

the radius of the stator. This model proves to be adequate for the electromagnetic parameters being examined, and produces results in reasonable time on a desktop computer with a 3-GHz processor and 2.5 GB RAM, ranging between 20 minutes and 2 hours for a simulation of a rotation of one segment pitch in steps of 1° mechanical.

4.5.2 Simulations

Two simulation methods were used to obtain the electromagnetic quantities of interest. In the first method, static electromagnetic fields quantities are obtained at specified electromagnetic conditions by invoking the static field solver. With a parameterization facility to automatically change the position of the components in the model, whilst maintaining the specified electromagnetic conditions, field solutions could be obtained for various rotor positions. Using this method the output electromagnetic quantity of interest is the flux linkage information in the stator coils. In the second method, the motion of the rotor is directly simulated by a time-stepping approach using the 'transient-with-motion' solver. With this simulation method, the relevant electromagnetic quantities are the voltages in the coils, forces and torques on the model components.

Among the electromagnetic quantities listed for evaluation, it is seen that only flux linkages can be deemed to be directly presented from the field solutions of FE analysis. The voltage on the coils is a quantity derived from the flux linkages, whilst the force or torque is calculated from the flux density by the "Maxwell stress" concept, within the FEA package.

4.6 Electromagnetic Evaluation of the Topologies

The eight feasible topologies evaluated in this investigation are shown in figure 4.4, together with the corresponding multi-phase flux linkages. For each topology configuration shown in the figure, the excitation is arranged to have constant current density in the field winding, at a current of 14 A.

The armature tooth flux linkages alternate between equal positive and negative peaks, loading the armature tooth in a true bipolar mode. The flux linkage waveforms for the six armature tooth windings may initially be construed as a set of six phases. By grouping the armature tooth flux linkages labelled A, B and C, in pairs for the 12-tooth

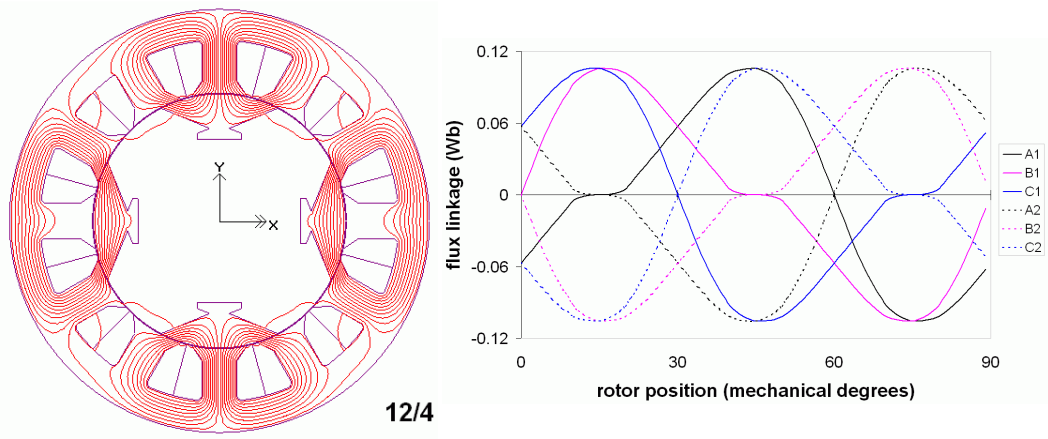

(a) 12/4 topology

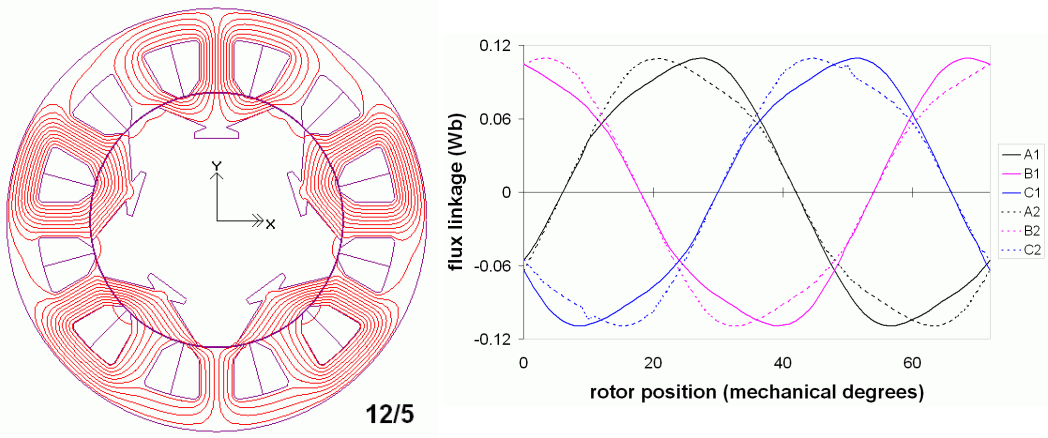

(b) 12/5 topology

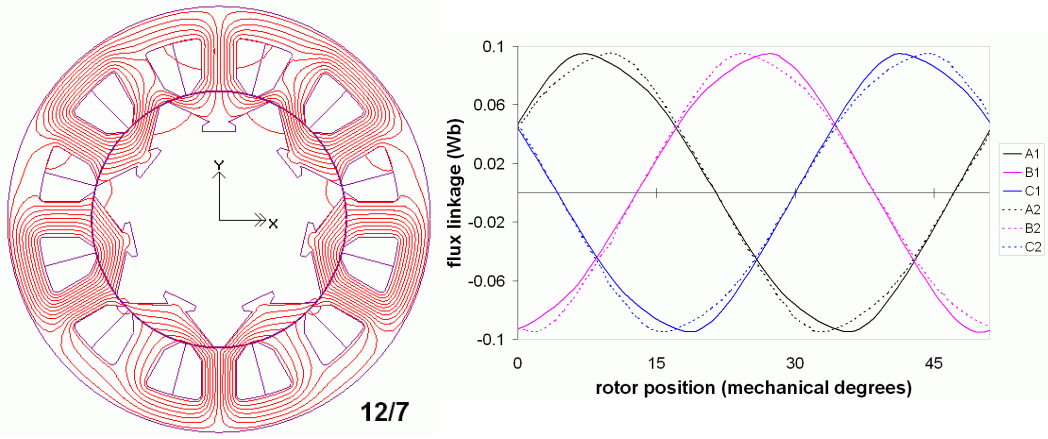

(c) 12/7 topology

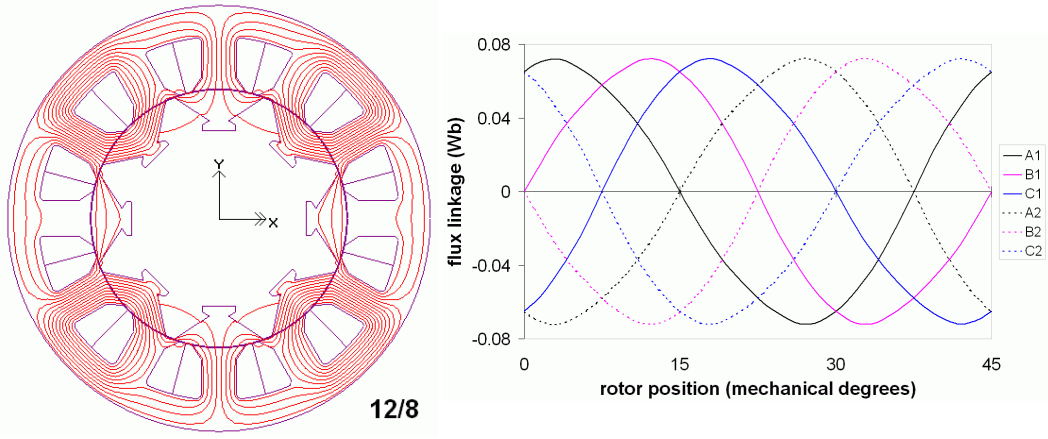

(d) 12/8 topology

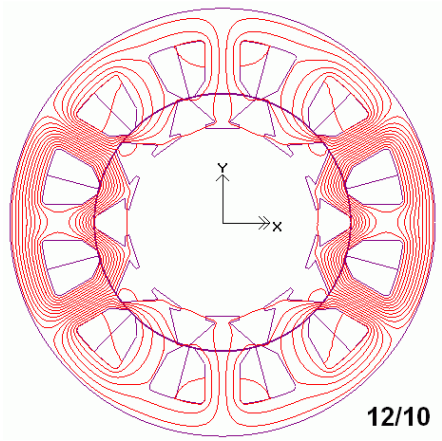

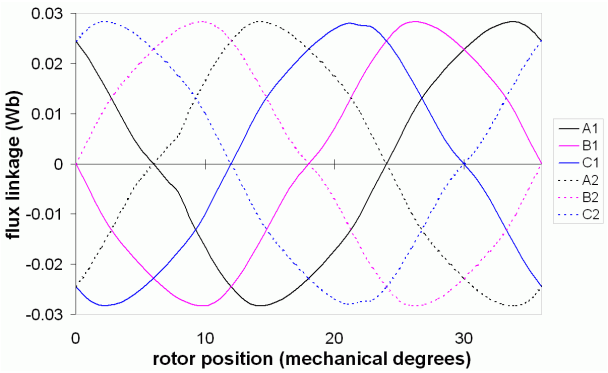

(e) 12/10 topology

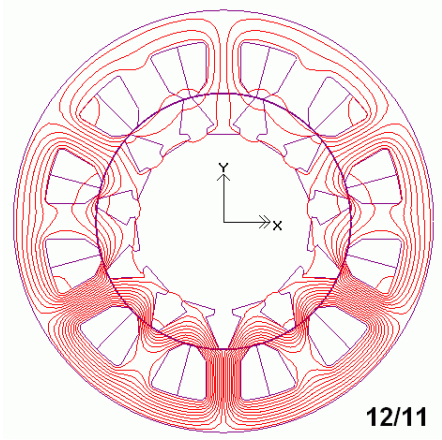

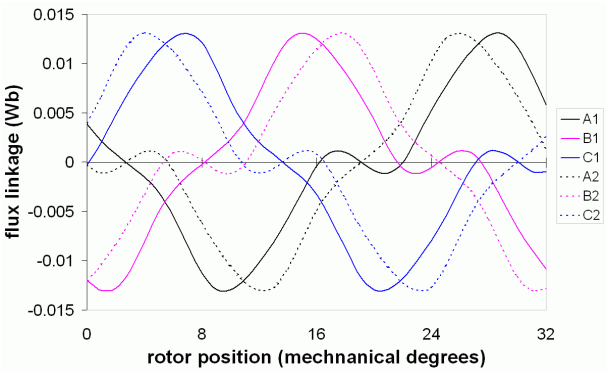

(f) 12/11 topology

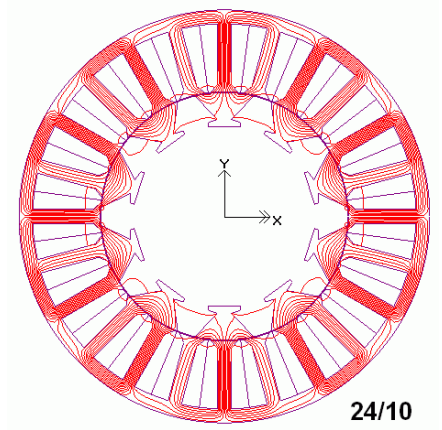

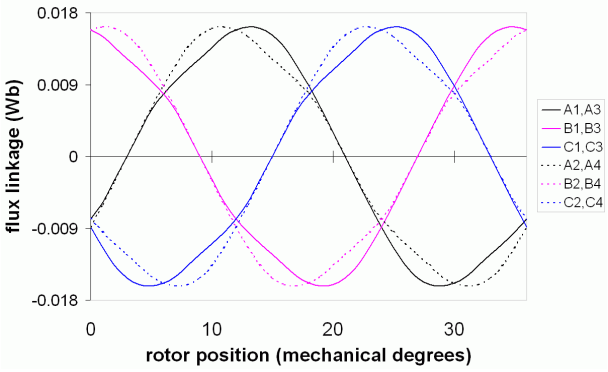

(g) 24/10 topology

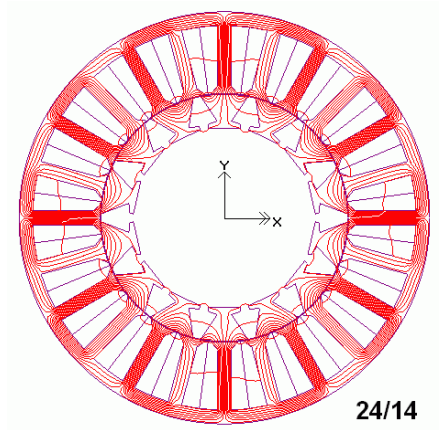

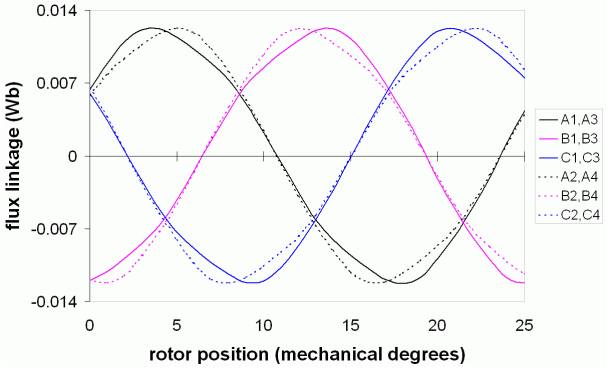

(h) 24/14 topology

Figure 4.4. Flux distribution and phase flux linkages against rotor position, with field excitation only at rated value and at a segment span which gives maximum armature peak flux linkage.

stator or in sets of four for the 24-tooth stator, a three phase system is constructed. In the 12/4, 12/8 and 12/10 topologies, the phase relationship between the tooth windings of a complementary pair is 180°. The approach taken is to construct each phase of the three phase system on the stator by connecting pairs or sets of complimentary armature tooth windings in cumulative-series.

In the following sections the electromagnetic characteristics of each topology are examined with variation of the segment span at rated field tooth flux density. Additionally, the characteristics of the topologies are compared against each other.

4.6.1 Peak armature flux Linkage

The peak flux linkages tend to increase with the segment span until the full teeth-segment alignment span is reached, equivalent to the span of two stator teeth and one slot-opening. The full teeth-segment alignment span as designed is 55° for the 12-tooth stator and 27.5° for the 24-tooth stator. Figure 4.5 shows the influence on the peak armature flux linkage of the segment span, normalised on the base of the segment pitch for each topology.

The highest armature peak flux linkage is obtained with the 12/4 topology at 0.21 Wb when the segment span is about 55°. The 12/5 topology can achieve 98% of this flux linkage at the same segment span, and this is maintained when the segment span exceeds 55°. At differently specified segment spans, close to the maximum permitted within the segment, the 12/7 and 12/8 topologies achieve about 88% and 71% of peak

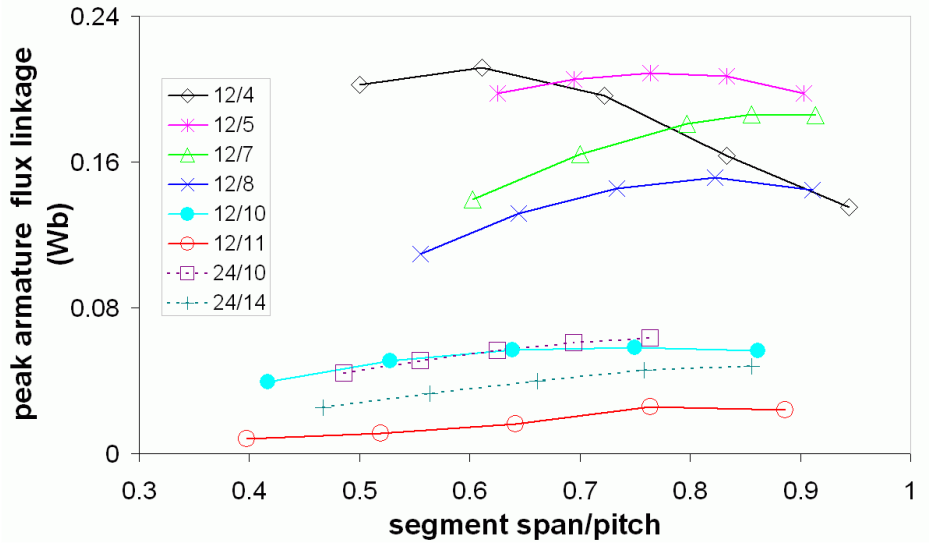

Figure 4.5. Armature peak flux linkage per phase.

flux linkages achieved in the 12/4 topology, respectively. The other topologies give achievable peak flux linkages in the range which is less than 30% of what is obtained with the 12/4 topology.

The results of low peak flux linkages are expected for topologies on the 24-tooth stator because the increased number of stator teeth causes a reduction in the level of field excitation when the total slot space is maintained. It seems remarkable that the topologies with 10 and 11 segments on a 12-tooth stator have similarly low flux linkages. With increased number of segments the maximum limit of the segment span remains further from the angle of full segment alignment. As the principles prescribe that optimal flux linkages are obtained when the segment span is equal to the angle of full-segment alignment segment, topologies with maximum permitted spans which substantially depart from this are expected to have a significant fall in performance. In the case of the 10- and 11-segment rotors, the maximum permitted segment span are 32° and 29°, respectively, corresponding to a compliance of 52 to 58% of the angle of full alignment span.

If there are fewer than seven segments on the rotor the segment pitch permits the segment span to be extended beyond 55°. Beyond this barrier there is likelihood of cross-coupling of flux in the phases, and the peak flux linkage falls with increasing segment span, as observed in the 12/4 and 12/5 topologies.

4.6.2 Induced armature rms EMF

The bipolar flux linkages in the armature coils produce induced EMF at the winding terminals. To a large extent, the variation of the rms value of the phase EMF with segment span, shown in Fig. 4.6, is similar to the variation of the peak armature flux linkages. On the 12-tooth stator, the 7-segment rotor gives the highest induced phase EMF of 49.1 V at a segment span of between 44° and 48°, followed by the 8-segment rotor at 44.6 V with a segment span of between 37° and 41°. Although the 4-segment rotor has the highest peak armature flux linkages, it produces a modest 70 % of the phase EMF produced by the 7-segment rotor at the same speed. This is a curious result at first glance, but on recalling that EMF is derived from the rate of change of flux linkages, it becomes apparent that, at similar speed, the change in flux linkages for a rotor with smaller segment pitch is more than for a rotor with a larger segment pitch. The 5-segment rotor can achieve a maximum possible phase EMF which is about 80%

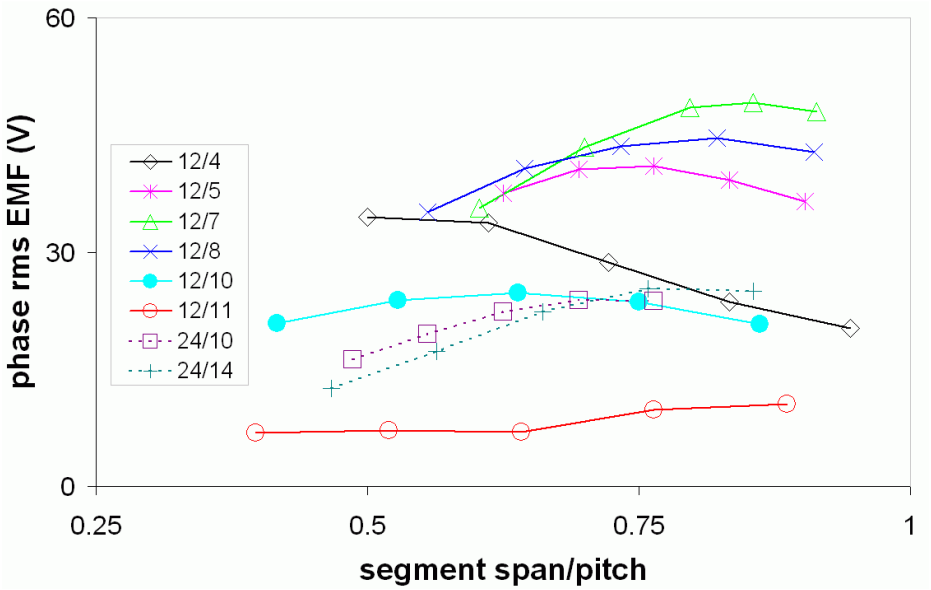

Figure 4.6. Induced rms EMF per phase.

of that achieved by the 7-segment rotor, while the 10- and 11-segment rotors achieve significantly lower values of the maximum possible EMF, at the less than 50% of what can be achieved by the 7-segment rotor.

For the 24-tooth stator, it is seen that both the 10-segment and 14-segment rotor can produce higher phase EMF than the 10 and 11-segment rotor on the 12-tooth stator. Between the two rotor topologies on the 24-tooth stator, the 14-segment rotor presents a slight edge over the 10-segment rotor.

4.6.3 EMF waveform distortion

The waveforms of the induced EMF for both phase and line quantities, as shown in figure 4.7 for maximum segment spans which give the maximum possible phase EMF at the same current density in the field winding, indicate a perceptible distortion from the ideal sinusoidal shape. Additionally, there is a lack of parity in the alternations of the phase EMF waveforms for the tooth windings for all topologies. This is clearly pure AC, with no DC component, and where there is a discrepancy in the amplitudes of the alternation this is compensated for by a corresponding discrepancy in the duration of the alternation, thereby maintaining equal areas under the EMF-time graph for the alternations.

However, if the phase EMF is considered, the lack of parity in the alternations of the resultant waveform is apparent only for topologies with even-numbered rotor segments on the 12-tooth stator. This is because the complementary tooth windings produce

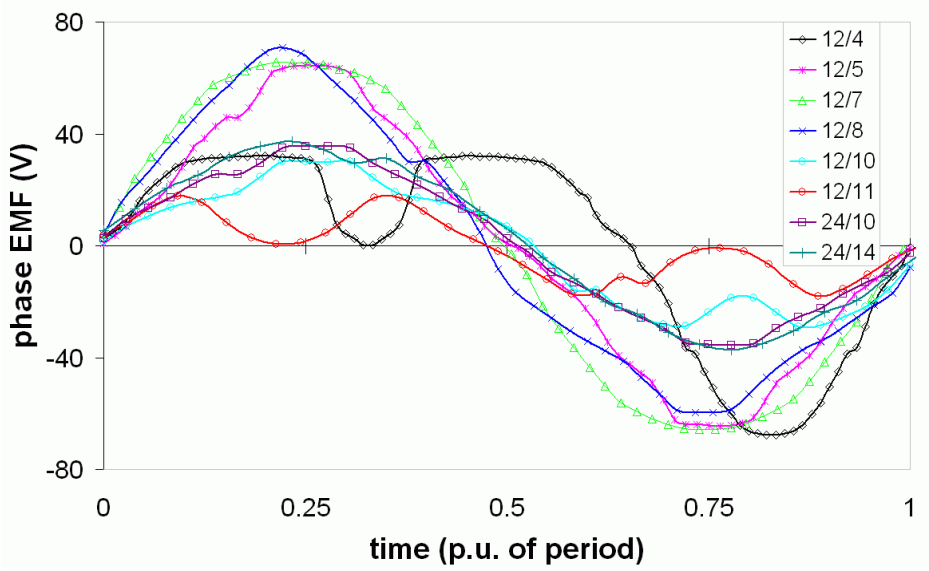

(a) phase EMF

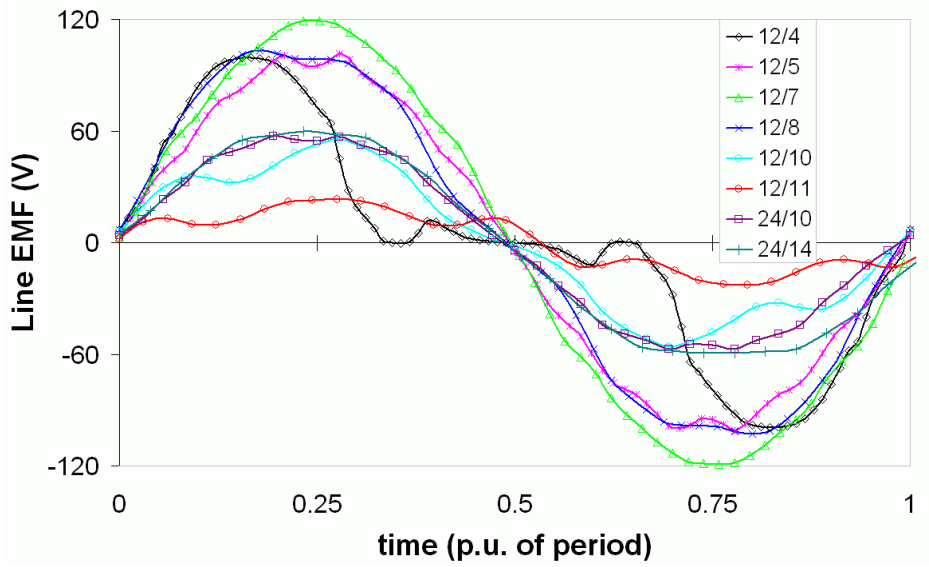

(b) line EMF

Fig. 4.7. Waveforms of induced EMF at 500 r/min in one period.

alternations which are identical on the time axis and are reproduced exactly in the series connection of forming a phase for topologies with even numbered rotor topologies. The case with odd-numbered rotor segments is different, as the complementary tooth winding produces alternations which interchange in shape on the time axis, resulting in a symmetrical phase EMF in the series connection. This is also the situation with the 10-and 14-segment rotor implemented on the 24-tooth rotor, where a phase comprises two pairs of complementary windings. Though the EMF waveforms of a pair of complementary winding are identical, the two pairs of complementary windings have alternations which interchange shapes on the time axis.

A scrutiny of the EMF waveform distortion in quantified form for both phase and line quantities are shown in figure 4.8. Waveform distortion appears to decrease with increase of segment span for topologies with even-numbered rotor segments on the 12-tooth rotor, with the lowest value of THD being with the 12/8 topology at 13 % on phase quantities. Of the odd-numbered rotor segment topologies, the variation of the phase THD of with segment span for the 11-segment rotor defies a simple characterisation but can be said to fluctuate at a high value of between 64% and 87%. The 5-segment and 7-segment rotors present low values of phase THD at less 17 % and less than 8%, respectively, and this trend is replicated even with line quantities.

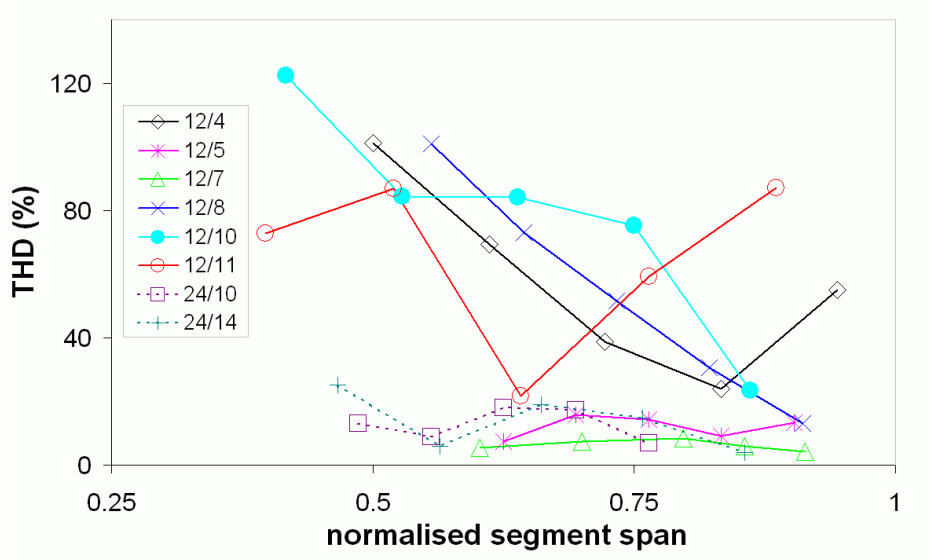

(a) phase EMF at various segment spans

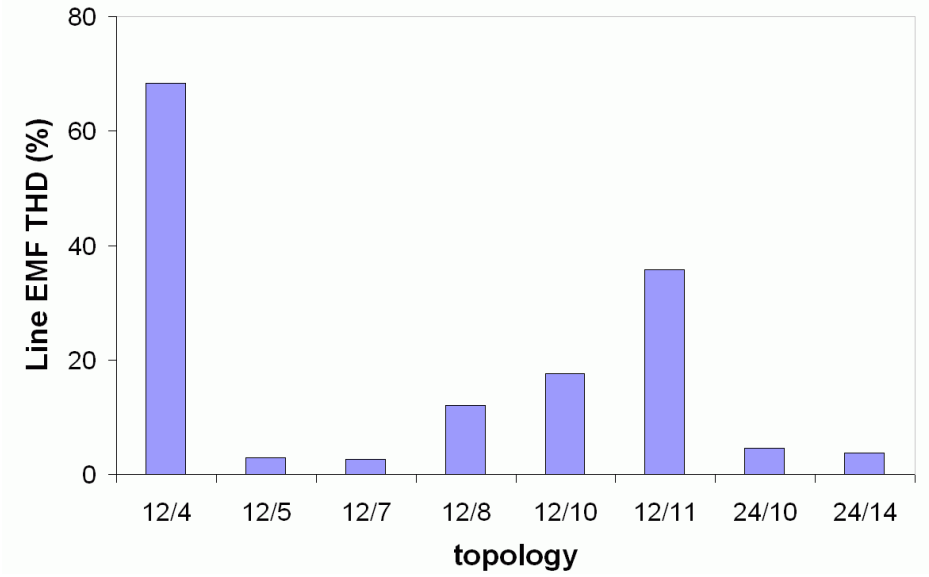

(b) line EMF at optimum at segment span for maximum EMF

Figure 4.8. THD of the EMF for various topologies.

On the 24-tooth stator, both the 10-segment and 14-segment rotors present phase THD which fluctuates with segment spans, but the fluctuation is limited to THD of between 6 and 25%.

Of all the topologies considered, the 12/7-topology presents the lowest phase and line THD, at about 4% phase THD when the segment span is 47°, and a corresponding line THD of 2.6%.

4.6.4 Electromagnetic torque

The armature flux linkages and induced EMF evaluated in the preceding sections are components of the magnetic loading. Since torque is proportional to the magnetic and electric loading, a segment span in each topology which produces the largest value of armature peak flux linkage and induced EMF is selected for comparison of the electromagnetic torque among the topologies. The control regime adopted in the simulations is one with constant speed, with sinusoidal currents in the armature windings placed in phase with the back-EMF.

As in similar machine topologies with double saliency and concentrated windings the FSM topologies are expected to present fluctuations of torque with time [177], as seen in torque waveforms of figure 4.9. This fluctuation of torque, technically known as torque ripple, is due to one or a combination of the following two main causes [178]:

- the interaction of the spatial and time harmonics between the magnetic field

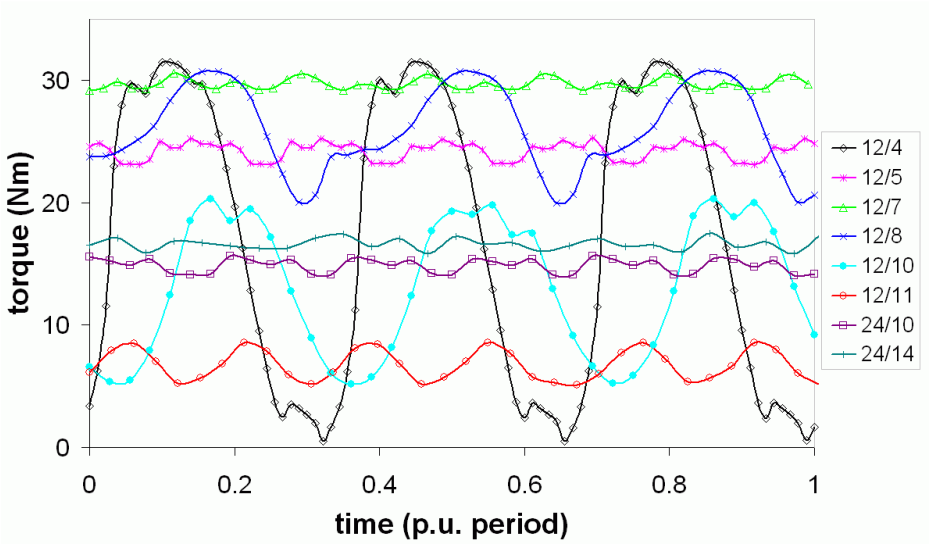

Figure 4.9. Torque waveforms for various topologies at rated load conditions, with DC field current and sinusoidal armature current.

produced by the field winding or PM and the magnetic field produced by the armature winding. Even when a sinusoidal current is supplied to the armature winding, the MMF produced is not a pure sinusoid because the slotting causes a concentration of MMF in space, and the resulting MMF has space harmonics. Similarly, the EMF induced in the armature winding by the field excitation as the rotor rotates is not sinusoidal because the excitation flux has spatial harmonics, seen as rotating at the same speed and direction as the rotor mechanical motion. Both these two effects are significant in the FSM topologies.

- the variation of the reluctance seen by the armature phase winding and the exciting field winding or permanent magnet, in the permanent magnet excited machines. The FSM topologies presents substantial variation of reluctance as seen by the armature and field winding as the rotor rotates, signified by the change from the aligned to unaligned positions of the rotor segments. In geometric terms, this effect is pronounced by slotting and the gaps separating the segments. When the armature is not energised this torque ripple still exists due the variation of the reluctance seen by the field winding or PM, and is generally known as cogging torque.

There is strong suggestion that both the two types of effects described above are making a significant contribution to the torque ripple, as the back-EMF has substantial harmonics and there is notable slotting on the stator accompanied by a presentation of isolated segments on the rotor.

The electromagnetic torque, T_e developed in an electrical machine generally consists of a reluctance torque component, T_{rel} and an excitation torque component, T_{exc},, and may be expressed in a polyphase arrangement as [179]

$$\begin{aligned} T_e &= \sum_k T_{\text{rel},k} + \sum_k T_{\text{exc},k} \\ &= \frac{1}{2}\sum_k i_k^2 \frac{dL_k}{d\theta} + \sum_k i_k \frac{d\psi_{exc}}{d\theta} \end{aligned} \tag{4.10}$$

where L_k is the phase winding inductance, ψ_{exc} is the flux linkage due to field excitation, i_k is the phase current, θ is the electrical angular position of the rotor and $k = a, b, c$ is the phase designation. As the operation of the FSM with sinusoidal current is with the current placed in phase with the back-EMF, the principal torque is due to T_{exc} and the contribution of T_{rel} is negligible, so that T_e can be expressed as

$$T_e = \frac{P_i(t)}{\omega_r} = \frac{\sum_k e_k(t) i_k(t)}{\omega_r} \approx \sum_k T_{\text{exc},k} \tag{4.11}$$

with P_i being the instantaneous power, ω_r the rotational speed and e_k the phase back-EMF.

Although the current, i_k is prescribed and supplied as sinusoidal, it has been seen that the back-EMF, e_k of the FSM in all topologies has significant harmonics, indicative of existence of spatial excitation flux harmonics. Thus, P_i and the resulting torque are subject to fluctuations of the first type, as observed in the overall effect in figure 4.9.

The second contribution to torque pulsations, attributed to cogging torque, has been a subject of recent investigations [180]-[182], in the pursuit of methods of minimising torque ripple in various configurations of electrical machines. A simple analytical model proposed in [182], [183] may be applied to characterise and define the nature and contribution of the cogging torque to the torque ripple of an electrical machine, based on the configurations of the stator teeth (or slots) and the rotor poles. Applying this approach, the cogging torque, T_{cog} may be described by a general Fourier series expansion for the FSM employing segmental rotors as

$$T_{\text{cog}}(\theta_r) = \sum_{h=1}^{\infty} T_h \sin(hN_{st}\theta_r + \varphi_h) \tag{4.12}$$

where N_{st} is the number of stator teeth, T_h and φ_h are the Fourier coefficients for the harmonic cogging torque magnitude and phase, respectively.

The number of periods, N_p of the cogging torque waveform over a rotation of one stator tooth pitch is given by

$$N_p = \frac{N_{seg}}{\text{HCF}\{N_{st}, N_{seg}\}} \tag{4.13}$$

where the denominator is defined as the highest common factor (HCF) between N_{st} and N_{seg}, and N_{seg} being the number of segments on the rotor as defined in chapter 3. Using the index N_p, the electrical angle of rotation, α_{cog} for each period of the cogging torque and the number of periods of cogging torque, N_e per electrical cycle are therefore

$$\alpha_{\text{cog}} = \frac{360^{\circ}}{N_p N_{st}} \tag{4.14}$$

and

$$N_e = \frac{N_p N_{st}}{N_{seg}} \tag{4.14}$$

respectively.

For the waveforms of the cogging torque obtained by the FE modelling for the topologies of the FSM considered, these parameters are shown in Table 4.3.

Interpreted according to the simplified model in [183], the quantity N_p is a useful index that indicates the relative phase angle alignment of the two types of elementary cogging torques, of which the cogging torque is composed. The superposition effect of the two types of elementary cogging torque produces two distinct results on the resultant cogging torque: a cumulative effect which amplifies the resulting torque and a spreading out effect which diminishes the resultant cogging torque. The first kind is associated with a low value of N_p and is indicative of the elementary torques tending towards being in phase, whilst a high value indicates the elementary torques leaning towards being out of phase.

Table 4.3. Cogging torque parameters for the considered topologies.

	Topology	**HCF(N_{st}, N_{seg})**	**N_p**	**N_p classification**	**α_{cog} [°]**	**Number of periods / elec. cycle**
even	12/4	4	1	low	30	3
	12/8	4	2	low	15	3
	12/10	2	5	high	6	12
	24/10	2	5	high	3	12
	24/14	2	7	high	2.1	12
odd	12/5	1	5	high	6	12
	12/7	1	7	high	4.3	12
	12/11	1	11	high	2.7	12

An examination of the results of the N_p index, shown in table 4.3, reveals that the 12/4 and 12/8 configurations have relatively low values of N_p, at 1 and 2, respectively, and are therefore expected to show high magnitudes of cogging torque. The remaining configurations in the table are identified with high indices of N_p, with the 12/11

configuration having the highest N_p at 11, and therefore expected to give the lowest cogging torque. The 12/7 and 24/7 configurations are expected to present the next lowest cogging torques for having N_p of 7, followed by the 12/5 and 24/10 configurations for having N_p of 5.

A harmonic decomposition of the cogging torques waveforms of figure 4.10, shown in figures 4.11- 4.13 are in agreement with the predictions produced by using the N_p index. The cogging torque is manifested as an integer multiple of triplen harmonics. From the predictions of table 4.3, while examining α_{cog}, all the topologies with an even number of segments on the 12-tooth stator are expected to have significant first order triplen harmonics, while the topologies with odd-number of segments on the 12-tooth stator and all topologies considered on the 24-tooth stator are expected to show prominent 4th order triplen harmonics. These further predictions, using N_e and α_{cog}, are confirmed by the harmonic spectra for the FE predictions results in figures 4.11-4.13. A comparison of the contribution of the cogging torque, in relation to the peak torque, is made in figure 4.14, where is it verified that the severest effect is in 12/4 topology.

In most cases, torque pulsations are undesirable and designs of high performance electrical machines apply techniques to eliminate or minimise them. The notable methods in designing for reducing cogging torque are listed as [181], [182]

a) ***Rotor pole or PM arc width***. A method generally applied to eliminate some of the cogging torque, and involves a computation of the optimum arc. Changing

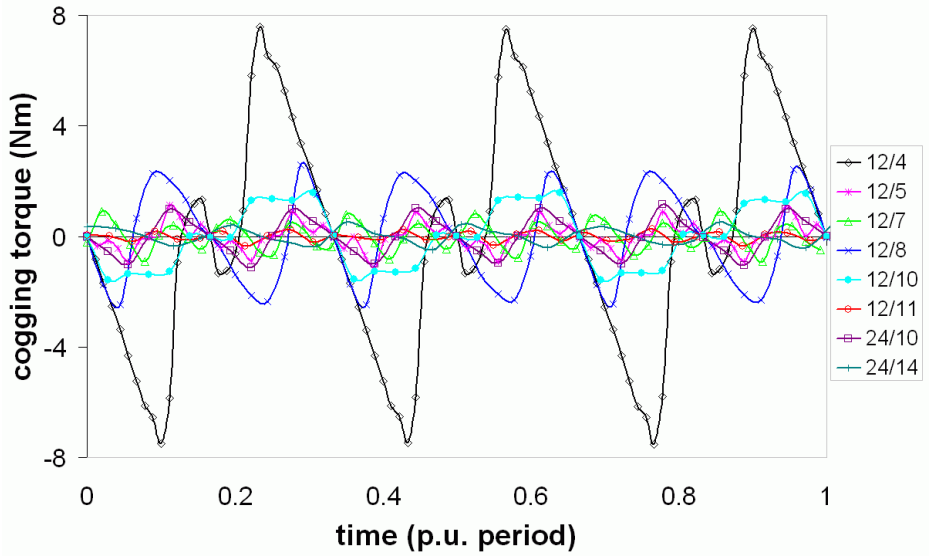

Figure 4.10. Cogging torque for various topologies.

the rotor or PM pole arc also has an effect on the form of the back-EMF, but the more difficult part to deal with is the computation of the optimum arc due to various variables involved.

b) ***Skewing of stator teeth or rotor magnets***. This is an effective method applied at design stage. For the cogging torque to be entirely eliminated, the skewing angle

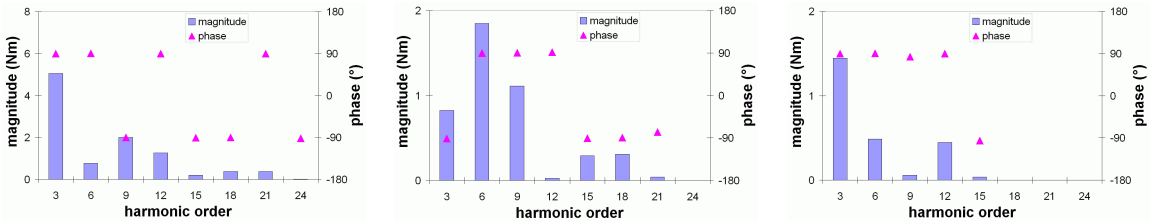

(a) 12/4 (b) 12/8 (c) 12/10

Figure 4.11. Cogging torque spectra for 12-tooth stator with even number of segments.

(a) 24/10 (b) 24/14

Figure 4.12. Cogging torque spectra for 24-tooth stator with even number of segments.

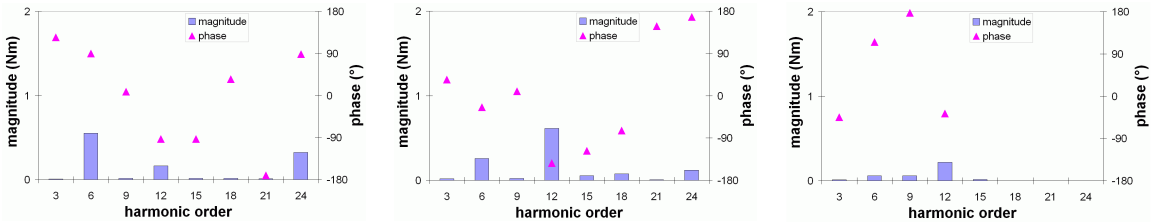

(a) 12/5 (b) 12/7 (c) 12/11

Figure 4.13. Cogging torque spectra for 12-tooth stator with odd number of segments.

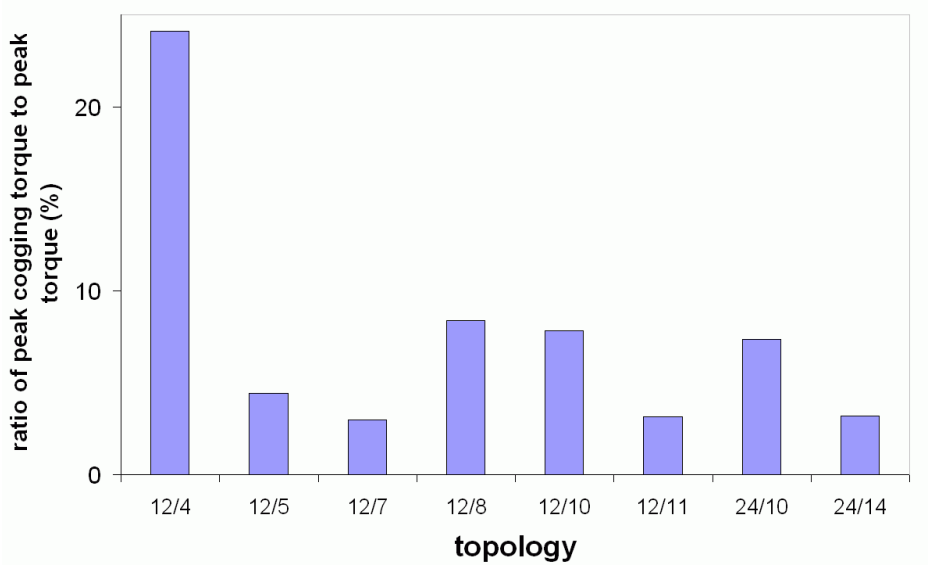

Figure 4.14. Ratio of peak cogging torque to peak output torque for all topologies.

must equal the angle of the mechanical period of the cogging torque. This said, it is easy to appreciate how this method poses manufacturing difficulties in automated and mass production lines. A variation applies this method in steps along the axial direction, in what is known as stepped skewing.

c) ***Rotor pole or PM shifting*** or (***circumferential pole skewing***). This method involves an adjustment of the mutual positions of the rotor poles or PMs on the rotor surface, in what appears as circumferential pole skewing, and has the same effect as the stepped skewing method. This method also generates the same design challenges as the skewing method.

d) ***Rotor pole or PM arcs of different width***. In this approach, magnets of different arc widths are employed, causing the effect of the elementary components of the cogging torque to be distributed along the pitch of the stator slot.

e) ***Stator teeth notches***. If dummy slots are introduced in the stator teeth, there is an increased interaction between rotor poles (or PMs) and stator slots, causing a reduction in the peak value of the cogging torque. A careful choice of the number of dummy slots is required so that the harmonics eliminated are the highest; otherwise a risk of only increasing the frequency rather reducing the amplitude of the cogging torque exists.

Of recent, rather approach the problem of torque pulsations at the design stage, reduction of torque is dealt with in operation of the machine by use of harmonic current injection or current profiling techniques [179], [184]-[191]. The attraction of this approach, apart from that it is quite effective, is that both the two causes of torque pulsations are addressed in one method.

The mean torque and the torque ripple are evaluated from the torque waveform data, and are shown in figure 4.15. Clearly, the 12/7 topology presents the largest mean torque at 29.7 Nm and the least amount of torque ripple at 4.7%. The 12/8 topology follows in ranking on mean torque at 26 Nm but has more torque ripple at 34.9%. The 12/5 topology gives a mean torque of nearly the same amount as the 12/8 topology at 24.4 Nm and has lower torque ripple at 8.6%. The two topologies on the 24-tooth stator present a mean torque which is about 50-55% of that in the 12/7 topology and have

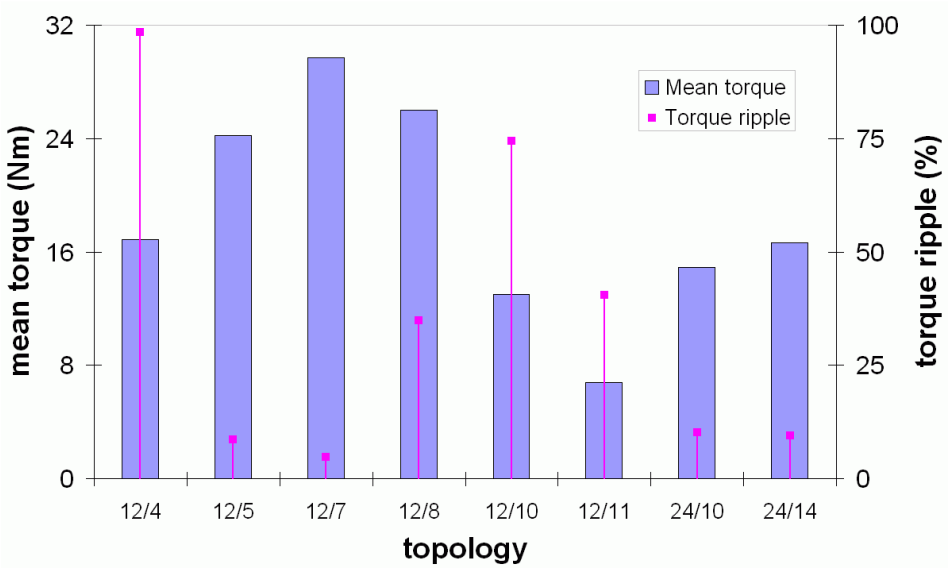

Fig. 4.15. Mean electromagnetic torque and torque ripple at rated load for all topologies.

relatively low torque ripple at about 10%, with the 14-segment rotor having an edge on both aspects. The poorest performance across all topologies is found in the 12/11 topology on mean torque and in the 12/4 topology on torque ripple.

4.6.5 Unbalanced magnetic force

The global force F acting at a point on a rotary body in a magnetic field has two components: the circumferential or tangential component, F_t which is responsible for the torque and the radial or normal component F_n which results in linear displacement. In rotating machines, if the radial component of the force is finite, i.e. not balanced, a magnetic side-pull on the rotor results and is generally known as the unbalanced magnetic force (UMF) or unbalanced magnetic pull (UMP).

The production of the global force on the rotor can be predicted by applying the Maxwell tensor stress approach to the airgap magnetic field distribution, $B(\alpha)$. The airgap field density at a point can be viewed as composed of the normal and tangential components $B_t(\alpha)$ and $B_n(\alpha)$, respectively, with α being the angular position with respect to a rotor reference position, θ, and normally defined as

$$\alpha = \theta + \omega t \tag{4.10}$$

The x-axis and y-axis components of the radial force, F_{nx} and F_{ny}, on the rotor of axial length l_a around the surface in the middle of the airgap which is at radius r, are [192], [193]

$$F_{nx} = \frac{rl_a}{\mu_0} \int_0^{2\pi} \left(B_t(\alpha)^2 - B_n(\alpha)^2\right) \cos\alpha d\alpha \tag{4.11}$$

$$F_{ny} = \frac{rl_a}{\mu_0} \int_0^{2\pi} \left(B_t(\alpha)^2 - B_n(\alpha)^2\right) \sin\alpha d\alpha \tag{4.12}$$

A geometric disposition of a rotating machine which causes a diametrically asymmetrical magnetic field distribution in the airgap round the rotor is likely to result in a finite value of UMF, rather than zero. This situation may arise by any of the several ways listed in the following situations.

- diametrically asymmetric phase windings inherent in the design topology [192]-[194];
- phase winding faults while in operation [194];
- rotor eccentricity [196];
- an odd number of rotor poles [197].

From the foregoing, there is therefore a justified expectation of UMF on the rotor for topologies considered in this investigation which have odd-numbered rotor segments.

The computation of the *x*-axis and *y*-axis forces using Maxwell's stress tensor equations is implemented within the FE analysis software and yields results for odd-numbered rotor segments which are discussed below. The topologies for discussion are the 12/5, 12/7 and 12/11 configurations.

The magnetic field distribution in the airgap, both at no-load and rated load, shows diametric asymmetry round the periphery of the rotor in all cases of topologies with odd-numbered topologies, as shown in figures 4.16, 4.17, and 4.18, and is consistent with the substantial values of the predicted UMF shown in part (b) of the figures. The magnitude of the UMF pulsates six times in one cycle between 960 and 1250 N for the 12/5 topology and between 800 and 1200 N for the 12/7 topology. The magnitude of the UMF for the 12/11 topology is steadier but is more than three times the maximum found in either the 12/5 or 12/7 topology. The UMF at no-load, for all cases considered, is nearly as much as the UMF at rated load. As the armature current is increased from no-load, the magnitude of the UMF falls gradually and reaches a minimum value at about half the rated armature current, before gradually rising again with current to reach the value at full-load, as in figure 4.19. The change between the minimum value and the

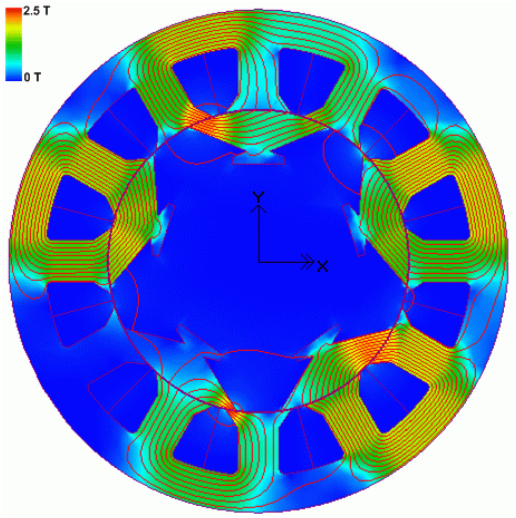

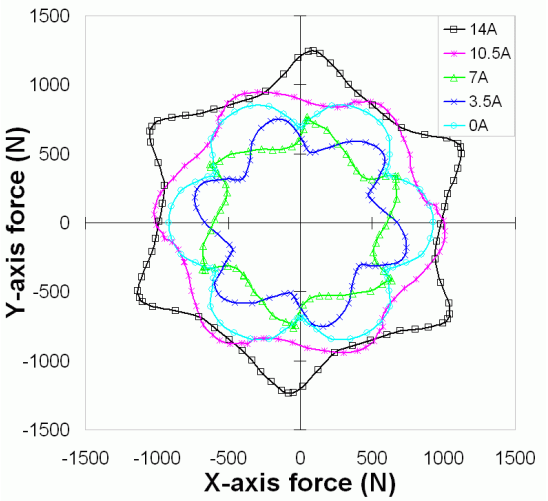

(a) field distribution at 14 A armature current *UMF at various armature currents*

Figure 4.16. Field distribution and UMF for 12/5 topology at 14 A field current.

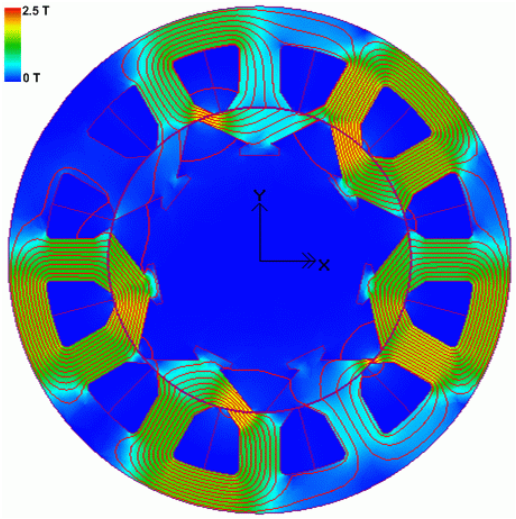

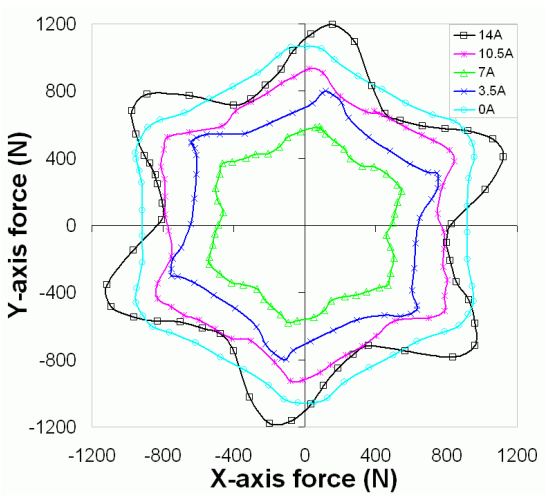

(a) field distribution at 14 A armature current *UMF at various armature currents*

Figure 4.17. Field distribution and UMF for 12/7 topology at 14 A field current.

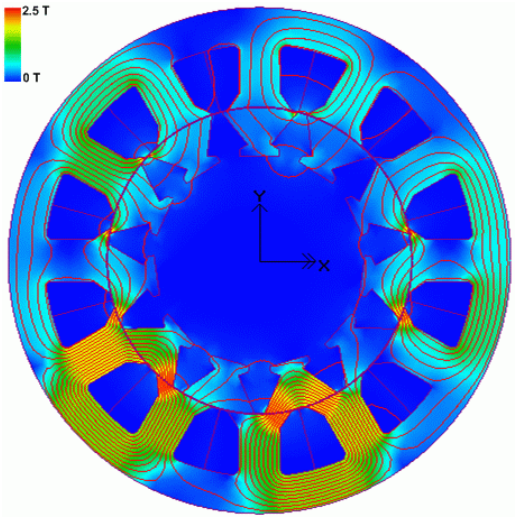

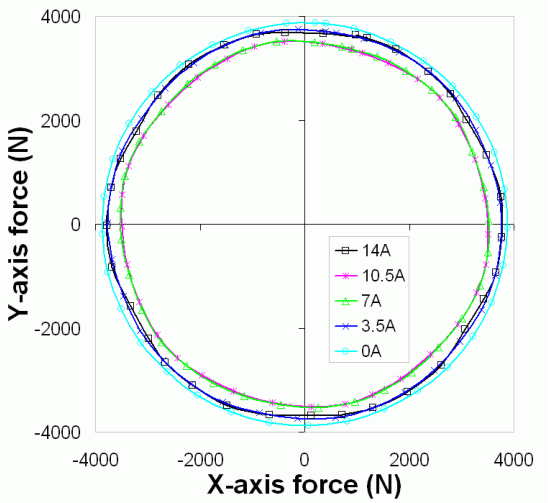

(a) field distribution at 14 A armature current *UMF at various armature currents*

Figure 4.18. Field distribution and UMF for 12/11 topology at 14 A field current.

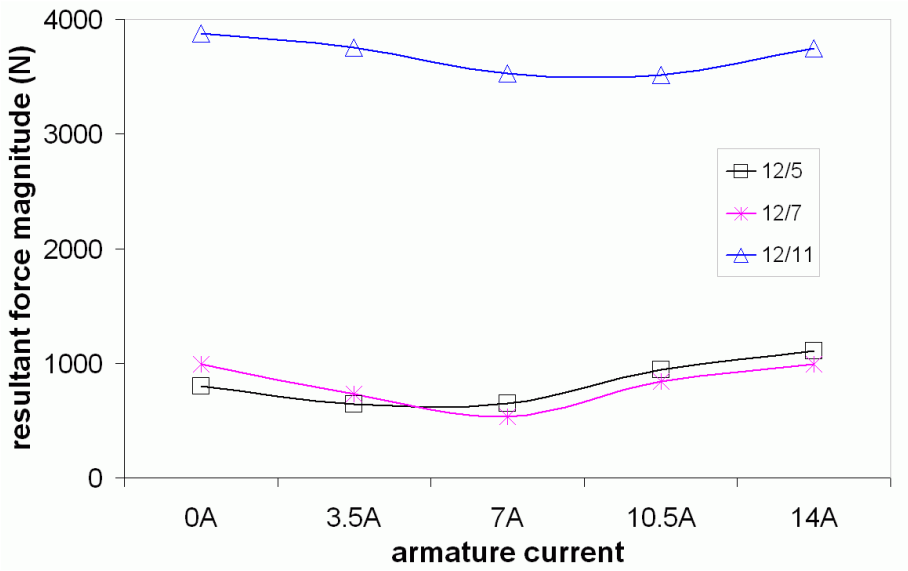

Figure 4.19. Variation of the mean UMF with armature current for topologies with odd-numbered rotor segments.

maximum value is 42, 47 and 9% of the maximum value for the 12/5, 12/7 and 12/11 topologies, respectively.

The presence of significant levels of UMF is obviously a drawback, culminating in excessive mechanical vibration and acoustic noise. Ultimately, the effect of the UMF is borne by the shaft bearings, and a judgement for tolerance of the UMF considers the type and quality of the bearings, together with requirements of the application.

4.7 Discussion and Conclusion

Topologies for three phase flux switching machines using a segmented rotor have been considered. The investigation has considered the requirements for stator teeth and the rotor segments. The flexibility in the rotor configuration has produced an extra variety of machine topologies over the choice presented by the stator configuration. Features of the machines have been examined and the topologies compared on the basis of the electromagnetic performance.

A stator with 12 teeth has been found to be the basic requirement for a three phase topology. Other stator configurations may appear in multiples of 12. This investigation has emphasised stator configurations with 12 and 24 teeth. Adaptation of a 24-tooth stator on similar dimensions of outside and inside diameter as the 12-tooth stator causes a significant reduction of the working flux density. Moreover, the resulting smaller tooth-width raises a concern for the mechanical strength of the 24-tooth stator structure.

Any number of rotor segments between 1 and 11 has been found to potentially produce a three phase topology on the basic 12-tooth stator, except for 3, 6 and 9 which confine the topology to single phase configuration. Notwithstanding this observation, feasible designs appear to subsist in the topologies with 4, 8 and 10 segments. If geometric balance is ignored, the choice for plausible designs is extended to topologies with 5, 7 and 11 segments.

It is has also been investigated how the segment span influences the performance parameters in each topology. Discounting the span of segment separation, the design of the rotor segment span in each of the topologies is constrained by the segment pitch and the angle of full segment overlap at alignment. Within these constraints, the optimum segment spans in each topology can be identified by examining the quantifiable electromagnetic parameters. As a general outcome, it has been found that the optimum segment spans tend to cluster near the maximum permissible segment span for cases where the alignment compliance factor is less than 1 and are equivalent to the angle of full segment overlap at alignment for the cases where the alignment compliance factor is 1. For the cases considered, all the topologies fall in the category with the alignment compliance factor less than 1, with the exception of the 12/4, 12/5 and 24/10 topologies which fall in the category with the alignment compliance factor equal to 1.

A comparison of the electromagnetic performance of the topologies shows that the 12/7 topology gives the highest performance, when considered on the parameters of achievable peak flux linkages, induced armature voltage and available torque. At the other end of the spectrum, the 12/11 topology gives the lowest performance on the same parameters. The 12/7 also gives the highest performance in terms of the secondary attributes on EMF waveform distortion and torque ripple. However, topologies with odd-numbered rotor segments, including the 12/7 topology, have shown remarkable UMF. If it is a condition of the design requirement to exclude topologies with potential UMF, the 12/8 topology ranks as the configuration with the best performance. There is undoubtedly a mixture of advantages and disadvantages in the other topologies including those on the 24-tooth stator, which may warrant consideration depending on the specifications and applications.

It is central to this study to end by mentioning that these general conclusions, derived by examining wound-field configurations, are equally applicable to configurations with

permanent magnet excitation, as long as the circumferential span of the magnet at the airgap periphery is the same as the span of the field tooth tip at the airgap periphery in the equivalent wound-field stator.

Chapter 5

Design and construction of three-phase segmental rotor machines

The design and construction of three-phase segmental-rotor flux switching machines for practical implementation as wound-field and PM configurations are considered in this chapter. The feasible topologies for three phase implementation using a segmental rotor were revealed in the previous chapter. It appears prudent to define a set of criteria and apply it to select the configurations for development of the representative machines. This is the approach followed in this chapter. Design optimisation may then be instituted on the preferred topology based on the defined criteria, and the approach and method of its construction may subsequently be considered.

5.1 Introduction

Although a 2-phase, wound-field, flux switching machine employing a segmental rotor [123] has been implemented, operated from a single-phase drive with sinusoidal current control, there is interest to implement practical configurations for three phase operation to overcome the limitation of single phase configurations. The advantages for considering three phase configurations have been presented at the beginning of chapter 4, and are as attractive as to outweigh the foreseeable disadvantages in applications accruing in output power of over a kilowatt. The single phase machine in [123] was implemented on an 8-tooth stator and a rotor with 4 segments in an 8/4 configuration.

5.2 Considerations on Choice of Topology

It is clear, from the investigations in chapter 4, that the configuration of a three phase flux switching machine employing a segmental rotor topology with a 12-tooth stator and 7 rotor segments, herein called the 12/7 topology, gives the best of the desired attributes. The 12/7 topology presents the highest torque capability, the least torque ripple, the most symmetrical phase EMF and the least distortion in the EMF waveform from a sinusoid. However, the use of an odd number of rotor segments entails an intrinsic unbalanced radial force in the rotary application, which has been shown to be significant. With this factor in consideration, it is natural to choose to develop the next best topology which avoids this penalty. Thus, the 12/8 topology is proposed for development. With all factors considered, it becomes the best topology, though it gives 87.5% of the torque capability, about 7 times the torque ripple, a more unsymmetrical EMF waveform and about 1.6 times the EMF THD of the 12/7 topology.

Alongside the 12/8 topology, the 12/5 topology may be considered for development to validate some features of flux switching by means of a segmental rotor which may not be exhibited by the 12/8 topology. The development of the 12/5 topology serves to validate or illustrate the following bundled features.

- Each of the two armature coils making a phase winding produces unsymmetrical EMF waveform with dissimilar alternations which is an intrinsic property of flux switching by means of a segmental rotor. In topologies with an even number of segments, the alternations of the two coils are synchronised while in topologies with odd number of segments, they are transposed. This has the effect of producing a

resultant EMF in the phase winding composed of the two complementing coils which is symmetrical for topologies with odd-numbered segment but unsymmetrical for topologies with even-numbered segments. The 12/5 topology, together with the 12/8 topology, gives a chance to validate this expectation.

- As developed from single phase principles, the ideal presentation of segment overlap at alignment position is to have the rotor segment fully and exactly overlapping two adjacent stator teeth, i.e. the segment span being equal to the span of two stator teeth and one stator slot. The span of segment separation may thus be allowed to be larger than the specified minimum, which is possible in the 12/5 topology in which the segment pitch can accommodate it. The facility of using a large segment separation eliminates a posturing that creates coupling between phase coils or between field coils and, as such, the mutual inductance between phases tends to be ideally zero.

A combination of all these considerations gives strong credence to develop the 12/8 and 12/5 topologies for implementation.

5.3 Stator Design

The winding disposition of the flux switching machine is predominantly a series of concentrated windings wound around each stator tooth. Therefore, the design considerations of the stator for the flux switching machine may be grounded in the accumulated research of machines with concentrated windings, rather than those with distributed windings. The common traditional machines employing concentrated windings on the stator are stepping motors, switched reluctance machines and some classes of modern permanent magnet machines. Unlike stator cores for distributed windings, where deeper concern is on slotting for the conductors, so that design of the slot openings is an important function to control machine performance, the design of stator cores for concentrated windings tends to place importance on the tooth or pole. This section considers both the geometry and dimensions of the stator teeth.

5.3.1 Tooth geometry for wound-field configuration

The general presentation of the shape of the stator tooth for concentrated winding arrangements is one with a radial structure jutting out from the back-iron or yoke and profiling the circular shape of the rotor on the mating side with the airgap. The development of such a structure from a basic shape with straight parallel sides to ones with refinement meeting specified functions is shown in figure 5.1 (a) [198], as applied to switched reluctance machines. In [198], the principles for the modification to the basic shape for a concentrated winding tooth are outlined and may be applied to progress to a judicious selection of the shape for this application.

Modification of the basic shape in part A of figure 5.1 (a) may be imparted to serve

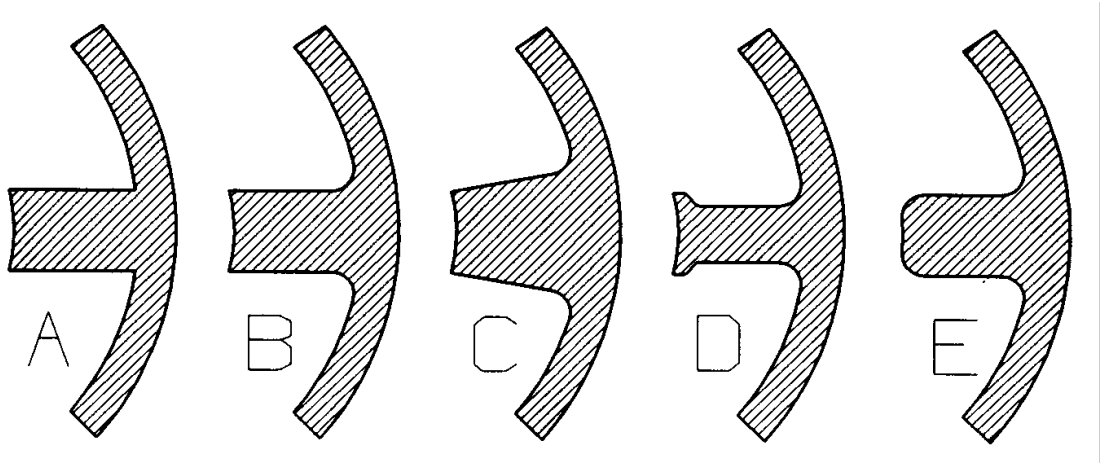

(a) Stator tooth geometries for concentrated windings [184]

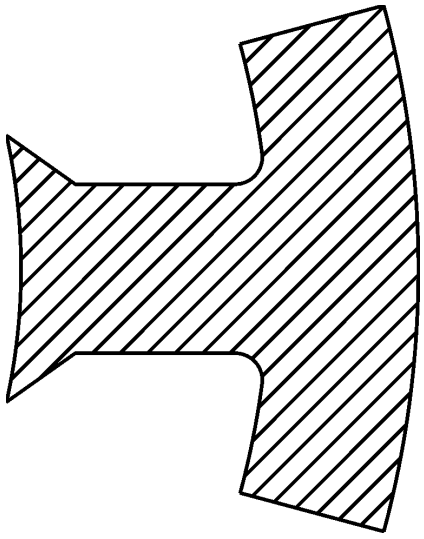

(b) Stator tooth geometry adopted for development

Figure 5.1. Stator-tooth shapes for concentrated windings.

various purposes. As a way to brace the tooth against vibrations in the circumferential direction, the sharp corners at the root connecting the yoke may be made with a radius as in part B. Tapering the sides of the tooth, as provided in part C, reduces the MMF drop in the tooth and concentrates the flux near the airgap. The modification made to the tip in part D, by providing overhangs, is similar to what is done for distributed winding arrangements as a way of adjusting the slot openings. In concentrated winding arrangements, this type of modification is not followed if the coils are made for insertion after winding but, where applied, it may be for one or both of the following two reasons. Firstly, the overhangs may be applied to soften the torque impulse that may arise at the start of overlap, and secondly the overhangs may serve as markers for supporting the coil in assembly. A modification rarely applied is one shown in part E, where the tooth tip corners are rounded. It is obvious that this modification increases the airgap, and may be too high a price for attempting to soften the torque impulse at the start of overlap, as is the envisaged purpose. A good deal of the modification in recent times, after considerations of bracing the tooth root, is done at the tips of the tooth for the advertent effect of minimising the torque ripple [199]-[202].

The shape of the stator tooth for the flux switching machine developed for this study is intended to gather as many of the benefits outlined above but also to have a simplicity that befits construction with standard machining equipment in the university's in-house workshop. The general tooth shape adopted has, ultimately, rounded corners at the root and, for simplicity, triangular overhangs at the tip. The tooth shape is still kept simple by adopting straight parallel sides, as the benefits of a tapering structure are minimal in the purpose of this study. Figure 5.1 (b) shows the outline shape of the stator tooth adopted, with details provided in appendix F.

5.3.2 Tooth geometry for permanent-magnet configuration

As pointed out in chapter 3, the segmental-rotor configuration with permanent magnet excitation has to have the magnets on the stator acting in a radial direction. Design and construction considerations favour locating the magnets at the tip of the stator teeth on account for the following benefits:

- a reduction of the number of sections on the stator, as the stator tooth requires no segregation if the magnets are at the tip.

- an increased volume of magnet is possible, which takes advantage of the permitted extended span of the tooth tip. The span of the tooth tip, by employing overhangs, is generally larger than the span across the parallel sides of the tooth.

- assembly of the magnets onto the stator is thought to be easier if they are to be fitted at the tip.

- at the tip of the tooth, the magnet is further from the heat source (coil slot) than at other positions on the tooth.

There are minor disadvantages for locating the magnets at the tips, as follows.

- the magnets may not be easily cooled if located at the tooth tips, and are unlikely to benefit fully from forms of forced convective cooling method on the outside surface of the stator.

- there is a risk of inflicting damage to the magnets during assembly of the rotor as the magnets are on the exposed side.

The choice to locate the magnets at the stator tooth tip presents several geometries for the magnet and modifies the shape of the field tooth significantly in relation to the armature. Figure 5.2 shows the geometries considered. The preferred profile of the magnet where it mates with the airgap is a curved surface so that the airgap length, l_g, is constant and the same over the armature field teeth. In all the designs of the magnet geometry, the magnet depth, l_m, is also fixed and is calculated from the magnetic field intensity required to produce the same MMF as with an equivalent wound-field tooth. In order to have the same overlap conditions over the magnet as over the armature tooth, the span of the magnet is made the same as that of the armature tooth.

The beginning of the tapered overhangs in A and C is designed to be the same as in the armature tooth, while in F the tapered overhang begins higher up on the field tooth to create a well-proportioned overhang for supporting the bonding of the magnet. In contrast the tapering overhangs D and E and the parallel overhangs in B are created on the magnet itself and start at the height of the magnet, l_m, from the airgap side. It is calculated that geometry A gives the same slot area as when a tooth similar to the armature is used, while D and E presents more slot area and the geometries in B, C and F present less area.

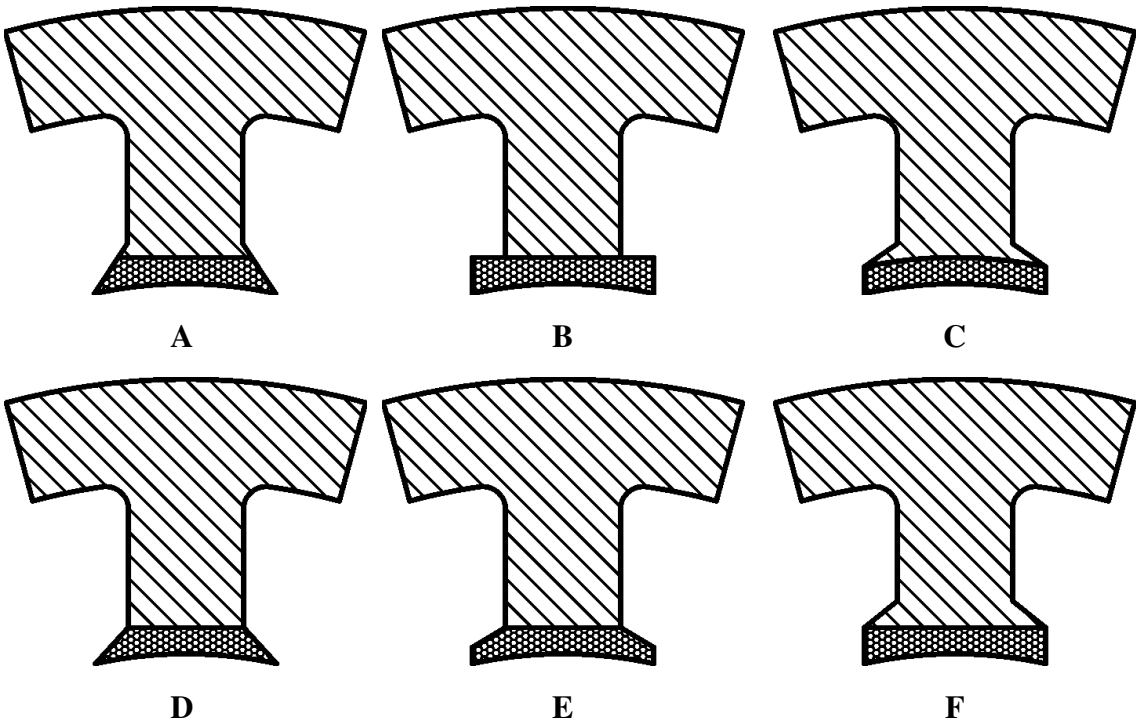

Figure 5.2. Geometries for magnets.

While the variety of the geometries of the combined field tooth and magnet shown in Figure 5.2 might appear to be differentiated only by aesthetics, their shapes may have an impact on the strength of the bonding and assembly and on the volume of the magnet, ultimately affecting performance. For instance, the geometries C and F may be preferred for the larger surface for bonding the magnets and increased torque output for the same armature current as shown in figure 5.3. On the other hand, output torque may be sacrificed and high torque ripple may have to be incurred for reduced THD of the induced EMF by preferring geometry D. While geometry F clearly presents the highest torque capability, there are small differences differentiating the performance of geometry C from that of A, B and E.

In building a demonstrator machine for this study, geometry F was favoured. This selection ensured ease and simplicity in propping of jigs for assembling the magnets on their flat surfaces, an expansive surface for the bonding area, whilst keeping the most favourable electromagnetic performance.

5.3.3 Stator teeth dimensions

The maximum overlap arc between segments and a field tooth determines the width of the field and armature teeth, along with the stator core-back depth and the segment depth, so that all regions have similar peak magnetic flux densities. Having identified a

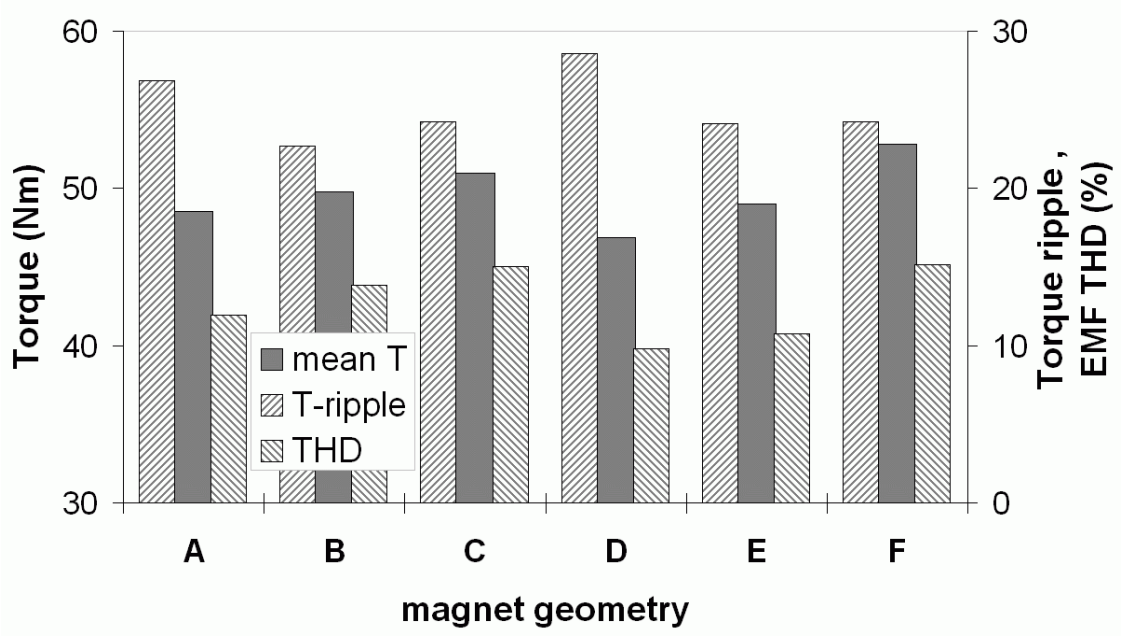

Figure 5.3. Outlook of performance for various magnet geometries, comparing mean electromagnetic torque capability, T, torque ripple, t-ripple, and THD of EMF waveform at assumed rated condition.

working peak flux density, the influence of the armature tooth width relative to a fixed field tooth width is investigated for both configurations with 8 and 5 segments, with all other parameters fixed. Determination of the width for the field tooth is performed with a simplifying outline design approach represented in appendix B.

The effect of reducing the armature tooth width on the performance parameters of rms EMF, E_a, electromagnetic torque, T_e and total harmonic distortion (THD), of the EMF waveform, is shown in figure 5.4. The per-unit (p.u.) quantities in the graph are with reference to the quantities of the baseline design with the armature tooth width equal to the field tooth. As the armature tooth width is reduced, more room is availed to the armature winding, and as such the graphs with solid lines represent the performance with proportionally adjusted armature winding turns, (keeping the current density and slot fill factor fixed), whilst the graphs in dashed line represent the cases with same armature turns as the field turns (i.e. the 1 p.u. case).

In respect of the rms EMF and electromagnetic torque, the optimal width of the armature tooth is when it is between 60-80% of the field tooth in the 12/8 configuration. However, in this configuration, the THD of the EMF waveform increases with reduction of armature tooth width, with the least THD presented when the armature tooth width is the same as the field tooth width.

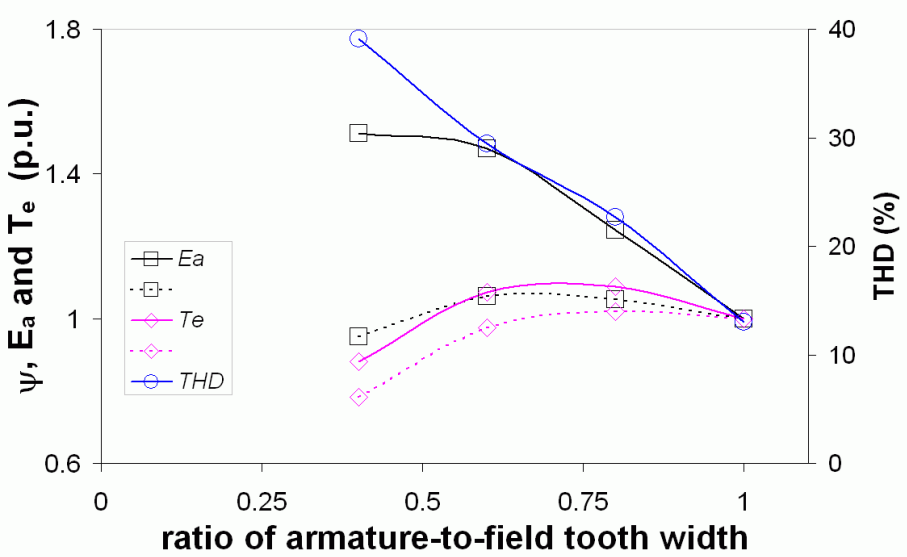

(a) 12/8 configuration

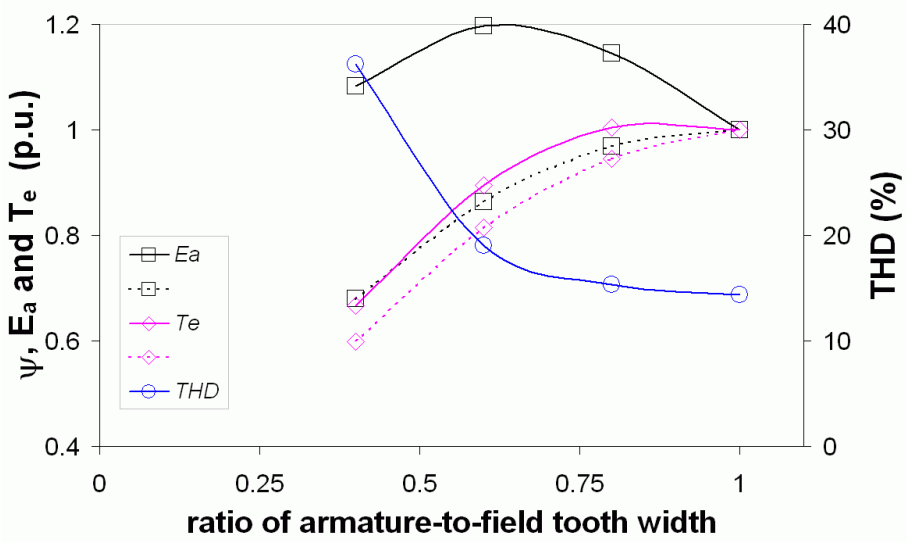

(b) 12/5 configuration

Figure 5.4. Influence of armature tooth width on performance.
Solid = with adjusted armature turns; dashed = without adjustment of armature turns

For the 12/5 configuration, the combination of EMF and electromagnetic torque is optimum at a width of the armature tooth which is in the range 80-100% of the field tooth. The THD decreases with increase of the width of the armature tooth, but is virtually unchanged in the range when the armature tooth width is 60-100% of the field tooth width. Due to this outcome, there is a reasonable case to have a reduced armature tooth width relative to the field tooth width by a margin of up to 40 % for optimum performance for a saving in core material.

It is seen that the performance parameters of torque, flux linkage and EMF generally appear to be unchanged until reduction of armature tooth width reaches about 70% of

the field tooth width, when it starts to fall, if the armature turns are not adjusted in relation to the proportionally freed slot space. This seems to suggest that there is a improvement in the utilisation of the magnetic circuit up to this point, beyond which the armature tooth is operating at saturation flux density and any further increase in performance is largely due the compensated increase in the armature turns.

The armature tooth width which is equivalent to the field tooth (the 1 p.u. case) is chosen as it gives the least THD of the EMF for both the 12/8 and 12/5 topologies, without conceding significant torque capability.

5.4 Segment Design

The principal use of magnetic segments in the flux switching machine is for provision of magnetic paths for flux to defined regions of the stator, while ensuring isolation of these paths. It is expected that the segment has to be a good receptacle of flux at the airgap periphery, and may be as deep as necessary in relation to the span, so that reasonable working flux densities subsist in the segment core.

5.4.1 Segment geometry

A rotor segment is invariably either solid or laminated magnetic steel isolated from other segments in the rotor by a non-magnetic medium. In rotary configurations, the surface profiling the airgap follows the prospective circular shape of the rotor, other parts may be modified to impress some electromagnetic property or serve a mechanical function. Figure 5.5 shows typical shapes applied in segmented rotors. The basic shape of the segment, viewed in the axial direction, has a circular arc as the main side and two tapering sides starting for the end tips of the arc. The tapered sides extend the same distance on each side and are closed by a generally straight edge or circular edge which may follow the profile of the non-magnetic shaft.

The shape design in part (a) shows one of the earliest geometries applied in synchronous reluctance machines [152], [153], [203], [204]. A notable modification from the basic shape is the channel in the middle of the arc, the position defined by the interpolar centre-line. The size of channel and the shape of the segment ends have a notable effect on the fringe and permeance factors [204] which impact on the quadrature axis reactance, and hence the available torque of the machine. This shape is quite basic

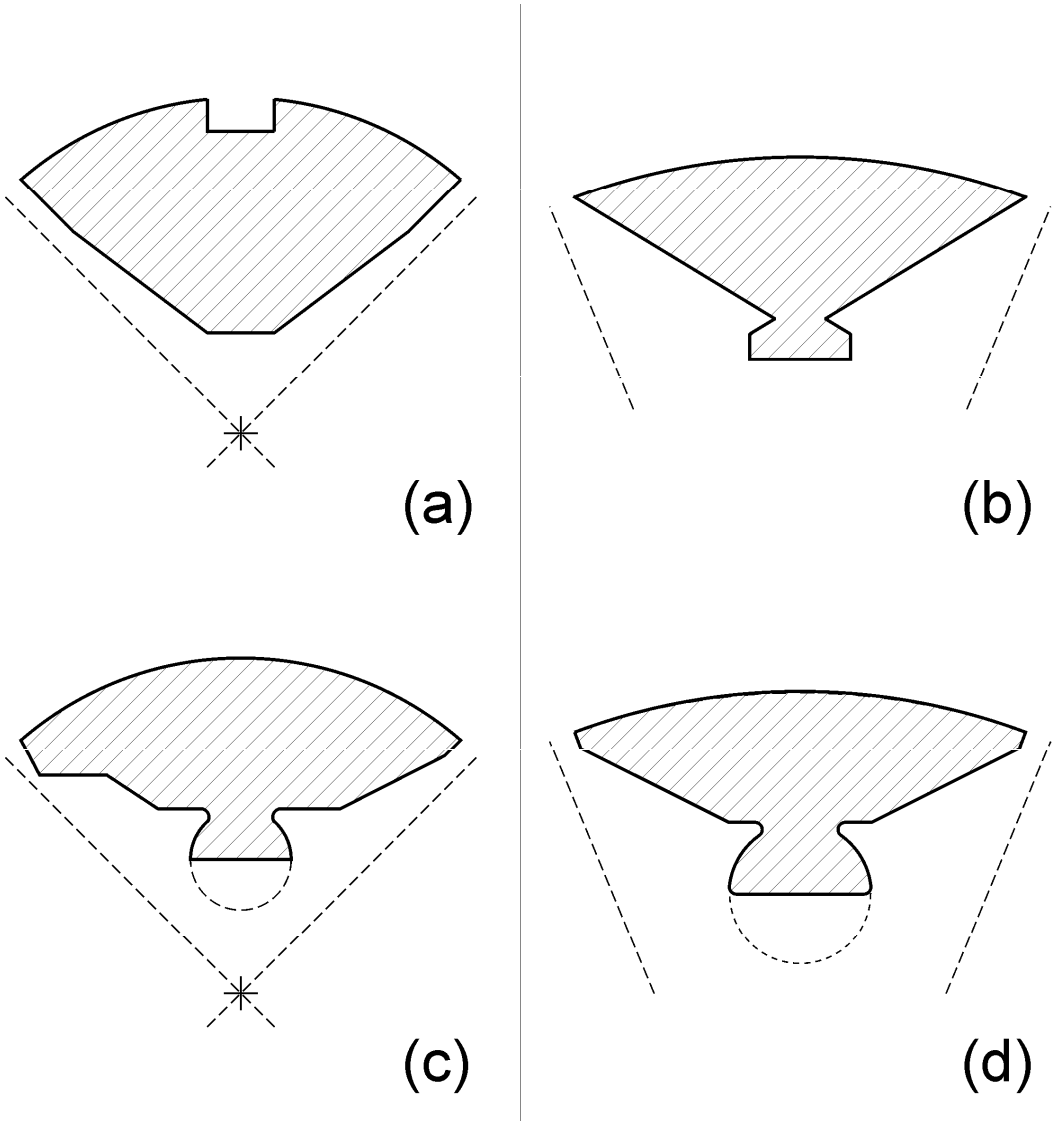

Figure 5.5. Geometries for rotor segments.

and without handles, so that a way to secure the segments on the through shaft of nonmagnetic stainless steel is by the clamping force exerted by axial bolts and nonmagnetic stainless-steel discs at the ends and, in some cases, in the centre. The design in part (b) was applied for an SRM [123], and has a handle at the seating of the segment. This shape of the segment permits circumferential location of the segment on the rotor by using the flat bottom of the handle. Retention of the segment against centripetal and magnetic radial forces is by application of non-magnetic steel wedges dovetailed into the handle and radially bolted on to the rotor shaft. The modifications applied for the FSMs [123], [205] are shown in parts (c) and (d). The first aspect of the modification is the thickening of the edges of the segments, believed to help relieve magnetic saturation on the edges on the segments at the start of overlap. The edges in part (c) are designed to present asymmetry, for self-starting capability in single phase applications. The second modification is on the handle of the segment for location and

retention of the segment, where a semi-circular protrusion is used. The protrusion is designed to fit in a similarly shaped semi-circular indentation on the non-magnetic rotor shaft, so that the resulting press-fit assembly is mechanically tight and strong. The assembly may be further strengthened mechanically by non-magnetic caps axially bolted at the ends of the rotor shaft. The geometry shown in part (d) is the one adopted for the rotor of FSMs in the 12/8 and 12/5 configuration of this study.

5.4.2 Segment dimension

Of the segment dimensions, the span is more likely to significantly influence performance than the depth. The segment depth is therefore adjusted only as deep as to avoid saturation and no deeper than the back-iron depth. The angle of full overlap at segment alignment for the stator with baseline dimensions incorporating tooth overhangs as adopted in the previous section is 55°. With allowance for segment separation of 4° on the chosen size of rotor, the segment span variation for the topology with 8 segments is limited to 41°, whereas for the topology with 5 segments it can vary up to the angle of full overlap at segment alignment. When the segment span is normalised, with the angle of the segment pitch as the base, the effect of changing the span on the performance has been investigated and presented in chapter 3. For the 12/8 configuration, the optimum performance on the basis of peak flux linkage and rms EMF when the span is varied from 25 to 41° occurs when the segment span is about 38°, but as in the case of changing armature tooth width, the THD is at optimum when the segment span is at maximum (i.e. 41°). The 12/5 topology, in which the range of span for this investigation is from 45 to 65°, gives a different outlook. As there is no influence of the segment span on THD, the parameters of peak flux linkage and rms EMF are applied to determine the optimum performance. The optimum performance is ascribed to the span of full segment alignment and occurs at 55° segment span for the stator design adopted.

5.5 Manufacturing and Assembly

The discussion in the previous section considered the shapes of the stator core and rotor segments, which are the principal magnetic material elements in the machines. This discussion concentrates on the manufacture and assembly or construction of these elements for the flux switching machine employing a segmental rotor. While consideration of the design of the principal elements is chiefly based on their

electromagnetic function, the important aspect of the processes of fabrication plays a significant role in the final decision. Designing for manufacturability considers specifying components that can be fabricated at minimum cost, of which the cardinal principles are simplicity and use of standard materials and components [206].

5.5.1 Consideration on manufacturing methods

The stator core for the flux switching machine with 12 teeth, as in this design, typifies core arrangements for concentrated windings, and benefits from the wealth of manufacturing techniques accrued in their development. The laminations for both the stator core and rotor segments may be manufactured by the standard or advanced processes of sheet metal cutting [207], of which the following are widely applicable.

- ***Shearing by guillotine or scissors***. This may be a preferred method for large-sized sheets to prepare the laminations before another cutting process. It is effective on soft alloys such as brass and mild steel but hard alloys such as stainless steel and silicon steels tend to work-harden due to plastic deformation on the cutting edges. However, it is not unusual to prepare laminations used for electrical machines for electrical testing in the single sheet or Epstein strip test [208] by this method.

- ***Shearing by punching***. It is the conventional and commonly applied cutting method for mass production of laminations and also the most cost effective. Like the guillotine, there is significant burr on the edges of the cutting, and often some means of relieving this by heat treatment are employed.

- ***Laser cutting***. As one of the advanced cutting methods with an in-built flexibility for use in a wide variety of situations, it competes strongly with conventional punching methods and it is not far-fetched to aim at improved overall efficiency of production by combining the two processes. Deep cuts and sharp corners can be difficult to execute, and are better avoided in this method. There is virtually no mechanical deformation on the cut edges, but there may be some adverse effects arising from localised high temperatures.

- ***Electrical discharge machining (EDM)***. With the two main variants of spark erosion and wire erosion, this cutting method also places some restrictions on the shapes that can be cut, tending to be avoided for deep slots and narrow openings. The surface finish can be as fine as laser cutting but if a high production rate is

required the removal of the bulk of the material should be done by conventional cutting methods.

Apart from undergoing the cutting process, the laminations may be subjected to a heat treatment process, for annealing and welding, and a compacting process, for stacking and sticking. Figure 5.6 shows the relative deformation at the edges of samples cut by different methods, which is proportional to the stress induced at the cut edges. In relative terms, the sample cut by the guillotine endures the most stress at the cut edge, followed by one produced by the punching method, whilst the one produced by laser cutting has virtually no deformation at the edges.

Apart from considering the variety of the manufacturing methods for laminations on cost and manufacturability, another far-reaching position is that each of the considered manufacturing process has significant effect on the magnetic properties of the electrical steel alloys [209]-[218]. Punching and laser cutting tend to increase the iron loss at 60 Hz by up to 10% and lower the permeability at 1.5 T by up to 20%. The iron loss at 1.5

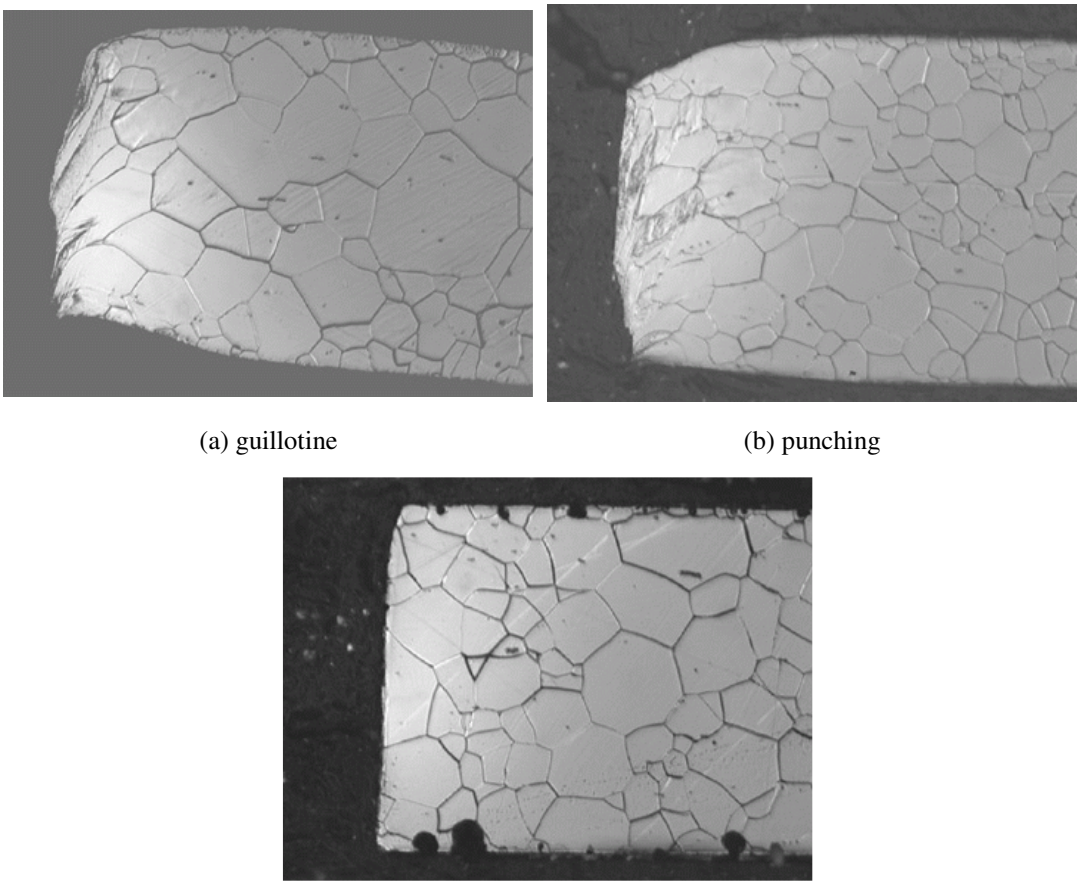

(a) guillotine (b) punching

(c) laser

Fig. 5.6. Edge profiles for different cutting methods [198].

T, after welding with six passes, may increase by as much as 15 % due to the short circuits created on laminations, whereas there are appears to be no significant effect of the pressing and sticking processes on the iron losses, reported at increase of less than 3%.

Manufacturers quote properties of steel lamination from tests performed on prepared specimens which undergo one of the cutting processes, usually by guillotine and punching, and it is clear why discrepancies exist between the quoted properties and those of the unprocessed lamination. The characterisation of the magnetic properties of laminations is rendered significantly deficient if preparation of the test specimen in the standard test subjects it to some form of deformation such as by a cutting process [208], [219], [220]. While it appears easy to rectify the deformation arising due to cutting processes by using heat-treatment, some researchers [221] also advocate incorporating the effects of lamination processing at the design stage of an electrical machine.

5.5.2 Consideration on the manufacturing approach

There are several ways to produce the stator of a rotating machine intended for concentrated winding configuration [222]. The choice of the approach for production of the stator may be influenced by a number of factors including the size of stator, scrap minimisation, production processes and assembly considerations. Some of the novel approaches to production of the stator laminations outlined in this section have been chiefly motivated by a desire to ease the assembly of coils, with benefits of low turn-around times and increased slot-fill factors. Four approaches are considered as fitting application to production of stators designated for concentrated winding configuration and are listed as follows [228]:

- ***Complete core.*** Using a punching process or one of the advanced machining processes, the whole cross-section of the stator core may be produced. This approach is known to produce considerable scrap, up to 90%, especially if the centre part remaining after cutting out the section is not intended for other use. A way to make good use of the left-out cutting is to produce laminations for smaller motors or the rotor of the same motor. Nonetheless, it is a traditional approach to produce laminations by the punching process for machines up to medium size frames (< 400 mm stator diameter).

- ***Modular core***. If the stator core is separated into equal sections for production, preferably along lines of symmetry, there may be substantial reduction in the amount of scrap. The number of sections defines the degree of modularisation, but if the ultimate case of modularising to one stator tooth section is employed, there is a possibility to wind the coils on the teeth before assembling the stator core. Figure 5.7 shows the possibilities of modularisation on a 12-tooth stator with six lines of symmetry. These possibilities are reduced by one if the configuration is for permanent magnet excitation.

  It is thought that the amount of scrap may be reduced in proportion to the degree of modularisation. For the case of the 12-tooth stator, the computed wastage of core steel with the degree of modularisation is shown in figure 5.8, where it is assumed the 150 mm diameter by 150 mm axial length single stator is manufactured from standard lamination sheets of 600 mm x 300 mm and the production requires margins of approximately 5 mm around the edges of the sheet for handling. These cases illustrate steel wastage being reduced from 84.6 %, if complete core laminations are produced, to 45.8 %, if one twelfth of core section modules are

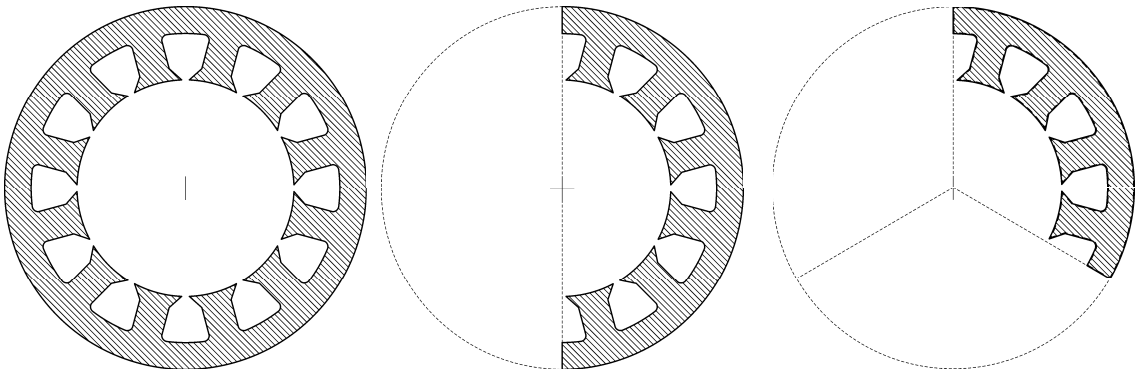

(a) 360° module (complete core) (a) 180° module (a) 120° module

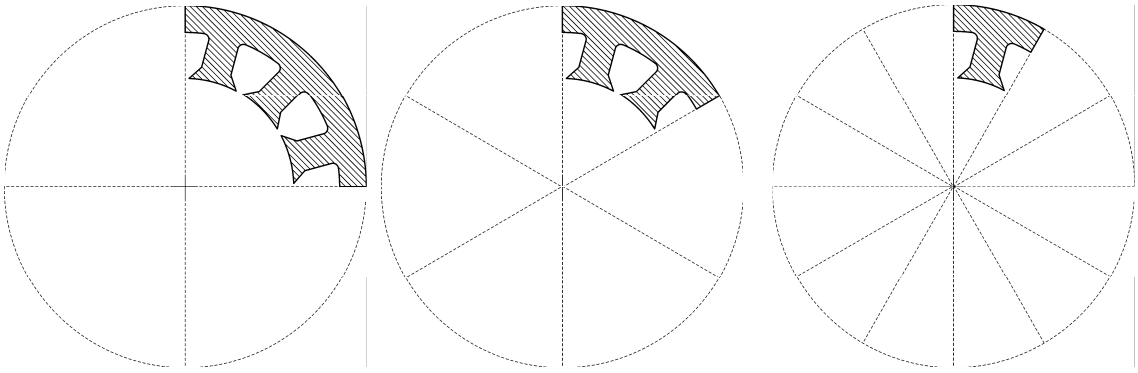

(a) 90° module (a) 60° module (a) 30° module

Fig. 5.7. Six degrees of modularisation of a 12-tooth stator.

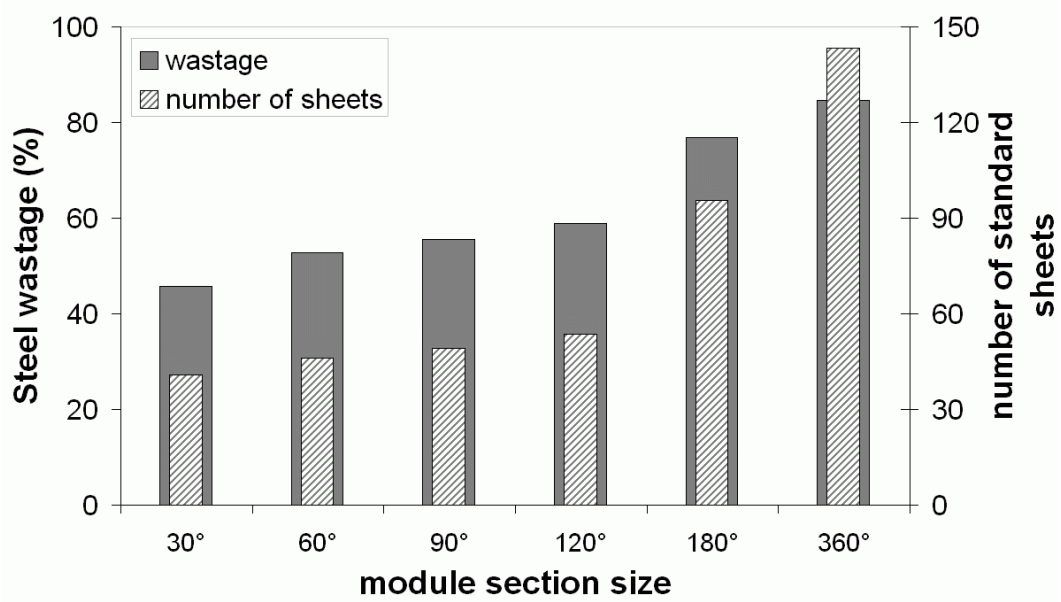

Figure 5.8. Effect of modularisation of core production on steel usage.

produced, with the number of standard sized steel sheets needed correspondingly being reduced. The cutting patterns per standard sheet for each case of modularisation for the wound-field FSM stator are presented in appendix D.

The modular core approach has the disadvantage of requiring further processing such as alignment and joining of the sections by welding or bonding agents. It is also prudent to consider that the bonding agent or small remnant airgaps between the sections may present a change in permeability along the flux paths. A hybrid approach of the complete core and the modular core is what is called the connected core, in which modular sections of the core are connected by thin bridges to form a complete core [223].

- ***Spiral laminated core***. In applications where the core-back is not too deep, a spiral laminated core is an attractive approach to production of the stator core. While it requires producing a long band of lamination from which slots are punched before being furled and welded, and effectively culminating into a complete core, the amount of scrap can be considerably less than in the traditional approach. It is thought that the furling process may affect the magnetic properties of the steel, but it is the requirement of special production machines and a limitation on the geometries that can be produced that count as apparent disadvantages.

- ***Joint-lapped core***. This approach, attributed to Akita et al [223], is novel and relatively new (the turn of the second millennium). It is similar to the production of

the modular core, except for the connections of the modular sections, and similarly reduces scrap. It relies on an arrangement where pairs of cylindrical convex and concave jointing areas on either faces of the joints on the modular sections are overlapped and jointed, making axes of rotation. The freedom to rotate at the jointing axis permits assembly of the modular sections into a complete core and the assembly is highly amenable for automation.

The first two approaches thus discussed for producing stator cores are equally applicable for rotor cores. Being smaller in size than the stator core, the material wastage due to scrap is relatively smaller and is not expected to vary significantly between the approaches. This observation is reinforced if the rotor is of a segmental configuration.

5.5.3 Coils

Before embarking on a review of the approaches to coil winding, some of them which are now standard but others completely novel and ingenuous, it is helpful to mention the factors considered in processing and assembling coils on electrical machines.

Foremost, a decision on the level of automation, dictated by cost, needs to be made from a wide range, starting from manual hand-winding to various levels of automation, with and without intelligent control. A simplified general guide is that if only a few samples of experimental or high performance dedicated machines are to be made, then the winding methods employing manual skills and some form of mechanical gearing and spindles suffice. However, an extended level of automation, up to intelligent correction with feedback systems, may be necessary for the winding processes that encounter frequent changes in winding patterns and parameters or for large volumes of mass production.

Next, the specification of the required or acceptable winding pattern needs to be determined. Even for single-tooth windings with parallel sides, there are inherent difficulties in implementing certain winding patterns [224], of which figure 5.9 is a good illustration. The orthocyclic winding pattern, so-called perfect winding, is the most practical winding pattern close to the ideal pattern in part (a), reaching a theoretical fill factor of 90.6%, and some fairly simple techniques of how to approach a pattern of this form with success have been devised [225].

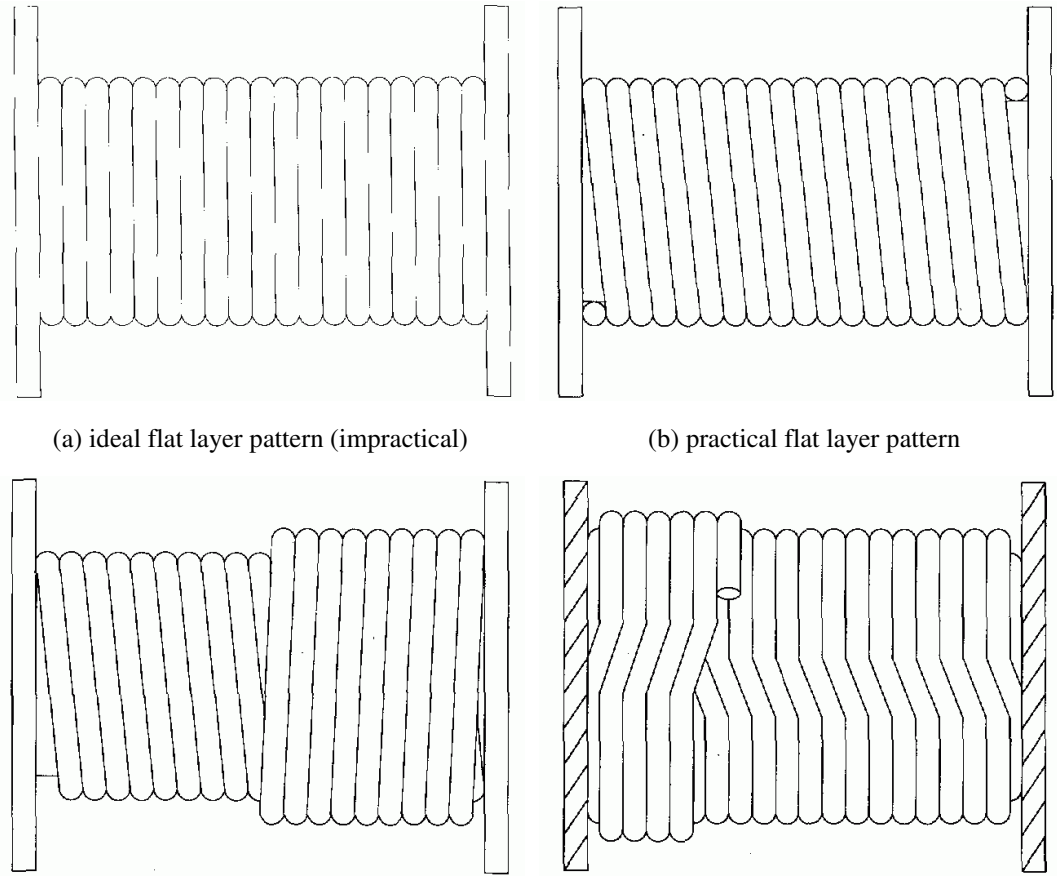

(a) ideal flat layer pattern (impractical) (b) practical flat layer pattern

(d) practical multilayer pattern (d) orthocyclic pattern (perfect)

Figure 5.9. Coil winding patterns [224].

A final consideration in the treatment of coil winding is the need for application of optimum tension in the wire. Tension in excess of the optimum tends to deform and change the characteristics of the wire while inadequate tension may let the wire wander during winding, creating unevenly spaced turns, even with automated controls. If winding is to done by automated machines, control of this tension may have to accommodate several factors [226], including the ever changing winding conditions. A recently invented technique for use with thick wire [227], along with application of the right tension, is the use of a 'reverse bend' for coils created on a form. If the traverse of the winding machine is made to advance by a pitch of the wire in a chosen direction, a reverse bend is achieved by passing the wire over the pulley system to make the wire lay flat against the coil form. The effect of this technique can be appreciated, even visually as seen in figure 5.10, in the straightening of the layers. Using this technique, it is possible to reduce the amount of wire in the coil by up to 15%.

Having considered the three factors of cost, winding pattern and the required tension in the wire, these may be be combined, together with the stator core geometry, to

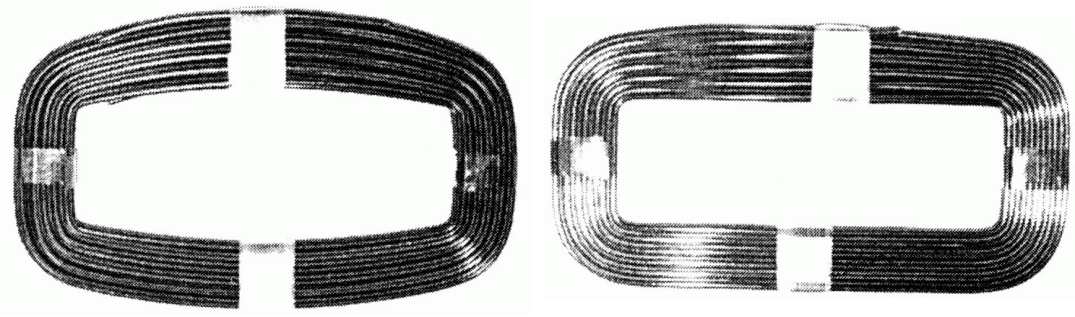

(d) without reverse bend (d) with reverse bend

Figure 5.10. Coil winding technique for thick wires [227].

determine the approach for the winding. The basic choice on the approach appears to be between winding by manual and machine. The process of manual winding can be slow and labour intensive but relatively high slot fill factors can be achieved. If only a prototype machine is to be produced or only a few samples of the machine are needed, this approach can be generally effective. The machine winding approach easily leads to automation and can rapidly produce large volumes of samples. A winding machine deploys one or two or all of the winding jigs: needle, nozzle and fly winder [228]. Since the wire-guiding jig needs room to manouver in the slot, there is invariably some space left unfilled in this winding approach and leads to lower fill factor, not exceeding 40%. However, if the coils are pre-wound before assembly the restrictions of the jigs are eased and can produce coils of remarkable fill-factor. There have been some remarkable designs of stator cores that exploit the method of prewinding the coils before assembly [223], [229], [230], which can be classified in two ways way, broadly following the complexity of the stator tooth geometry:

- ***Stator tooth tips without overhangs.*** In single-tooth configurations, this type of stator core is manifested as one with open slots and the coils have to be fixed to the core by some means. As the tips are straight, pre-winding the coil winding is relatively easier, even when the stator core is not modularised. The slot fill factor may increase, up to 60%, but since the motor characteristics are affected in different ways by the open slots whose form is specific to the type of motor, they need to be weighed against the benefits of easy assembly.

- ***Complex tooth tips***. Tooth presentations of tips with any form of overhangs may be considered as complex tooth tips. One arrangement may be made to have the teeth to be straight before winding, which are then pressed by a special tool into the required shape of the overhang after winding [229], illustrated in figure 5.11 (a).

The forming of the tooth tip into shape after winding causes considerable distortion and deformation of the tooth tips, but may be an excellent choice for joint-lapped cores. Another type of arrangement [230], shown in figure 5.11 (b), uses asymmetrical modularisation of the stator core so that preformed coils may be easily slipped onto the tooth from one end and avoids forming the tooth tips into shape

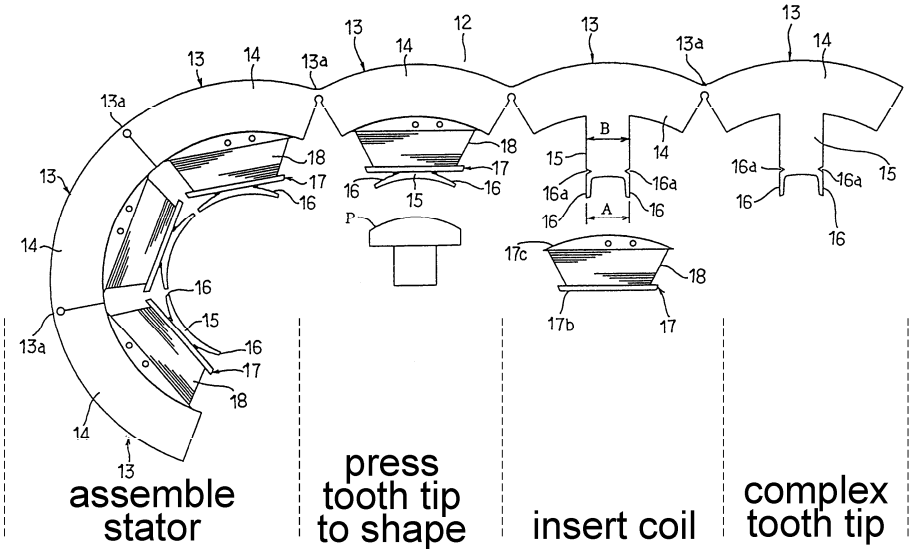

(a) sequence of assembly for formable complex tooth tips [229]

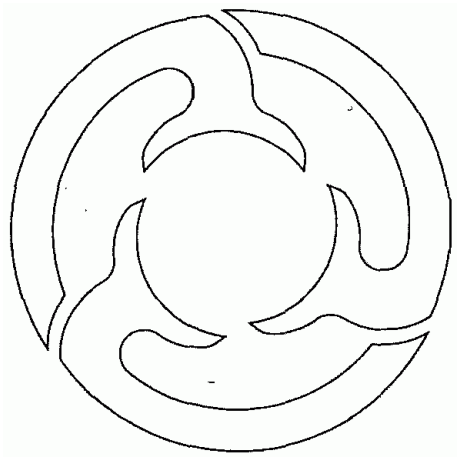

(b) asymmetric modularisation of stator core for easy insertion of single-tooth pre-formed windings [230]

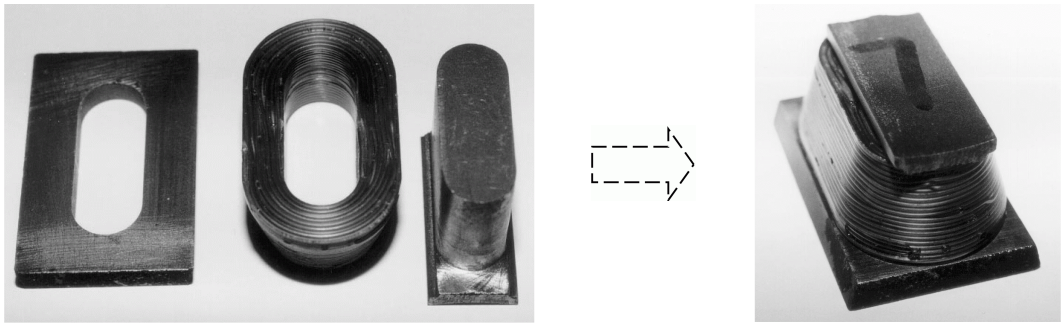

(c) accommodation of pre-wound coils on stator teeth with complex tips [231]

Figure 5.11. Modern production approaches for stator cores.

after assembly. If the teeth can be produced separately from the yoke [231] (figure 5.11(c)), as may occur with isotropic materials, an opportunity arises to pre-form and possibly pre-press the coils on a former for high fill factor before slipping them on to the teeth and assembly. The work in [231] has demonstrated that a machine with preformed and pre-pressed windings is superior to conventionally wound machine if the stator is of soft magnetic composite (SMC) rather than laminated iron core, taking special advantage of the isotropic properties of SMC.

In concluding this section on the consideration of approaches to windings for single-tooth arrangements, it is reiterated that as there several ways to produce single-tooth windings, the number of factors that are involved need to be considered to determine the best choice on the defined criteria. Simplicity, low cost and an easy bent on automation are qualities generally sought for mass production, but these factors may be waived in considering production of prototypes or a few samples of a machine.

5.5.4 The 12-tooth stators

The two stators for wound-field and permanent-magnet implementation were produced using two different approaches and two different production methods. The complete core and modular section were the approaches applied separately to either one of the two types of stator cores, whilst the laser and EDM cutting methods were the production methods for laminations applied to either one of the two stator cores. The geometries followed for the stator teeth for both types of stators and for the magnets have been discussed in the previous sections. Some of the features and production stages of two types of the stators are shown in figure 5.12.

The stator for the wound-field implementation was prepared as 30°-modular section laminations from non-oriented silicon steel and manufactured by the laser-cutting method. Stacking of the laminations along the axis was aided by a bonding agent and application of moderate pressure. The teeth assemblies were then manually pre-wound with single-strand solid wire before assembling the wound-stator sections to form the complete stator core. Winding before assembly, as followed in the wound-field arrangement, achieved a slot fill-factor of 48.2% using 1.4-mm diameter wire. Specially prepared but simple jigs and spiders were used to centre and align the stator sections on the circumferential layout.

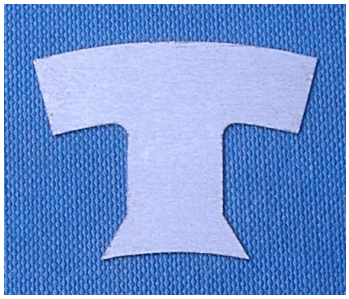

(a)modular stator section lamination

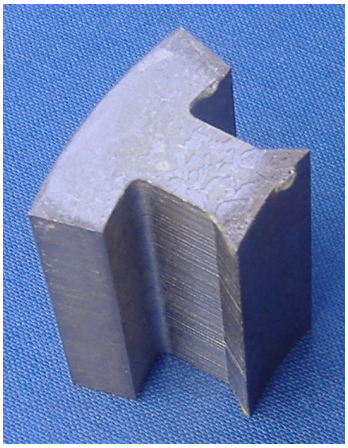

(b) assembled stator section

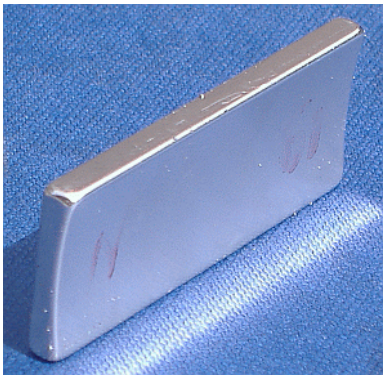

(c) magnet for pm stator showing curved airgap surface

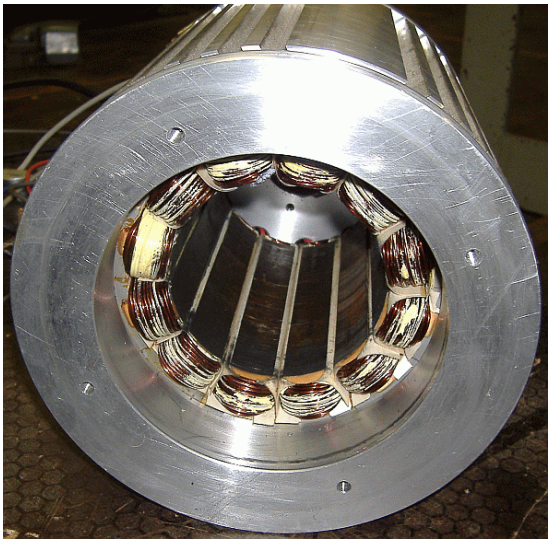

(d) assembled wound-field stator

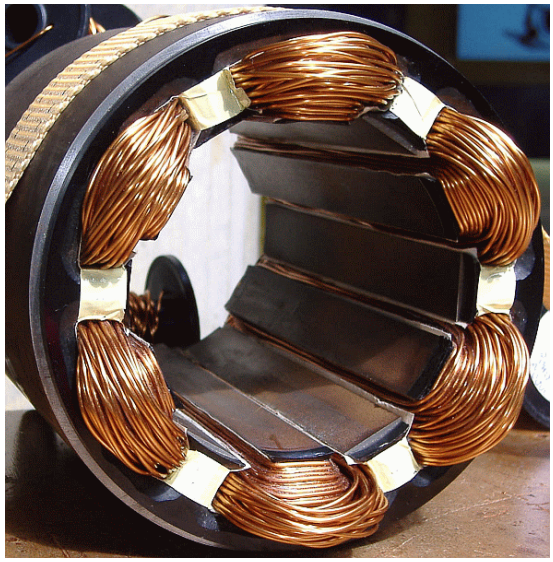

(e) assembled PM stator

Figure 5.12. 12-tooth stators' components and assembly.

Contrasted with the wound-field construction, the stator for the permanent magnet implementation was prepared as complete core laminations. The stator laminations were stacked and bonded with adhesive and application of high pressure before cutting into shape by wire-erosion EDM. The inner outline of the stator comprising the airgap needed to be of a fine finish and so, in addition to the initial rough pass, a second and fine-finish pass of cutting was applied on this outline. The outcome, after completion of cutting, was a complete stator core ready for winding. A reverse bending winding approach was contemplated to fill the slot with the required number of turns but restrictions of working space in practice and the large number of layers of windings compared to the wound-field arrangement counted against it. The coils were laid by looping the wire over the tooth and applying the regular forward bend, a method which seemed more practical and successful for the manual hand-winding approach. Due to

springing of the wire on the straight runs, a property of the forward bend, and variable tension in different parts of the coil, it became increasing difficult to lay coils after the 7th or 8th layer. As a result, 65% of the coil turns were laid by looping the wire over the tooth and the remaining 35% were laid by threading the wire through the slot. A slot fill-factor of 47.2% using 1.25 mm diameter wire was achieved by this method.

Rare earth magnets (Neodymium-iron-boron) were prepared as three sections along the axial length and bonding to the tip of the stator teeth was accomplished with a strong industrial adhesive. As there was strong axial repulsion of magnets placed next to each other, the two outer magnets were placed in first, with the middle magnet following to easily slip in between the two. The flat surfaces on the bonding surfaces of the magnet and the tooth tip ensured ease of placement of the magnetised magnets.

5.5.5 The 8- and 5-segment rotors

The rotor laminations and the shaft were cut into shape by wire-erosion EDM. The segment laminations for both the 8- and 5-segment rotor were produced with semi-circular protrusions and the non-magnetic shaft was of high-strength aluminium alloy grooved with matching semi-circular indentations to enable firm press fitting on assembly. Parallel to the flat side of the semi-circular protrusion and tangent to the curved surface of the outline of the protrusion, were two flat resting surfaces for circumferential location of the segments. This gives a simple, but mechanically strong arrangement which can be replicated for mass production. Once pressed into the grooves, the laminations were further tightly held in place by aluminium discs bolted at both ends of the shaft. The views in figure 5.13 show components of the rotor, including semi-circular protrusions, the matched indentation on the shaft and the process of assembling the laminations into a complete rotor.

5.5.6 Auxiliary components

Machine components that are not participating in the electromagnetic behaviour of the machine are classified as auxiliary components. Their principal function is structural support or thermal consideration or both, and, to some extent, aiding assembly of the machine. The auxiliary components playing a role in the structural composition of the machine are the rotor shaft and the stator casing. The stator casing is also usually

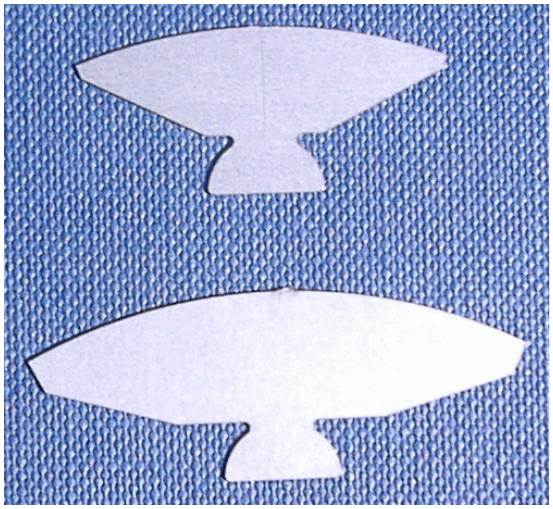

(a) The 8- and 5 segment laminations

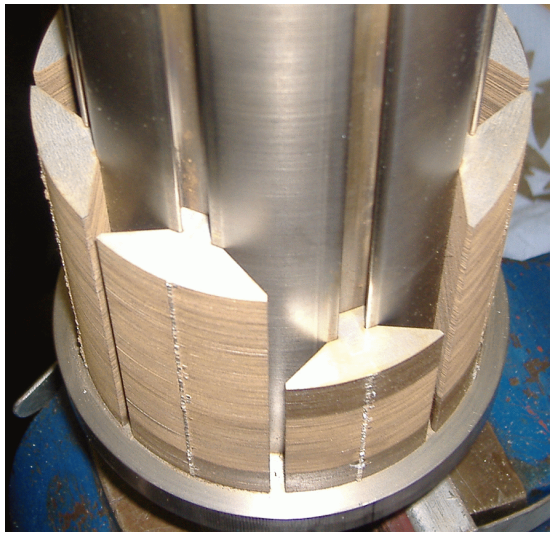

(b) assembling the 8-segment rotor

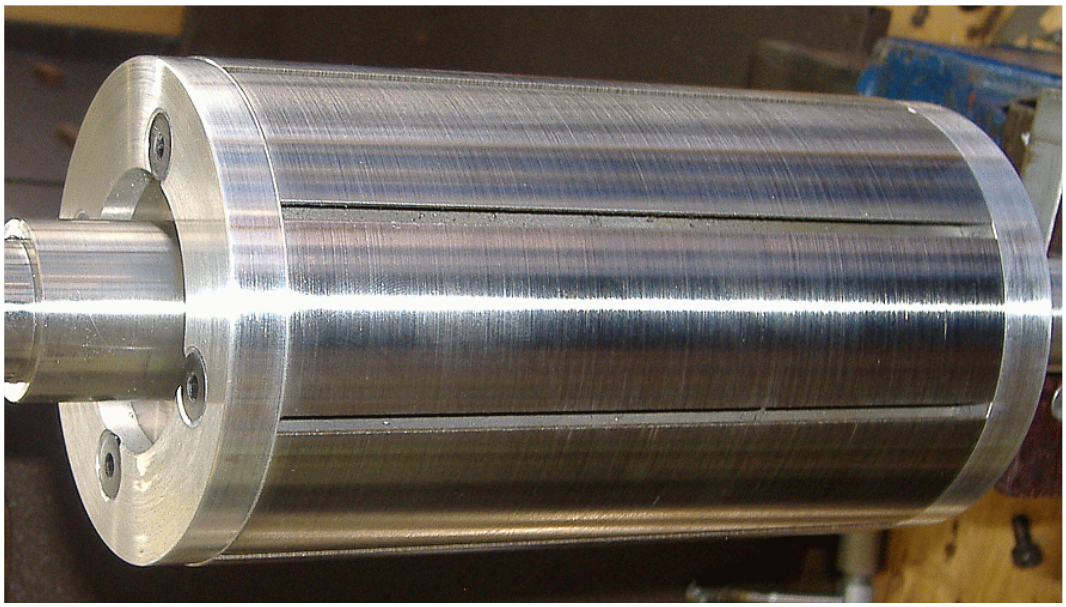

(c) The fully assembled and turned 8-segment rotor

Figure 5.13. The 8- and 5-segment rotors' components and assembly.

designed with thermal considerations in mind. The components considered to be aiding assembly are the end-discs on the rotor.

The rotor shaft was built in two parts, designated as an inner and outer part. The outer part, forming the sleeve for supporting the segment laminations, is built of duralumin, this material is selected for its nonmagnetic property, high strength and good durability. Ironically, by the requirement of being nonmagnetic, it may be considered in the main to be taking part in the electromagnetic behaviour of the machine. The support of the laminations is attained through the semi-circular grooves located on the circumference of the sleeve which mate with the semi-circular protrusions of the segment laminations,

illustrated by figure 5.13 (b). The sleeve could be made of nonmagnetic stainless steel for ultimate strength and durability but, in practice, it is difficult to ensure that the steel graded as nonmagnetic has permeability close to that of air. The inner part of the rotor is solid cylinder of standard steel stainless steel, for strength and rigidity against deflections normal to the axial direction. This cylinder has stepped extensions of smaller diameters on either side for sequentially locating the bearings and terminal couplings for the feedback device coupling or loads. As can be seen in figure 5.14, a lip is essential at one end of the cylinder for bracing the sleeve at one position on the axis of shaft, whilst a keyway in the inner part of the sleeve ensures the sleeve is locked against rotational slip on the shaft.

Since the two discs at the ends of the sleeve are in direct contact with the segment lamination, they are required to be made of a nonmagnetic material. In this application duralumin was also employed for the discs. Loading of the machine is expected not to exceed current density of 10 A/mm^2 so that cooling of the machine on the surface is by natural convection of air or forced-air convection at high and prolonged loading. Thus, the outer casing of aluminium alloy can be of simple cylindrical shape, but may be enhanced for this type of cooling by having grooves on the surface, as seen in figure 5.10 (d), to increase the surface area and direct the air-flow.

5.6 Conclusion

In this chapter, an account has been given of the considerations for the design and construction of three phase flux switching machines with segmental-rotors. Although there is a myriad of factors and parameters to consider in designing and construction of an electrical machine, this consideration has drawn on the wealth of information accumulated for similar configurations of machines such as those of concentrated windings and segmental rotors. Inevitably, as these types of machines are new inventions, there have been some fresh considerations and new methods devised to satisfy their design and construction requirements.

The choice to design the 12/8 and 12/5 topologies for construction is intended to develop a topology with optimum performance and to test the varied and intricate characteristics of the flux switching principle using segmental-rotors in three phase arrangements. In both configurations, the stator tooth and rotor segment dimensions applied in the design are the optimum on the basis of electromagnetic torque capability

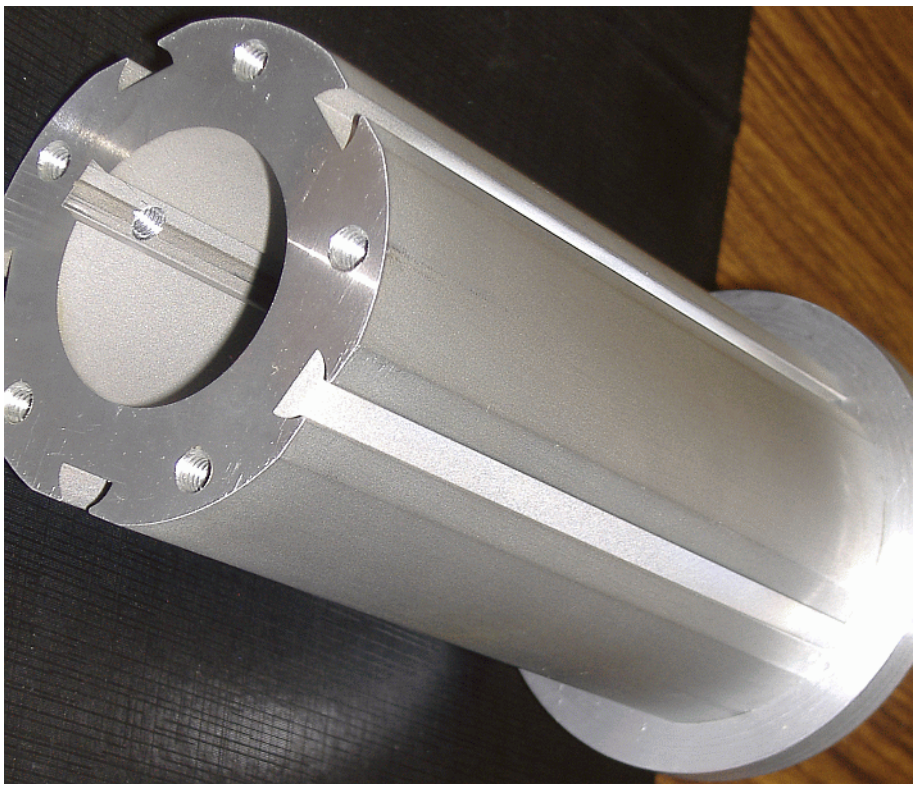

(a) outer sleeve for 5-segment rotor

(b) inner shaft

Figure 5.14. Rotor shaft components.

and total harmonic distortion of the induced EMF. As the topology of the machine on the 12-tooth stator configuration is distinguished by number of segments on the rotor, the wound-field and PM stators are intentionally designed to fit either of the two types of rotors, so that is possible to configure two wound-field machines and two PM machines using two rotors only.

Considerations of the approach and methods of manufacturing of machines of this type have been presented, highlighting the attraction of simplicity and low overall cost of the construction process. The stators and rotors for this study have been produced by

variation and combination of more than one of the modern production methods and construction approaches. The production methods and construction approaches employed have been fully described and contrasted.

Performance measurement and testing on the two wound-field and two PM configurations are the subject of the next two chapters.

Chapter 6

Testing and performance of wound-field machines

This chapter reports the test results and performance measurements of the three-phase wound-field machines whose design and construction have been considered in the last chapter. Two configurations of the experimental machines are tested: the 12/8 and 12/5 configurations. The tests include the no-load running test, the static load test and thermal characterisation. The performance of the 12/8 machine is measured by operating in synchronous mode as a motor, up to full load and the available DC link voltage of the drive. Finally, a comparison with the established machine types of similar configurations is made.

6.1 Introduction

For the wound-field configurations, the field orientation has to be one polarity for a field tooth and of the other polarity for the next field, so that the excitation is constant for each individual tooth but alternates up one tooth and down the other. In practice, this is achieved by connecting the coils in series to a single DC source supply and by reverse-connecting every other field coil. The DC source employed is adjustable so that variable field current may be easily applied. Figure 6.1 shows the configurations of topologies and the connection scheme of the field coils for all the practical measurements on the 12/8 and 12/5 configurations.

6.2 No-load Test: Induced EMF

Induced EMF at no-load is a form of initial parameter measurement and involved coupling the rotor of the motor under test to a brushless servomotor which acted as a prime mover. The test machine with field-only excitation was then driven by the servomotor at required speed. The armature EMF was observed using a high bandwidth (350 MHz) digital oscilloscope. Initially the EMF was observed at a fixed speed of 500 rpm and subsequently, the speed was varied from 100 to 1500 r/min. The measured EMF (waveform and rms) were compared directly against the 2D FE predictions. Predicted EMF was obtained by the "flux linkage" concept from within the finite element modelling package by invoking the transient analysis solver on the 2D model.

6.2.1 The 12/8 configuration

With the first case of fixed speed at 500 r/min and variable excitation from 3.5 to 14 A, and the second case of fixed excitation at 14 A and variable the speed from 100 to 1500 r/min, the measured and predicted EMF waveforms are shown in figure 6.2. and 6.3, whilst a comparison of rms EMF is made in figure 6.4. The general appearance of the EMF waveform at low excitation is one with a trapezoidal shape in one alternation and a stepped trapezoidal shape in the other alternation, and conforms to a good degree to the expectation described in the idealised principle of operation. The linear relationship between the generated EMF and the field excitation, with indication of saturation at high excitation, is evidently apparent and so is the linear relationship between the EMF and the speed, when the speed is varied between 100 and 1500 r/min at fixed excitation.

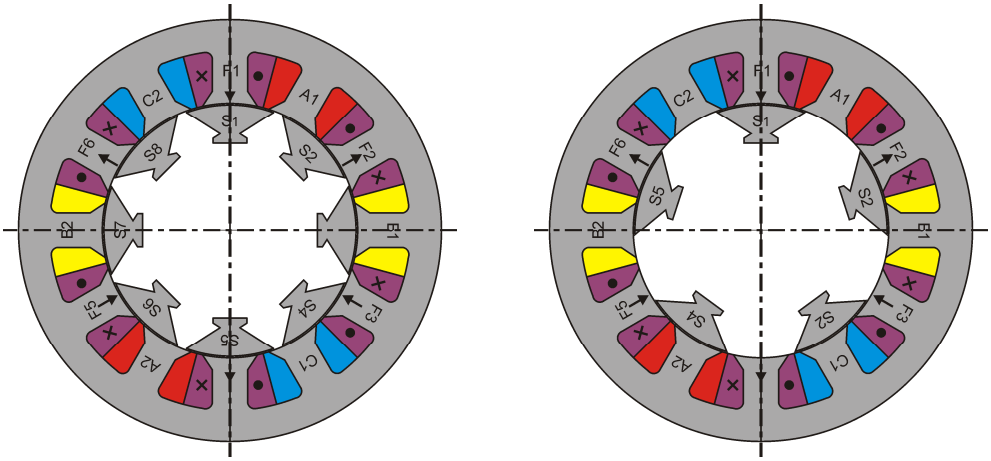

(a) 12/8 FSM (b) 12/5 FSM

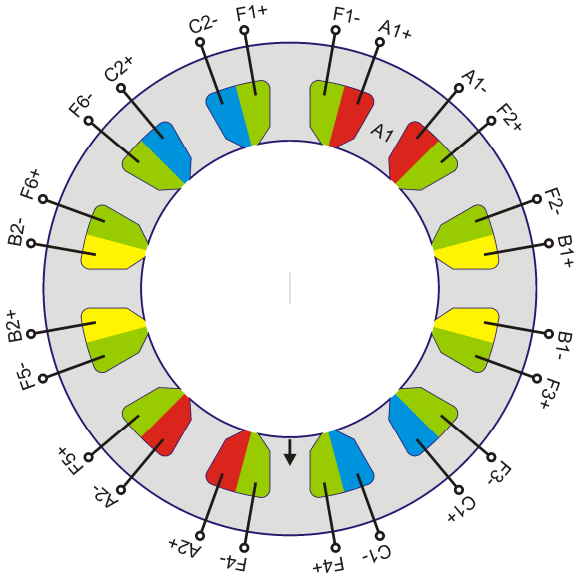

(c) coil designation

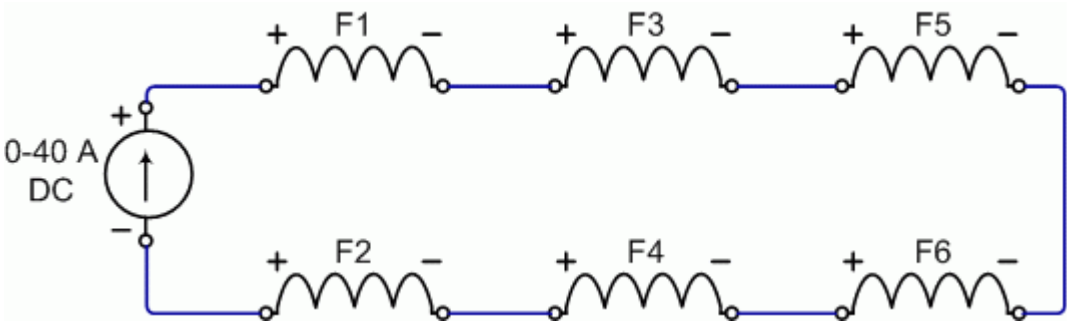

(d) Scheme for field connection for flux switching

Figure 6.1.Topology deployment and coil terminal designation in wound-field FSM.

Whilst the EMF waveforms are quasi-sinusoidal, the lack of similarity and symmetry between the alternations is striking but this is expected for the 12/8 arrangement. As predicted in chapter 4, each of the armature coils in the flux switching arrangement employing a segmental rotor produces unsymmetrical alternations of the EMF waveform and the alternations of the complementary coils which constitute a phase

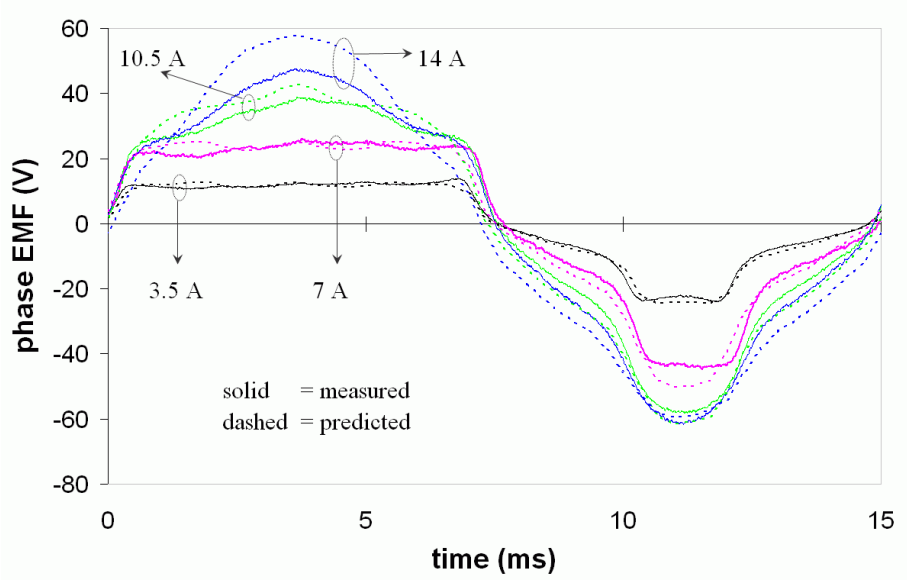

(a) phase EMF waveforms

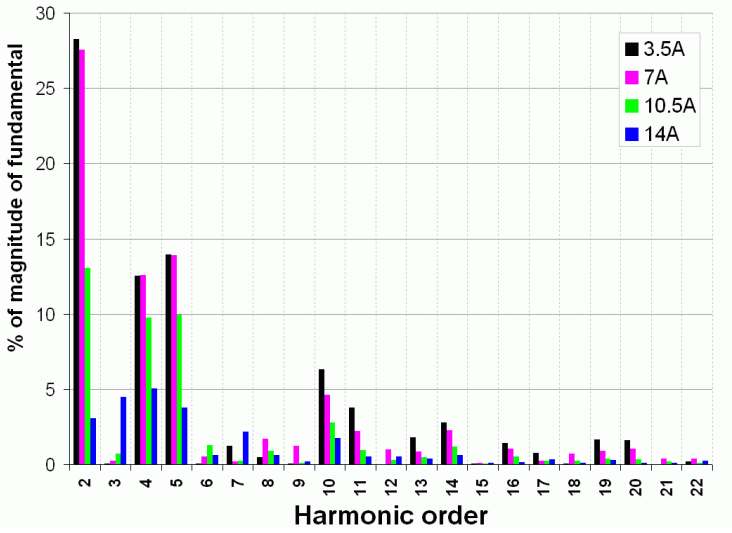

(b) harmonic decomposition of predicted phase EMF

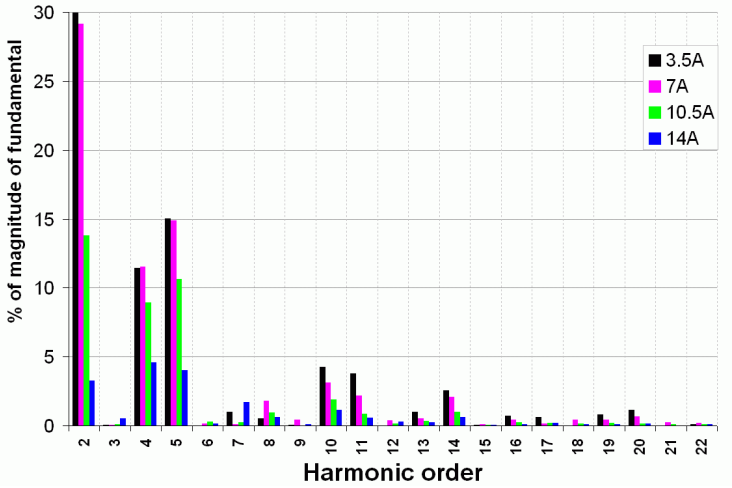

(c) harmonic decomposition of predicted line EMF

Figure 6.2. Induced phase EMF waveforms at 500 r/min and various field excitations for the 12/8 configuration.

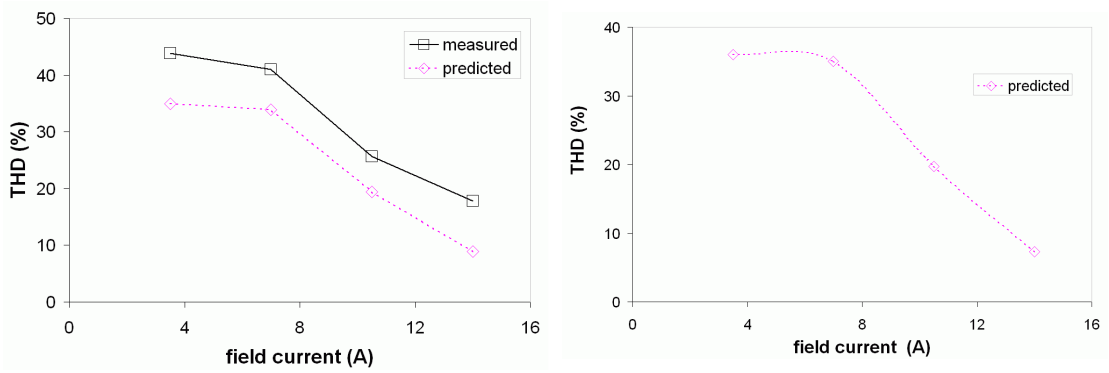

(a) phase EMF (b) line EMF

Figure 6.3. THD with varying field excitation for 12/8.

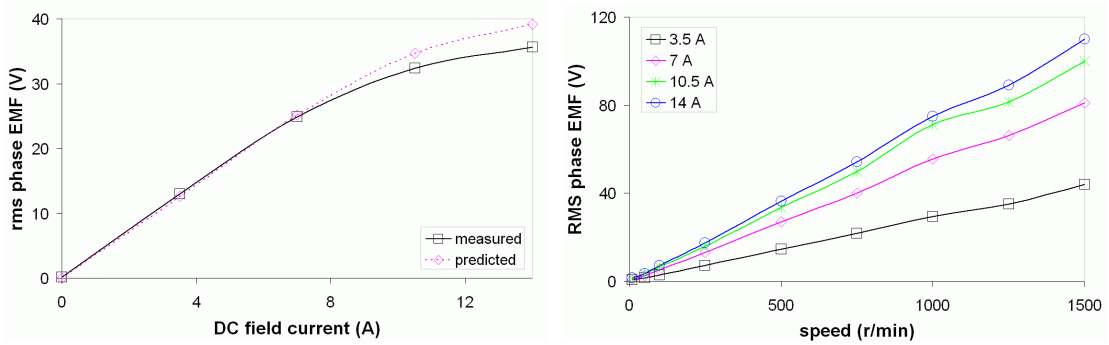

(a) with field excitation at 500 r/min (b) with speed at various field excitations

Figure 6.4. RMS armature phase voltage

remain synchronised and in phase. The resultant phase EMF is therefore unsymmetrical. The effect of the field excitation is also remarkable, wherein it is seen that the waveform tends to be less unsymmetrical and more sinusoidal with increase of field current. The harmonic spectrum up to the 22nd harmonic are shown in figure 6.2 (b) and (c) for four levels of excitations. Considering the measurement results, the total harmonic distortion of the phase EMF falls from 43.8% at 3.5 A to 17.8 % at 14 A of field current as shown in figure 6.3. There is no significant difference between the phase and line EMF in the behaviour of the THD with field current, but the harmonic spectra show that the triplen harmonics are notably absent in the line EMF.

The predicted results show reasonable agreement with the measurement results when field excitation is less than 10 A, with the error not exceeding 5%. There is an overestimation of the predicted rms EMF values for field currents over 10 A, but this error is limited to within 10%. The error in the predicted instantaneous EMF, as compared in the positive alternation of the waveform with 14 A field excitation, is close to 18%. These deviations are within the expectations of employing 2D FE modelling.

6.2.2 The 12/5 configuration

A set of tests similar to the one performed on the 12/8 configuration were repeated on the 12/5 configuration for the induced EMF. It must be pointed out beforehand that the variation of the rms EMF with field current at fixed speed and with speed at fixed field current are almost identical to that of the 12/8 configuration in figure 6.4. Both the 12/5 and 12/8 configurations produce nearly the same phase rms EMF (37.5 and 35.6 V, respectively) at the rated field current of 14 A when running at 500 r/min. These results are in agreement with predictions from the FE models. As the 12/8 configurations produces more electrical cycles in a fixed period of time than the 12/5 topology by a factor of 8/5 (= 1.6), the EMF produced by the 12/8 configuration is predicted, from basic principles, to be greater than that of the 12/5 by this factor. However, it may be recalled from chapter 4 that the 12/5 configuration produces a peak armature flux linkage which is greater than that of the 12/8 topology by a factor of 1.47. By accounting for these differences as quantified by these factor, it is becomes clear why the EMF of the 12/5 and 12/8 topology are nearly the same.

Despite the similarity in the behaviour of the rms value of the EMF, there is an important distinction between the EMF waveforms for the 12/5 and12/8 configurations which has been verified by measurement. The alternations of the phase EMF waveform for the 12/5 are identical and symmetrical, as shown in figure 6.5. The alternations of the EMF of the complementary coils that constitute a phase are dissimilar and unsymmetrical, as in all considered configurations of FSM with a segmental rotor, but the alternations in configurations with an odd number of segments are transposed in time, so that the series combination of the two coils to make a phase results in the phase EMF which has identical and symmetrical alternations. The harmonic spectrum of the phase EMF of the 12/5 configuration, as shown in figure 6.5 (b) , is composed of odd harmonics of which the 3rd harmonic is dominant after the fundamental, when field current is high, while the 9th is equally prominent when field current is low. However, the line EMF harmonic spectrum is devoid of the triplen harmonics as seen figure 6.5 (c). The symmetry of both the phase and line EMF for the 12/5 configuration is reflected in the absence of even harmonics in the spectra, and the improvement in the quality of the waveforms towards a sinusoid is reflected in the lower values of the THD, more so for line than phase quantities, as shown in figure 6.6.

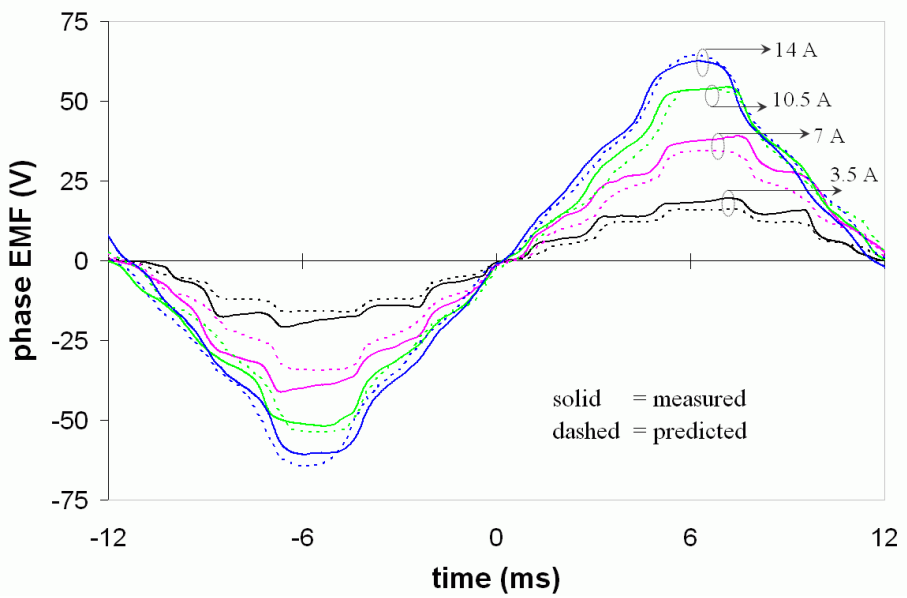

(a) phase EMF waveforms

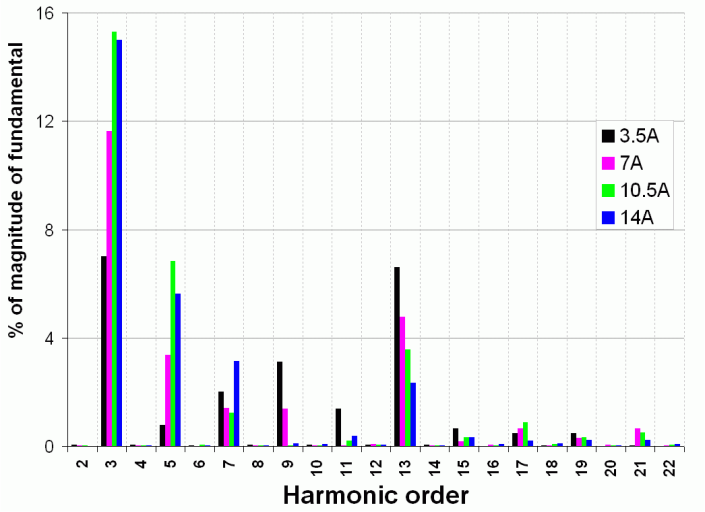

(b) harmonic decomposition of predicted phase EMF

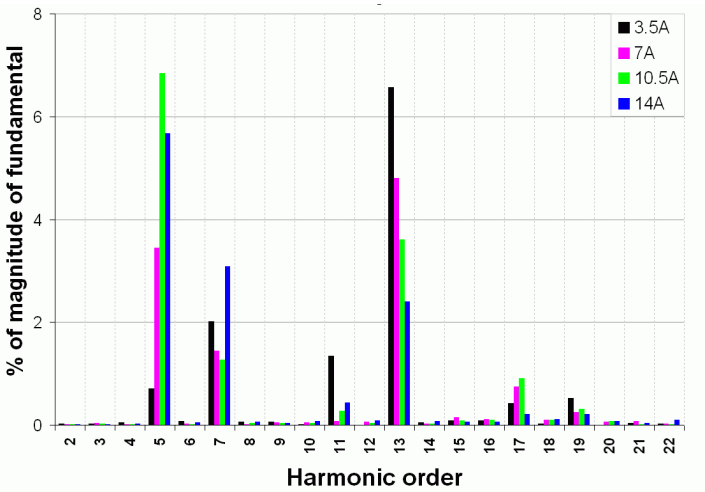

(c) harmonic decomposition of predicted line EMF

Figure 6.5. Induced EMF waveforms at 500 r/min and various field excitations for the 12/5 configuration.

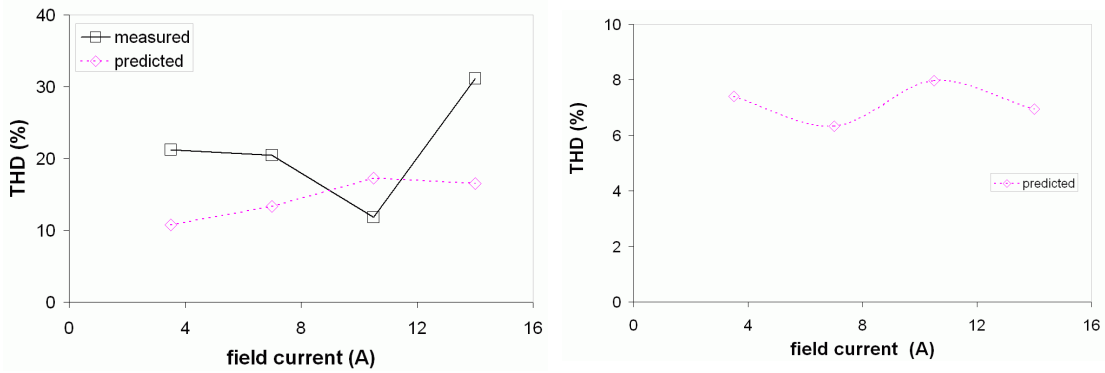

(a) phase EMF (b) line EMF

Figure 6.6. THD with varying field excitation for 12/5.

The error between the measurement and the prediction of the EMF waveform does not exceed 13%. A surprising outcome is that the error appears to be such that the measured values are higher than the predicted values for field currents up to 10.5 A. This is apparently due to the significant fluctuation of the DC field current even at no-load, which was not the case with the 12/8 configuration. The DC field current settings were primed on the measuring oscilloscope set to rms value, but the reading of DC supply's inbuilt meter reflected a mean value which did not account for the fluctuating AC component. This seems to suggest that the machine was actually excited with mean DC currents higher than the DC current depicted in the measurements set. The ripple on the DC current at no-load was entirely unexpected and explains the decision to initially ignore the distinction of the mode of the reading (rms or mean) as they are indistinguishable when there is no ripple.

6.3 Load Test: Static Torque

Static torque test results were measured using an in-line torque transducer with the rotor shaft locked on a rotary dividing-head, with defined positions over one electrical cycle. A snapshot of the instance of the three phase operating condition may be represented by connection of three phase winding to a single DC supply in one of the two ways. The first way is when the current is at $\frac{\sqrt{3}}{2}$ of the positive peak in one phase and at $\frac{\sqrt{3}}{2}$ of the negative peak in the second phase, while there is zero current in the third. This can be realised by connecting the first two phases in series but opposing polarity to the DC current source, and leaving the third unconnected. The second way is when the current is at positive peak in the one phase and half the negative peak in the other two phases. This is implemented by connecting one phase in series with the parallel combination of

the other two phases to DC supply. The second method has the advantage that there is more even distribution of the heating sources, depicted by the energised of the phases, around the machine than in the first. However, this method assumes that the two parallel-connected phase windings are exactly identical to share the current equally, in amounts half that of the series phase. In practice, it is not unusual to find slightly unbalanced phase windings and the error that may arise due to the assumption of identical windings is avoided by using the first method. The second method, whose scheme connection on the FSM is depicted in figure 6.7, was employed for the illustrated test results for the 12/8 configuration, with field winding supplied from a separate DC source and connected as shown previously in figure 6.1. The first method was employed for the illustrated test results of the 12/5 configuration.

In both the 12/8 and 12/5 the measured torque was compared directly with predictions made using the "Maxwell Stress" concept within the finite element simulations. These measurements were taken at several levels of field excitation, in steps of 3.5 A for field current and 5 A for armature current.

6.3.1 The 12/8 configuration

Figure 6.8 shows the results of the static torque at the rated field current of 14 A for 12/8 configuration. There is a possible 7.2 % error band in comparing the values of simulation and measurement results on the position scale, arising from the digitization in steps of 1° (mechanical) from independent starting positions. Low values of the measurement set were also particularly susceptible to errors due to poor stability of the readings on the lower end of the range. Allowing for these errors and the assumptions

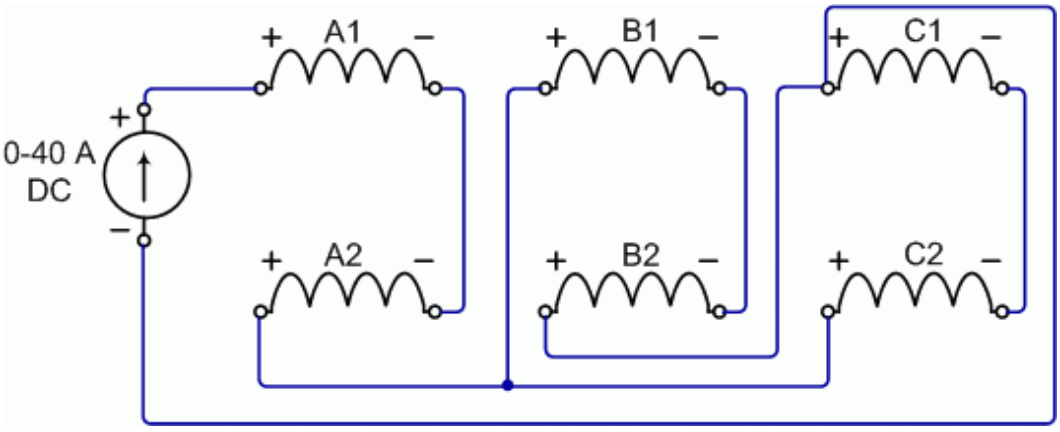

Figure 6.7.Schemtatic connection of armature coils three phase static torque test on the 12-tooth stator.

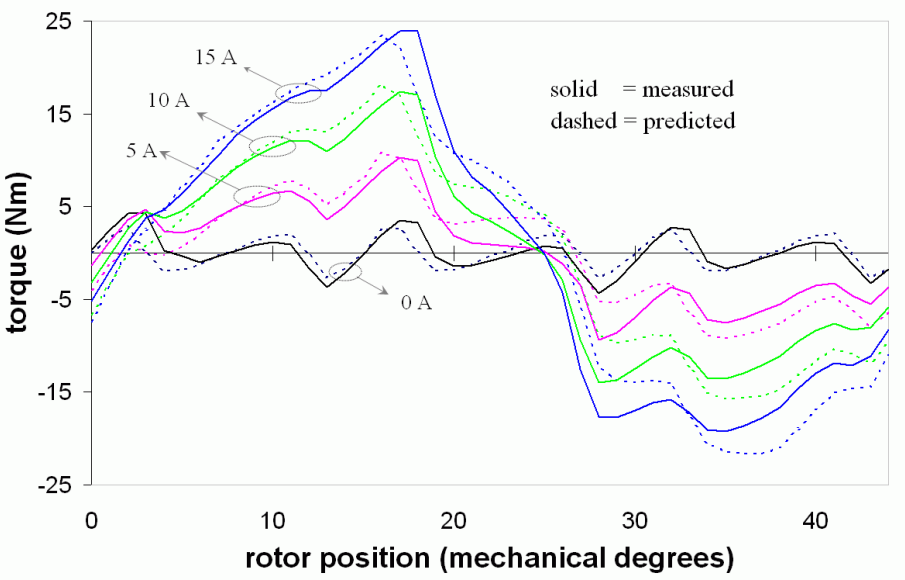

Figure 6.8. Static torque at 14 A field current and various armature currents for the 12/8 configuration.

of the 2D model, the measurement results agree within these reasons with the simulation results, with the worst mismatch in the peak values being at about 2% difference for the highest armature current used and at about 35.5% difference when no armature current is applied.

The torque increases approximately linearly to a maximum as the dominant rotor segment moves from the aligned position with the armature tooth and starts to reduce sharply as the next segment builds overlap from the other side of the tooth. Torque changes polarity at the point where an armature tooth is overlapped in equal measure by both a receding and an approaching segment. It is also obvious to see that this is a point of torque instability with respect to position. After this position torque has changed polarity and tends to be at a constant value until there is no overlap of the first segment with the armature tooth. The torque then falls sharply but linearly as the next segment builds overlap with the armature tooth up to the alignment position, when the new cycle begins.

The cogging torque in this machine, measured when there is no current in the armature, is significant. It is manifested as six sub-cycles in one electrical cycle (i.e. dominated by the 2nd order triplen harmonic cogging torque) corresponding to the effect described in chapter 4, and profiles the overall torque curve with undulations when the armature is energized. Some methods to reduce the cogging torque and the torque ripple in general have been presented in chapter 4.

Conventional machines with distributed windings give a sinusoidal presentation of static torque with position. In this machine, the results show the expected discrepancy in the positive and negative alternations of the torque, similar to the presentation of the EMF waveform.

6.3.2 The 12/5 configuration

The variations with rotor position of the positive and negative parts of the static torque, from the position of zero torque, are identical for the 12/5 configuration. This result is illustrated in figure 6.9 for rated current in the windings and is in agreement with the expectation for this configuration whose phase EMF alternations are also symmetrical and identical. The variation of the torque with rotor position closely resembles the sinusoidal shape and is similar to the presentations of static torque for conventional AC machines. The cogging torque is lower than that of the 12/8 topology at the same field excitation by factor of about ½ and only slightly ripples the profile of the total static torque. The magnitude of static torque with field excitation and armature current varies in proportion with the level of the current, similar to the 12/8 configuration.

The prediction of the static torque closely follows that of the measurement, when the armature is energised, but the error between measurement and prediction appears to be high for cogging torque. Reading the measurements when there was no current in the armature was generally unreliable as the values were at the low of end of the full scale

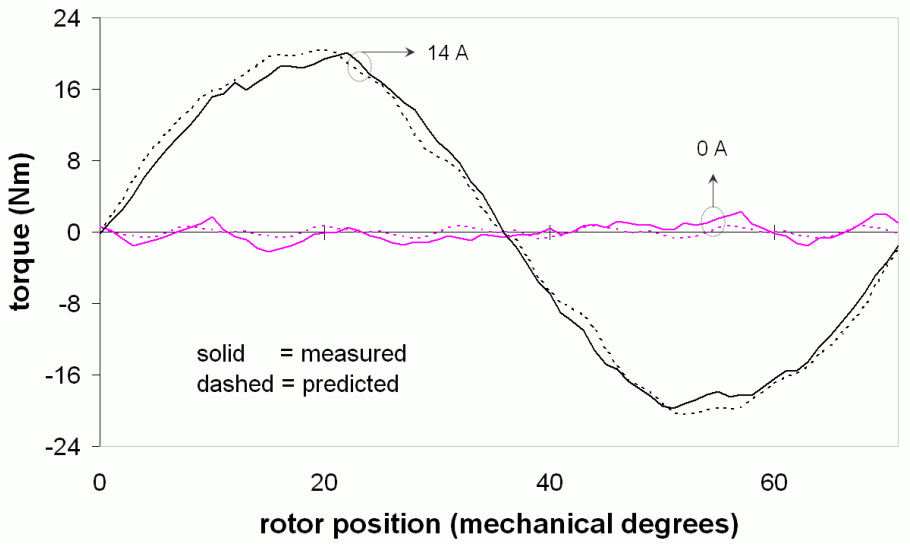

Figure 6.9. Static torque at 14 A field current and two values of armature current for 12/5 configuration.

of 50 Nm, and may account for this significant discrepancy, in which the measured cogging torque appears to be higher than the predicted cogging torque. Additionally, the torque meter has an accuracy error of ±0.5% of full-scale-deflection, giving a starting error of ±0.25 Nm.

6.4 Thermal Characteristic

A test was performed to establish the basic thermal behaviour of the wound-field machines, in which both the field and armature systems generate heat. As the thermal capacity of the 12-tooth stator harbouring an 8-segment rotor is nearly the same as when harbouring a 5-segment rotor, only the 12/8 configuration was tested. The machine had two thermocouples, one attached to the winding conductor in the slot and the other to the casing of the machine. The general test involved energising all the coils, connected in series for even dissipation and transfer of heat, with a moderate current (approximately half of the anticipated full-load current, i.e. 6.5 A) from ambient conditions and observing the conductor and casing temperature for 90 min.

The characteristic shown in figure 6.10, was with a desk-fan placed about 40 cm from the machine and blowing a steady stream of air perpendicular to the axis of the casing at a specified airflow of about 2100 m^3/h. Under these operating conditions, the thermal characteristics for the machine were derived and are shown in Table 6.1.

Table 6.1. Basic parameters of thermal characteristics for wound-field machine

Thermal time constants	**slot-to-casing (conduction)**	4.05 min
	casing-to-ambient (convection)	10.56 min
100°C temperature rise in conductor	**Power loss**	458.6 W
	rms current	13.6 A

6.5 Synchronous Performance

The performance of the 12/8 configuration was investigated when run as a synchronous motor. Two identical commercial three phase AC drives, one for the test motor and the other for load machine, were applied to perform the tests initially at a fixed speed of 500

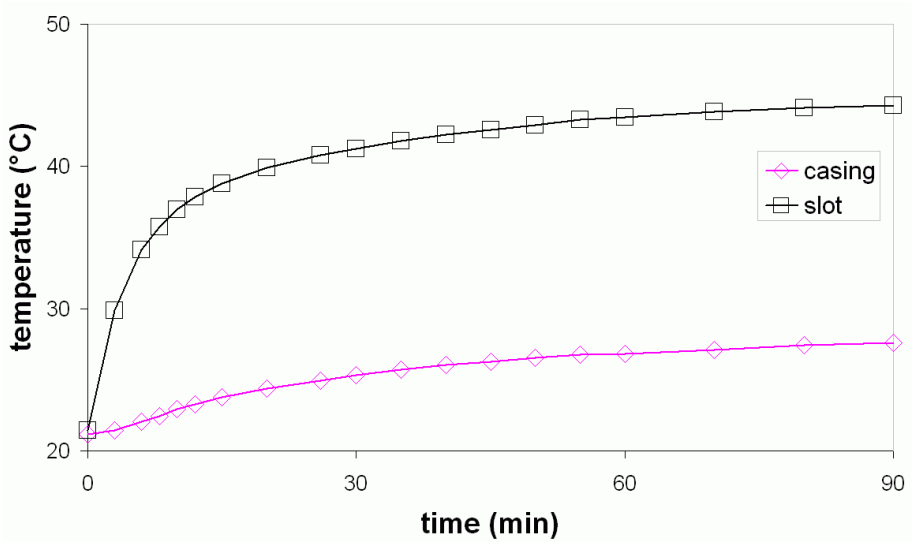

Figure 6.10. Thermal behaviour of the wound-field machine.

rev/min and then at various speeds up to nearly the base speed. The test motor was coupled to a permanent magnet servo-machine with a regenerative drive which acted as the load machine. The drive for testing the motor is designated for universal operation of three phase AC machines, and consequently, running of the motor required adaptation to the most appropriate operating mode, 'servo mode' in this case, which for operation of traditional AC motors uses the rotor flux reference frame with stator currents placed in the quadrature axis [232]. This mode of operation, in effect, implements the $i_d = 0$ control method [233]. To use this drive, the 12/8-experimental machine was translated as an equivalent 16-pole conventional permanent-magnet synchronous motor. With closed loop speed control selected for the motor drive, the AC drive applied sinusoidal current control implemented as a PWM scheme at a selected maximum switching frequency of 6 kHz. Rotor position feedback was employed using an absolute encoder.

6.5.1 Torque

The graphs for torque in figure 6.11 verify the flexible characteristic of the torque, controllable by both the field current and the armature current. The mean torque output increases proportionally with the armature current and with the field current. At high currents, saturation effects come into play. Knowing that the measurement graphs are for the mechanical output torque and the predicted graphs are for the electromagnetic torque, which includes windage and friction, the differences, which range from 1.2% at low loading and 9.5% at the highest loading, are expected and also serve to underline the 2D simulation assumptions and some mismatched measuring conditions. The

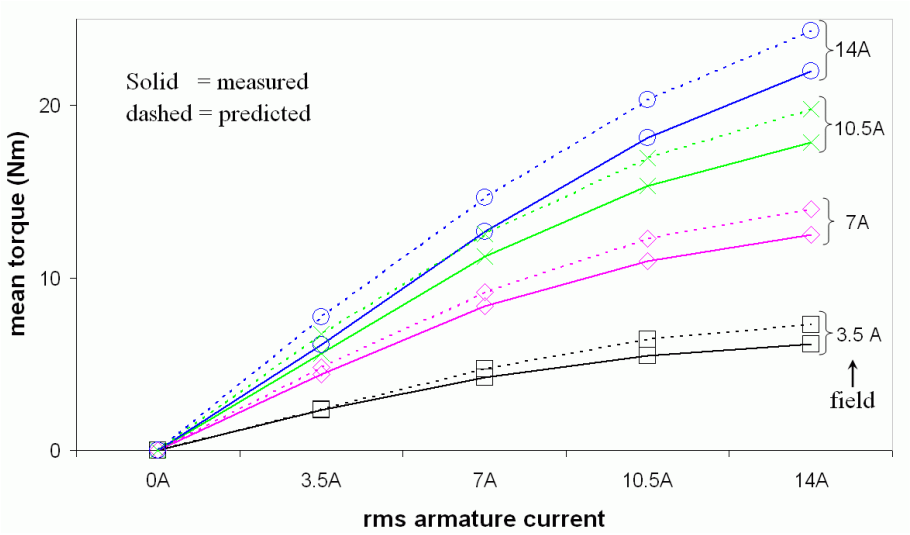

(a) variation of mean value with currents

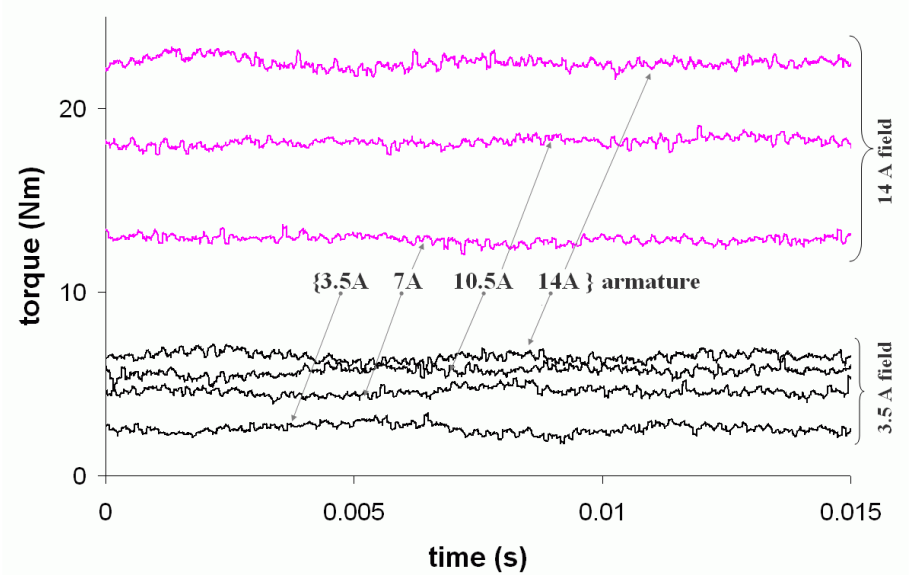

(b) waveforms

Figure 6.11. Output torque at 500 r/min.

measured AC armature currents used to benchmark the points for recording mechanical torque contained harmonics while the simulation values assumed pure sinusoidal armature currents, which made the actual fundamental rms value of the measurement somewhat lower at every benchmark point. Additionally, the measured DC field current, whose waveform is examined in the next section, presented a ripple while the simulations used steady and constant DC values.

As shown in figure 6.11 (b), torque ripple was noticeable in the measurement results, more at low field currents and high armature currents than at other conditions. This is in contrast to the appreciable ripple in the electromagnetic torque predicted by simulations at similar operating conditions and presented in chapter 4. It is thought that, in practice

and in these tests, the inertia of the rotating mass has the tendency to smoothen the torque.

6.5.2 Armature and field current waveforms

The armature current waveform was a good sinusoid, underlying a robust current control scheme of the PWM drive, although a slight distortion appeared at high loading. Current ripple in the DC field circuit was present at all load conditions, although barely perceptible at light loads. As can be seen for the situation with rated currents in figure 6.12, the ripple was at three times the electrical frequency and the peak-to-peak variation was at approximately 19% of the mean DC value. The content of current ripple observed across the range of loadings in this three phase arrangement appears to be substantially lower than that in the single-phase arrangement reported in [123], where the extent of the oscillations interfered with the stability of current control. The postulation was that three phase configurations would eliminate current ripple in the DC field winding by coupling a resultant null effect. Evidence in this investigation shows a noticeable reduction of the ripple. This outcome is expected because the EMF induced in the field winding by the armature reaction flux is, for this design, still substantially distorted from a sine wave. With the presence of a fluctuating field excitation, the contribution of this effect on the form of the torque, and particularly the torque ripple, should be acknowledged.

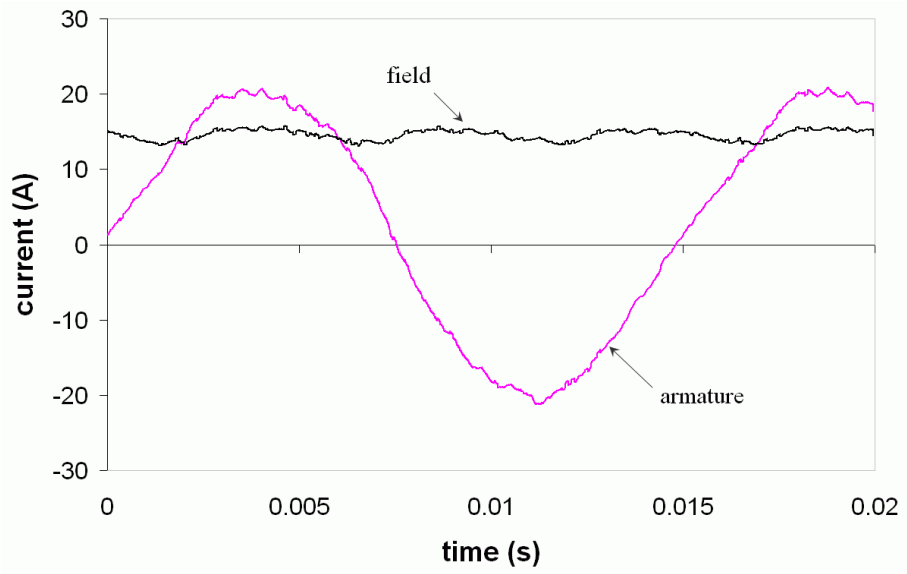

Figure 6.12. Current waveforms at rated currents and 500 r/min.

6.5.3 Power, efficiency and power factor

This section deals with power measurement results at a fixed speed of 500 r/min. The measured output power was proportional to the field and armature currents, in agreement with theoretical expectations. The total efficiency, including losses in the field winding, initially rises with loading of the armature but starts to fall after reaching a maximum value, except when the field current is possibly 3.5 A and less. This is illustrated in the measurement results in figure 6.13, where the maximum efficiency of 68.65% at 3.5 A field current occurs at the lowest armature loading and progressively falls with increasing armature current to the minimum of 46.5% when armature loading is at maximum. At field currents greater than 3.5 A, the maximum efficiency is obtained

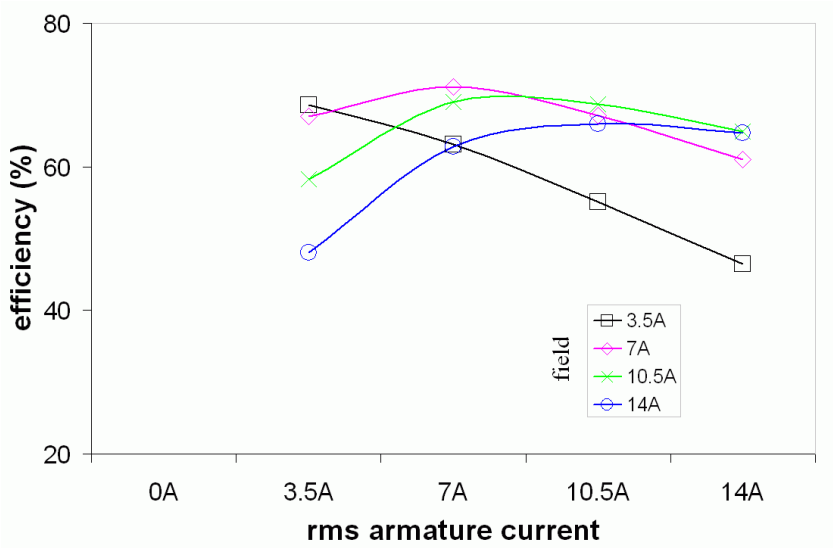

(a) total efficiency variation with armature current

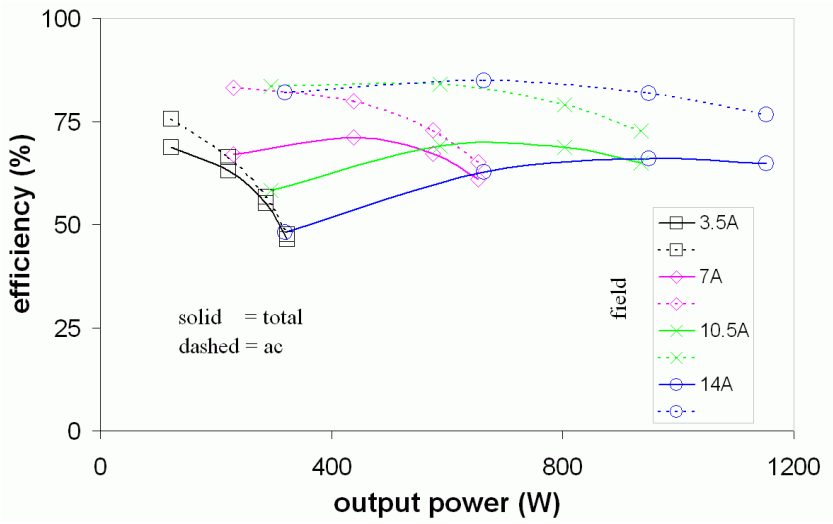

(b) with varying output power

Figure 6.13. Variation of efficiency with load.

when armature current is between 50 to 80% of the full-load value and is in the range 66-71%, depending on the field current. The range of output power, for locating the efficiency curves, is influenced by both the field and armature current, as seen in figure 6.13 (b). The contribution of the losses of the field circuit to the total efficiency is illustrated in figure 6.13 (b), where the total efficiency is plotted alongside the ac efficiency. The ac efficiency is evaluated as the efficiency without taking into account the losses in the field circuit. The total efficiency when field current is low, i.e. less than 3.5 A, is not significantly higher than the ac efficiency, but the difference between the two becomes substantial as the field current, and hence the power range, is increased.

The power factor, according to the measurement results illustrated in figure 6.14 (a), varies inversely with the armature currents at all levels of field excitation. On the other hand, at any specified armature current, the power factor appears to be linearly proportional to the field current. It is a combination of a high field current and a low armature current that gives the maximum power factor, measured at 0.9 when field current is 14 A and armature current is 3.5 A in the considered tests. At rated conditions and compared to other AC machines, the power factor is poor. It is thought that an increase of field turns and a reduction of the armature turns in the design may help improve the power factor.

The line-to-line terminal voltage increases approximately linearly with the armature current, as shown in figure 6.14 (b), but appears to be less affected by the change in the field current. For instance, at 14 A armature current, the change in the terminal line voltage as field current changes from 3.5 A to 14 A is a reduction of 12% in the required terminal voltage. The trend of demanding a lower terminal voltage with increase of field current is maintained at all levels of field excitation except when field current is less than 5 A, when it is reversed.

The complex behaviour of the power factor and terminal voltage as the field and armature are varied can be studied theoretically by the equivalent circuit representation of these quantities as mapped on a vector diagram. The field current influences the terms with open-circuit flux linkage, whilst the armature current influences the voltage drop terms of the armature resistance and inductance in the representation. The influence of both the field and armature current is indeed complex, but the measurement results for the operating power factor and terminal voltage at specified values of field

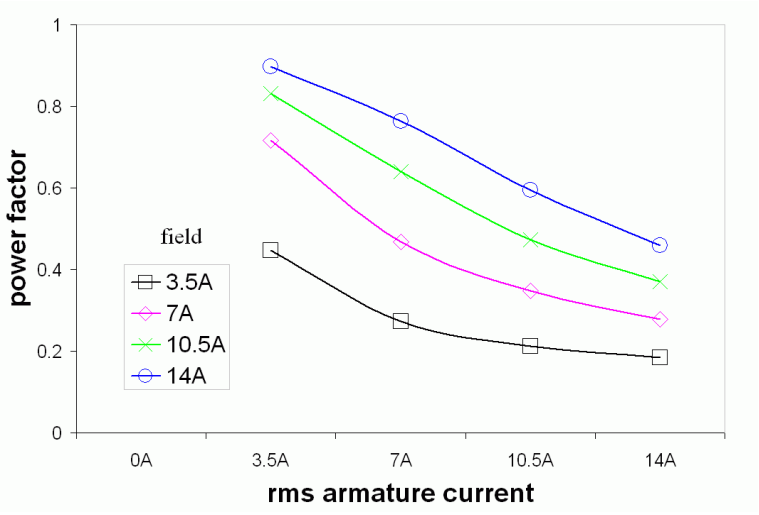

(a) power factor

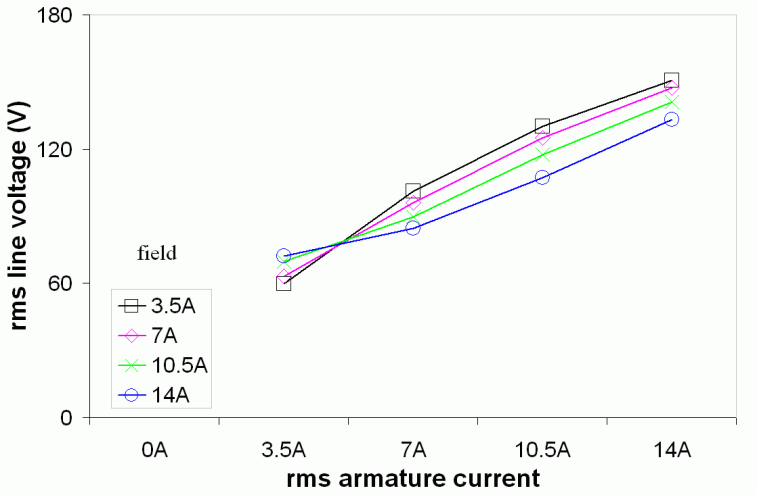

(b) terminal voltage

Figure 6.14. Variation of power factor and armature terminal voltage with load.

and armature current for motoring in the FSM have been revealed and are consistent with the behaviour of the conventional wound-field synchronous motor.

The armature reaction increases proportionally with current and is the principal cause of the fall of power factor and the rise of terminal voltage with current. The simplified phasor illustration in figure 6.15 (b) for constant field excitation and speed, shows both the power factor angle, ϕ and terminal armature voltage, V_a rising, for the case of doubling the armature current of figure 6.15 (a).

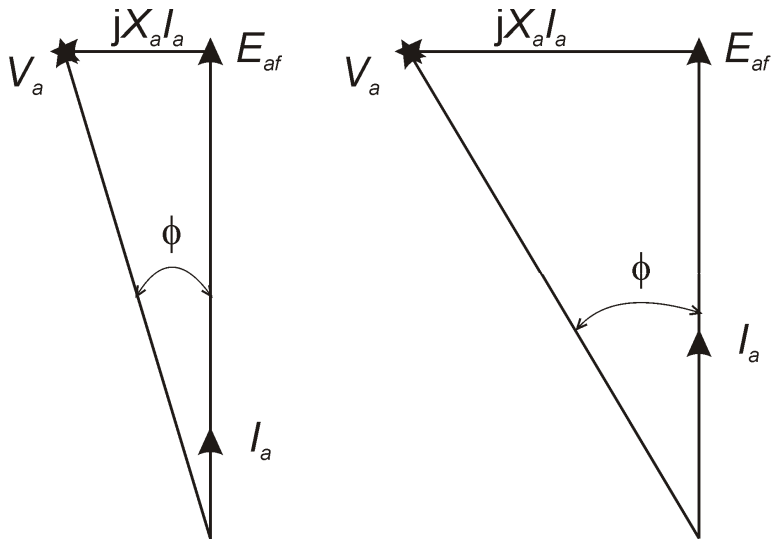

(a) high power factor (b) low power factor

Figure 6.15. Effect of armature reaction on power factor and terminal voltage

6.5.4 Performance with speed variation

In the tests, values of output torque for a speed range of 100-1250 r/min at a rated field current of 14 A were recorded to reveal the performance characteristics with speed, shown in figures 6.16-6.19.

At constant armature current the torque speed-curve is a straight line with a small droop, typically about -1.5 x 10^{-3} Nm per r/min, shown by figure 6.16. The point of instability for speed control occurred at a progressively lower speed with increase of armature current but was difficult to capture with good precision as the operation of the drive depended on a constant speed. The base speed of the motor at 14 A field excitation on the 400-V drive would be determined by locating the speed at which the drive, set to speed control, starts to lose stability of controlling the speed as speed is increased. This was found to be about 1500 rev/min at no-load and about 1300 rev/min at rated load (14 A field and armature currents) and is the point of inception of field weakening.

Characteristic of electrical machines, the efficiency increases with speed as shown in figure 6.17 and it appears that maximum efficiency at a specified torque or armature current would occur at maximum possible speed, while maximum efficiency at a specified speed would occur at maximum torque or armature current, the field current remaining fixed.

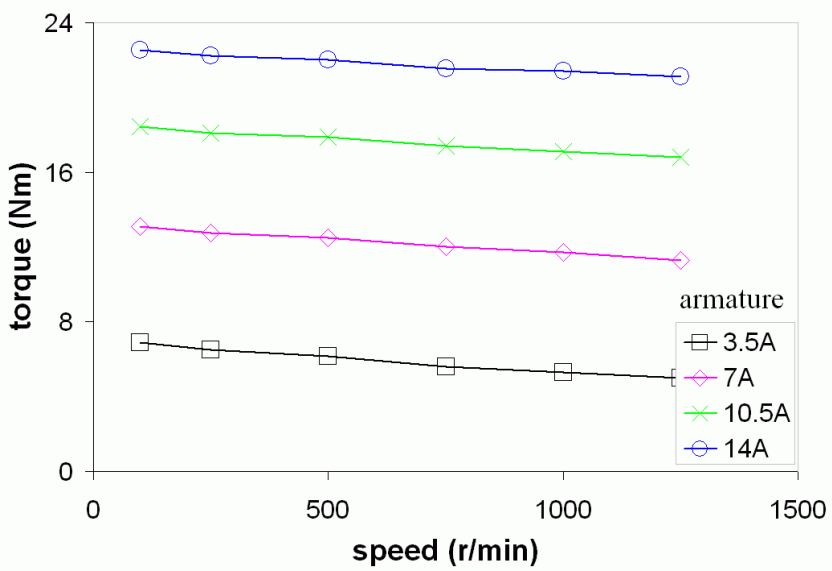

Figure 6.16. Mean output torque with speed

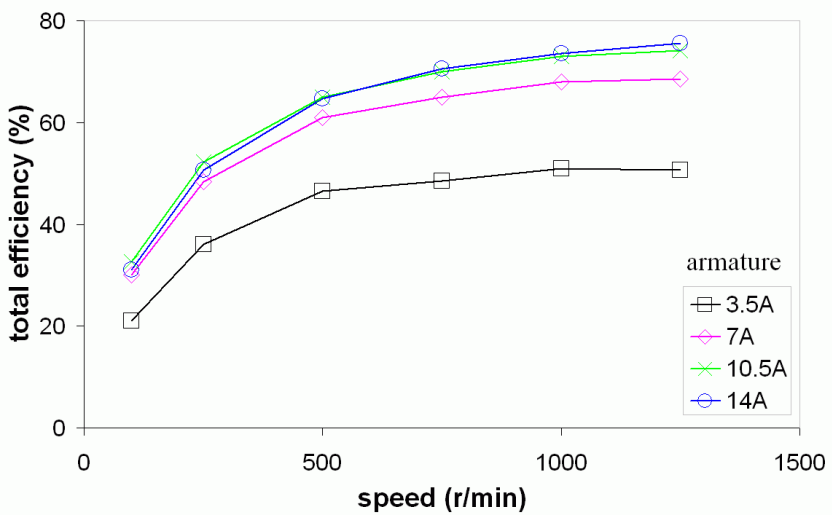

Figure 6.17. Total efficiency with speed

Although the power factor falls with increase of speed at constant field current, as seen in figure 6.18, the change is not significant for high armature current, but may be in the order of about 50% for low armature currents, between the lowest and highest speeds in the considered range. The variation of the terminal voltage with speed at the specified field current and various armature currents is proportionally linear and is illustrated in figure 6.19 for 14 A field current. This relationship may be applied to infer the base speed of the motor on a drive of specified voltage. For instance, in this application with a 400-V drive, it is observed that if the voltage-speed curves are extrapolated beyond the recorded value 1250 r/min, the curve meets the 400 V level close to 1500 r/min, the speed beyond which the drive starts to run out of volts and must operate in the field weakening mode if equipped by the control. This is in good agreement with the approach described at the beginning of this section where the base speed of the 400-V

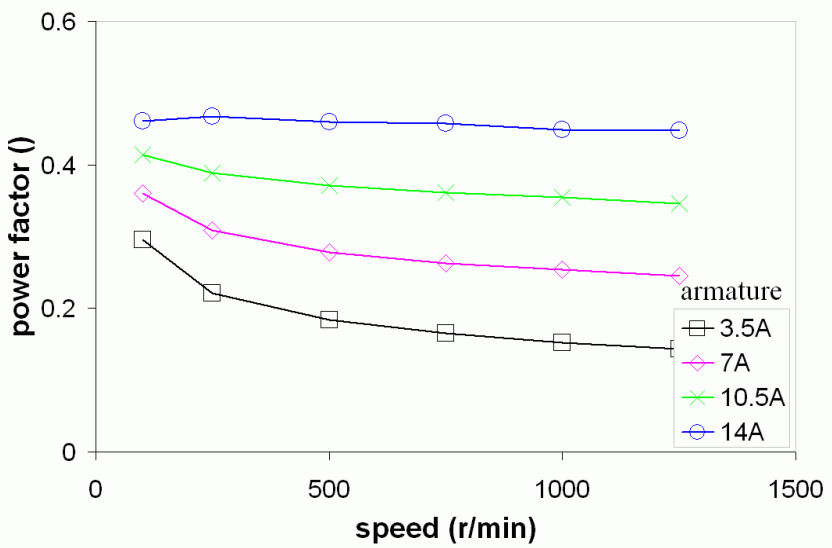

Figure 6.18. Power factor with speed.

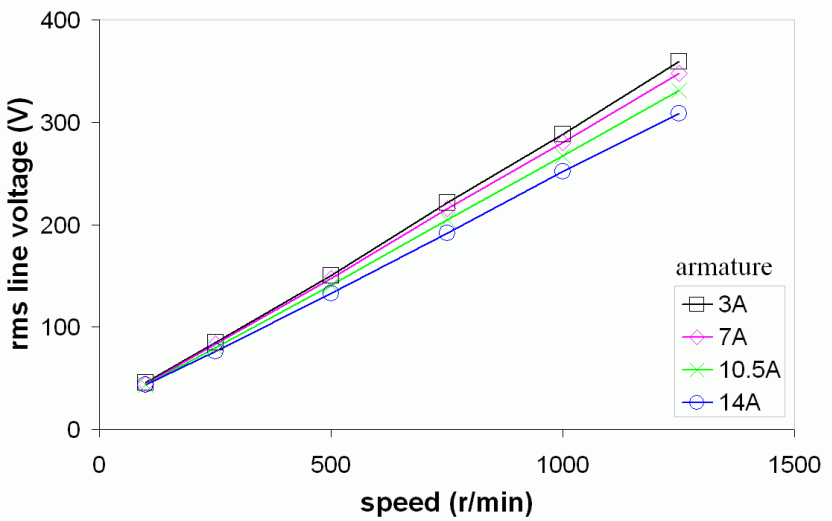

Figure 6.19. Terminal line voltage with speed.

drive was revealed by estimating the speed at which stability of speed control is disturbed.

6.6 Comparison with Other Similar Machines

The principles of the wound-field flux-switching motor employing a segmental rotor are a relatively new concept but the ultimate configuration of the motor bears resemblance to configurations of some well-established motors. It is thought that the physical configuration of a synchronous reluctance motor, especially the type with a segmental rotor [153], may be similar to the FSM employing a segmental rotor and differs in the main on the assignment of the stator coils the field and armature systems in the FSM. Another type of well-established motor with resemblance to the FSM employing a

segmental rotor is the switched reluctance motor, typically those employing a segmental rotor [155]. They differ from the FSM employing a segmental rotor only in that all the coils typically carry a switched dc current. A comparison is made of the FSM with a synchronous reluctance motor employing a segmental rotor, based on FE simulation results and with a series of different types of switched reluctance motors, based on practical measurement results.

6.6.1 Synchronous reluctance motor

Following the geometry and specifications of the 12/8 FSM employing a segmental rotor, an equivalent synchronous reluctance motor SyRM may be realised. The design of the rotor for the SyRM takes various forms [151], thus:

- toothed rotors
- segmental rotors
- flux barrier rotors (typically, axially laminated with distributed anisotropy)

Designs with salient-pole toothed rotors are known to have relatively low reluctance torque and poor power factor due to their low saliency ratio. Rotors with segments or flux barriers give significant improvement to the performance of the SyRM. For strong resemblance to FSM employing a segmental rotor, this comparison is made with a configuration of the SyRM employing a segmental rotor. Using eight rotor segments, the equivalent SyRM is an 8-pole motor, with semi-closed slots carrying a concentrated single-tooth winding (figure 6.20 (a)). This winding design configuration gives comparatively low torque. For a fairer comparison, an alternative winding configuration in the form of concentrated winding with overlapping winding is used as in figure 6.20 (b).

As can be seen in table 6.2, the 12/8 wound-field FSM has torque capability and torque density at 300 W winding loss which are more than twice the values for an equivalent 8-pole SyRM. Although this may not be used as a general or definitive relation of the performance between the FSM and SyRM, as there are other improved forms of rotors for SyRM with L_d/L_q = 10-12 [151], this comparison serves to show in one way the gain of arranging machines for production of excitation torque rather than for reluctance torque.

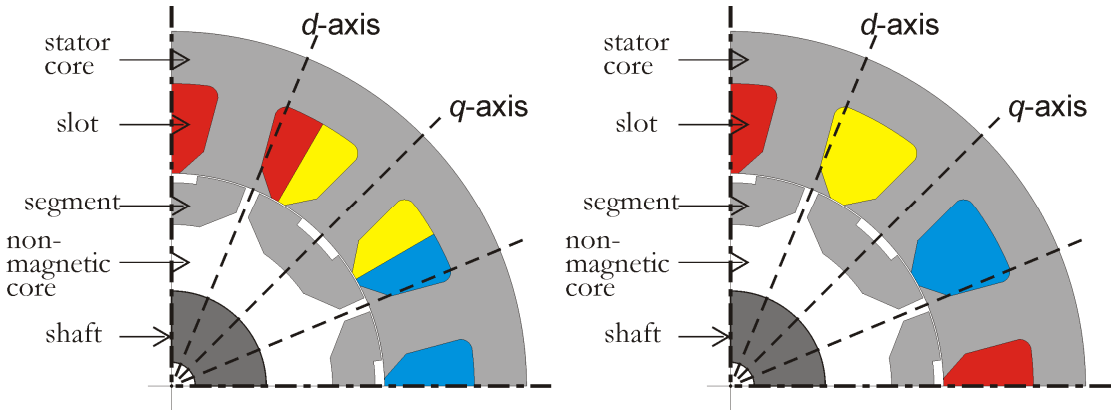

(a) concentrated single-tooth winding (b) concentrated overlapping winding

Figure 6.20. Configuration of 8-pole SyRM on the 12-tooth stator.

Table 6.2. Comparison of FSM with SyRM

Type of motor	**Saliency ratio, L_d/L_q** ( )	**Torque Capability** (Nm)	**Torque density** (kNm/m^3)	**Torque ripple, (of max.)** (%)
12/8 wound-field FSM	-	26	27.2	34.9
SyRM: single-tooth	2.22	3.33	3.5	69.0
SyRM: overlapping	4.52	9.96	9.96	61.2

6.6.2 Switched reluctance motors

A series of SRMs, with the same stack length, outside diameter, and similar slot-fill factor [156], is compared on torque density with the experimental wound-field FSM operating as synchronous motor. The comparison in table 6.3 is on the torque density at a winding loss of 300 W, corresponding to rms current of about 11 A (current density of 7.2 A/mm^2), against three types of switched reluctance motors, ranging from the conventional to the high performance configurations.

As designed, the wound-field synchronous motor has a torque density comparable to that of the conventional toothed-rotor motor, but substantially lower than that of the optimised high performance segmental rotor machine. The 12/8 wound-field motor in this study is a preliminary design and improvements in this value of torque density can be expected with optimisation of other parameters.

Table 6.3. Comparison of torque density with SRMs

Type of motor	**Torque density** (kNm/m^3)
12/8 wound-field FSM	19.9
12/8 toothed SRM	19.3
12/8 segmental SRM	28.7
12/10 segmental SRM	28.9

6.7 Conclusion

Testing and measurement of performance of the wound-field FSMs employing a segmental rotor have verified the characteristics portrayed from the predictions by FE simulations. Additionally a thermal characterisation has identified the loading capability of the experimental machines.

The tests reveal an AC induced EMF in the phase of the 12/8 configuration which is rich in harmonics and with dissimilar and unsymmetrical alterations of the EMF waveform. The EMF waveform for the 12/5 configuration was found to be largely symmetrical with less harmonics than the 12/8 topology. In both types of configurations of the machine, the distortion of the EMF waveform appears to be influenced by the field current, with high field current generally producing less distortion. These findings are consistent with the predictions from FE simulations, and the remarkable features have been fully explained.

As the alternations of the induced EMF waveforms were found to be unsymmetrical in the 12/8 configuration, it was not surprising that the static torque measurements showed unequal positive and negative torque presentation in the test representing an instance of three phase loading. However, the presentation of the measured static torque for the 12/5 was with equal positive and negative torque presentations, as was the alternations of the EMF. The cogging torque, strongly anticipated in the FSM, was reliably detectable by tests in the 12/8 configuration. In the 12/5 configurations, the cogging torque was predicted to be relatively lower than in the 12/8 configurations and presented uncertainties in its measurements, causing larger errors in the measurement values.

The 12/8 configuration was successfully operated as a synchronous motor with variable field excitation and variable load. The synchronous motor performance measurements demonstrated steady-state motor performance characteristics similar to the conventional

synchronous motor with field-winding excitation at a fixed speed. Torque capability was virtually constant with variable speed, save for a gentle droop arising from the change in voltage drop over the motor impedance elements. A base speed of about 1500 r/min was inferred from the test on the 400-V drive with speed control.

When compared on torque density, the motor appears to present torque density similar to a conventional SRM, but significantly higher than an equivalent SyRM with a segmental rotor by a factor of nearly 2.

Chapter 7

Testing and performance of permanent-magnet machines

The design and construction of the experimental three-phase permanent-magnet flux switching machines (PMFSM) employing segmental rotors has been considered in chapter 5. This chapter presents the test results and performance measurements of the experimental machines. Two configurations of the experimental machines, in 12/8 and 12/5 arrangements, are considered. The test and measurement methods follow much of the arrangements employed in the tests and measurements performed on the wound-field machines reported in chapter 6. As such, much of the description of methods are avoided in this chapter and referred in the appropriate text to chapter 6. As with the wound-field machines in chapter 6, the tests cover the no-load running test, the static load test and thermal characterisation. The experimental machine on the 12/8 configuration was operated as a synchronous motor up to full load and the available DC link voltage of the AC drive, providing results for performance evaluation. Finally, comparisons of performance with the wound-field machine and the conventional AC permanent-magnet machine are made.

7.1 Introduction

The important difference between the wound-field and permanent magnet machines, as the terms suggest, is in the type of field excitation. As the properties of the magnets are invariable on the machine, there is no variation of field excitation in the operation of the permanent-magnet machine. Therefore, there are fewer parameters for measurement and investigation and fewer pieces of equipment to deploy in the permanent magnet machine than the wound-field machine. The electrical supplies, which include DC supplies for static no-load tests and three phases AC drives for motoring, and the metering instruments are all for deployment on the armature system. The topology arrangement and the coil terminal connections are as provided in figure 7.1.

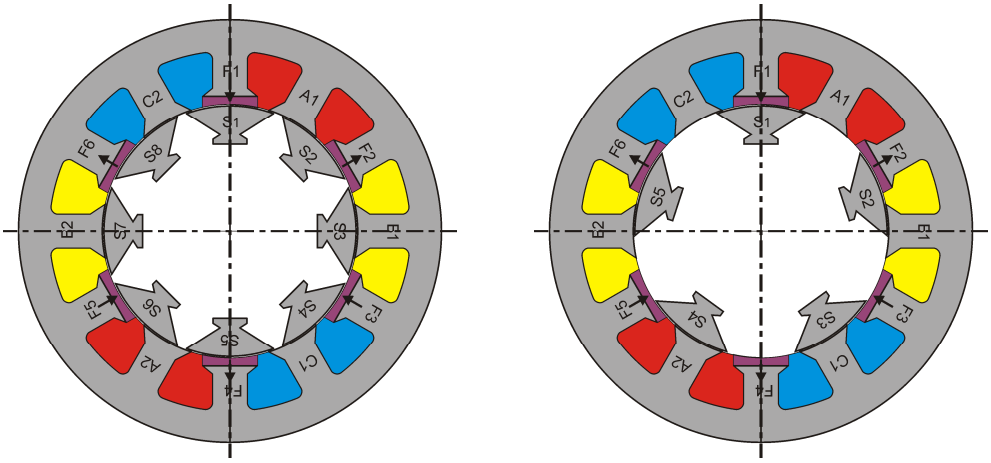

(a) 12/8 PMFSM (b) 12/5 PMFSM

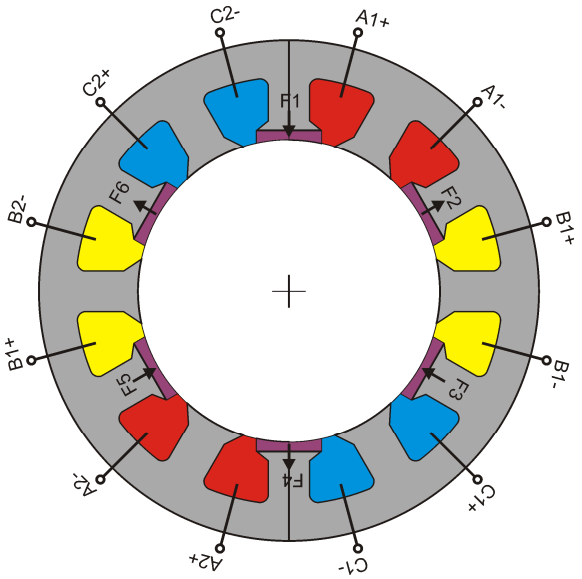

(c) coil designation

Figure 7.1.Topology deployment and coil terminal designation in the PMFSM.

7.2 No-load Test: Induced EMF

The test set-up for measurement of the no-load induced EMF in the armature system is the same as described for the wound-field machine in chapter 6. The EMF was observed in the phase winding at a fixed speed of 500 r/min in the 12/8 and 12/5 configurations.

7.2.1 The 12/8-configuration

The EMF waveform is quasi-sinusoidal, as shown in figure 7.2. The alternations of the EMF are dissimilar and the phase waveform yields significant harmonics, the 2nd harmonic being the largest after the fundamental at 7.2% of the fundamental in the measurement results. The triplen harmonics are absent in the observation of the line EMF. There is general good agreement between the measurement and predicted EMF waveforms, but there appears to be an overestimation of the predicted EMF in the peak value of the positive alternation by 28.4%. This appearance of an unusually high peak in the positive alternation is yet to be fully accounted for. There are also noticeable differences in the harmonic spectra between the measurement and the prediction. This difference is believed to be due to the difference in the resolution of the data range between the measurement and predicted waveforms, by which the measurement uses about 4000 data points and the predictions uses 45 data points for one electrical cycle in the computation of the harmonic spectrum. The measurement set of results produces a THD of 11.7% whilst the prediction has a THD of 13.3% for phase EMF. The predicted THD for line EMF is even lower, at 7.5%.

7.2.2 The 12/5 configuration

The AC waveform for the 12/5 configuration, shown in figure 7.3, is also quasi-sinusoidal but appears to be more sinusoidal than that for the 12/8 configuration. Unlike that for the 12/8 configuration, the waveform for the 12/5 configuration is symmetrical and has identical alternations. The inclination to symmetry and sinusoidal shape is reflected in the near absence of the even harmonics in the harmonic spectrum. After the fundamental, the third harmonic is the dominant harmonic at 5.8% of the fundamental in the measurement results of phase EMF. As in the 12/8 configuration, the are no triplen hanmonics when line EMF is considered. The phase EMF waveform presents a THD of 7.6 % in the measurement, compared to 7.9 % in the prediction, whilst the

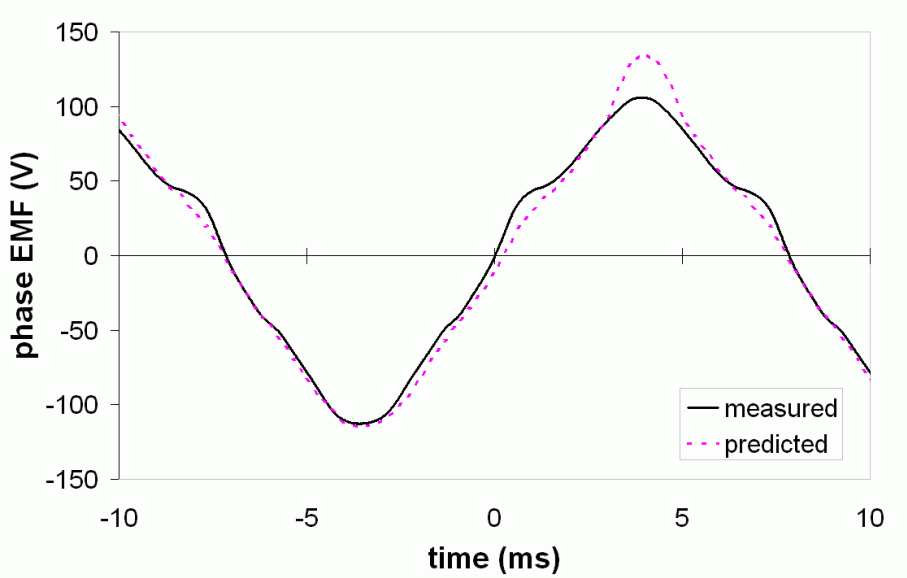

(a) phase waveform

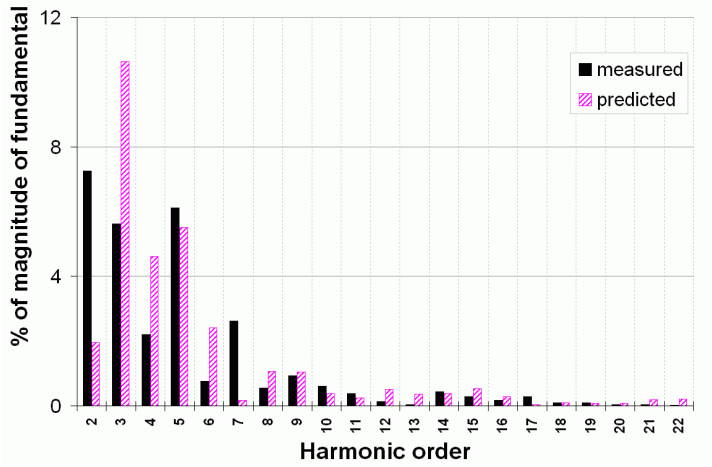

(b) spectrum of phase EMF

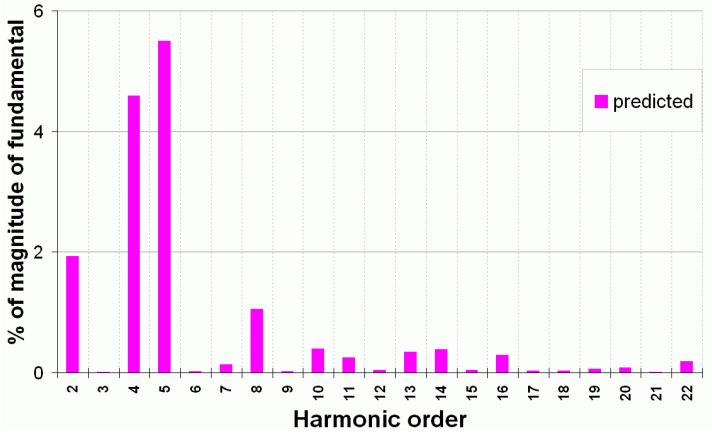

(c) spectrum ofline EMF

Figure 7.2. EMF for 12/8 configuration at 500 r/min.

predicted THD for the line EMF is appreciably lower, at 4.5%. The THD in the

measurement set is significantly lower than that for the 12/8 configuration, and underpins the preliminary assertion that the sinusoidal quality of the waveform for the

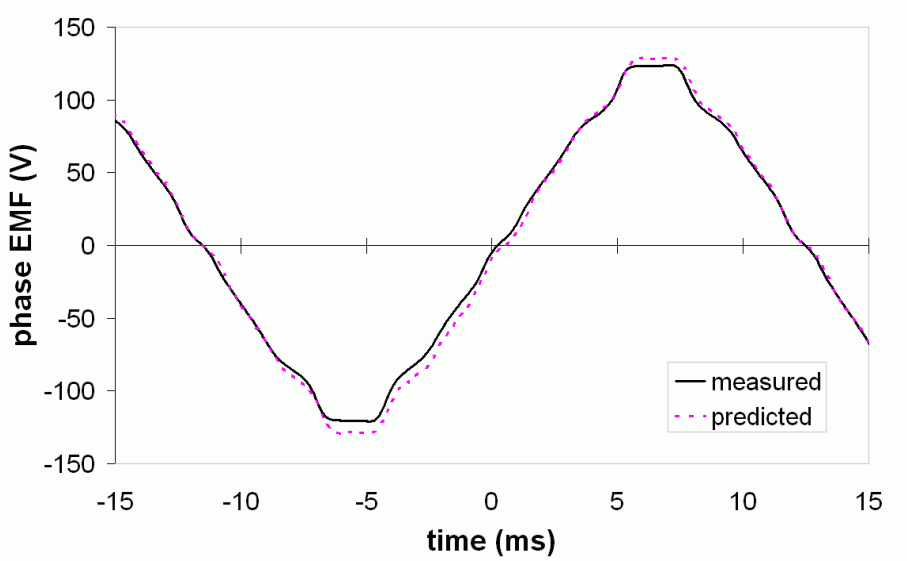

(a) phase waveform

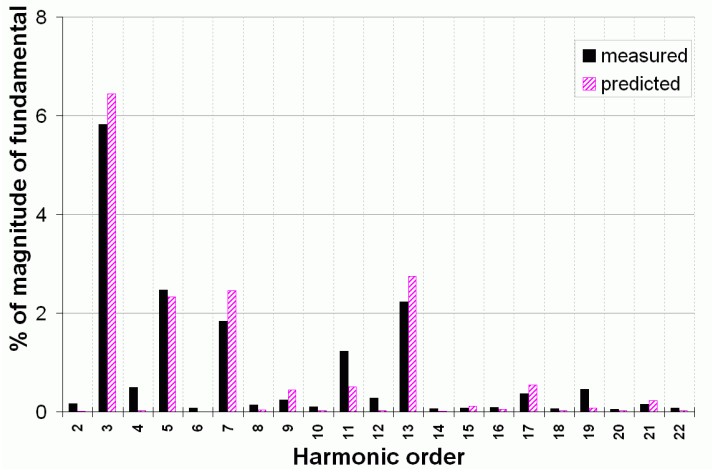

(b) spectrum of phase EMF

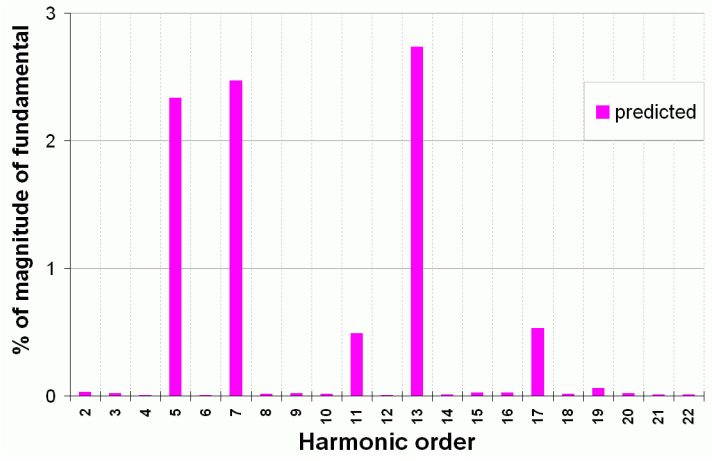

(c) spectrum of line EMF

Figure 7.3. EMF for 12/5 configuration at 500 r/min.

12/5 configuration is better than that for the 12/8 configuration. The error between the measured and predicted peak value of the phase EMF waveform is around 4.6%, with the predicted being higher than the measured value.

The grounds accounting for a presentation of identical alternations in the phase EMF for the 12/5 configuration and a presentation of dissimilar alternations in the 12/8 configuration have been advanced in chapter 6 for the wound-field configurations, and are equally applicable for the permanent magnet configurations.

7.3 Load Test: Static Torque

The static torque test results presented in this section were produced from the three phase connection described in chapter 6, where one phase carries positive peak current and the other two phases carry half the negative peak current. The merits and demerits of the approach to represent a three phase situation have been discussed. In the following subsections the results of the test for permanent-magnet configurations of the experimental machines are presented.

7.3.1 The 12/8-configuration

The static torque profile for the 12/8 permanent-magnet configuration, shown in figure 7.4, is similar to that of the 12/8 wound-field configuration described in chapter 6. It reveals similar and substantial cogging torque, which is superimposed on the torque of the loaded machine, evidenced by the undulations at the same frequency of the cogging torque on the total profile. Due to the nature of the 12/8 topology, the profile and peak values of the positive torque are not identical to those of the negative torque. Whilst the positive torque can reach peak torque of 31.4 Nm, the negative torque reaches 36.5 Nm for the same dc armature current of 12 A.

7.3.2 The 12/5-configuration

The major differences in the static torque profile of the 12/5 configuration, shown in figure 7.5, compared to that of the 12/8 configuration, are that the positive and negative torque profiles are identical and the cogging torque is significantly lower in the 12/5 configuration. The exceptionally low values of cogging torque in the 12/5 configurations also appears to be a source of errors in the measurement value set for cogging torque, so that that the measured values tend to be higher than the predicted

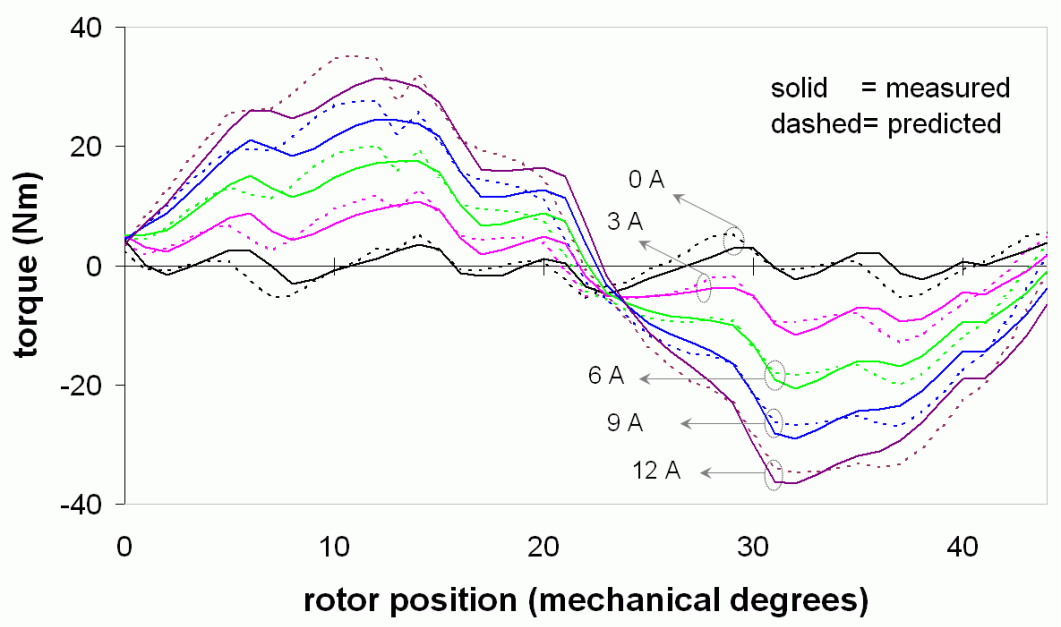

Figure 7.4. Static torque for 12/8 configuration at various armature currents.

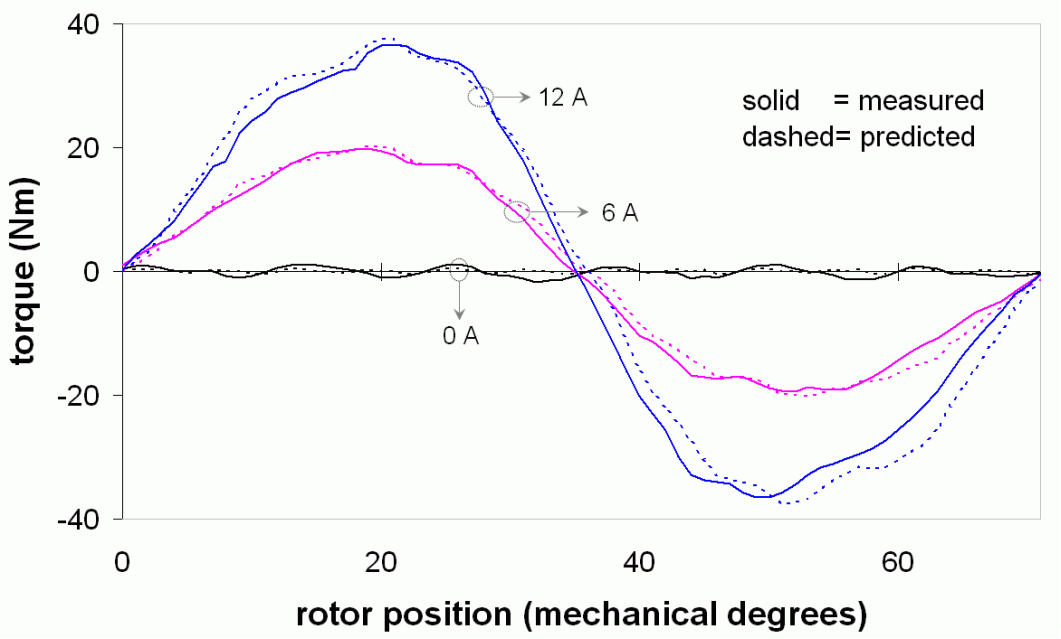

Figure 7.5. Static torque for 12/5 configuration at various armature currents.

values. On the overall, the predicted static torque matches the measured torque reasonably well when the armature is loaded, with a 2.3 % error in the peak value at 12 A armature current. The major observations on the measured static torque for the 12/5 configurations with wound-field excitation in chapter 6 are applicable to this configuration with permanent magnet excitation. However it is worth repeating here that the presentation of the torque profile of the 12/5 configuration, even with permanent magnet excitation, approaches that of conventional AC machines in appearance.

7.4 Thermal Characteristic

A thermal test, similar to that executed on the wound-field machine and described in chapter 6, was performed on the permanent magnet machine with an 8-segment rotor. The difference in the permanent magnet arrangement, arising from the configuration, is that there are six series-connected coils to energize, which act as heat sources, presenting a different arrangement of thermal sources to that the wound-field machine at the same current.

The thermal curves in figure 7.6 show the temperature responses of the conductor in the slot and the surface of the casing with time for two cases of assisted and unassisted cooling. The thermal parameters derived from the curves are shown in table 7.1.

Table 7.1. Basic parameters of thermal characteristics for permanent-magnet machine

		Unassisted cooling	**Assisted cooling**	**Units**
Thermal time constants	**slot-to-casing (conduction)**	4.13	3.34	min
	casing-to-ambient (convection)	40.26	32.19	min
100 °C temperature rise in conductor	**power loss**	381.5	504.2	W
	rms current	9.8	11.4	A

The use of an ordinary desk fan to aid cooling is tentative but its effect on increasing the loading capability, shown by the change in the response time constants, is significant. The fan had a specified airflow of about 2100 m^3/h and was positioned about 40 cm from the test machine. By using such a fan, the current loading in the conductor may be increased from 7.9 A/mm^2 to 9.3 A/mm^2, to achieve the same temperature rise of 100°C in the slot conductors, as computed from the response parameters in Table 7.1.

7.5 Synchronous Performance

The 12/8 permanent magnet experimental machine was set up for synchronous motor operation in the manner described for the wound-field machine in chapter 6. In the following subsections the results of synchronous operation up to rated load torque, initially at a fixed speed of 500 r/min and subsequently at variable speed, are presented.

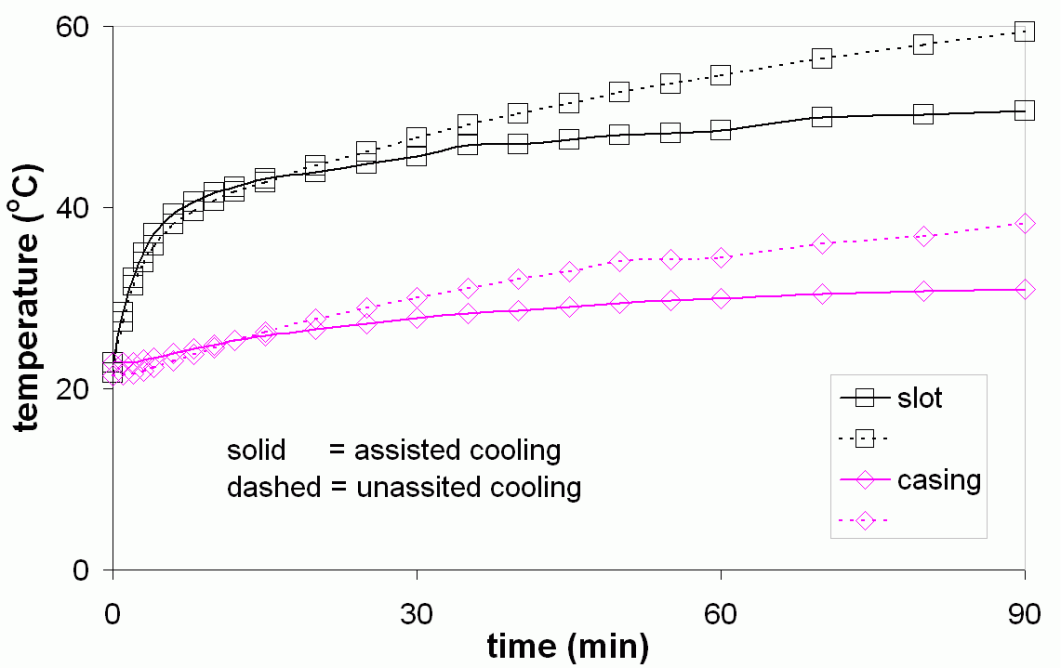

Figure 7.6. Thermal response of permanent-magnet machine.

7.5.1 Torque

The output torque varies linearly with armature current at fixed speed. The motor produces an output torque of 40.7 Nm at a motor current of 12 A (J = 9.8 A/mm^2), which is nearly the rated motor current, with assisted cooling as determined from the thermal test. Figure 7.7 shows the variation of measured output torque with motor current alongside the predicted electromagnetic torque. There is a noticeable discrepancy between the measured and predicted torque, estimated at 12.3% at the

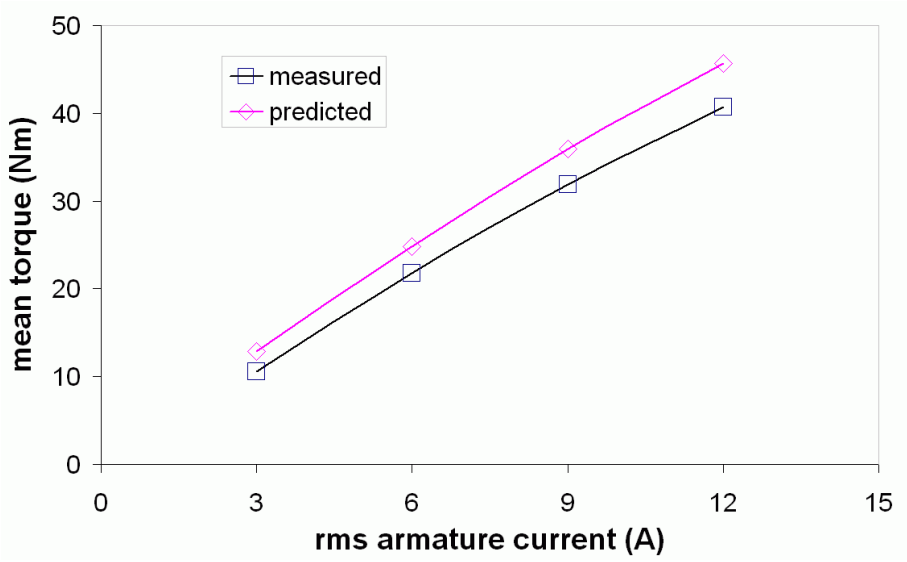

Figure 7.7. Output mean torque for 12/8 PM motor.

maximum output torque. Part of the discrepancy is attributed to the prediction value not discounting the frictional and windage torque, which is any case expected to be quite small, but the main part of the discrepancy is thought to be due to limitations posed by the 2D modelling. A combination of neglecting end-winding effects and leakage flux in the stator frame has been known to produce errors of up to 10 % in the EMF of PM machines [234].

Although torque ripple is predicted to be significant in the permanent magnet configuration, the measurement results showed hardly any ripple. As in the wound-field machine, much of the torque ripple is thought to be smoothened by the inertial mass system of the motor and load, but the apparently more smoothened torque in the PM motor is also due to the steady flux supplied by the magnets.

7.5.2 Power, efficiency and power factor

The power output of the motor was found to be linearly proportional to the armature current, attaining a value of 2.13 kW with a motor current of 12 A at 500 r/min. Figure 7.8 shows that the efficiency of the motor at 500 r/min is relatively high when motor current is low, with a value of about 81% for motor current between 3 and 6 A, and starts to fall as current is increased. At the maximum current of 12 A, the efficiency has dropped to 71.4 %, suggestive of the dominance of the copper loss in the total loss at high loading.

At a fixed speed of 500 r/min, the terminal voltage, shown in figure 7.8 increases proportionally with armature current up to 415 V when maximum motor current is reached, while the power factor falls with increase of current from 0.9 at 3 A to 0.52 at 12 A. As with efficiency, it appears advantageous to operate with a low current to get a high power factor at the test speed of 500 r/min. Compared with other AC machines, the power factor is relatively poor at rated conditions, although it is better than for the wound-field FSM at the same conditions.

7.5.3 Performance with speed variation

Performance on load was measured for a speed range 100-1400 r/min for the permanent-magnet motor. The motor current applied in this test was limited to 11 A, corresponding to the capacity limit of the load machine to measure the torque.

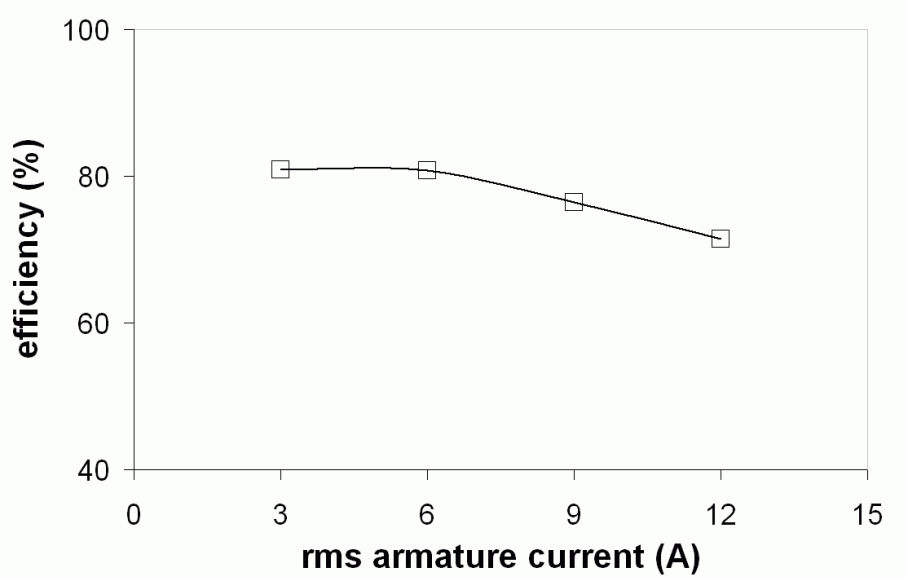

Fig. 7.8. Efficiency against armature current.

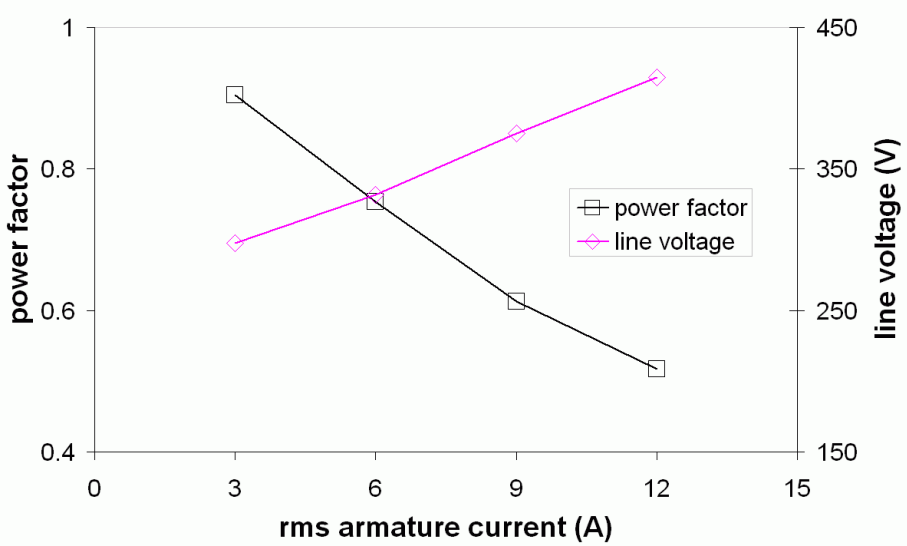

Figure 7.9. Power factor against current and terminal line voltage against current.

Inception of instability (i.e., when converter runs out voltage) occurred between 900-1400 r/min, depending on the load. The higher the torque, the lower the point of instability, with lowest being a little above 900 r/min when motor current is at its possible maximum of 11A. This range of stability in speed control at a specified motor current is slightly higher than that with the wound-field machine, possibly due to the steadier field flux in the PM motor.

The torque-speed curves at various loads are shown in figure 7.10. They reveal a drooping characteristic which is typical of the conventional PM synchronous motor. The torque-speed curve is almost a straight line droop, whose gradient is influenced by

the per unit impedance of the phase winding. The sudden change of torque at the upper end of the speed reached is indicative of inception of flux-weakening.

The effect of the speed on the efficiency is shown in figure 7.11. Generally, efficiency increases with speed at any particular motor current, but the increase is substantially lower at high speeds than at low speeds, in the speed range considered. As the efficiency also appears to increase with motor current at a particular speed, particularly in the lower speed range, it is a fair observation to generally note that the efficiency increases with output power. A presentation of the maximum efficiency is at a value of 83.3% when the speed is about 100 r/min with an armature current of 6 A.

At any particular speed, the power factor falls with increase in motor current, as shown in figure 7.12. There appears to be no change in the power factor with speed when the

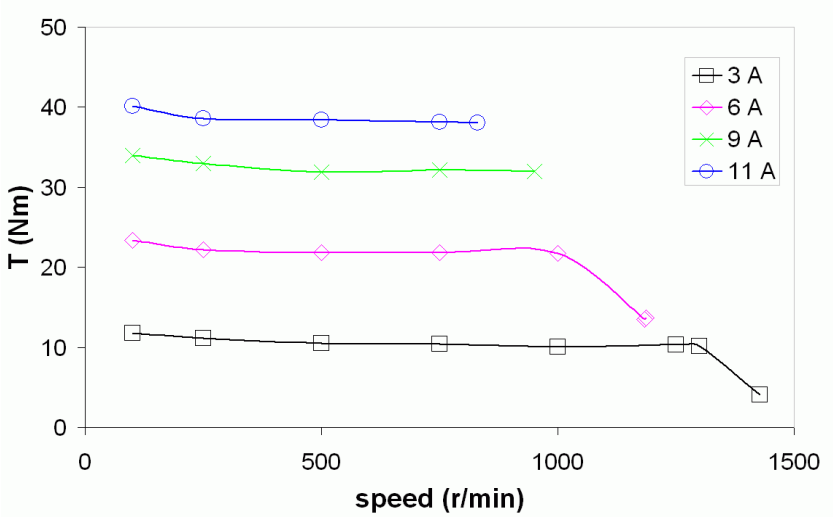

Figure 7.10. Mean output torque with speed

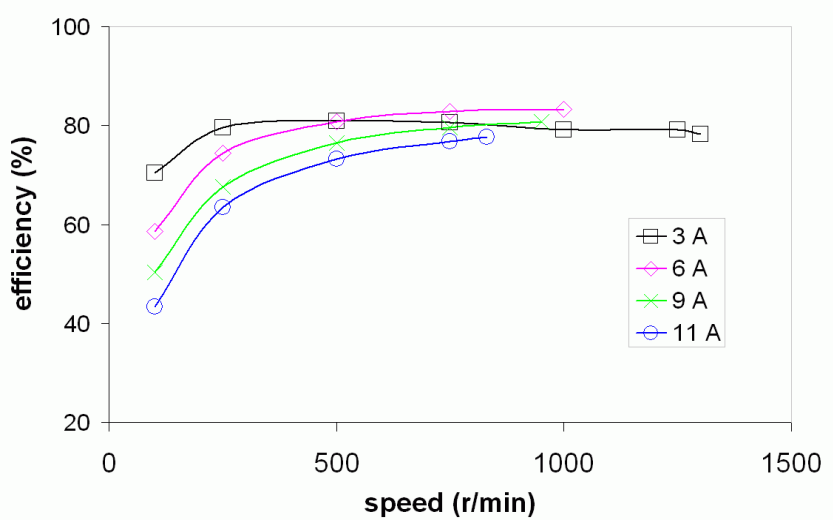

Figure 7.11. Efficiency with speed

motor current is at 6 A. However, in the speed range up to 500 r/min, when current is above 6 A, the power factor has a linear droop with speed, and when the load current is above 6 A the power factor tends to increase with speed. At speeds above 500 r/min, the power factor tends to be constant with speed, regardless of the motor current.

The terminal voltage is observed to be inversely proportional to the motor current at a specified speed, as illustrated in figure 7.13 and noted in the measurement with fixed speed. However, when speed is varied, the terminal voltage is proportional to the speed at any specified load current. As a result of this characteristic, the terminal voltage reaches the limit set by the dc link voltage of the drive at a higher speed for low motor currents.

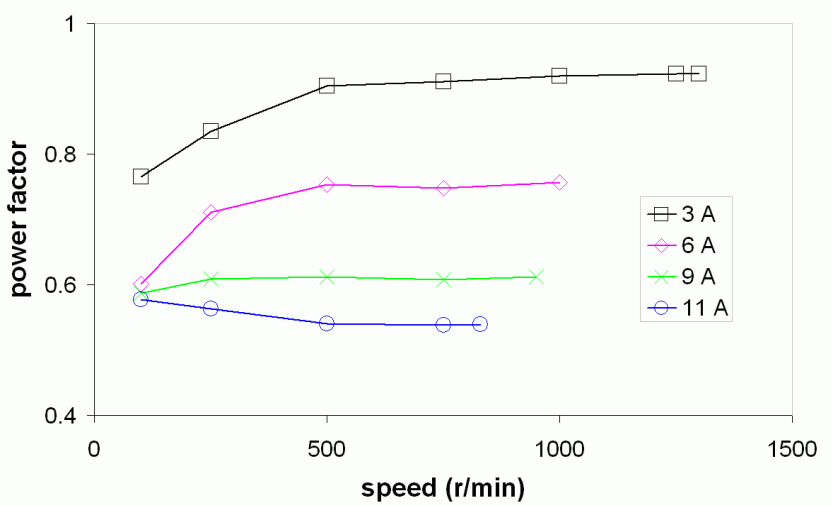

Figure 7.12. Power factor with speed

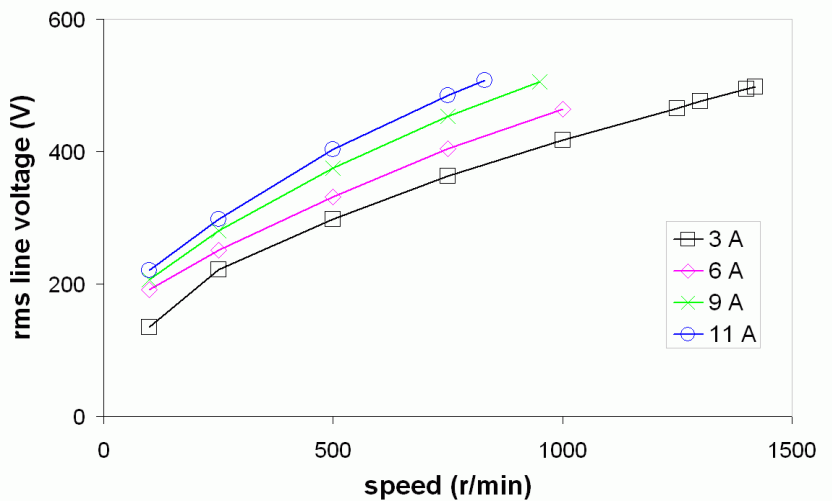

Figure 7.13 Terminal line voltage with speed.

7.6 Comparison with Other Machines

The permanent magnet flux switching synchronous motor employing a segmental rotor is being studied for the first time. As pointed out in chapter 2, permanent magnet flux switching motors that have been studied in the last 13 years employ a toothed-rotor and the action and placement of the PM magnets are significantly different from that of the PMFSM employing segmental rotor introduced in this thesis. For the purpose of comparison, the wound-field flux switching synchronous motor studied in this thesis, and which differs from the permanent-magnet motor mainly in the manner of field excitation, is considered. It also appears interesting to compare the permanent magnet flux switching synchronous motor employing a segmental rotor with the established and convention permanent synchronous motors with magnets on the rotor. In the following subsections, the permanent magnet flux switching synchronous motor employing a segmental rotor is compared with these two types of motors.

7.6.1 Wound-field synchronous flux switching motor

The permanent-magnet synchronous flux switching motor, like most permanent-magnet motors, is expected to give a higher torque capability than a wound field-field motor for the same general size of machine. Table 7.2 shows the comparison of the permanent-magnet and wound-field flux switching synchronous motor on selected measured performance parameters.

Table 7.2. Comparison of PMFSM and wound-field FSM

		PMFSM	**Wound-field FSM**
Torque capability (at thermal limit)	Nm	40.7	22
Torque density (at 300 W loss)	kNm/m^3	31.7	19.9
Torque ripple (from prediction)	% mean	23.5	38.0
Estimated base speed (at rated torque)	r/min	830	1250
Rated power (at rated speed)	kW	3.3	3.4
Power factor (at rated load, speed)	-	0.54	0.45
Efficiency (rated load, speed)	%	77.6	75.6

The two motor types have identical dimensions and operating criteria, except for the mode of field excitation. The depth of the magnets was calculated to give the same flux density in the stator teeth as would the field excitation of the wound-field machine with open-circuit armature windings, with the assumption of linearity in the magnetisation.

Due to space freed by a field winding, the PM motor has more armature turns than wound-field motor, by a factor of 2.27 in this case.

The torque capability, at thermal limit, of the permanent-magnet motor is nearly twice that of wound-field motor. The increased torque capability of the permanent-magnet motor is largely due to the augmented slot area for the conductors, so that the electrical loading may ideally be doubled. In practice, as copper loss is the main component of the loss, it requires a higher current (increased electrical loading) in the permanent-magnet motor than in the wound-field motor to produce a winding loss that results in the same temperature rise. The subtler effects, in the differences that arise due to thermal structures, though extensively examined in these comparisons, are believed to add the observed differences in the torque capabilities of the two types of motors. When compared at the specific winding loss of 300 W, a loss which is on the margins of the operating loading with unassisted cooling, the torque density of the permanent-magnet motor is about 1.6 times that of wound-field motor.

Aside of the torque, the torque ripple predicted from FE simulations is also lower for the permanent-magnet motor than for the wound-field motor by nearly half, with prospects of the permanent-magnet motor being quieter than the wound-field motor. Although the permanent-magnet motor shows only marginal improvements in the power factor and efficiency, there is significant lowering of the base speed at rated torque of the permanent motor, principally due to producing a noticeably higher back-EMF. The rated output power of the permanent-magnet motor, considered at the base speed is, however, practically the same as that of the wound-field motor.

7.6.2 Permanent magnet synchronous motor

There are several configurations for conventional AC permanent magnet synchronous motors [235]. One main variety can be conceived by the manner of the winding type, either with distributed or concentrated stator windings. Another major variety may be produced by the arrangement of the magnets on the rotor. In respect of the variety due to rotor magnet configurations, there are four major types identified by the location of the magnets: interior, insert, surface and flux concentration configurations. As the PMFSM in this study implements a concentrated winding arrangement, a choice of this type of winding on the PMSM presents a fairer comparison. There are equally good reasons premised on fairness, to avoid comparing the PMFSM with the PMSM

employing either flux concentration magnets or interior magnets. In practice, the flux concentration arrangements of the magnets on the rotor for PMSM are usually applied for designs with low flux-density magnet materials. On the other hand, while the type of torque in the synchronous PMFSM is largely due the excitation torque produced by placing the current in phase with back-EMF, the PMSM with interior magnet configurations are designed to also exploit the reluctance torque availed by their substantial saliency. Therefore, the comparison of the PMFSM employing a segmental rotor in the 12/8 configuration is made with the PMSM employing insert and surface magnets in an 8-pole configuration. As there were no experimental PMSM machines of similar size available, the comparisons are from modelled performance results using FE simulations, with the models having similar stator and rotor dimensions, including the airgap, based on the constructed 12/8 PMFSM. Figures 7.14 and 7.15 show the presentation of the 8-pole PMSM motors employed in the comparison with 12/8 PMFSM.

Although the machines all employ permanent magnet excitation, the PMSMs have about 35% higher torque capability than the PMFSM, principally due to the higher volume of the magnets of the same depth that the PMSM machines can accommodate on the rotor in an 8-pole arrangement. With 8 magnets on the rotor for the PMSM and 6 magnets on the stator for the PMFSM, the ratio of the volume of the magnets for either insert or surface PMFM to that for the PMFSM is approximately 2.1. Accordingly, the torque density, evaluated at 300 W loss, is higher for the PMSMs than the PMFSM by a factor of 1.6. A tabulated summary of the comparison on the selected principal indices is shown in table 7.3.

As there are serious implications of the usage of magnets on cost, a fairer comparison of torque capability, which takes into account the mass of the applied magnets, is shown in the 4th row of table 7.3. It is then seen that the PMFSM surpasses the PMSM in torque capability per unit mass of applied magnets, at thermal limit, by factor of about 1.48.

Despite presenting a higher torque capability, both configurations of the PMSM incur a higher torque ripple than the PMFSM, the surface magnet configuration significantly further higher than the insert magnet configuration, as shown in the summary. The cogging torque of the PMFSM is appreciably lower than that found in the PMSM.

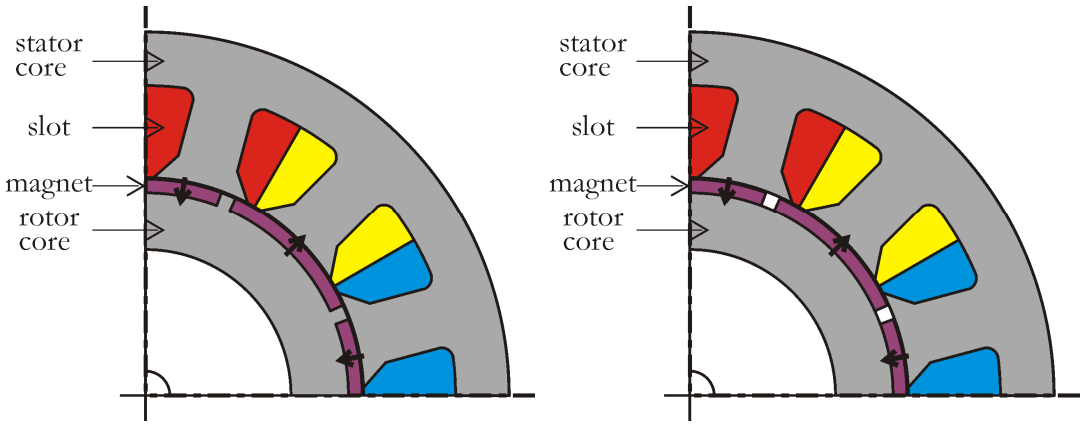

(a) insert-magnet configuration (b) surface-magnet configuration

Fig. 7.14. Conventional 8-pole double-layer single-tooth winding PMSM configurations.

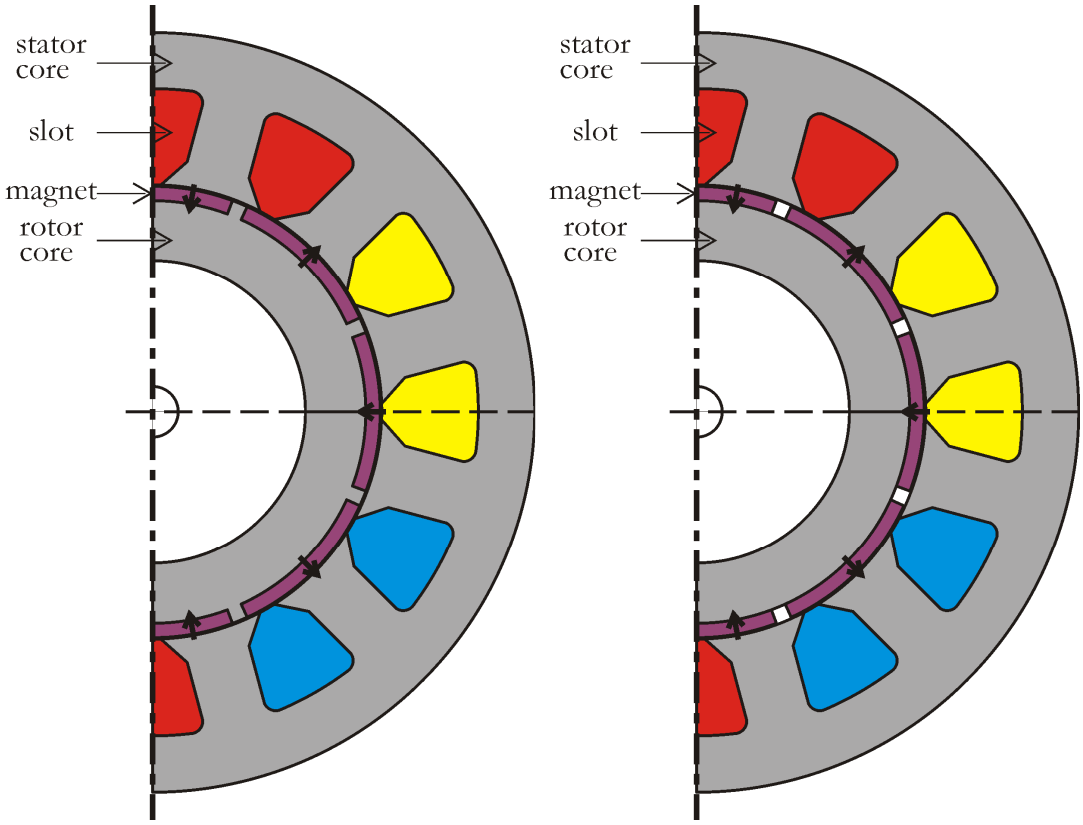

(a) insert-magnet configuration (b) surface-magnet configuration

Fig. 7.15. Conventional 8-pole single-layer single-tooth winding PMSM configurations.

According to the findings, when expressed as a percentage of the mean torque capability, the peak value of the cogging torque for both the insert and surface magnet configurations of the PMSM is more than double that of the PMFSM.

Table 7.3. Comparison of PMFSM and PMSM

		PMFSM	PMSM			
			Double-layer		Single-layer	
			insert	surface	insert	surface
Total volume of magnets	mm^3	51, 003	106,824			
Torque capability (at thermal limit)	Nm	45.7	67.6	69.8	64.7	66.3
Torque density (at 300 W loss)	kNm/m^3	31.7	51.8	53.5	49.6	50.8
Torque ripple of mean	%	23.5	30.7	36.0	15.3	30.0
Torque capability per unit mass of magnets	Nm/kg	119.5	84.4	87.1	80.8	82.8
Peak cogging torque	Nm	5.5	15.4	14.5	15.5	14.5
Peak cogging torque/torque capability	%	12.0	22.8	20.7	23.9	21.9
EMF at 500 r/min per phase	V	76.5	106.0	105.6	106.4	106.1
EMF THD	%	13.3	20.7	14.5	20.5	14.3

The higher back-EMF predicted in both configurations of the PMSM are in correspondence with the resultant torque capabilities, but the nature of the EMF waveform is widely different across the machines under comparison. Using the index of the THD, the PMSM with surface magnets presents a THD of the EMF of 14.5%, which is nearly the same as that of the PMFSM, while the PMSM with insert magnets incurs higher THD at 20.5%, which is more than 1.4 times that of the PMFSM. There are no even harmonics, as shown by the harmonic spectrum of the of the EMF of the insert and surface magnet configuration of the PMSM in figure 7.16, but the difference between the two in the THD is accounted for through the dominant 5th harmonic, which is 1.4 times greater for the insert than the surface magnet configuration. By inference, through the presentation of the phase induced EMF, it is expected that the PMSM motors would attain a lower base speed than PMFSM on the same drive-supply, due to higher values of the back-EMF. This presentation of the torque ripple, cogging torque and EMF THD for PMSM is not typical of well-designed PMSMs, which usually employ a distributed

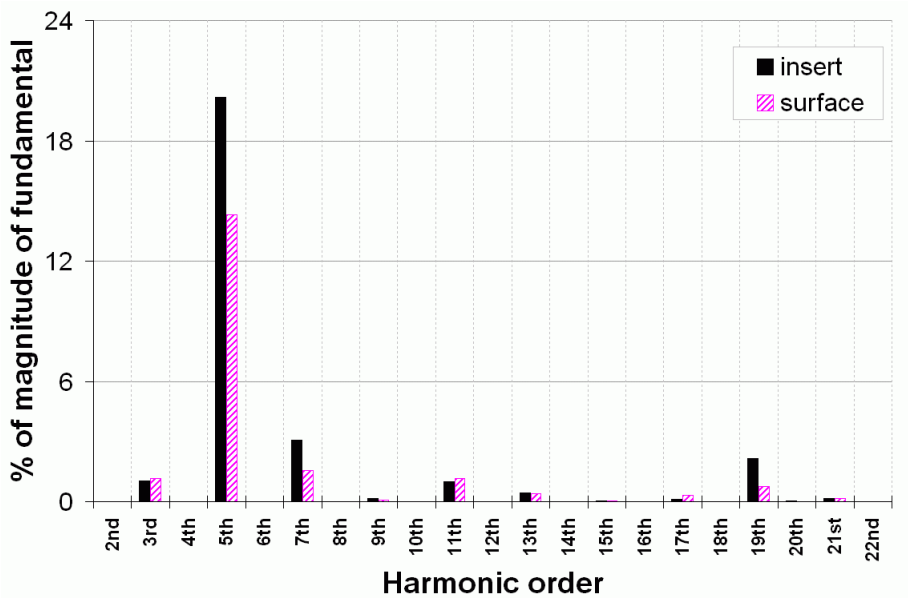

Figure 7.16. Harmonic spectrum of phase EMF of insert and surface magnet PMSM.

winding for sinusoidal back-EMF, and if concentrated winding is employed, then trapezoidal armature current is normally employed.

7.7 Conclusion

The findings in the testing and performance of the permanent magnet synchronous machines have revealed characteristics which are consistent with the predictions from FE modelling, allowing for the errors arising from the applied assumptions in the modelling. However, as with wound-field machines, the torque ripple predicted in the FE modelling is hard to verify in practice on the running tests due the influence of inertia. A better chance of verifying torque ripple in practice was in measuring the torque in the static tests, whose results were, to a large degree, also consistent with the predictions.

The EMF waveform of the permanent magnet flux switching motor employing a segmental rotor has an induced EMF waveform which is quasi-sinusoidal and therefore with substantial harmonics in both the 12/8 and 12/5 configurations. However the EMF waveform for the 12/8 configurations has dissimilar alternations while that for the 12/5 configuration has identical alternations.

The PMFSM employing a segmental rotor has a static torque characteristic with unequal positive and negative torque in the 12/8 configuration but with equal positive and negative torque in the 12/5 configuration, in correspondence with the characteristics

of the induced EMF waveform. An interesting finding, predicted in the FE model and verified by the measurement, is in the presentation of cogging torque, which has been found to be lower in the 12/5 configuration than in the 12/8 configuration.

When operated as a synchronous motor, the PMFSM employing a segmental rotor produced torque proportional to the *q*-axis directed motor current, and which was virtually constant with speed. The characteristics of the power factor, efficiency and terminal voltage with motor current and speed have been measured and were found to be consistent with characteristics found in conventional permanent-magnet synchronous motors.

A comparison of the PMFSM employing a segmental rotor with the wound-field motor reveals almost a doubling the measured available torque in the permanent magnet motor, but there are also subtle features in the performance, differentiated in the individual measured parameters. When compared with the conventional concentrated-winding PMSM with either inset or surface magnets of similar size, on the basis of FE models, the available torque capability of the PMFSM is less than that of the PMSM, but when usage of the magnets taken into account, the PMFSM provides higher torque capability than the PMSM. Although it is not a generally trend of well-designed PMSMs, the torque ripple, cogging torque and THD of the considered concentrated-winding PMSM are higher than those of the PMFSM.

Chapter 8

Representation of Segmental-rotor Synchronous Motors using the *dq* Model

The classical *dq*-representation is lauded as a simplifying approach to modelling three phase AC machines and is a ubiquitous method in AC machine analysis. The steady-state performance of the flux switching synchronous motors, as presented in chapter 6 and 7, may be more rapidly predicted with a *dq*-equivalent model than FE simulation if a valid representation can be developed. In this chapter, the process for representation of both the wound-field and permanent magnet flux switching synchronous motors employing a segmental rotor is explored. As the motors present an unusual topology and mechanism of operation, a need to establish a justification for adopting the application of the *dq* model is required, together with the foundations of the underlying assumptions. The performance predicted using the derived *dq* parameters is compared with the performance measurement results from chapter 6 and 7, for accuracy of the model.

8.1 Introduction

The transformation of the stator reference frame, which applies *abc* parameters, to the synchronous reference frame, which uses the *dq* modelling to apply *dq* parameters, was originally formulated for machines with a rotating excitation system on the rotor and distributed windings on the stator [236]. The appeal for working with *dq* parameters, which are fixed to the synchronous reference frame and therefore tied to the rotor, lies in the resultant simplification of the prediction equations. However, the underlying assumptions for *dq* modelling may at first appear to exclude its application to many types of real AC machines. These restrictive assumptions are that, firstly the machine has to have a distributed winding, a condition required to provide sinusoidal armature flux linkage and back-EMF; and secondly, the behaviour of magnetic structures has to be linear. In practice, the condition aligned to the second assumption is difficult to fulfil with real materials, but the design of a sizeable proportion of conventional synchronous AC machines strives to conform to the first assumption, and such machines may be deemed to have sinusoidal parameters to a degree.

There is a compelling argument in [236] that the *dq* transformation may be deemed to be a purely mathematical formulation so that transformation of the prediction parameters from *abc* to *dq*, even in the face of violating the ideal assumptions, gives valid prediction expressions. Allied work in [237] investigated the validity of a *dq* model as applied to PM synchronous motor with non-overlapping concentrated windings and showed reliable predictions, drawing attention, as in other works, to the effect of saturation on the characteristic of the *dq* inductances.

The flux switching synchronous motor employing a segmental rotor, apart from having concentrated single-tooth windings, presents a further and significant two-fold departure from the conditions under which the *dq* transformation was formulated. In the first fold, as the excitation system, either by field winding or permanent magnets, is stationary and located on the stator, it is not obvious to establish a correspondence with a revolving field system which has either the field or armature system in motion, on which the transformation is founded. This uncertainty is resolved by the work in [238], which shows the equivalence of a system with an excitation field on the rotor, such as in a synchronous PM machine, to one with an excitation field in the stator, as found in FSM with toothed-rotor, using fundamental transform concepts. In the second fold, the

departure from ideal assumptions is allied to the use of a segmental rotor for flux switching, which results in the frequency of variation of phase inductance with rotor position appearing to be the same as the electrical frequency, as opposed to twice the electrical frequency in conventional machines. It is expected that this situation may present hitherto unexplored characteristics of the *dq* inductances and possibly question the simplifications that may be derived from applying the *dq* transformations to this type of machine.

In this consideration, rather than assume sinusoidal variation of the inductance in obtaining the *dq* model, the stator frame *abc* inductances are taken as they occur in the machine, accounting for the effect of both direct and cross-saturation. The variation of inductances is also taken to vary both with position and current in a complex and unknown manner.

8.2 Modelling

The route to predicting the performance of the AC machine and its drive in using electrical circuit parameters is by applying the voltage relationship with current. The circuit path per phase consists of a term due to the change of the flux linkages and another term due the resistance voltage drop. Ultimately, to be consistent with the circuit parameter stipulation, the term due the change of flux linkage may be represented as one due to the change of inductances. The torque equation may be derived from considering the change and storage of energy, embodied in the term for flux linkage or inductance. In three phase systems, the expressions for voltage and torque may be complicated and cumbersome, due to mutual coupling of circuits and dependence of the flux linkages on both the rotor position and current.

8.2.1 Modelling in *abc* stator reference frame

For a general AC machine with a rotating field provided by a field winding, the *abc* three phase voltages $\boldsymbol{v}_{abcf}$ are given in terms of the phase currents $\boldsymbol{i}_{abcf}$ by

$$\boldsymbol{v}_{abcf} = R\boldsymbol{i}_{abcf} + \frac{d}{dt}\left(\boldsymbol{\psi}_{abcf}\right) \tag{8.1}$$

where $\boldsymbol{\psi}$ is the flux linkage and R is the resistance per phase.

The flux linkages of each phase is dependent on the currents and may be generally expressed as

$$\boldsymbol{\psi}_{abcf} = \boldsymbol{\psi}_{abcf}(i_a, i_b, i_c, i_f) \tag{8.2}$$

so that the inductance matrix $\boldsymbol{\mathcal{L}}_{abcf}$ is the defining relationship between the column matrices of flux linkages and the currents, as in

$$\boldsymbol{\psi}_{abcf} = \boldsymbol{\mathcal{L}}_{abcf}\boldsymbol{i}_{abcf} \tag{8.3}$$

The inductance $\boldsymbol{\mathcal{L}}_{abcf}$ is generally acknowledged to be dependant on the rotor position θ_r, and referred to as $\boldsymbol{L}_{abc}$, so that (8.3) may written as

$$\boldsymbol{\psi}_{abcf} = \boldsymbol{L}_{abcf}(i_a, i_b, i_c, i_f, \theta_r)\boldsymbol{i}_{abcf} \tag{8.4}$$

The elements of the inductance matrix, may be denoted by

$$\boldsymbol{L}_{abcf} = \begin{bmatrix} L_{aa} & L_{ab} & L_{ac} & L_{af} \\ L_{ab} & L_{bb} & L_{bc} & L_{bf} \\ L_{ac} & L_{bc} & L_{cc} & L_{cf} \\ L_{af} & L_{bf} & L_{cf} & L_{ff} \end{bmatrix} \tag{8.5}$$

with the alike-paired subscripts indicating the self-inductance terms and the unlike-paired subscripts indicating mutual inductance terms.

The voltage given by (8.1) and the resulting electromagnetic power P_i, evaluated by

$$P_i = v_a i_a + v_b i_b + v_c i_c + v_f i_f \tag{8.6}$$

from which the torque expression may derived, are quite complicated expressions, even when the quantities are taken to vary in a sinusoidal manner.

8.2.2 Modelling in *dq* synchronous reference frame

The Park transformation [239] enables a change of the three-winding *abc* quantities viewed from the stator reference frame to the two-winding *dq* quantities viewed from the synchronous reference frame. For synchronous motors, the synchronous reference

frame is fixed to the rotor and appears to be the natural reference frame for machines operating in this mode. In the generalised treatment, which includes excitation by a field winding, the Park transformation matrix $\boldsymbol{P}$ is a 3 x 4-matrix, given by [237]

$$\boldsymbol{P} = \frac{2}{3}\begin{bmatrix} \cos\theta & \cos(\theta - 2\pi/3) & \cos(\theta + 2\pi/3) & 0 \\ -\sin\theta & -\sin(\theta - 2\pi/3) & -\sin(\theta + 2\pi/3) & 0 \\ 0 & 0 & 0 & 3/2 \end{bmatrix} \tag{8.7}$$

where $\theta = N_{seg}\theta_r$, N_{seg} being the number of segments on the rotor.

Applying the transformation to the generalised *abcf* currents, the flux linkages of (8.3) are modified as follows:

$$\boldsymbol{i}_{dqf} = \boldsymbol{P}\boldsymbol{i}_{abcf} \tag{8.8}$$

$$\boldsymbol{\psi}_{dqf} = \boldsymbol{P}\boldsymbol{\psi}_{abcf} = \boldsymbol{P}\boldsymbol{L}_{abcf}\boldsymbol{P}^{-1}\boldsymbol{i}_{dqf} = \boldsymbol{L}_{dqf}\boldsymbol{i}_{dqf} \tag{8.9}$$

where L_{dqf} is the *dq* equivalent of the *abcf* inductances, and can be directly computed from

$$\boldsymbol{L}_{dqf} = \boldsymbol{P}\boldsymbol{L}_{abcf}\boldsymbol{P}^{-1} \tag{8.10}$$

Under general conditions, the inductance matrix can be assumed to be full, so that the flux linkages $\boldsymbol{L}_{dqf}$ are given by

$$\boldsymbol{L}_{dqf} = \begin{bmatrix} L_d & L_{dq} & L_{df} \\ L_{dq} & L_q & L_{qf} \\ \frac{3}{2}L_{df} & L_{qf} & L_f \end{bmatrix} \tag{8.11}$$

Under special conditions prescribed as follows,

- quantities are of sinusoidal variation
- phase quantities are displaced 120° electrical
- self-inductance terms are varying at twice electrical frequency and mutual inductance terms at electrical frequency

which are valid for most types of conventional AC machines, the *dq* inductance expression reduces to

$$\boldsymbol{L}_{dqf} = \begin{bmatrix} L_d & 0 & L_{df} \\ 0 & L_q & 0 \\ \frac{3}{2}L_{df} & 0 & L_f \end{bmatrix}. \tag{8.12}$$

Both the *dq* voltage and torque expressions, given by (8.13) and (8.14), do not have a θ term and the expressions have undergone great simplification. In steady-state operation, the electrical frequency, $\omega = \dfrac{d\theta}{dt}$, is a constant.

$$\begin{bmatrix} v_d \\ v_q \\ v_f \end{bmatrix} = \begin{bmatrix} R & \psi_d & 0 \\ \psi_q & R & 0 \\ 0 & 0 & R_f \end{bmatrix} \begin{bmatrix} i_d \\ i_q \\ i_f \end{bmatrix} + \frac{d}{dt} \begin{bmatrix} \psi_d \\ \psi_q \\ \psi_f \end{bmatrix} + \omega \begin{bmatrix} -\psi_q \\ \psi_d \\ 0 \end{bmatrix} \tag{8.13}$$

$$T_e = \frac{3}{2} p\left(\psi_d i_q - \psi_q i_d\right) \tag{8.14}$$

8.2.3 Steady-state flux switching motor *dq* equations

There is no fundamental change to (8.13) and (8.14) as a result of whether the excitation system is supplied by a DC current of a field winding or permanent magnets but only the terms with the *f*-subscript may be appropriately adjusted to reflect this distinction. Assuming ideal conditions in the *dq* transformation when applying phasor quantities, the synchronous motor steady-state voltage equation, after transformation to the *dq* orthogonal axes, is [233]

$$\begin{bmatrix} V_d \\ V_q \end{bmatrix} = \sqrt{3} I_e \begin{bmatrix} R & -\omega L_q \\ \omega L_d & R \end{bmatrix} \begin{bmatrix} -\sin\beta \\ \cos\beta \end{bmatrix} + \sqrt{3}\omega\psi_e \begin{bmatrix} 0 \\ 1 \end{bmatrix} \tag{8.15}$$

where β is the leading angle of armature phase current from the *q*-axis, the subscript *e* denotes effective values, and ψ_e is the armature flux linkage to due field excitation.

With adequate field excitation provided by the field current or permanent magnets, normal operation is by the $i_d = 0$ control method, in which the current is placed in the *q*-axis, with zero *d*-axis component. The current phase angle β from the *q*-axis is effectively zero, and thus the measurable motor parameters of rms voltage, V_e, average electromagnetic torque, T_e, and motor power factor, $\cos\phi$, evaluated with the aid of the vector diagram in figure 8.1, are given by

$$V_e = \sqrt{(\omega L_q I_e)^2 + (RI_e + \omega\psi_e)^2} \tag{8.16}$$

$$T_e = pI_e\psi_e \tag{8.17}$$

$$\cos\phi = \cos(\delta - \beta) \tag{8.18}$$

where

$$\tan\delta = \frac{\omega L_q I_e}{RI_e + \omega\psi_e} \tag{8.19}$$

In the circumstances of the flux switching motor, where conditions of transformation to the *dq* model are not ideal, the effect of the coupling terms in the *dq* inductance matrix in the derivation of the average electromagnetic torque must be included, so that ψ_e is modified to include the coupling effect of L_{dq} as in

$$T_e = \frac{3}{2} p(\psi_{fd} + L_{dq} I_q) I_q \tag{8.20}$$

8.3 Motor Parameters

The phases *abc* of the flux switching synchronous motor employing a segmental rotor in 12/8 configuration are composed of phases constructed by pairs of coils on six stator armature teeth A, B, and C, shown in figure 8.2, for half the section of the motor. Interspaced between the armature teeth are six field teeth, F1-F6, bearing single-tooth

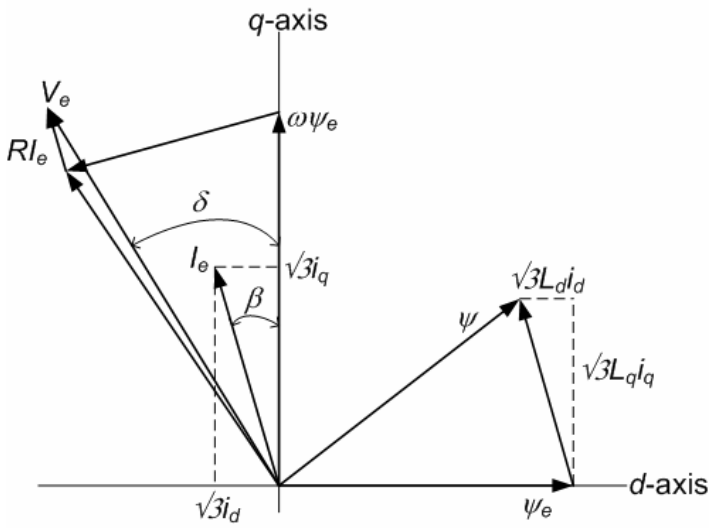

Figure 8.1. General *dq* vector diagram.

field coils in the case of wound-field motor and supporting magnets at the tips in the case of the permanent-magnet motor. The magnetisation of the field coils are arranged such that the armature tooth flux alternates between positive and negative maximum values as the segments on the rotor move. A full description of the principle of operation and descriptions of the three phase arrangements is in chapter 3 and 4 of this thesis, but it is useful to repeat here that each complete rotation of the rotor produces eight cycles of induced AC EMF in armature coils.

The description of the arrangement of this type of synchronous motor exudes early signs of substantive departure from the conditions of ideal transformation. The armature windings are concentrated, foretelling a non-sinusoidal back-EMF in the phase winding. The distortion from sinusoidal presentation of the phase flux linkage, verified by FE results in figure 8.3, results in the non-sinusoidal back-EMF, shown in figure 8.4.

While this departure from a sinusoidal waveform is partly attributed to the type of winding, saturation of the magnetic structures is also a significant factor, as evidenced by the change in the no-load EMF waveform and its THD as field excitation is varied. The total harmonic distortion (THD) of the EMF is as high as 35% at a low field current of 3.5 A, and drops to 8.9% with increase of field current to the nominal value of 14 A.

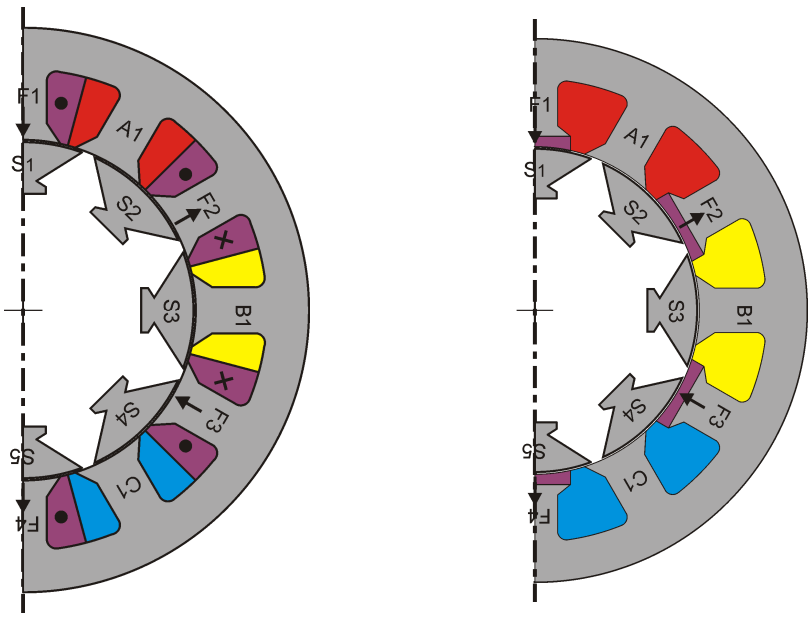

(a) FSM (b) PMFSM

Figure 8.2. Configurations of flux switching synchronous motors employing a segmental rotor.

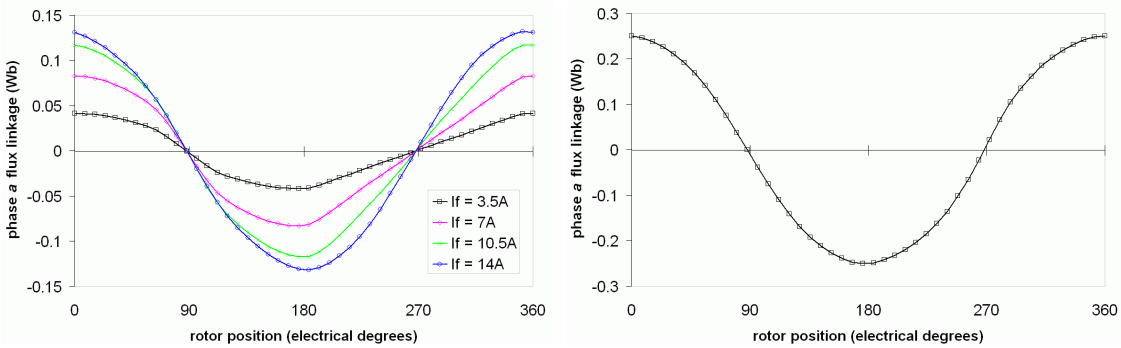

(a) FSM (b) PMFSM

Figure 8.3. Phase flux linkage.

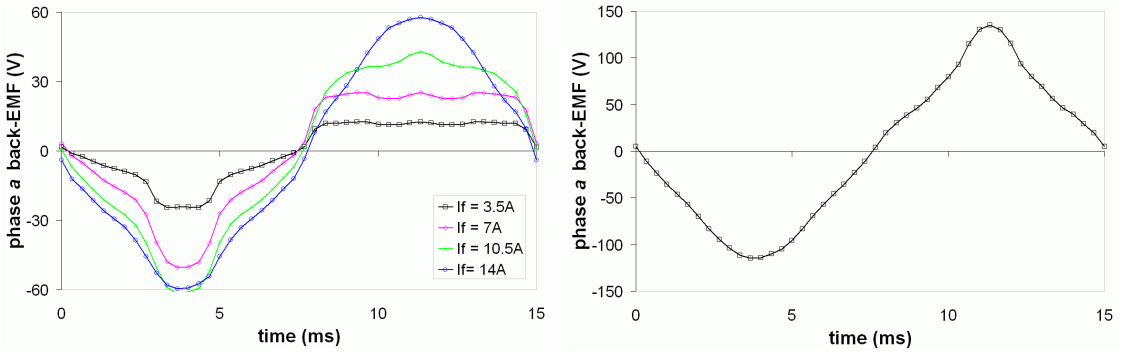

(a) FSM (b) PMFSM

Figure 8.4. Back-EMF at 500 r/min .

8.3.1 *abc* parameters

The inductances of the machine are influenced by two parameters: the rotor position θ_r, and the winding currents $\boldsymbol{i}_{abcf}$. Equation (8.3) gives the relationship between the flux linkages $\boldsymbol{\psi}_{abcf}$, and the winding currents, to define the inductance matrix $\boldsymbol{L}_{abcf}$. The inductance matrix comprises self- and mutual inductances according to (8.4).

In the FSM employing a segmented rotor, the three phase winding arrangement is symmetrical, presenting a balanced arrangement and therefore the phase inductances may be taken to be equal but displaced by 120°. The equivalent per phase inductances may then be represented by phase a inductance, so that the self-inductance, L_{aa}, and mutual inductance with adjacent phase b, L_{ab} are affected by both position and current and deemed to follow yet undetermined functions g_1 and g_2 as follows.

$$L_{aa} = g_1(\theta_r, i_{abcf}) \tag{8.21}$$

$$L_{ab} = g_2(\theta_r, i_{abcf}) \tag{8.22}$$

An examination of the phase self- and mutual inductances from FE simulations, obtained by the method described in [127], shows the extent to which these quantities are affected by rotor position, and phase and field currents.

The self-inductance, shown in figure 8.5, for rated field current or PM excitation, is seen to vary with position in a near sinusoidal manner at the same pace as the electrical frequency. The dc component and amplitude of the variable component change with phase current. The same pattern is observed even when the field excitation is below the rated value, but the dc component tends to increase with reduction of field current. The mutual inductance, in the same figure, is barely affected by the phase currents and is nearly constant at most positions except around where the segment is deemed to be

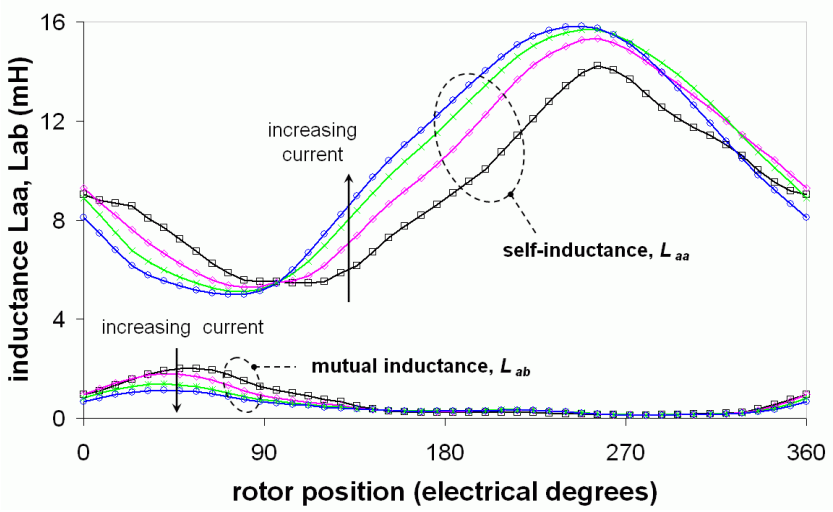

(a) wound-field FSM

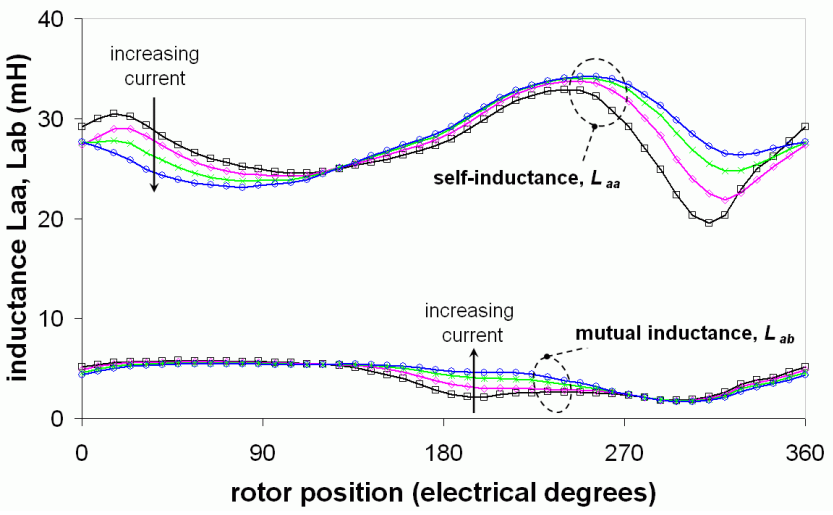

(b) PMFSM

Figure 8.5. Self- and mutual inductances with position at rated field excitation and varying rms phase current from 3.5 to 14 A.

centred with phase armature teeth, where it presents a gentle undulation. If the field excitation is reduced for the case of the wound-field motor, the mutual inductance reduces only slightly and assumes more of a constant value than at situations of rated field excitation. In general, considering the average or dc components only, the value of self inductance is higher than that of the mutual inductance between phases by a factor of about 17.4 for the wound-field motor and about 6.7 for the PM motor.

Figure 8.6 shows, for the field winding of the wound-field motor, the self-inductance and the mutual inductance to a phase winding. While the self-inductance is nearly constant with position, the change of the mutual inductance with position is nearly sinusoidal and is at the rate of the electrical frequency, with zero dc-component.

8.3.2 *dq* parameters

In the application of *dq* theory to the ideal situation where the self- and mutual inductances vary in sinusoidal manner at twice the electrical frequency, the *dq* model has constant flux linkage in the *d*-axis, constant *d*- and *q*-axis inductances and zero coupling inductance, L_{dq}. If it is taken that the frequency of the variation of self-and mutual inductances is the same as the electrical frequency, as encountered in the FSM with a segmented rotor, a Park transformation of the sinusoidal *abc* inductances to the *dq* form reveals that L_d and L_q expressions have $\sin\theta$ and $\cos\theta$ terms, some terms to the order of 3, suggestive of a complex variation with position. The Park transformation is applied with an open mind of being a mere mathematical mapping, without aiming for

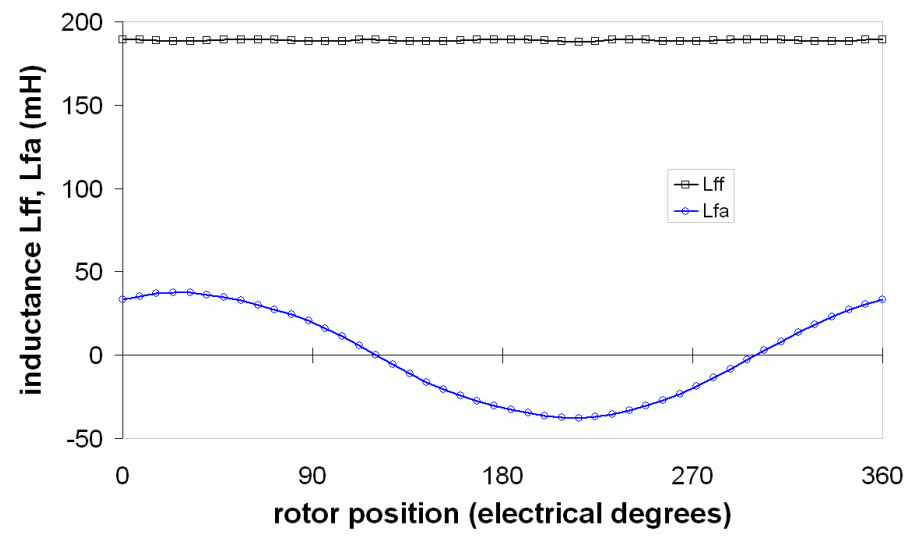

Figure 8.6. Self- and mutual inductances of field winding with position at 14 A field current.

simplification of the *dq* inductances.

Equations (8.7)-(8.11) are the basis for obtaining the *dq* inductances L_{dqf} by a transformation of the known *abc* inductances. The *abc* inductances in this investigation are availed by FE simulations, as in the previous section, but it is possible to use other predictive analytical methods. As the motor topology is significantly different from the convectional AC machine, coupled with a lack of an obvious rotating magnetic field and its reference, there is a need to identify the equivalent *d*- and *q*-axes with respect to a known reference.

The illustrations in figures 8.7 and 8.8 are for the wound-field motor, but the outcome is identical to that with the PM motor, as long as the correspondence of the magnetisation due the field winding to that due to the magnets is maintained on the field teeth. With respect to phase *a* winding (coil around tooth A) in figure 8.7, the *q*-axis on the rotor is identified by the position of the segment S1, where there is zero flux linkage in phase *a*, with field winding excitation only. There are two such positions in a cycle, unique and different in presentation, and are identified as the positions when a segment is centred with the phase armature tooth (mode 1) and when the two adjacent segments equally overlap the phase armature tooth (mode 2), as shown in figure 8.8 (c) and (d). Retarding or advancing the rotor by 90° electrical (equal to 11.25° mechanical) identifies the *d*-axis, when there is maximum flux linkage in phase *a*, as shown in figure 8.8 (a) and (b). The inductance L_d is evaluated with *abc* phase currents placed in the *d*-axis whilst the L_q inductance is evaluated with the phase currents in the *q*-axis. The inductance L_{dq} is evaluated with *abc* phase currents placed at any arbitrary known angle with respect to the *d*-axis, for instance 45°, and with previously computed values of either L_d or L_q, when the flux linkage expression is applied to yield L_{dq}. As the inductances are evaluated at discrete positions of the rotor through one electrical cycle, it entails knowledge of the corresponding discrete values of the *abc* phase currents at these rotor positions that place the currents in the *d*- and *q*-axis and another known arbitrary phase angle. The applicable expressions for these evaluations are in appendix C.

The behaviour of the *dq* inductances with rotor position, as observed in figures 8.9 and 8.10, can be divided into two parts as defined by two regions. The two regions are measured from 0° when the rotor is at the *q*-axis position with respect to phase *a*. The first region comprises the bands from approximately 0 to 90° and 270 to 360°, while the

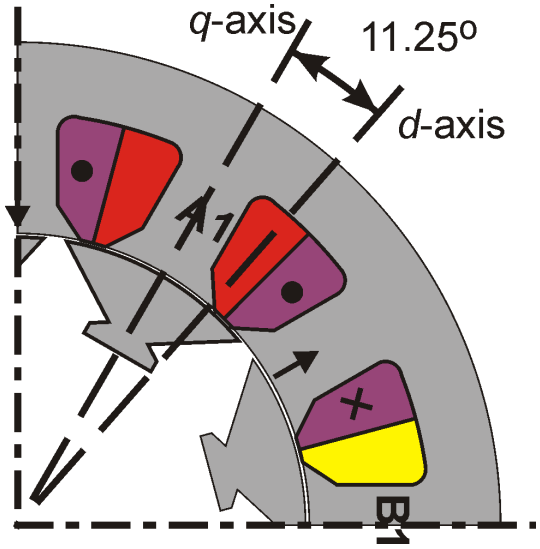

Figure 8.7. Identification of *d*-and *q*-axis.

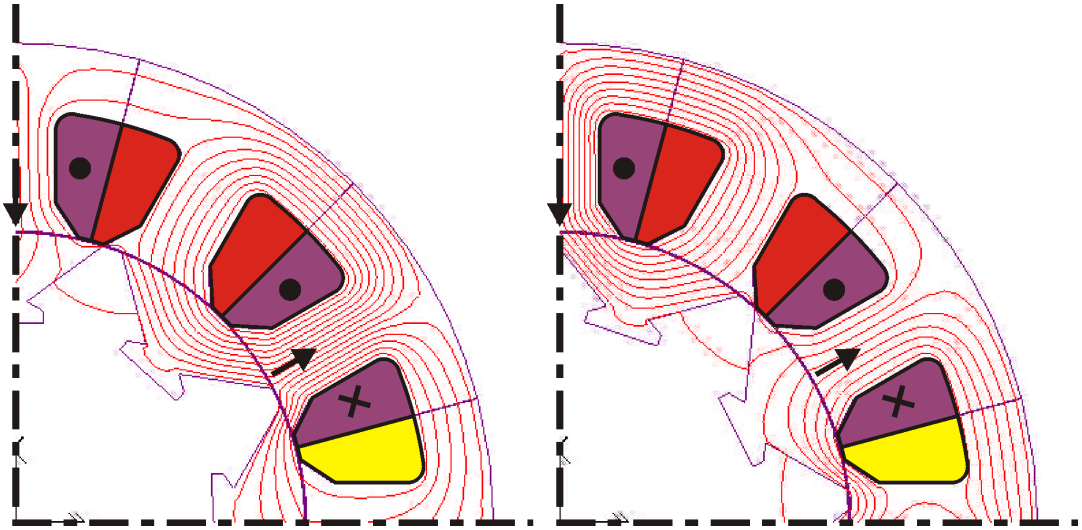

(a) positive maximum flux linkage

(b) negative maximum flux linkage

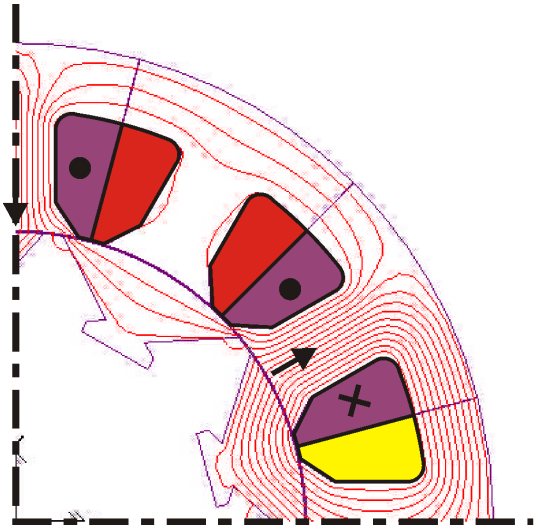

(c) zero flux linkage, mode 1

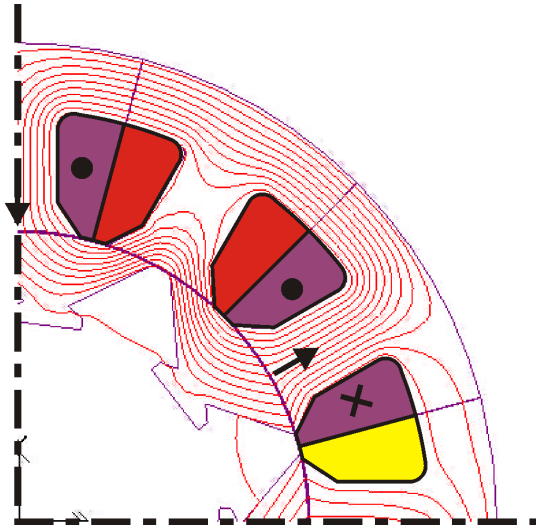

(d) zero flux linkage, mode 2

Figure 8.8. Flux linkages of phase *a* at peak and zero, with field excitation only.

second region lies between 90 and 270°. All the *dq* inductances appear to have higher values in the first region than in the second region. There is, however, no defined change of the field winding *dq*-inductance L_f, across these regions, which appears to be constant with position and whose mean value falls with increase of field current, as seen in figure 8.11. The inductances L_{fd} and L_{fq}, in part (b) of figure 8.11, behave in the same manner with position and field current as L_f but are much smaller, with mean values of 9.9 and 2.7 mH, respectively.

It is interesting that the regions classified above are related to the constitution of the permeance seen by the phase winding. The permeance of the phase winding in the first region is constituted by the magnetic circuit path through the segment to either one of

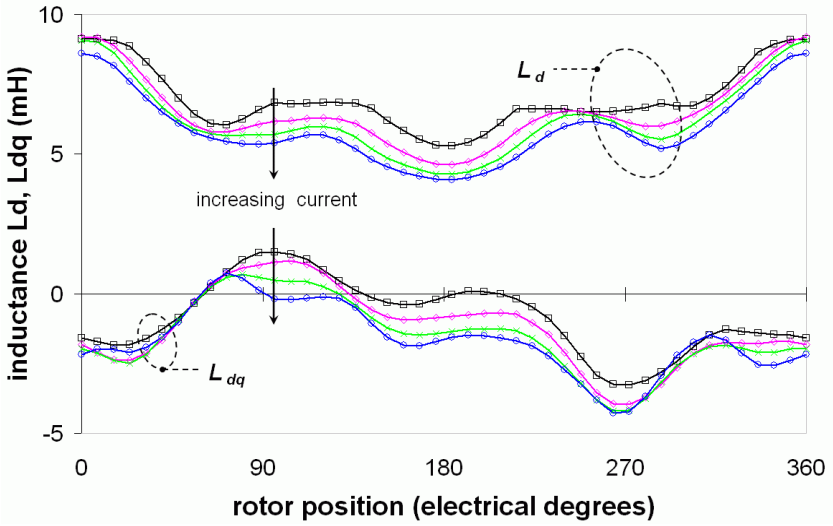

(a) wound-field FSM

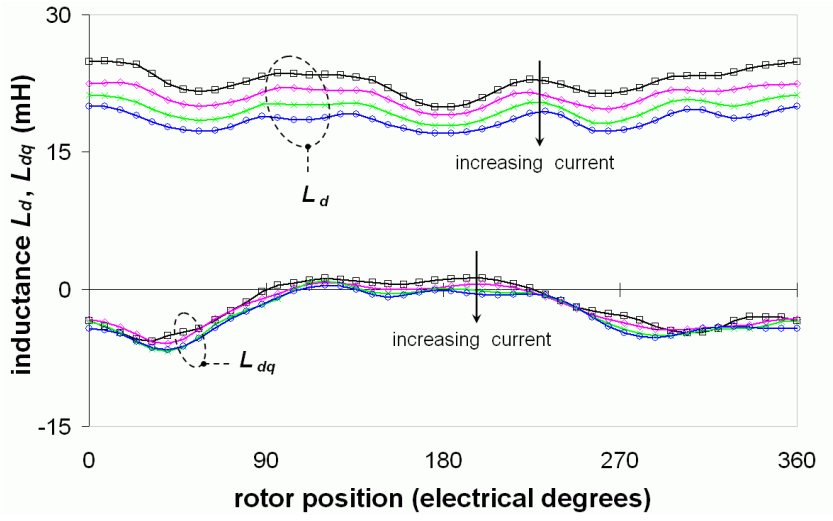

(b) PMFSM

Figure 8.9. *d*-axis and *dq*-coupling inductances at rated field excitation and various phase currents.

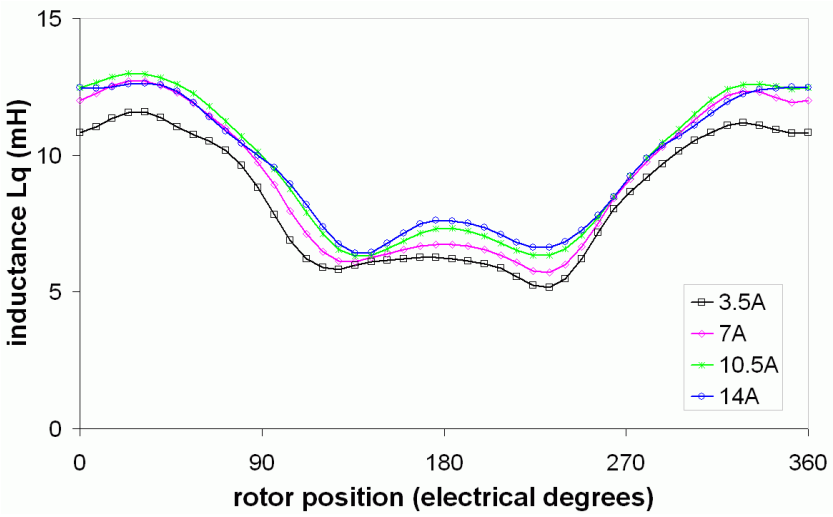

(a) wound-field FSM

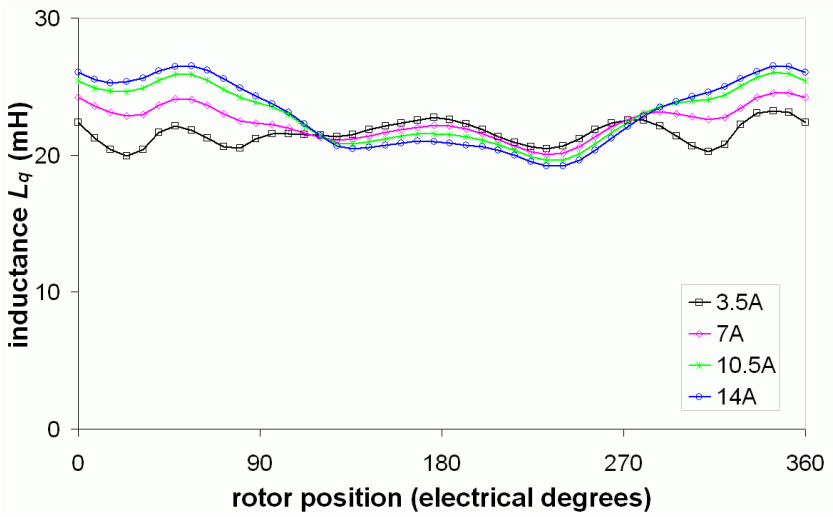

(b) PMFSM

Figure 8.10. *q*-axis inductances at rated field excitation and various phase currents.

the adjacent field teeth. The permeance in the second region is constituted by the parallel combination of two sub-circuits, created by the two simultaneous paths to the adjacent field teeth.

In contrast to conventional synchronous AC motors and PMFSM employing toothed rotors, L_d and L_q for the flux switching synchronous motors with a segmented rotor appear to vary appreciably with rotor position and L_{dq} has a finite value.

8.3.3 Effect of current on *dq* inductances

It is understood, and has been suggested in [236], [237], that the current may have significant influence on the inductance, due to the non-linear of effect of saturation. As

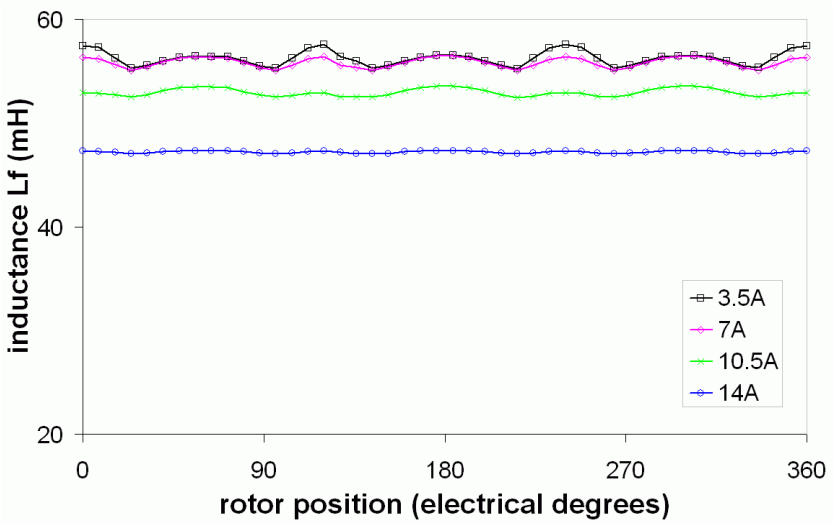

(a) L_{fd}

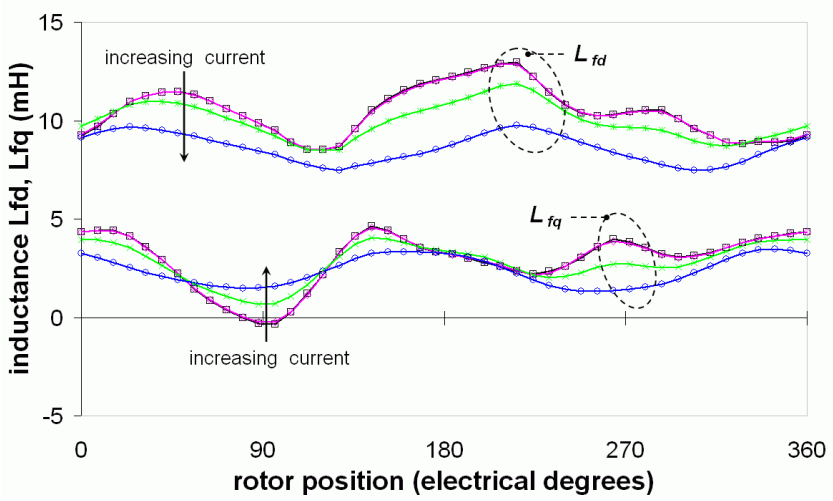

(b) L_{fd} and L_{fq}

Figure 8.11. *dq*-axis inductances of the field winding at various field excitation.

the *dq*-inductances appear to vary appreciably with position in the flux switching synchronous motor, it is expected that their mean values over once cycle are to be applied for representation in steady-steady prediction. Figure 8.12 shows the influence of the phase current on the *d*- and *q*-axis inductances for both the wound-field and PM motor, and at various levels of field excitation for the wound-field motor. The inductance L_d appears to fall with increase of phase current for the PM motor. In the wound-field motor at low excitation, the behaviour of L_d is similar, but there is little effect of the phase current on the inductances when the field excitation is high. On the other hand, the increase of phase current is accompanied by an increase of the inductance L_q for the PM and wound-field motor at high excitation. At low excitation L_q falls with increase of phase current, similar to the behaviour of L_d with phase current.

At rated field current, the saliency ratio L_d / L_q falls linearly with phase current over the range considered from 0.8 to 0.6 for the wound-field motor and from 1.0 to 0.8 for the PM motor. As a general observation, it is seen that the PM motor shows lower saliency than the wound-field motor due to the dominating influence of the reluctance of the permanent magnets in the magnetic circuit. When compared at rated field excitation and phase current excitation, L_d for the PM motor is 3.1 times that for the wound-field motor, while L_q for the PM motor is 2.4 times that of wound-field motor. This substantial difference in inductances between the wound-field and PM motors is apparently due to employing different armature coil turns, wherein the wound-field motor applies 88 turns per phase and the PM motor applies the 200 turns per phase.

The behaviour of the coupling inductance L_{dq} with current, which is shown alongside L_d in part (a) of figure 8.12, is similar to the behaviour of L_d for both the wound-field and

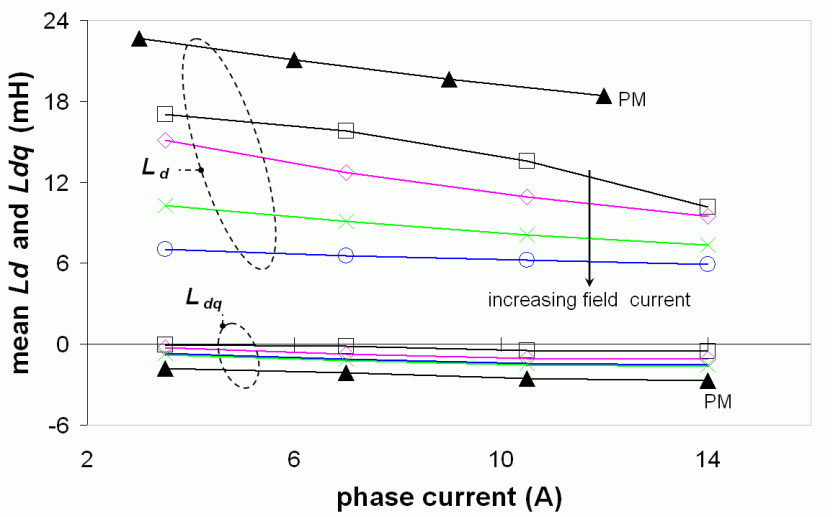

(a) d-axis inductance, L_d and coupling inductance, L_{dq}

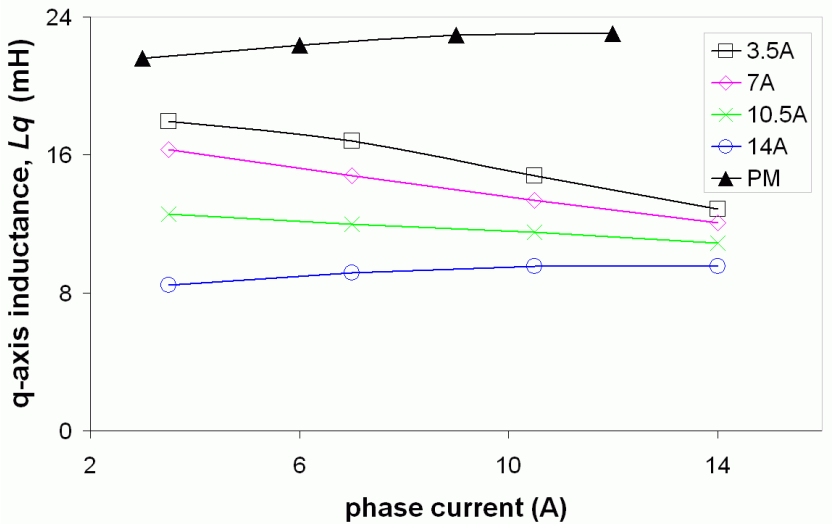

(b) q-axis inductance L_q

Figure 8.12. Variation of mean value of dq inductances with phase current.

PM motor. However, the mean values of L_{dq} for both the wound-field and PM motor are negative. Additionally, the magnitudes of the mean values for the PM motor across the range of the phase current are appreciably higher than those for the wound-field motor, by a factor ranging between 1.6 and 2.2, when the PM motor is compared with wound-field motor at 14 A field excitation. From the minimum phase current of 3 A to the maximum value of 12 A, L_{dq} changes from -0.81 to -1.65 mH for the wound-field motor at 14 A field excitation, whilst it changes from -1.8 to -2.7 mH for the PM motor. At rated excitation and phase current, the mean coupling inductance L_{dq} is 27.8% of the d-axis inductance L_d for the wound-field motor while the figure is 14.7% for the PM motor

8.4 Prediction of steady-state performance

Equations (8.16)-(8.20) are applied to predict the steady-state motor performance on the key parameters of terminal fundamental line voltage, power factor and torque. Corresponding values of the derived *dq* inductances are used for each operating condition of field excitation and armature phase currents.

The prediction by *dq* modelling and the measurements on the test motors are performed under the following conditions:

- The obvious complication posed by the variation of the *dq* inductances with rotor position is resolved by taking the dc component or mean value over a rotation of one cycle.

- For the purpose of testing the validity of the prediction, the phase resistance R is obtained from direct measurement on the phase winding of the test motors, but in actual application where a physical machine is not required, this may be estimated to a high degree of accuracy by known methods that take into account both the physical dimensions and electromagnetic effects. In both the wound-field and PM motor, while the effect of operating temperature is acknowledged, the phase resistance values at ambient temperature are applied and have values of 0.28 and 1.05 Ω, for the wound-field and PM motor, respectively.

- The voltage is presented as the fundamental of the voltage in the prediction expression whilst a 500-Hz low-pass filter was applied for the measured voltage in

the measurements. Inevitably, the power factor computation takes the fundamental values of the voltage and current, while the instrumentation for the measurement takes the true rms voltage as presented by the drive in evaluating power factor.

- The prediction avails the mean electromagnetic torque whilst the measurement avails the output mechanical torque. It is expected that the predicted electromagnetic torque contains a component for loss due to mechanical effects.

Despite the conditions highlighted above, it appears fair to directly compare the prediction and the measurements, as long as these conditions are borne in mind.

8.4.1 Line voltage and power factor at fixed speed

As can be seen in figure 8.13 for the representative comparisons at rated excitation (14 A for wound-field) and rated phase current (14 A for wound-field and 12 A for PM)), the voltage essentially varies linearly with phase current, as discerned from (8.16). Under no-load, the motor is required to supply a voltage of a least the value of the back-EMF, identified by the extrapolating through to the zero-phase current on the graph and represented by the term $\omega\psi_e$ in the voltage expression. The power factor, while represented by a more cryptic expression in (8.18) and (8.19), is seen to vary approximately linearly with phase current. The prediction and the measurement are reasonably matched in magnitudes and behaviour with phase current, within the conditions outlined above. For the wound-field motor, the mismatch of the prediction with the measurement voltage and power factor at the rated level of field excitation are -1.8 % and 6.1 % at the lowest considered phase current, respectively, and -5.3 % and 24.5 % a the highest considered phase current, respectively. The respective percentages for mismatch for the PM motor are 1.9% and 4.1% at the lowest current and -6.6% and 13.7% at the highest current.

8.4.2 Line voltage and power factor with variable speed

Although the percentage mismatch of the prediction with the measurement reduces with the speed while keeping motor current (and torque) constant, the absolute value of the mismatch in both the voltage and power factor appear to be constant for the both the wound-field and PM motor, as seen in figure 8.14. The mismatch in the power factor appears larger than the mismatch in voltage, mainly due to dissimilar comparison conditions outlined above. It must be borne in mind from results in the previous section

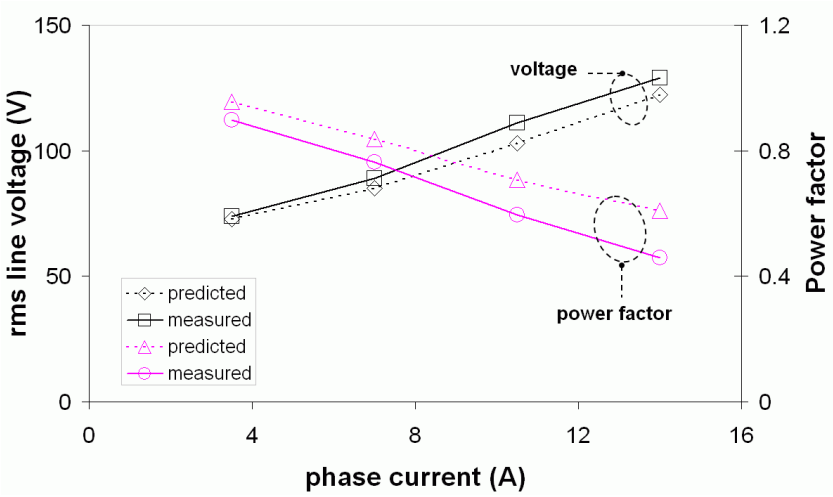

(a) wound-field FSM

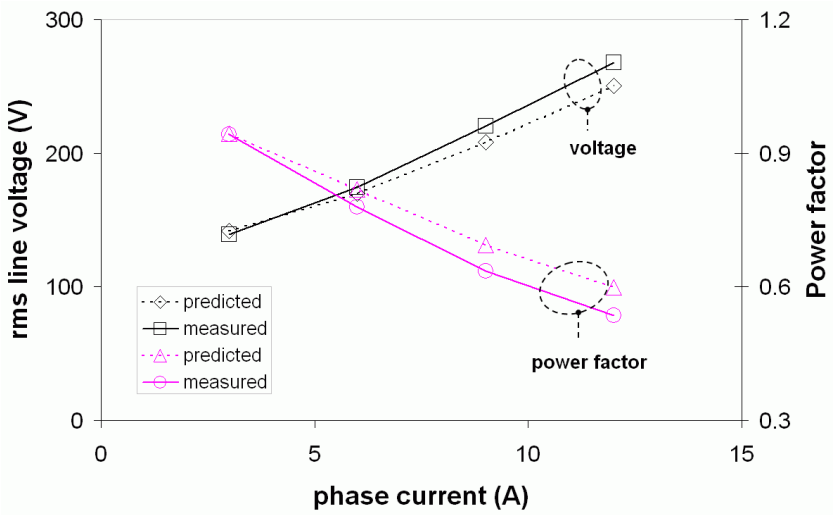

(b) PMFSM

Figure 8.13. Line voltage and power factor against phase current at 500 r/min and rated field excitations.

that operating at rated phase current gives the largest mismatch where there is an option of varying phase current. At the highest considered speed, the mismatch in voltage and power factor is -2.9% and 31.4% for the wound-field motor, respectively, and -6.3% and 10.1% for the PM motor, respectively.

8.4.3 Torque

Equation (8.17) predicts a linear relationship between mean electromagnetic torque and phase current when speed is fixed at a constant value. The comparison of the prediction with measurement, for both the wound-field and PM motor, is illustrated in figure 8.15 for a fixed speed of 500 r/min. The measurement results show the mechanical output torque increasing with phase current, not strictly in a linear manner, but with a reduction

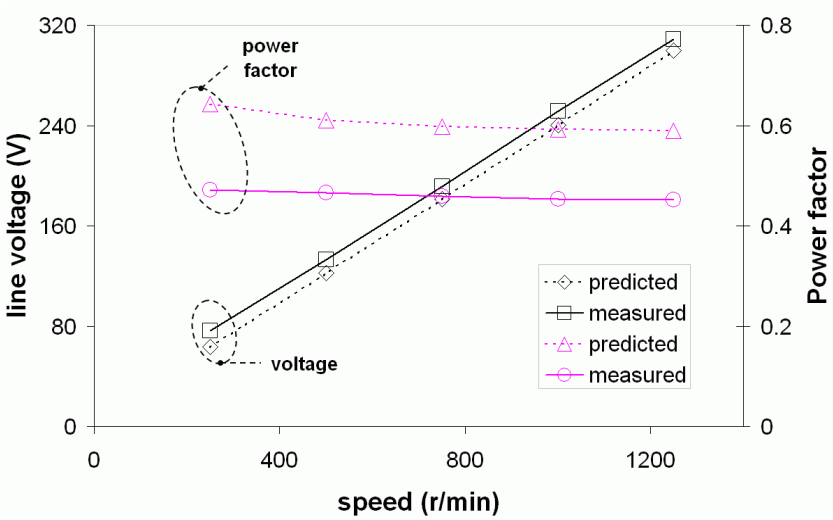

(a) wound-field FSM

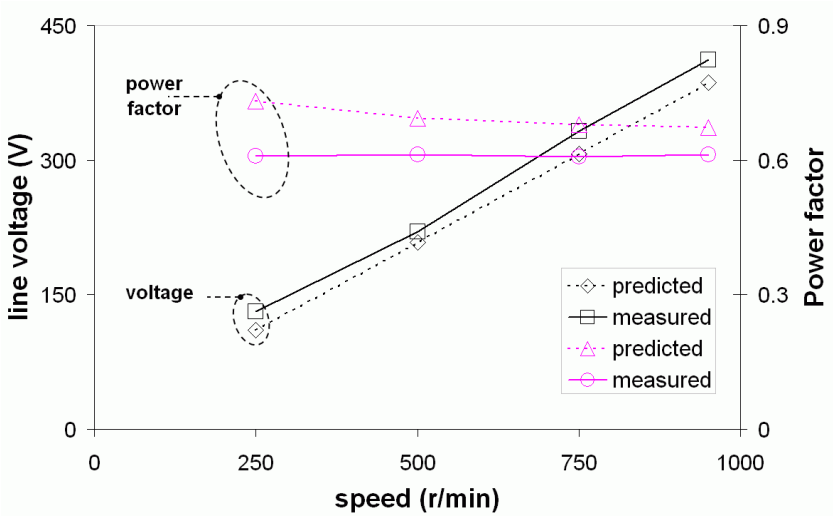

(b) PMFSM

Figure 8.14. Line voltage and power factor against speed at rated phase current and field excitation.

of the rate of increase at higher phase currents. This outcome produces an average mismatch of predicted torque over the considered current range of about 29.2% for the wound-field motor and 16.9% for the PM motor.

An alternative prediction approach, which takes into account the coupling of the *dq* inductances and represented by (8.20), produces a prediction of the electromagnetic torque which appears to track the measurement more closely than the prediction which assumes decoupled *dq* inductances. Taking account of the L_{dq} inductance affects the armature phase flux linkage, ψ in the manner illustrated in the phasor diagram of figure 8.16, and appears to be a more realistic representation for the FSM employing a segmental rotor. If L_{dq} is positive, ψ is affected to appear as ψ^{+}, and if L_{dq} is negative it

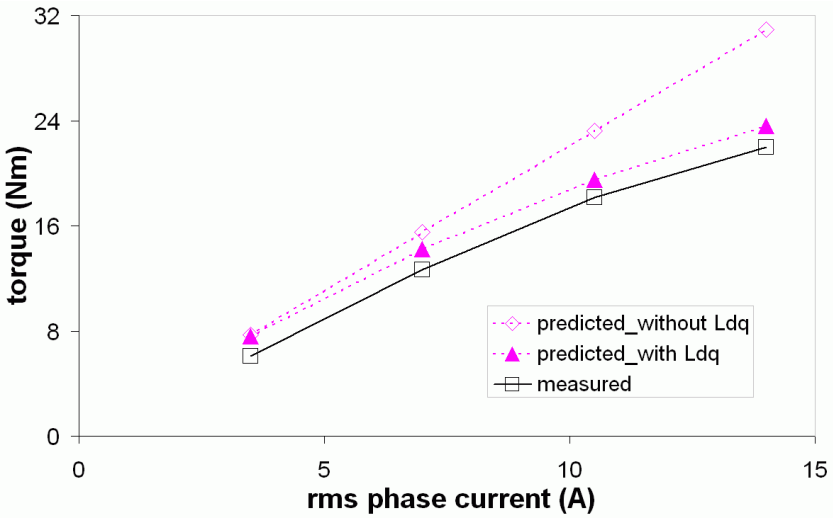

(a) wound-field FSM

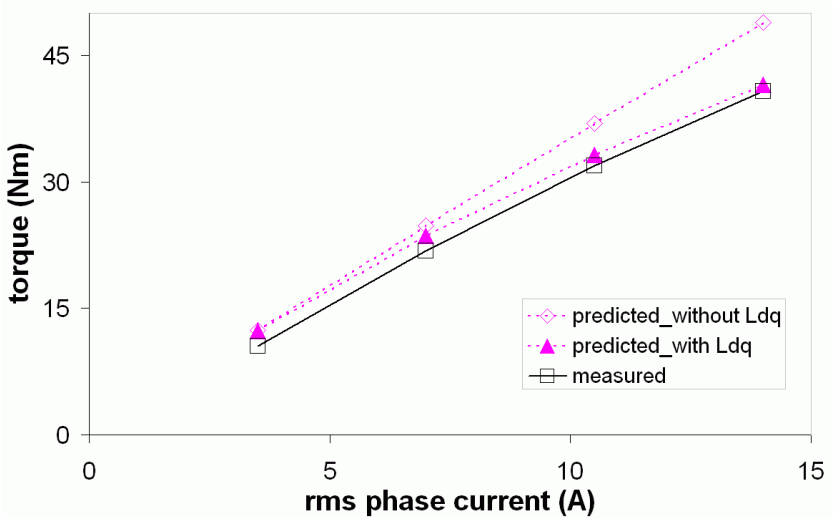

(b) PMFSM

Figure 8.15. Torque against phase current at rated field and 500 r/min.

is affected to appear as $\overline{\psi}$, in figure 8.16. The average mismatch in the electromagnetic torque, using this approach, falls to 12.8%, for the wound-field motor, and to 7.9%, for the PM motor. As the mean value of the coupling inductances over the electrical cycle of rotation is negative, it is easy to appreciate the reduction effect of the torque term with L_{dq} on the resultant electromagnetic torque, so that the rate of increase of resultant torque with current is diminished at higher currents, as in the measurement results.

8.5 Conclusion

After laying a foundation for employing *dq* modelling in conventional AC machines, the substantive departures from ideal requirements of *dq* transformation of the flux switching synchronous motor employing a segmental rotor have been considered. Due

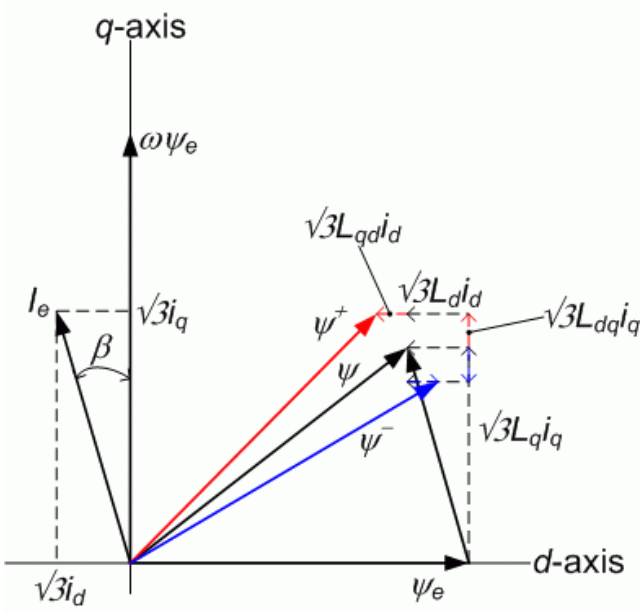

Figure 8.16. Vector diagram accounting for L_{dq} and L_{qd} coupling.

to their unusual topology, the flux switching motors employing a segmental rotor require additional exigent considerations, which are apparent in both the stator reference frame *abc* model and in the synchronous frame *dq* model. Since the resultant *dq* parameters obtained by direct transformation of the *abc* parameters are not simplified constant parameters as in conventional AC machines, their interpretation and application in the predictive expressions is judiciously exercised to have credibility.

An adopted *dq* model gives a prediction of the terminal voltage and power factor that matches reasonably closely with the measurement over a range of phase current and operating speed. The prediction of torque is reasonably close to the measurement at low motor currents, but diverges significantly at high motor current. However, it is found that the prediction of the torque is substantially improved across the operating range of current if the model is made to incorporate the coupling effect of the *dq* inductance.

The use of a *dq*-model for the synchronous motor with credible predictive accuracy for the steady state performance paves the way for applying analytically-derived models in characterising motor performance from motor design stage to interaction with the drive. As pointed out in chapter 3, an analytical approach, such as the magnetic equivalent circuit approach, especially if it adaptively incorporates real effects, may be made as accurate as the FE approach applied here, but with the advantage of less computing time and resources. The main challenge appears to be devising such an analytical model that incorporates the cross-coupling effects.

Chapter 9

Conclusion

Flux switching machines employing segmental rotors have been characterised in this thesis by their principle of operation and basic topological arrangement. The stages of treatment in the study, from concept and design to construction and testing of demonstrator machines, have served to elicit both the fundamental and peculiar properties of flux switching machines employing a segmental rotor. The treatment on construction and manufacturing considerations is centred on the resultant structure of the feasible three-phase arrangements with either a field winding or permanent magnets. Testing of the performance of machines has verified the concepts and afforded a comparison of the machines on specific output against those of conventional configurations of similar arrangements. A *dq*-equivalent model, derived under distorted conditions, has also been tested for validity under synchronous steady-state operation of the motor.

9.1 Overview

The four principal broad objectives of this study were to conceive, design, construct and test three-phase flux-switching machines employing segmental rotors. Substantive outcomes have been produced for each of these objectives.

Concept

The concept of flux-switching using a segmental rotor has been developed using elementary rectilinear structures, and extended to describe and define rotary concepts for single-phase and polyphase arrangements. This treatment of the basic configurations reveals both fundamental and subtle characteristics of the concept including similarities and differences with the schemes employing a toothed-rotor.

Design

The design process considers the best configuration on the basis of predefined performance characteristics. With a specified outside diameter, a number of parameters in the configuration and geometry of the resultant three phase arrangements have been investigated to consider the best topology for three-phase presentations. Modelling for the designs is done with 2D FE, the large number of design configurations benefiting from the more rapid solutions and less requirement of computing resources than 3D FE modelling, albeit with some considered loss of accuracy due to the encumbrances of the applied assumptions of 2D modelling. The 2D approach has proved reliable at the design stage, as the results have been mainly for relative comparison of performance.

Construction

In constructing demonstrator machines, modern manufacturing methods have been considered, compared and applied to determine an efficient production approach which favours simplicity and avoids wastage of materials. As there has been a chance to produce more than one prototype, the production methods have been also been varied for different prototypes to experience and contrast the effect of the different methods.

Testing

Static measurement of torque, no-load running test and loaded motoring tests have been performed on the demonstrator machines. The characteristics elicited by the FE models have been directly tested and verified by the measurement. Where applicable, it has proved useful to compare directly the measurement results with the FE models' results

and gauge the reliability of the FE modelling by indicating the deviations. The motoring tests have been performed using a standard three-phase AC drive with a defined and known control strategy, providing the testing opportunity for one of the principal motor operating modes. A comparison on the output torque, with similarly arranged and sized conventional machines, on the basis of measurements on physical machines and FE models, exposes the machines to scrutiny in the context of established electrical machines.

9.2 Characteristics of Flux-Switching Machines

The concept of flux-switching using a segmental rotor has been developed around a representation of elementary rectilinear structures, centred on four stator teeth and two rotor segments, of which half the stator teeth are designated as the field and the other half as the armature. For the arrangement to produce AC flux in the armature teeth by motion of the rotor segments, the orientation of the field flux in one field tooth must be opposite to that on the next adjacent field tooth. Further to this, the basic principle is valid regardless of whether field excitation is produced by a DC winding or permanent magnets. Based on this concept, rotary arrangements for single-phase presentation may be developed in which the ratio of the number of stator teeth to the number of segments is an even integer. When the ratio is a positive rational number greater than 1, other than an even integer, a polyphase presentation is the outcome.

While most of the properties of flux switching by means of a segmental rotor are similar to those of the relatively older schemes employing a toothed rotor, the most important yet subtle distinction between the schemes is in the magnetisation of the magnetic sections that convey bipolar flux. The scheme with a segmental rotor has a magnetisation trajectory for a change of flux from negative to positive maximum which is quite different from that from positive to negative, and results in dissimilar alternation in the EMF waveform and unequal peaks of positive and negative torque. The focal points of this difference is in the presentation of two types of zero flux linkage of an armature tooth coil by different positional presentations of the rotor segments, one when a rotor segment is centred with the coil tooth and the other when a rotor slot is centred with the coil tooth. The difference in the magnetisation trajectory has also been found to be influenced to a degree by the relationship of the span of rotor slot to that of coil tooth, and to a lesser degree by the level and type of field excitation.

9.3 Three Phase Configurations with Segmental Rotors

With a specified outside stator and rotor diameter, a number of parameters including the number of stator teeth and rotor segments, segment span and stator tooth width have been investigated to consider the best topology for three-phase presentations. In pursuing three-phase configurations, eight topologies have been conceived, of which six are practically feasible on the 12-tooth stator and by transposition, a further two are feasible on a 24-tooth stator.

Among the eight feasible three-phase configurations, the configuration with 12 stator teeth and 8 rotor segments appears to the best practical topology, selected on the basis of the results of an evaluation of the resulting performance in output torque, harmonic distortion of the EMF waveform and presence of unbalanced magnetic pull. On the basis of output torque and harmonic distortion alone, the configuration with 12 stator teeth and 7 rotor segments produces the best of the desired results but it has significant UMP, which makes it to be precluded in the overall consideration.

The output torque appears to increase with the segment span and the highest torque for the 12/8-configuration is obtained when the segment span is at its maximum allowable, equivalent to segment pitch less the minimum permitted rotor slot span. At this segment span the THD is also at the lowest. The ratio of the armature-tooth width to the field-tooth width affects the performance parameters in a disparate manner. Output torque is at its largest when the ratio is between 0.6-0.8, while the least THD for the EMF waveform is presented when the ratio is unity.

9.4 Construction

The shape or geometry of the stator and rotor component cores significantly influences the choice of the manufacturing method. Although the geometry is principally determined by functional and structural considerations, there appears to be gains in designing for manufacture, where the shapes have simple outlines, their production and construction are amenable to automation and where there is low wastage of materials. The shapes of the stator teeth and rotor sections have thus been determined in an intimate balance of these factors. Modularisation of the stator cores to the smallest possible section enables utilisation of the least amount of core sheet materials and produces the least percentage of waste for the type of stator designed. Designing the

shape of the main body of the rotor segment is less complicated than the stator core but considerations on the shape for its root are leveraged more by the need for retention capability on the rotor shaft than by manufacturing concerns.

Suitable shapes of the stator teeth and rotor segments have been selected according to the interplay of the above factors. The stator core for the wound-field machines has been produced as a modularised assembly and that for the permanent-magnet machine as a complete core, presenting an occasion for both pre-winding the stator teeth before assembly and needle-winding by threading the wire. The designs of the shapes of the stator and rotor component cores and the selected methods of their production have proved to be robust and their results have been borne in the tests the ensued. Four demonstrator machines have been constructed of which one pair of the wound-field scheme is in 12/8 and 12/5 configurations and another pair of the permanent-magnet scheme is also in 12/8 and 12/5 configurations.

9.5 Performance Results

The results of the performance tests on the wound-field and permanent-magnet demonstrator machines have verified both the principle of operation and performance characteristics of flux switching machines employing segmental rotors. The predictions results from 2D FE models have matched the measurements results to an acceptable degree of accuracy.

The static torque of the machines in 12/8 configurations have been shown to have unequal positive and negative peak torques as predicted from FE simulation. Similarly, as predicted from the models, the induced EMF in the armature phase winding has been shown in measurements to have unequal alternations in the waveform. However, for the 12/5 configurations, there has been the expected equivalency of the peaks of the static torque and symmetry of the alternations of the induced EMF waveforms. The proportional response of the induced EMF to the excitation and the torque to both the field excitation and armature current has been evident in the tests, including the effect of saturation of the magnetic core.

In running both the wound-field and permanent-magnet machines as synchronous motors, performance characteristics similar to those of the conventional synchronous motors have been revealed, with the wound-field motor exhibiting extended torque

control by way of field current. Of particular note are the torque-speed characteristics, which demonstrate a base speed delimited by the drive's output voltage and the motor's intrinsic property of per unit reactance.

For the frame size of the machines studied, the wound-field machine running as synchronous motor appears to have the specific torque close to that of a conventionally configured SRM, but significantly higher, by a factor of nearly 2, than that of the segmental-rotor synchronous reluctance motor, of which it has extensive similarities in structure. It is thought that the permanent-magnet machine running as a synchronous motor has similarities in function to the conventional PMSM, but a comparison of the performance on specific torque has shown that it has about 64% the torque capability of a similarly sized PMSM.

9.6 Classical *dq* model

Despite the flux-switching synchronous motor presenting several violations of the assumptions of *dq* theory, the steady-state performance of the motor may be reliably represented in *dq* modelling by including the effect of the coupling *dq* inductance. It is a characteristic of the flux switching synchronous motor with either a field-winding or permanent-magnet excitation, which has been revealed after transforming the three phase *abc* inductances to orthogonal *dq* inductances, that the coupling *dq* inductance is finite and negative. Furthermore, the *dq* inductances have been found to vary with rotor position, unlike in the classical application with sine wave distributed windings and a rotating field on the rotor in which they emerge as constant. For this reason, the mean value or dc component of the *dq* inductances is applied in the representation. Although the inductances also vary with current, due mainly to saturation of the steel, their values are closely-defined with respect to the operating current, so that the representation applies the corresponding inductances at the applicable operating current.

It is thought that the *dq* model, whose derivation may benefit from modern nonlinear adaptive magnetic equivalent circuit approach, may provide a more rapid and less expensive method of prediction of steady-state performance for the flux-switching synchronous motor than FE modelling.

9.7 Further Work

This work has considered the concept, characterisation and some design aspects of the flux switching machines employing a segmental rotor. While the main aspects of the objectives have been addressed, interesting ideas arising in the course of this work have emerged, and whose pursuance may increase understanding and application of these types of machines. Below is an outline of some of these ideas.

- Further optimisation of the designs for 12/8 configuration is possible. Although the influence of the span of stator tooth in relation to the span of the rotor slot has been gleaned in the treatment with elementary rectilinear structures, it appears interesting to investigate how performance fares when these parameters are varied in the 12/8 configuration. Additionally, as the size of design has been based on a typical integral TEFC industrial motor, it is suggested that optimisation may be improved in different sizes of motor by investigating the influence afforded by varying the ratio of the rotor to stator diameter and the airgap length.

- From the predictions, the torque ripple is as notoriously a nuisance in this type of motors as in SRMs, even with synchronous sinusoidal current operation. Methods to minimise the torque ripple at design stage or in operating regimes may increase the range of application of these types of motors.

- Effects of locating the magnets near the airgap in the PM machine require further study. It is known that demagnetisation of magnets is likely with magnets at similar positions in FRMs.

- An analysis of the losses for the flux switching machine, including a development of loss models, is suggested, especially if high-performance applications are envisaged.

- In this work, motoring operation has been directed at applying synchronous sinusoidal current. It remains to be considered what the performance of the motor is if square wave current with electronic commutation is applied.

- Development of nonlinear adaptive analytical expressions for the inductances of the machines is work which may complement the power of using a *dq* model to predict steady-state performance.

References

[1] Finley, W., Veerkamp, B., Gehring, D., and Hanna, P., 'Improving Motor Efficiency Levels Globally,' IEEE Industry Applications Magazine, vol. 15 , no. 1, January/February 2009, pp. 39-49.

[2] Boteler, R., and Malinowski, J., 'Review of Upcoming Changes to Global Motor Efficiency Regulations,' IEEE Annual Pulp and Paper Industry Technical Conference, PPIC '09, Birmingham, Alaska, USA, 21-26 June 2009, pp. 26-30.

[3] Benhaddadi, M., and Olivier, G., 'Barriers and Incentives Policies to High-Efficiency Motors and Drives Market Penetration,' Symposium on Power Electronics, Electrical Drives, Automation and Motion, SPEEDAM'08, Ischia, Italy, 11-13 May 2008, pp. 1161-1164.

[4] de Almeida, A.T., Ferreira, F.J.T.E., Fong, J.A.C., and Brunner, C.U., 'Electric Motor Standards, Ecodesign and Global Market Transformation,' IEEE/IAS Industrial and Commercial Power Systems Technical Conference, ICPS'08, Clear Water Beach, Florida, USA, 4-8 May 2008, pp. 1-9.

[5] Benhaddadi, M., Olivier, G., and Yelle, J., 'Premium Efficiency Motors Effectiveness,' Symposium on Power Electronics, Electrical Drives, Automation and Motion, SPEEDAM'10, Pisa, Italy, 14-16 June 2010, pp. 1607-1612.

[6] Ionel, D.M., 'High-Efficiency Variable-Speed Electric Motor Drive Technologies for Energy Savings in the US Residential Sector,' 12th International Conference on Optimization of Electrical and Electronic Equipment, OPTIM 2010, Brasov, Romania, 20-22 May 2010, pp. 1403-1414.

[7] Benhaddadi, M., Olivier, G., Labrosse, D., and Tetrault, P., 'Premium Efficiency Motors and Energy Saving Potential,' IEEE International Electrical Machines and Drives Conference,' IEMDC'09, Miami, Florida, USA, 3-6 May 2009, pp. 1463-1468.

[8] Finley, W.R., Veerkamp, B., Gehring, D., and Hanna, P., 'Advantages of Using High Efficiency Motors Such as NEMA Premium® Around the World,' IEEE 44th Petroleum and Chemical Industry Technical Conference, PCIC '07, Calgary, Alberta, Canada, 17-19 September 2007, pp. 1-14.

[9] Mecrow, B.C., Jack, A.G., Atkinson D.J., and Haylock J.A., 'Fault Tolerant Drives for Safety Critical Applications,' IEE Colloquium on New Topologies for Permanent Magnet Machines (Digest No: 1997/090), 1997, pp. 5/1-5/7.

[10] Boglietti, A., Cavagnino, A., Ferraris, L., and Lazzari, M., 'Energy-Efficient Motors,' IEEE Industrial Electronics Magazine, December 2008, pp. 32-37.

[11] Mecrow, B.C., and Jack, A.G., 'Efficiency Trends in Electric Machines and Drives,' Energy Policy, vol. 36, no. 12, December 2008, pp. 4336-4341.

[12] Jahns, T.M. and Owen, E.L., 'AC Adjustable-Speed Drives at the Millennium: How Did We Get Here?' IEEE Transactions on Power Electronics, vol. 16, no. 1, January 2001, pp. 17-25.

[13] Lorenz L., 'Power Semiconductors Development Trends,' CES/IEEE 5th International Power Electronics and Motion Control Conference, IPEMC'06, Shanghai, China, 13-16 August 2006, pp. 1-7.

[14] Lorenz L., 'Key Power Semiconductor Devices and Development Trends,' 11th IEEE International Conference on Electrical Machines and Systems, ICEMS'08, Wuhan, China, 17-20 October 2008, pp 1137-1142.

[15] Toliyat, H.A., 'Recent Advances and Applications of Power Electronics and Motor Drives-Electric Machines and Motor Drives,' IEEE 34th Annual Industrial Electronics Conference, IECON'08, Orlando, Florida, USA, 10-13 November 2008, pp. 34-36.

[16] Bose, B.K., 'Power Electronics and Motor Drives Recent Progress and Perspective,' IEEE Transactions on Industrial Electronics, vol. 56, no. 2, February 2009, pp. 581-588.

[17] Blaabjerg, F., Consoli, A., Ferreira, J.A., and van Wyk, J. D., 'The Future of Electronic Power Processing and Conversion,' IEEE Transactions on Industry Applications, vol. 41, no. 1, January/February 2005, pp. 3-8.

[18] Lorenz L., 'Power Semiconductors State-of-Art annd Development Trends,' 7th IEEE Internatonal Conference on Power Electronics, ICPE'07, Daegu, South Korea, 22-26 October 2007, pp. 683-686.

[19] Huang, A., 'Recent Advances and Applications of Power Electronics and Motor Drives-Power Semiconductor Devices,' IECON'08, Orlando, Florida, USA, 10-13 November 2008, pp. 28-29.

[20] Capolino, G.A., 'Recent Advances and Applications of Power Electronics and Motor Drives- Advanced and Intelligent Control Techniques,' IEEE 34th Annual Industrial Electronics Conference, IECON'08, Orlando, Florida, USA, 10-13 November 2008, pp. 37-39.

[21] Hayes, J.P, 'Technology Changes in Personal Computers,' IEEE Transactions on Systems, Man and Cybernetics, vol. 10, no. 8, August 1980, pp. 476-480.

[22] Nunnally, C.E., 'Requiring PC's -Status Update: 7 Years,' IEEE Proceedings of Southeastcon '91, Williamsburg, Virginia, USA, 7-10 April 1991, pp. 957-958.

[23] Trybus, D., Kucerovsky, Z., Ieta, A., Doyle T.E., and Flatley, M., 'Performance Analysis of a Dual Processor Workstation,' Proceedings of the IEEE Canadian Conference on Electrical & Computer Engineering, Winnipeg, Manitoba, 12-15 May 2002, pp. 640-645.

[24] Alberti, L., Bianchi, N., and Bolognani, S., 'A Very Rapid Prediction of IM Performance Combining Analytical and Finite-Element Analysis,' IEEE Transactions on Industry Applications, vol. 44, no. 5, September/October 2008, pp. 1505-1512.

[25] Alberti, L., Bianchi, N., Baldassari, P., and Wang, R., 'Thermal Assisted Finite Element Analysis of Electrical Machines,' 18th International Conference on Electrical Machines, ICEM'08, Vilamoura, Portugal, 6-9 September 2008, pp. 1-4.

[26] Shuhong, W., Qingfu, L., Mingxing, T., and Qunfeng, L., 'A New Method for Design and Analysis of a Parameterized Electrical Machine Electromagnetic Fields Finite Element Package,' IEEE 6th International Conference on Electrical Machines and Systems, ICEMS'01, Beijng, China, 9-11 November 2003, pp. 823-826.

[27] Parrish, J., Moll, S., and Schaefer, R.C., 'Plant Efficiencies Benefit by Selection of Synchronous Motor,' 42nd IEEE Industry Applications Annual Meeting, IAS'07, New Orleans, Louisiana, USA, 23-27 September 2007, pp. 1229-1237.

[28] Hayashi, H., Nakamura, K.,Chiba, A., and Fukao, T., 'Efficiency Improvements of Switched Reluctance Motors with High-Quality Iron Steel and Enhanced Conductor Slot Fill,' IEEE Transactions on Energy Conversion vol. 24 , no. 4, December 2009, pp. 819-825.

[29] Hayashi, H., Chiba, A., and Fukao, T., 'Efficiency Comparison of Switched Reluctance Motors with Low Loss Materials,' IEEE Power Engineering Society General Meeting, PES'07, Tampa, Florida, USA, 24-28 June 2007, pp. 1-6.

[30] Kirtley, J.L., Cowie, J.G., Brush, E.F., Peters, D.T., and Kimmich, R., 'Improving Induction Motor Efficiency with Die-cast Copper Rotor Cages,' IEEE Power Engineering Society General Meeting, PES'07, Tampa, Florida, USA, 24-28 June 2007, pp. 1-6.

[31] Kim, Y.G., Bae, C.B., Kim, J.M., and Kim, H.C., 'Efficiency Improvement by Changeover of Phase Windings of Multiphase Permanent Magnet Synchronous Motor with Outer-Rotor Type,' IEEE 25th Annual Applied Power Electronics Conference and Exposition, APEC'10, Palm Springs, California, USA, 21-25 February 2010, pp. 112-119.

[32] Sanada, M., and Morimoto, S., 'Efficiency Improvement in High Speed Operation using Slot-less Configuration for Permanent Magnet Synchronous Motor,' IEEE Power Engineering Society General Meeting, PES'07, Tampa, Florida, USA, 24-28 June 2007, pp. 1-6.

[33] Mellor, P.D., Wrobel, R., McNeill, N., and Drury, D., 'Impact of Winding and Rotor Design on Efficiency and Torque Ripple in Brushless AC Permanent Magnet Traction Motors,' IET 4th International Conference on Power Electronics, Machines and Drives, PEMD 2008, York, UK, 2-4 April 2006, pp. 240-244.

[34] Yung, C., 'Improving Electric Motors by Better Designing,' IEEE Industry Applications Magazine, vol. 13 , no. 6, November/December 2007, pp. 12-20.

[35] Krishnan, R., 'An Energy-Efficiency-Enhanced Switched Reluctance Motor,' IEEE Industrial Electronics Magazine, vol. 1, no. 1, 2007, pp. 4-6.

[36] Sanada, M., Morimoto, S., 'Efficiency Improvement at High-Speed Operation using Large Air-Gap Configuration For PMSM,' 18th International Conference on Electrical Machines, ICEM'08, Vilamoura, Portugal, 6-9 September 2008, pp. 1-6.

[37] Kosaka, T., Kume, A., Wakayama H., and Matsui, N., 'Development of High Torque Density and Efficiency Switched Reluctance Motor with 0.1mm Short Airgap,' 12th European Conference on Power Electronics and Applications, EPE'07, Aalborg, Denmark, 2-5 September 2007, pp. 1-9.

[38] Bianchi, N., Bolognani, S., and Frare, P., 'Design Criteria for High-Efficiency SPM Synchronous Motors,' IEEE Transactions on Energy Conversion, vol. 21, no. 2, June 2006, pp. 396-404.

[39] Lee, D.Y., Jung, C.G., Yoon, K.J., and Kim, G.T., 'A Study on the Efficiency Optimum Design of a Permanent Magnet Type Linear Synchronous Motor,' IEEE Transactions on Magnetics, vol. 41, no. 5, May 2005, pp. 1860-1863.

[40] Gupta, R.K., and Mohan, N., 'A Three-Phase Permanent Magnet Brushless DC Motor for Low-Power Low-Speed Fan Applications-Optimizing Cost and

Efficiency,' 42nd IEEE Industry Applications Annual Meeting, IAS'07, New Orleans, Louisiana, USA, 23-27 September 2007, pp. 846-852.

[41] Hur, M., and Sung H.G., 'Development of High-efficiency 42V Cooling Fan Motor for Hybrid Electric Vehicle Applications,' IEEE Vehicle Power and Propulsion Conference, VPPC'06, Windsor, UK, 6-8 September 2006, pp. 1-6.

[42] Rodger, D., Lai, H.C., Hill-Cottingham, R.J., Coles, P.C., and Robinson, F., 'A New High Efficiency Line Start Motor with High Starting Torque,' IET 3rd International Conference on Power Electronics, Machines and Drives, PEMD 2006, Dublin, Ireland, 4-6 April 2006, pp. 551-555.

[43] Woody, J.E., 'Improving Efficiency in Fractional Horsepower Motors for Air-Moving Applications,' Electrical Insulation Conference and Electrical Manufacturing Exposition, EEIC 2005, Indianapolis, Indiana, USA, 26-26 October 2005, pp. 351-356.

[44] Jack, A.G., 'Impact of New Materials on the Design of Electrical Machines,' IEE Colloquium on Impact of New Materials on Design, 1995 , pp. 1/1-1/5.

[45] Moses, A.J., 'Iron Based Amorphous Magnetic Materials - Present and Future,' IEE Colloquium on New Magnetic Materials, Digest no. 1998/259, 1998, pp. 9/1-9/2.

[46] Alam, F., Kamal, M.M., and Asgar, M.A., 'Study of Magnetostriction in Iron and Cobalt Based Amorphous Magnetic Materials,' 34th International Conference on Electrical and Computer Engineering, ICECE'06, Dhaka, Bangladesh, 19-21 December 2006, pp. 366-369.

[47] Paker, R.J., 'Survey of Rare Earth Permanent Magnet Applications,' IEEE Transactions on Magnetics, vol.17, no. 6, November 1981, pp. 2985-2987.

[48] Knoch, K.G., 'Rare Earth Permanent Magnet Materials and their Properties,' IEE Colloquium on Impact of New Materials on Design, 1995 , pp. 8/1 - 8/5.

[49] Schrefl, T., Fidler, J., and Scholz, W., 'Modeling and Limits of Advanced HT-Magnets,' IEEE Transactions on Magnetics, vol. 36, no. 5, September 2000, pp. 3394-3398.

[50] Gallagher, K., Venkatesan, M., and Coey, J. M. D., 'Magnetic Properties of Mechanically-Alloyed Sm–Co Nanophase Hard Magnets,' IEEE Transactions on Magnetics, vol. 37, no. 4, July 2001, pp. 2528-2530.

[51] Renyuan, T., 'Research and Development of Rare Earth Permanent Magnet Machines,' IEEE 5th International Conference on Electrical Machines and Systems, ICEMS'01, Shenyang, China 18-20 August 2001, pp. 28-34.

[52] Thompson, M.T., 'Practical Issues in the Use of NdFeB Permanent Magnets in Maglev, Motors, Bearings, and Eddy Current Brakes,' Proceedings of the IEEE vol. 97, no. 11, November 2009, pp. 1758-1767.

[53] Driscolt, D., Dombrovski, V., and Zhang, B., 'Development Status of Superconducting Motors,' IEEE Power Engineering Review, May 2000, pp. 12-15.

[54] Kalsi, S.S., 'Development Status of Superconducting Rotating Machines,' IEEE Power Engineering Society Winter Meeting, New York, New York, USA, 27-31 Juanuary 2000, pp. 401-403.

[55] Gamble, B.B., Kalsi, S., Snitchler, G., Madura, D., and Howard, R., 'The Status of HTS Motors,' IEEE Power Engineering Society Summer Meeting, Chicago, Illinois, 25-29 July 2002, pp. 270 – 274.

[56] Kalsi, S.S., Gamble, B.B., Snitchler, G., and Ige, S.O., 'The Status of HTS Ship Propulsion Motor Developments,' IEEE Power Engineering General Meeting, Chicago, Illinois, 18-22 June 2006, pp. 1-5.

[57] Bennett, J.W., Mecrow, B.C., Jack, A.G., and Atkinson, D.J., 'A Prototype Electrical Actuator for Aircraft Flaps,' IEEE Transactions on Industry Applications, vol. 46, no. 3, May/June 2010, pp. 915-921.

[58] Wolmarans, J., Polinder, H., Ferreira, J.A. Clarenbach, D., 'Design of a Fault Tolerant Permanent Magnet Machine for Airplanes,' IEEE 11th International Conference on Electrical Machines and Systems, ICEMS'08, Wuhan, China, 17-20 October, 2008, pp. 2882-2887.

[59] Schramm, A., and Gerling, D., 'Researches on the Suitability of Switched Reluctance Machines and Permanent Magnet Machines for Specific Aerospace Applications Demanding Fault Tolerance,' Sympoisum on Power Electronics, Electrical Drives, Automation and Motion, SPEEDAM'06, Toarmina, Italy, 23-26 May 2006, pp. 56-60.

[60] Bennett, J.W., Mecrow, B.C., Jack, A.G., Atkinson, D.J., Sheldon, S., Cooper, B. Mason, G., Sewell C., and Cudley, D., 'A Prototype Electrical Actuator for Aircraft Flaps and Slats,' IEEE International Electrical Machines and Drives Conference,' IEMDC'05, San Antonio,Texas, USA, 15-18 May 2005, pp. 41-47.

[61] Atkinson, G.J., Mecrow, B.C., Jack, A.G., Atkinson, D.J., Sangha, P., Benarous, M., 'The Design of Fault Tolerant Machines for Aerospace Applications,' IEEE International Electrical Machines and Drives Conference,' IEMDC'05, San Antonio,Texas, USA, 15-18 May 2005, pp. 1863-1869.

[62] Naidu, M., Gopalakrishnan, S., and Nehl, T.W., 'Fault-Tolerant Permanent Magnet Motor Drive Topologies for Automotive X-by-Wire Systems,' IEEE Transactions on Industry Applications, vol. 46, no. 2, March/April 2010, pp. 841-848.

[63] Abolhassani, M.T., and Toliyat, H.A., 'Fault Tolerant Permanent Magnet Motor Drives for Electric Vehicles,' IEMDC'09, Miami, Florida, USA, 3-6 May 2009, pp. 1146-1152.

[64] Abolhassani, M.T., 'Novel Multiphase Fault Tolerant High Torque Density Permanent Magnet Motor Drive for Fuel Cell Powered Vehicles,' IEEE 3rd Vehicle Power and Propulsion Conference, VPPC'07, Arlington, Texas, USA, 9-12 September 2007, pp. 160-167.

[65] Bianchi, N., Bolognani, S., and Pr´e, M.D., 'Design of a Fault-tolerant IPM Motor for Electric Power Steering,' IEEE 36th Power Electronics Specialists Conference, PESC '05, Recife, Brazil, 12-18 June 2005, pp. 2873-2880.

[66] Bianchi, N., and Bolognani, S., 'Fault-Tolerant PM Motors in Automotive Applications,' IEEE 1st Vehicle Power and Propulsion Conference, VPPC'05, Chicago, Illinois, USA, 7-9 September 2005, pp. 747-755.

[67] Abolhassani, M.T., 'Novel Multiphase Fault Tolerant High Torque Density Permanent Magnet Motor Drive for Traction Application,' IEEE International Electrical Machines and Drives Conference,' IEMDC'05, San Antonio,Texas, USA, 15-18 May 2005, pp. 728-734.

[68] Polinder, H., Lendenmann, H., Chin, R., and Arshad, W.M., 'Fault Tolerant Generator Systems for Wind Turbines,' IEEE International Electrical Machines and Drives Conference,' IEMDC'09, Miami, Florida, USA, 3-6 May 2009, pp. 675-681.

[69] Gopalakrishnan, S., Omekanda, A.M., and Lequesne, B., 'Classification and Remediation of Electrical Faults in the Switched Reluctance Drive' IEEE Transactions on Industry Applications, vol. 42, no. 2, March/April 2006, pp. 479-486.

[70] Fahimi, B., Emadi, A., and Sepe, R.B., 'A Switched Reluctance Machine-Based Starter/Alternator for More Electric Cars,' IEEE Transactions on Energy Conversion, vol. 19, no. 1, March 2004, pp. 116-124.

[71] Jack, A.G., Mecrow, B.C., and Haylock, J.A., 'A Comparative Study of Permanent Magnet and Switched Reluctance Motors for High-Performance Fault-Tolerant Applications,' IEEE Transactions on Industry Applications, vol. 32, no. 4, July/August 1996, pp. 889-895.

[72] Raminosoa, T., Gerada, C., and Galea, M., 'Design Considerations for a Fault Tolerant Flux Switching Permanent Magnet Machine,' IEEE Transactions on Industrial Electronics, in press (2010).

[73] Zhao, W., Cheng, M., Hua W., and Jia, H., 'A Redundant Flux-Switching Permanent Magnet Motor Drive for Fault-Tolerant Applications,' IEEE Vehicle Power and Propulsion Conference, VPPC'08, Harbin, China, 3-5 September 2008, pp. 1-6.

[74] El-Refaie, A.M., 'Fault-Tolerant PM Machines: A Review,' IEEE International Electrical Machines and Drives Conference,' IEMDC'09, Miami, Florida, USA, 3-6 May 2009, pp. 1700-1709.

[75] Klontz, K.W., Miller, T.J.E., McGilp, M.I., Karmaker, H., and Zhong, P., 'Short-Circuit Analysis of Permanent-Magnet Generators', IEEE International Electrical Machines and Drives Conference,' IEMDC'09, Miami, Florida, USA, 3-6 May 2009, pp. 1080-1087

[76] Raminosoa, T., Gerada, C., and Othman N., 'Rating Issues in Fault Tolerant PMSM,' IEEE International Electrical Machines and Drives Conference,' IEMDC'09, Miami, Florida, USA, 3-6 May 2009, pp. 1592-1599.

[77] Hao, Z., Hu, Y., Huang, W., Yu, W., and Huang, X., 'The Research on Key Technologies of Fault-Tolerant Permanent Magnet Motor in the Drive System of Electric Vehicle,' IEEE Vehicle Power and Propulsion Conference, VPPC'08, , Harbin, China, 3-5 September 2008, pp. 1-4.

[78] Mecrow, B.C., Jack, A.G., Atkinson, D.J., Green, S.R., Atkinson, G. J., King, A., and Green, B., 'Design and Testing of a Four-Phase Fault-Tolerant Permanent-Magnet Machine for an Engine Fuel Pump,' IEEE Transactions on Energy Conversion, vol. 19, no. 4, December 2004, pp. 671-678.

[79] Mecrow B.C., Jack A.G., Haylock J.A., Coles, J., 'Fault-Tolerant Permanent Magnet Machine Drives,' IEE Proceedings-Electric Power Applications, vol. 143, no. 6, November 1996, pp. 437-442.

[80] Parsa, L., and Toliyat, H.A., 'Fault-Tolerant Interior-Permanent-Magnet Machines for Hybrid Electric Vehicle Applications,' IEEE Transactions On Vehicular Technology, vol. 56, no. 4, July 2007, pp. 1546-1552.

[81] Mitcham, A.J., Antonopoulos, G. and Cullen. J.J.A., 'Favourable Slot and Pole Number Combinations for Fault-Tolerant PM Machines,' IEE Proceedings-Electric Power Applications, vol. 151, no. 5, September 2004, pp. 520-525

[82] El-Refaie, A.M., 'Fractional-Slot Concentrated-Windings Synchronous Permanent Magnet Machines: Opportunities and Challenges,' IEEE Transactions on Industrial Electronics, vol. 57, no. 1, January 2010, pp. 107-121.

[83] Bianchi, N., Pr´e, M.D., Grezzani, G., and Bolognani, S., 'Design considerations on fractional-slot Winding Configurations of Synchronous Machines,' IEEE Transactions on Industry Applications, vol. 42, no. 4, July/August 2006, pp. 997-1006.

[84] Bianchi, N., Pr´e, M.D., Grezzani, G., and Bolognani, S., 'Design Considerations on Fractional-Slot Fault-Tolerant Synchronous Motors,' IEEE International Electrical Machines and Drives Conference,' IEMDC'05, San Antonio,Texas, USA, 15-18 May 2005, pp. 902-909.

[85] Barcaro, M., Bianchi, N., and Magnussen, F., 'Configurations of Fractional–Slot IPM Motors with Dual Three-Phase Winding,' IEEE International Electrical Machines and Drives Conference,' IEMDC'09, Miami, Florida, USA, 3-6 May 2009, pp. 936-942.

[86] Aghili, F., 'Fault-Tolerant Torque Control of BLDC Motors,' IEEE Transaction on Power Elecronics, in press (2010).

[87] Pan, Z., and Amhad, R., 'A Novel Motor / Converter Topology for High-Speed, High-Power Motor Applications,' IEEE 39th Power Electronics Specialists Conference, PESC '08, Rhodes, Greece, 15-19 June 2008, pp. 2301-2307.

[88] Wolmarans, J., Gerber, M.B., Polinder, H., de Haan, S.W.H., Ferreira, J.A. and Clarenbach, D., 'A 50kW Integrated Fault Tolerant Permanent Magnet Machine and Motor Drive,' IEEE 39th Power Electronics Specialists Conference, PESC '08, Rhodes, Greece, 15-19 June 2008, pp. 345-351.

[89] Desai, P., Krishnamurthy, M., Schofield, N., and Emadi, A., 'Novel Switched Reluctance Machine Configuration with Higher Number of Rotor Poles than Stator Poles: Concept to Implementation,' IEEE Transactions on Industrial Electronics, vol. 57, no. 2, February 2010, pp. 649-659.

[90] Zhao, W., Cheng, M., Hua, W., Zhu, X., and Zhang, Y., 'Fault-Tolerant Operation of Brushless Machines Having Magnets in the Stator,' IEEE International Electrical Machines and Drives Conference,' IEMDC'09, Miami, Florida, USA, 3-6 May 2009, pp. 1420-1425.

[91] Reinap, A., Hagstedt , D., Marquez, F., Loayza, Y., and Alakula, M., 'Development of a Radial Flux Machine Design Environment,' 18th International Conference on Electrical Machines, ICEM'08, Vilamoura, Portugal, 6-9 September 2008, pp. 1-4.

[92] Kano, Y., Kosaka, T., and Matsui, N., 'A Simple Nonlinear Magnetic Analysis for Axial-Flux Permanent-Magnet Machines,' IEEE Transactions on Industrial Electronics, vol. 57, no. 6, June 2010, pp. 2124-2133.

[93] Marignetti, F., Di Stefano, R., and Coia, Y., 'Analysis of Axial Flux PM Machines Including Stator and Rotor Core Losses,' IEEE 34th Annual Industrial Electronics Conference, IECON '08, Orlando, Florida, USA, 10-13 November 2008, pp. 2035-2040.

[94] Loureiro, L.T.R., Filho, A.F.F., Zabadal, J.R.S., and Homrich, R.P., 'A Model of a Permanent Magnet Axial-Flux Machine Based on Lie's Symmetries,' IEEE Transactions on Magnetics, vol. 44, no. 11, November 2008, pp. 4321-4324.

[95] Locment, F., Semail, E., and Piriou, F., 'Design and Study of a Multiphase Axial-Flux Machine,' IEEE Transactions on Magnetics, vol. 42, no. 4, April 2006, pp. 1427-1430.

[96] Jinhao, S., Yongbin, L., and Wenpeng, Z., 'Survey on the Development of Transverse Flux Machines,' IEEE 6th International Conference on Electrical Machines and Systems, ICEMS'03, Beijing, China, 9-11 November, 2003, pp. 137-140.

[97] Baserrah, S., Rixen, K.,and Orlik, B., 'Transverse Flux Machines with Distributed Windings for In-Wheel Applications,', IEEE 8th International Conference on Power Electronics and Drive Systems, PEDS'09, Taipei, Taiwan, 2-5 November, 2009, pp. 102-108.

[98] Leskovec, J., Pevec, B., Lahajnar, F., and Miljavec, D., 'Optimization of the Transverse-Flux Motor Based on Design of Experiments,' IEEE 8th International Conference on Power Electronics and Drive Systems, PEDS'09, Taipei, Taiwan, 2-5 November, 2009, pp. 932-937.

[99] Dubois, M.R., Polinder, H., and Ferreira, J.A., 'Transverse-Flux Permanent Magnet Machine with Toothed Rotor,' IET 1st International Conference on Power Electronics, Machines and Drives, PEMD 2002, Bath, UK, 16-18 April 2002, pp. 309-314.

[100] Fu, W.N., and Ho, S.L., 'A Novel Axial-Flux Electric Machine for In-wheel Gearless Drive in Plug-in Hybrid Electric Vehicles,' 14th Biennial IEEE Conference on Electromagnetic Field Computation, CEFC 2010, Chicago, Illinois, USA, 9-12 May 2010, pp. 1-1.

[101] Versele, C., De Greve, Z., Vallee, F., Hanuise, R., Deblecker, O., Delhaye, M., and Lobry, J., 'Analytical Design of an Axial Flux Permanent Magnet In-Wheel Synchronous Motor for Electric Vehicle,' 13th European Conference on Power Electronics and Applications, EPE'09, Barcelona, Spain, 8-10 September 2009, pp. 1-9.

[102] de la Barriere, O., Ben Ahmed, H., and Gabsi, M., 'Axial Flux Machine Design for Hybrid Traction Applications,' IET 4th International Conference on Power Electronics, Machines and Drives, PEMD 2008, York, UK, 2-4 April 2006, pp. 174-178.

[103] Chang, J., Lee, J., Kim, Ji., Chung, S., Kang, D., and Weh, H., 'Development of Rotating Type Transverse Flux Machine,' IEEE International Electrical Machines and Drives Conference,' IEMDC'07, Antalya, Turkey 3-5 May 2007, pp. 1090-1095.

[104] Guo, G., Zhu, J.G., Watterson, P.A., and Wu, W., 'Development of a PM Transverse Flux Motor with Soft Magnetic Composite Core,' IEEE Transactions on Energy Conversion, vol. 21, no. 2, June 2006, pp. 426-434.

[105] Patterson, D.J., Colton, J.L., Mularcik, B., Kennedy, B.J., Camilleri, S., and Rohoza, R., 'A Comparison of Radial and Axial Flux Structures in Electrical Machines,' IEEE International Electrical Machines and Drives Conference,' IEMDC'09, Miami, Florida, USA, 3-6 May 2009, pp. 1029-1035.

[106] Marignetti, F., Colli, V.D., and Carbone, S., 'Comparison of Axial Flux PM Synchronous Machines with Different Rotor Back Cores,' IEEE Transactions on Magnetics, vol. 46, no. 2, February 2010, pp. 598-601.

[107] Hewitt, A.J., Ahfock, A., and Suslov, S.A., 'Magnetic Flux Density Distribution in Axial Flux Machine Cores,' IEE Proceedings-Electric Power Applications, vol. 152, no. 2, March 2005, pp. 292-296.

[108] Cavagnino, A., Lazzari, M., Profumo, F., and Tenconi, A., 'A Comparison Between the Axial Flux and the Radial Flux Structures for PM Synchronous Motors,' IEEE Transactions nn Industry Applications, vol. 38, no. 6, November/December 2002, pp. 1517-1524.

[109] Arshad, W. M., Backstrom, T., and Sadarangani, C., 'Analytical Design and Analysis Procedure for a Transverse Flux Machine,' IEEE International Electrical Machines and Drives Conference,' IEMDC'01, Cambridge, Massachussetts, USA, 17-20 June 2001, pp. 115-121.

[110] Zhang, J., Cheng, M., Hua, W., and Zhu, X., 'Influence of Winding Configuration on Characteristics of Doubly Salient Permanent Magnet Machine,' IEEE 12th Biennial Conference on Electromagnetic Field Computation, CEFC'06, Miami, Florida, USA, 30 April-3 May 2006, pp. 318.

[111] Baek, J., Rahimian, M.M., Toliyat, H.A., 'Optimal Design and Comparison of Stator Winding Configurations in Permanent Magnet Assisted Synchronous Reluctance Generator,' IEEE International Electrical Machines and Drives Conference,' IEMDC'09, Miami, Florida, USA, 3-6 May 2009, pp. 732-737.

[112] Wang, J., Howe, D., and Lin, Z., 'Comparative Study of Winding Configurations of Short-Stroke, Single Phase Tubular Permanent Magnet Motor for Refrigeration Applications,' IEEE 42nd Industry Application Society Annual Meeting, IAS'07, New Orleans, Louisiana, USA, 23-37 September 2007, pp. 311-318.

[113] Cros, J., and Viarouge, P., 'Synthesis of High Performance PM Motors with Concentrated Windings' IEEE Transactions on Energy Conversion, vol. 17, no. 2, June 2002, pp. 248-253.

[114] Walker, J.H., 'The Theory of the Inductor Alternator,' Journal of IEE, vol. 89, 1942, pp. 227-241.

[115] Rauch, S.E. and Johnson, L.J., 'Design Principles of Flux-Switch Alternators,' Transactions of AIEE, Power Apparatus and Systems, vol. 74, no. 3, part III, January 1955, pp. 1261-1268.

[116] Dasgupta, A.K., 'Analytical Method to Find the Best Number of Stator and Rotor Teeth of Inductor Alternator for 3-Phase Sinusoidal Voltage Generation,' Transactions of AIEE, Power Apparatus and Systems, vol. 79, no. 50, October 1960, pp. 674-679.

[117] Dasgupta, A.K., 'Mathematical Analysis of Inductor Alternators,' AIEE Transactions on Power Apparatus and Systems, vol. 79, no. 50, October 1960, pp. 684-689.

[118] Subbiah, M., and Krishnamurthy, M.R., 'Single-Winding Single-Phase Inductor Alternator,' IEEE Transactions of Aerospace and Electronic Systems, vol. 12, no. 6, November 1976, pp. 689-697.

[119] Subbiah, M., and Krishnamurthy, M.R., 'Certain Design Aspects of Single-Winding Three-Phase Inductor Alternators,' IEEE Transactions of Aerospace and Electronic Systems, vol. 10, no. 5, September 1976, pp. 648-657.

[120] Dasgupta, A.K., and Dash, P.K., 'Derivation of the Basic Constants of Three-Phase Inductor Alternators in Terms of Winding Parameters,' IEEE Transactions on Power Apparatus and Systems, vol. 88, no. 5, May 1969, pp. 566-574.

[121] Dash, P.K., and Dasgupta, A.K., 'Design Aspects of Three-Phase Inductor Alternators,' IEEE Transactions on Power Apparatus and Systems, vol. 88, no. 11, November 1969, pp. 1718-1724.

[122] Pollock, C., and Wallace, M., 'The Flux Switching Motor, a DC Motor Without Magnets or Brushes,' IEEE 34th Industry Applications Society Annual Meeting, IAS'99, Pheonix, Arizona, USA, 3-7 October 1999, vol.3, pp. 1980-1987.

[123] Mecrow, B.C., Bedford, T.J., Bennet, J.W., and Celik, T., 'The Use of Segmental Rotors for 2-Phase Flux-Switching Motors,' 17th International Conference on Electrical Machines, ICEM'06, Chania, Greece, 2-5 September 2006, paper 608.

[124] Cheng, Y., Pollock, C. and Pollock, H., 'A Permanent Magnet Flux Switching Motor for Low Energy Axial Fans,' IEEE 40th Industry Applications Society Annual Meeting, IAS'05, Hong Kong, China, 2-6 October 2005, vol.3, pp. 2168-2175.

[125] Hoang, E. Ben-Ahmed, A.H., and Lucidarme, J., 'Switching Flux Permanent Magnet Poly-Phased Synchronous Machines,' 7th European Conference on Power Electronics and Applications, EPE'97, Trondheim, Norway, September, 1997, vol.3, pp.903-908.

[126] Deodhar, R.P., Andersson, S., Boldea, I., and Miller, T. J.E., 'The Flux Reversal Machine: A New Brushless Doubly-Salient Permanent-Magnet Machine,' IEEE Transactions on Industry Application, vol. 33, no. 4, July/August 1997, pp. 925-934

[127] Zhu, Z.Q., Pang, Y., Howe, D., Iwasaki, S., Deodhar, R., and Pride, A., 'Analysis of Electromagnetic Performance of Flux-Switching Permanent Magnet Machines by Nonlinear Adaptive Lumped Parameter Magnetic Circuit Model,' IEEE Transactions on Magnetics, vol. 41, no.11, 2005, pp. 4277-4287.

[128] Zhang, J., Cheng, M., and Zhang Y., 'Single Phase Doubly Salient Permanent Magnet Generator with Full-pitched Winding,' IEEE International Conference on Electric Machines and Drives, IEMDC'09, Miami, Florida, USA, 3-6 May 2009, pp. 311 - 316.

[129] Wang, C. Nasar, S.A., and Boldea, I., 'Three-Phase Flux Reversal Machine (FRM),' IEE Proceedings on Electrical Power Applications, vol. 146, no. 2, March 1999, pp. 139-146.

[130] Wang, C. X., Boldea, I., and Nasar, S. A., 'Characterization of Three Phase Flux Reversal Machine as an Automotive Generator,' IEEE Transactions on Energy Conversion, vol. 16, no. 1, March 2001, pp.74-80.

[131] Goodier, E.R.T., and Pollock, C., 'Homopolar Variable Reluctance Machine incorporating an Axial Field Coil,' IEEE Transactions on Industry Application, vol. 38, no. 6, November/December 2002, pp. 1534-1541.

[132] Goodier, E.R.T., and Pollock, C., 'Design and Control of a Variable Reluctance Drive with Axially Orientated DC Flux Assistance,' IEEE 36th Industry Applications Society Annual Meeting, IAS'01, Chicago, Illinois, USA, 30 September-4 October 2001, vol.3, pp. 2065-2072.

[133] Chen Y, Chen S., Zhu, Z.Q., Howe, D., and Ye, Y.Y., 'Starting Torque of Single-Phase Flux-Switching Permanent Magnet Motor,' IEEE Transactions on Magnetics, vol. 42, no.10, 2006, pp. 3416-3418.

[134] Pang Y., Zhu, Z.Q., Howe, D., Iwasaki, S., Deodhar, R., and Pride, A., 'Eddy Current Loss in the Frame of a Flux-Switching Permanent Magnet Machine,' IEEE Transactions on Magnetics, vol. 42, no.10, 2006, pp. 3413-3415.

[135] Hua, W., Zhu, Z.Q., Cheng, M., Pang, Y., and Howe, D., 'Comparison of Flux-Switching and Doubly-Salient Permanent Magnet Brushless Machines,' IEEE 8th International Conference on Electric Machines and Systems, ICEMS'05, Nanjing, China, 4-6 November 2005, vol. 1, pp. 165-170.

[136] Hua, W., Ming, C., Jia, H., and Fu, X., 'Comparative Study of Flux-Switching and Doubly-Salient Permanent Magnet Brushless Machines Particularly on Torque Capability,' IEEE 43rd Industry Applications Society Annual Meeting, IAS'08, Edmonton, Alberta, Canada, 5-9 October 2008, pp. 1-8.

[137] Owen R.L., Zhu, Z.Q. Thomas, A.S., Jewell, G.W. and Howe, D., 'Fault-Tolerant Flux-Switching Permanent Magnet Brushless AC Machines,' IEEE 43rd Industry Applications Society Annual Meeting, IAS'08, Edmonton, Alberta, Canada, 5-9 October 2008, pp. 1-8.

[138] Thomas, A.S., Zhu, Z.Q., Owen, R.L., Jewell, G.W., and Howe, D., 'Multi-Phase Flux Switching Permanent Magnet Machines for Aerospace Application,' IEEE Transactions on Industry Applications, vol. 45, no. 6, 2009, pp. 1971-1981.

[139] Chen, J.T., Zhu, Z.Q., Thomas, A.S and Howe, D., 'Optimal Combination of Stator and Rotor Pole Numbers in Flux-Switching PM Brushless AC Machines,' IEEE 11th International Conference on Electric Machines and Systems, ICEMS'08, Wuhan, China, 17-20 October 2008, pp. 2505-2510.

[140] Hua, W., Cheng M, Zhu, Z.Q., and Howe, D., 'Analysis and Optmistion of Back-EMF Waveform of a Novel Flux-Switching Permanent Magnet Motor,' IEEE Transactions on Energy Conversion, vol. 23, no.3, 2008, pp. 727-733.

[141] Zhu, Z.Q., Chen, J.T, Pang, Y., Howe, D., Iwasaki, S., and Deodhar, R., 'Analysis of a Novel Multi-Tooth Flux-Switching PM Brushless AC Machine for High Torque Direct-Drive Applications,' IEEE Transactions on Magnetics, vol. 44, no.11, 2008, pp. 4313-4316.

[142] Chen, J.T, Zhu, Z.Q., and Howe, D., 'Stator and Rotor Pole Combinations for Multi-Tooth Flux-Switching Permanent-Magnet Brushless AC Machines,' IEEE Transactions on Magnetics, vol. 44, no.12, 2008, pp. 4659-4667.

[143] Pollock, H., Pollock, C., Walter, R.C., and Gorti, V.B., 'Low Cost, High Power Density, Flux Switching Machines and Drives for Power Tools,' IEEE 38th Industry Applications Society Annual Meeting, IAS'05, Salt Lake City, Utah, USA, 12-16 October 2005, vol.3, pp. 1451-1457.

[144] Pollock, C., Pollock, H., and Brackley, M., 'Electronically Controlled Flux Switching Motors: A Comparison with an Induction Motor Driving an Axial Fan,' IEEE 29th Industry Electronics Society Annual Conference, IECON'03, Roanoke, Virginia, USA, 2-6 November 2003, vol.3, pp. 2465-2470.

[145] Hoang, E., Lecrivain, M., and Gabsi, M., 'A New Structure of a Switching Flux Synchronous Poly-Phased Machine with Hybrid Excitation,' 12th European Conference on Power Electronics and Applications, EPE'07, Aalborg, Denmark, 2-5 September 2007, pp. 1-8.

[146] Hoang, E., Hlioui, S., Lecrivain, M., and Gabsi, M., 'Experimental Comparison of Lamination Material Case of Switching Flux Synchronous Machine with Hybrid Excitation,' 13th European Conference on Power Electronics and Applications, EPE'09, Barcelona, Spain, 8-10 September 2009, pp. 1-7.

[147] Owen, R.L., Zhu, Z.Q., and Jewell, G.W., 'Hybrid-Excited Flux-Switching Permanent-Magnet Machines with Iron Flux Bridges,' IEEE Transactions on Magnetics, vol. 46, no. 6, June 2010, pp. 1726-1729.

[148] Mecrow, B.C., El-Kharashi, E.A., Finch, J.W., and Jack, A.G., 'Segmental Rotor Switched Reluctance Motors with Single-Tooth Windings,' IEE Proceedings on Electric Power Applications, vol. 150, no. 5, September 2003, pp. 591-599.

[149] Mecrow, B.C., 'New Winding Configurations for Doubly Salient Reluctance Machines,' IEEE Transactions on Industry Applications, vol. 32, no. 6, November/December 1996, pp. 1348-1356.

[150] Mecrow, B.C., 'Fully Pitched-Winding Switched-Reluctance and Stepping-Motor Arrangements,' IEE Proceedings-B, vol. 140, no. 1, January 1993, pp. 61-70.

[151] Boldea, I., 'Reluctance Synchronous Machines and Drives,' Oxford University Press, New York, 1996, pp. 26-28.

[152] Lawrenson, P.J., and Agu, L.A., 'Theory and Performance of Polyphase Reluctance Machine,' IEE Proceedings, vol. 111, no.8, 1964, pp. 1435–1445.

[153] Lawrenson, P.J., and Gupta, S.K., 'Developments in the Performance and Theory of Segmental-Rotor Reluctance Machines,' IEE Proceedings, vol. 114, no. 5, 1967, pp. 645–653.

[154] Lipo, T., 'Novel Reluctance Machine Concepts for Variable Speed Drives,' IEEE 6th Mediterranean Electrotechnical Conference, MELECON'91, Ljubljana, Slovenia, 22-24 May 1991, pp. 34-43.

[155] Mecrow, B.C., Finch, J.W., El-Kharashi, E.A., and Jack, A.G., 'Switched Reluctance Motors with Segmental Rotors,' IEE Proceedings on Electric Power Applications, vol. 149, no. 4, Jul. 2002, pp. 245-254.

[156] Mecrow, B.C., El-Kharashi, E.A., Finch, J.W., and Jack, A.G., 'Preliminary Performance Evaluation of Switched Reluctance Motors with Segmental Rotors,' IEEE Transactions on Energy Conversion, vol. 19, no. 4, 2004, pp. 679-686.

[157] Laithwaite, E.R., 'Magnetic Equivalent Circuits for Electrical Machines,' IEE Proceedings, vol. 114, no. 11, 1967, pp. 1805-1809.

[158] Carpenter, C.J., 'Magnetic Equivalent Circuits,' IEE Proceedings, vol. 115, no. 10, 1968, pp. 1503-1511.

[159] Ostovic, V., 'A Simplified Approach to Magnetic Equivalent-Circuit Modeling of Induction Machines,' IEEE Transactions on Industry Applications, vol. 24, no. 2, 1988, pp. 308-316.

[160] Kano, Y., Kosaka, T., and Matsui, N., 'Simple Nonlinear Magnetic Analysis for Permanent-Magnet Motors,' IEEE Transactions on Industry Applications, vol. 41, no. 5, 2005, pp. 1205-1214.

[161] Kokernak, J.M., and Torrey, D.A., 'Magnetic Circuit Model for Mutually Coupled Switched-Reluctance Machine,' IEEE Transactions on Magnetics, vol. 36, no. 2, 2000, pp. 500-507.

[162] Yilmaz, M., and Krein, P.T., 'Capabilities of Finite Element Analysis and Magnetic Equivalent Circuits for Electrical Machine Analysis and Design,,' IEEE Power Electronics Specialists Conference, PESC'08, Rhodes, Greece, 15-19 June 2008, pp. 4027-4033.

[163] Fang, Z.X., 'Design and Analysis of a Novel Flux-Switching Permanent Magnet Integrated-Starter-Generator,' 4th IET Conference on Power Electronics, Machines and Drives, PEMD 2008, York, UK, 2-4 April 2008, pp.106-110.

[164] Hua, W., Cheng, M., and Howe, D., 'Design of Flux-Switching Permanent Magnet Machine Considering the Limitation of Inverter and Flux-Weakening Capability,' IEEE 41st Industry Applications Society Annual Meeting, IAS'06, Tampa, Florida, USA, 8-12 October 2006, vol.5, pp. 2403-2410.

[165] Brittain, J.E., 'The Tesla Alternating-Current Power System,' Proceedings of the IEEE vol. 72 , no. 2 , 1984 , pp. 165-165.

[166] Fitzgerald, A.E., Kingsley, C., and Umans, S.D., 'Electric Machinery,' 6th edition, McGrall-Hill, New York, USA, 2003, pp. 201-206.

[167] Parsa, L., and Hao, L., 'Interior Permanent Magnet Motors with Reduced Torque Pulsation,' IEEE Transactions on Industrial Electronics, vol. 55, no. 2, February 2008, pp. 602-609.

[168] Parsa, L., Toliyat, H.A., and Goodarzi, A., 'Five-Phase Interior Permanent-Magnet Motors with Low Torque Pulsation,' IEEE Transactions on Industry Applications, vol. 43, no. 1, January/February 2007, pp. 40-46.

[169] Parsa, L., and Toliyat, H.A., 'Five-Phase Permanent-Magnet Motor Drives,' IEEE Transactions on Industry Applications, vol. 41, no. 1, January/February 2005, pp. 30-37.

[170] Williamson, S., and Smith, S., 'Pulsating Torque and Losses in Multiphase Induction Machines,' IEEE Transactions on Industry Applications, vol. 39, no. 4, July/August 2003, pp. 986-993.

[171] Miller, T.J.E., 'Switched Reluctance Motors and their Control,' Magna Physics, Hillsboro, Ohio and Oxford University Press, New York, USA, 1993, p. 47.

[172] Parsa, L., 'On Advantages of Multi-Phase Machines,' 31st IEEE Annual Conference of Industrial Electronics Society, IECON'2005, City, Country, dd/month/2005, pp. 1-6.

[173] Gataric, S., 'A Polyphase Cartesian Vector Approach to Control of Polyphase AC Machines,' IEEE 35th Industry Applications Annual Meeting, IAS'00, Rome, Italy, 8-12 October 2000, vol.3, pp. 1648-1654.

[174] Choy, C.T., and Leung, W.S., 'A.C. Servomotors with Concentrated Stator Windings,' IEE Proceedings, vol. 120, no.1, January 1973, pp. 67-72.

[175] Miller, T.J.E., 'Brushless Permanent-Magnet and Reluctance Motor Drives,' Oxford University Press, New York, USA, 1989, pp. 20-24.

[176] Shmilovitz, D., 'On the Definition of Total Harmonic Distortion and its Effect on Measurement Interpretation,' IEEE Transactions on Power Delivery, vol. 20, no. 1, January 2005, pp. 526-528.

[177] Sahin, F., Ertan, H.B., and Leblebicioglu, K., 'Optimum Geometry for Torque Ripple Minimization of Switched Reluctance Motors,' IEEE Transactions on Energy Conversion, vol. 15, no. 1, March 2000, pp. 30-39.

[178] Hsu, J.S., Scoggins, B.P., Scudiere, M.B., Marlino, L.D., Adams, D.J., and Pillay, P., 'Nature and Assessment of Torque Ripples of Permanent Magnet Adjustable-Speed Motors,' IEEE 30th Industry Applications Annual Meeting, IAS'95, Orlando, Florida, USA, 8-12 Octoberr1995, pp. 2696-2702.

[179] Zhu, X., Cheng, M., Chau, K.T., and Yu, C., 'Torque Ripple Minimization of Flux-Controllable Stator-Permanent-Magnet Brushless Motors using Harmonic Current Injection,' Journal of Applied Physics, vol. 105 , no. 7, February 2009, pp. 07F102-07F102-3.

[180] Zhu, Z.Q., and Howe, D., 'Analytical Prediction of the Cogging Torque in Radial-field Permanent Magnet Brushless Motors,' IEEE Transactions on Magnetics, vol. 28, no.2, March 1992, pp. 1371-1374.

[181] Tasker, J., 'Cogging Torques,' IEE 8th International Conference of Electrical Machines and Drives, EMD'97, Cambridge, UK, 1-3 September 1997, pp. 205-209.

[182] Bianchi, N., and Bolognani, S., 'Design Techniques for Reducing the Cogging Torque in Surface-Mounted PM Motors,' IEEE Transactions on Industry Applications, vol. 38, no. 5, September/October 2002, pp. 1259-1265.

[183] Schlensok, C, Kurzidem, M., Hameyer, K., 'Novel Method for Fast Analysis of Cogging-Torque Harmonics in Permanent-Magnet Synchronous-Machines,' IEEE 12th Biennial Conference on Electromagnetic Field Computation, CEFC 2006, Miami, Florida, USA, 30 April- 3 May 2006, pp. 330- 330.

[184] Madani, A., Barbot, J.P., Colamartinot, F., and Marchand, C., 'Reduction Of Torque Pulsations by Inductance Harmonics Identification of a Permanent-Magnet Synchronous Machine,' 1995., IEEE 4th Conference on Control Applications, Albany, New York, USA, 28-19 September 1995, pp. 787 – 792.

[185] Stephenson, J.M., Hughes A., and Mann, R., 'Torque Ripple Minimisation in a Switched Reluctance Motor by Optimum Harmonic Current Injection,' IEE Proceedings on Electric Power Applictions, vol. 148, no. 4, 2001, pp. 322-328.

[186] Han, S.H., Jahns, T.M., and Soong, W.L., 'Torque Ripple Reduction in Interior Permanent Magnet Synchronous Machines using the Principle of Mutual Harmonics Exclusion,' IEEE 42nd Industry Applications Annual Meeting, IAS'07, New Orleans, Louisiana, USA, 23-27 Septemebr 2007, pp. 558-565.

[187] Bianchi, N., Bolognani, S., Bon, D., and Dai Pre, M., 'Torque Harmonic Compensation in a Synchronous Reluctance Motor,' IEEE Transactions on Energy Conversion vol. 23 , no. 2, June 2008 , pp. 466- 473.

[188] Lee, G.H., Kim, S.I., Hong, J.P., and Bahn, J.H., 'Torque Ripple Reduction of Interior Permanent Magnet Synchronous Motor Using Harmonic Injected Current,' IEEE Transactions on Magnetics, vol. 44, no. 6, June 2008, pp. 1582-1585.

[189] Rahimi, M., Abbaszadeh, K., and Radan, A., 'Torque Ripple suppression of Surface Mounted Permanent Magnet Synchronous Motor Using Harmonic Injected Currents,' IEEE 1st Power Electronic, Drive Systems and Technologies Conference, Tehran, Iran, 17-18 February 2010, pp. 279-283.

[190] Jia, H., Cheng, M., Hua, W., Zhao, W., and Li, W., 'Torque Ripple Suppression in Flux-Switching PM Motor by Harmonic Current Injection Based on Voltage Space-Vector Modulation,' IEEE Transactions on Magnetics, Vol. 46, No. 6, June 2010, pp. 1527-1530.

[191] Njeh, M., Cauet, S., Coirault P., and Martin, P., 'Torque Harmonic Reduction in Hybrid Vehicles,' American Control Conference, ACC 2010, Baltimore, Maryland, USA, 30 June-2 July 2010, pp. 5838-5843.

[192] Jang, G.H., Yoon J.W., Park, N.Y., and Jang, S.M., 'Torque and Unbalanced Magnetic Force in a Rotational Unsymmetric Brushless DC Motors,' IEEE Transactions on Magnetics, vol. 32, no. 5. September 1996, pp. 5157-5159.

[193] Zhu, Z. Q., Ishak, D. Howe, D., and Chen, J., 'Unbalanced Magnetic Forces in Permanent-Magnet Brushless Machines with DiametricallyAsymmetric Phase Windings,' IEEE Transactions on Industry Applications, vol. 43, no. 6, November/December 2007, pp. 1544-1553.

[194] Bi, C., Liu, Z.J., and Low, T.S., 'Effects of Unbalanced Magnetic Side-Pull in Spindle Motors,' IEEE Transactions on Magnetics, vol. 33, no. 5, September 1997, pp. 4080-4082.

[195] Miller, T. J. E., 'Faults and Unbalanced Forces in the Switched Reluctance Machine,' IEEE Transactions on Industry Applications, vol. 31, no. 2, March/April 1995, pp. 319–328.

[196] Tenhunen, A., 'Finite-Element Calculation of Unbalanced Magnetic Pull and Circulating Current Between Parallel Windings in Induction Motor with Non-Uniform Eccentric Rotor,' Proceedings of Electromotion Conference, Bologna, Italy, 19-20 June 2001, pp. 19-24.

[197] Chen, J. T., and Zhu, Z.Q., 'Comparison of All and Alternate Poles Wound Flux-Switching PM Machines Having Different Stator and Rotor Pole Numbers,' IEEE 1st Energy Conversion Congress and Exposition, ECCE'09, San José, California, USA, 18-24 Septemebr 2009, pp. 1705-1712.

[198] Miller, T.J.E., 'Switched Reluctance Motors and their Control,' Magna Physics, Hillsboro, and Oxford University Press, Oxford, 1993, pp. 48-49.

[199] Garip, M., Ozoglu, Y., and Mese, E., 'An Approach to Torque Ripple Reduction in Fully Pitched Switched Reluctance Motors by Pole Tip Shaping,' 11th IEEE Mediterranean Electrotechnical Conference, MELECON 2002, Cairo, Egypt, 7-9 May 2002, pp. 157-161.

[200] Ozoglu, Y., Garip, M., and Mese, E., 'New Pole Tip Shapes Mitigating Torque Ripple in Short Pitched and Fully Pitched Switched Reluctance Motors,' IEEE 37th Industry Applications Society Annual Meeting, Pittsburgh, Pennsylvenia, 13-18 October 2002, vol.1, pp. 43-50.

[201] Bhiwapurkar, N., Jain, A.K., and Mohan, N., 'Study of New Stator Pole Geometry for Improvement of SRM Torque Profile,' IEMDC'05 , IEEE International Conference on Electrical Machines and Drives, 15 May 2005, pp. 516 – 520.

[202] Zhu, Z.Q., Ng, K., and Howe, D., 'Design and Analysis of High-Speed Brushless Permanent Magnet Motors,' 8th IEE International Conference on Electrical Machines and Drives, EMD97, Cambridge, U.K., 1-3 September 1997, pp. 381-385.

[203] Lawrenson, P.J., Gupta, S.K., and Murthy Vamaraju, 'Multispeed Performance of Segmental-Rotor Reluctance Machines,' IEE Proceedings, vol. 115, no. 5, May 1968, pp. 695–702.

[204] Lawrenson, P.J., 'Fringe And Permeance Factors for Segmented-Rotor Reluctance Machines,' IEE Proceedings, vol. 117, no. 5, May 1971, pp. 669–674.

[205] Zulu, A., Mecrow, B.C., and Armstrong, M. 'A Wound-Field Three-Phase Flux-Switching Synchronous Motor with All Excitation Sources on the Stator,' 1st IEEE-Energy Conversion Congress and Exposition, ECCE'09, 18-24 September 2009, San Jose, California, USA, pp. 1502-1509.

[206] Bralla J., 'Design for Maufacturability Handbook,' 2nd edition, McGraw-Hill, New York, U.S.A., 1999, pp. 1.17-1.25.

[207] Kalpakjian S., and Schmid, S., 'Manufactring Engineering and Technology,' 6th edition, Prentice Hall, Singapore, 2010, pp. 381-431, 759-783.

[208] Aouli, R., Akroune, M., Dami, M.A., and Mouillet, A., 'Chacterisation of Electric Alloys for Electric Drives,' IEE Proceedings on Science, Measurement and Technology, vol. 143, no. 3, May 1996, pp. 173-176.

[209] Schoppa, A., Schneider, J., and Wuppermann, C.D., 'Influence of the Manufacturing Process on the Magnetic Properties of Non-Oriented Electrical Steels,' Jounal of Magnetism and Magnetic Materials, vol. 215-216, June 2000, pp. 74-78.

[210] Smith, A.C., and Edey, K, 'Influence of Manufacturing Processes on Iron Losses,' 7th IEE International Conference on Electrical Machines and Drives, EMD'95, Durham, UK, 11-13 September 1995, pp. 77-81.

[211] Emura, M., Landgraf, F.J.G., Ross, W., and Barreta, J.R., 'The Influence of the Cutting Technique on the Magnetic Properties of Electrical Steels,' Journal of Magnetism and Magnetic Materials, vol. 254-255, January 2003, pp. 358-360.

[212] Boglietti, A., Cavagnino, A., Lazzari, M., and Pastorelli, M., 'Effects of Punch Process on the Magnetic and Energetic Propoerties of Soft Magnetic Material,' IEEE International Electric Machines and Drives Conference, IEMDC'01, Cambridge, Massachussetts, USA, 17-20 June 2001, pp. 396-399.

[213] Ossart, F., Hug, E., Hubert, O., Buvat, C., and Billardon R., 'Effect of Punching on Electrical Steels: Experimental and Numerical Coupled Analysis,' IEEE Transactions on Magnetics, vol. 36, no. 5, Sepetember 2000, pp. 3137-3140.

[214] Kedous-Lebouc, A., Cornut, B., Perrier, J.C., Manfe, P., Chevalier, T., and 'Punching Influence on the Magnetic Properties of the Stator Teeth of an Induction Motor,' Jounal of Magnetism and Magnetic Materials, vol. 124-255, January 2003, pp. 124-126.

[215] Boglietti, A., Cavagnino, Ferraris, L., and A., Lazzari, M., 'Effects of Punch Process on the Magnetic and Energetic Propoerties of Soft Magnetic Material,' IEEE International Electric Machines and Drives Conference, IEMDC'03, Madison, Wisconsin, USA, 1-4 June 2003, pp. 503-508.

[216] Schoppa, A., Schneider, J., and Roth, J.O., 'Influence of the Cutting Process on the Magnetic Properties of Non-Oriented Electrical Steels,' Jounal of Magnetism and Magnetic Materials, vol. 215-216, June 2000, pp. 100-103.

[217] Rygal, R., Moses, A.J., Derebasi, N., Schneider, J., and Schoppa, A., 'Influence of Cutting Stress on the Magnetic Field and Flux Density Distribution in Non-Oriented Electrical Steels,' Jounal of Magnetism and Magnetic Materials, vol. 215-216, June 2000, pp. 687-689.

[218] Schoppa, A., Schneider, J., Wuppermann, C.D., and Bakon, T., 'Influence of Welding and Sticking of Laminations on the Magnetic Properties of Non-Oriented Electrical Steels,' Jounal of Magnetism and Magnetic Materials, vol. 254-255, January 2003, pp. 367-369.

[219] Akroune, M., Aouli, R., Dami, M.A., and Mouillet, A., 'Chacterisation of Nonoriented Electric Alloys under Nonconventional Conditions,' IEE Proceedings on Science, Measurement and Technology, vol. 143, no. 1, January 1996, pp. 35-40.

[220] Dami, M.A., Akroune, M., Aouli, R., and Mouillet, A., 'New Approach to Characterisation of Electric Alloys under Rotating Magnetic Flux Density,' IEE Proceedings on Science, Measurement and Technology, vol. 143, no. 6, November 1996, pp. 399-405.

[221] Arshad, W.M., Ryckebusch, T., Magnussen, F., Lendenmann, H., Soulard, J., Eriksson, B., and Malmros, B., 'Incorporating Lamination Processing and Component Manufacturing in Electrical Machine Design Tools,' IEEE 42nd Industry Applications Annual Meeting, IAS'07, New Orleans, Louisiana, USA, 23-27 September 2007, pp. 94-102.

[222] Meier, F., 'Permanent-Magnet Synchronous Machines with Non-Overlapping Concentrated Windings for Low-Speed Direct-Drive Applications,' Ph.D. Thesis, School of Electrical Engineering, Royal Institute of Technology, Stockholm, Sweden, 2008, pp. 72-75.

[223] Akita, H., Nakahara, Y., Miyake, and N. Oikawa, T., 'New Core Structure and Manufacturing Method for High Efficiency Permanent Magnet Motors,' 38th IEEE Industry Applications Annual Meeting, IAS'03, Salt Lake City, Utah, USA, 12-16 October 2003, vol.1, pp. 367-372.

[224] Delis, J.S., 'Design Considerations, Machinery and Control Option in Coil Winding,' IEEE Electrical Insulation Magazine, vol. 9, no. 4., July/August 1993, pp. 16-22.

[225] Williams, K.L., 'Perfect Layer Winding,' IEEE Electrical Insulation Conference and Electrical Manufacturing and Coil Winding Conference, Chicago, Illinois, USA, 22-25 September 1997, pp. 731-732.

[226] Thomas, M.A., 'Tension Control during the Coil Winding Process,' IEEE Electrical Insulation Conference and Electrical Manufacturing and Coil Winding Conference, Indianapolis, Indiana, USA, 23-25 September 2003, pp. 527-530.

[227] Broomfield, T., Willard, S., and Taylor, A., 'Foil and Heavy Wire Winding and Tensioning,' IEEE Electrical Insulation Conference and Electrical Manufacturing and Coil Winding Conference, Chicago, Illinois, USA, 22-25 September 1997, pp. 245-250.

[228] Rahman, Z., Peyghaleh, M., and Matin, K., 'A Novel Coil Winding Technique Applicable to Multiple Strand Concentrated Wound Electric Motors for Low Voltage-High Torque Applications,' IEEE International Symposium on Electrical Insulation, Indianapolis, Indiana, U.S.A., 19-22 September 2004, pp. 8-11.

[229] Yamada, T. Kawamara, T. Mizutani, N. Sato, T. Miyaoka, K., and Mochizuki, M., 'Stator for Dynamoelectric Machine and Method for Making the Same,' European Patent Application, EP 0871282, 1998.

[230] Mecrow, B.C, Jack, A.G, Haylock J.,, Hoefer, U., and Dickinson, P., 'Simplifying the Manufacturing Process for Electrical Machines,' IEE 2nd International Conference on Power Electronics, Machines and Drives, PEMD 2004, Edinburgh, UK, 31 March - 2 April 2004, vol. 1, pp. 169-174.

[231] Jack, A.G., Mecrow, B.C., Dickinson, P.G., Stephenson, D., Burdess, J.S., Fawcett, N., and Evans, J.T., 'Permanent-Magnet Machines with Powdered Iron Cores and Prepressed Windings,' IEEE Transactions on Industry Applications, vol. 41, no. 5, July/August 2000, pp. 1077-1084.

[232] Control Techniques Advanced Users' Guide for Unidrive SP, 'Universal Variable Speed AC Drive for Induction and Servomotors,' Issue 7, 2004, pp. 83.

[233] Morimoto, S., Takeda, Y., and Hirasa, T., 'Current Control Methods for Permanent Magnet Synchronous Motors,' IEEE Transactions on Power Electronics, vol. 5, no. 2, April 1990, pp. 133-139.

[234] Zhu, Z. Q., Pang, Y., Hua, W., Cheng, M., Howe, D., 'Investigation of End Effect in Permanent Magnet Brushless Machines Having Magnets on the Stator,' Journal of Applied Physics, vol. 99 , no. 8, 2006 , pp. 08R319 - 08R319-3.

[235] Hanselman, D.C., 'Brushless Permanent-Magnet Motor Design,' McGraw-Hill, New York, USA, 1994, pp. 103-105.

[236] Miller, T.J.E., Popescu, M., Cossar, C. and McGilp, M.I., 'Computation of the Voltage-Driven Flux-MMF Diagram for Saturated PM Brushless Motors,' 40th IEEE Industry Applications Society Annual Meeting, Hong Kong, China, 2-6 October 2005, vol.2, pp. 1023-1028.

[237] Meier, F., and Soulard, J., 'Dq Theory Applied to a Permanent Magnet Synchronous Machine With Concentrated Windings,' 4th IET- Power Electronics Machines and Drives Conference, York, UK, 2-4 April 2008, pp. 194-198.

[238] Jia, H., Cheng, M., Hua, W., Lu, W., and Fu, X., 'Investigation and Implementation of Control Strategies for Flux-Switching Permanent Magnet Motor Drives,' 43rd IEEE Industry Applications Society Annual Meeting, Edmonton, Alberta, 5-9 October, 2008, pp. 1-6.

[239] Fitzgerald, A.E., Kingsley, C., and Umans, S.D., 'Electric Machinery,' 6th ed., McGraw-Hill, New York, USA, 2003, pp. 248-252, 657-667.

Appendix A

Analytical derivation of torque

It has been stated in [123], [205] that the electromagnetic torque T developed by the flux switching machine is proportional to field current i_f and armature current i_a, and is given by

$$T = i_f i_a \frac{dM_{fa}}{dt} \tag{A1}$$

where M_{fa} is the mutual inductance between the field and armature coils. In the following sections, the derivations of the torque and mutual inductance, using linear concepts, for the wound-field flux switching machine employing a segmental rotor are provided.

A.1 Torque and Stored Energy

For a lossless closed system with electrical and mechanical terminals depicted in figure A1, voltage e, current i and flux linkage ψ can be accessed at the electrical terminals while torque T and angular displacement θ can be accessed at the mechanical terminals. Such a system has stored energy W in the magnetic field.

Performing an energy balance on the system, while assuming input energy is from electrical sources, output energy is in mechanical form and the system is lossless, the stored energy changes with respect to time t is given by

$$\frac{dW}{dt} = ei - T\frac{d\theta}{dt} \tag{A2}$$

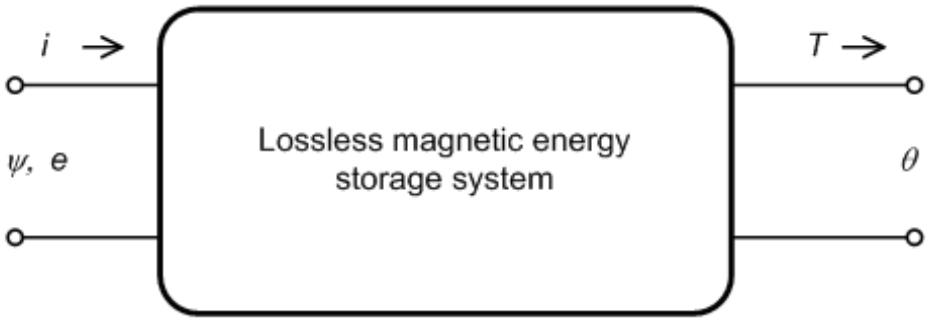

Figure A1: An electromechanical system.

Using faraday' law for flux linkages

$$e = \frac{d\psi}{dt} \tag{A3}$$

(A3) becomes

$$dW = id\psi - Td\theta \tag{A4}$$

Torque can now be solved as a state function of flux and angular position in the following way.

$$dW(\psi,\theta) = id\psi - Td\theta \tag{A5}$$

$$dW(\psi,\theta) = \left.\frac{\partial W}{\partial \psi}\right|_{\theta} d\psi + \left.\frac{\partial W}{\partial \theta}\right|_{\psi} d\theta \tag{A6}$$

Comparing (A5) with (A6), yields

$$i = \left.\frac{\partial W(\psi,\theta)}{\partial \psi}\right|_{\theta} \tag{A7}$$

$$T = \left.\frac{\partial W(\psi,\theta)}{\partial \theta}\right|_{\psi} \tag{A8}$$

A.2 Torque Using Co-Energy Concept

The torque is obtained from the stored energy magnetic W as,

$$T = \left.\frac{\partial W(\psi,\theta)}{\partial\theta}\right|_{\psi=CONSTANT} \tag{A9}$$

The stored energy is a state function of two variables: flux linkage ψ and position θ.

Using the concept of co-energy facilitates obtaining the torque expression directly as a function of the current i and position. Figure A2 illustrates the regions of the co-energy and stored energy on the flux linkage-current relationship diagram.

From this, Co-energy W' is then defined as

$$W'(i,\theta) = \psi i - W(\psi,\theta) \tag{A10}$$

and may be calculated as

$$W'(i,\theta) = \int_0^i \psi(i,\theta)di \tag{A11}$$

The torque is then derived as

$$T = \left.\frac{\partial W'(i,\theta)}{\partial\theta}\right|_{i=CONSTANT} \tag{A12}$$

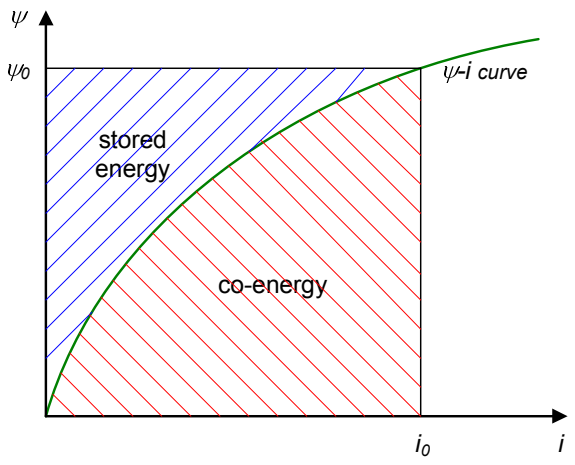

Figure A2. Stored energy and co-energy concepts.

For linear systems the flux linkage of the coil is dependent only on the inductance L and the current in the following way

$$\psi = L(\theta)i \tag{A13}$$

For a singly-excited system the torque reduces to

$$T = \frac{1}{2} i^2 \frac{dL(\theta)}{d\theta} \tag{A14}$$

A.3 Torque in a Multiply-Excited System

For a multiply-excited system, the flux linkage expression of (A14) develops to become a column vector, expressed in terms of the inductance matrix and current vector

$$\begin{pmatrix} \psi_1 \\ \psi_2 \\ \vdots \\ \psi_n \end{pmatrix} = \begin{pmatrix} L_{11} & L_{21} & \cdots & L_{n1} \\ L_{12} & L_{22} & \cdots & L_{n2} \\ \vdots & \vdots & \cdots & \vdots \\ L_{1n} & L_{2n} & \cdots & L_{nn} \end{pmatrix} \begin{pmatrix} i_1 \\ i_2 \\ \vdots \\ i_n \end{pmatrix} = \begin{pmatrix} L_1 & M_{21} & \cdots & M_{n1} \\ M_{12} & L_2 & \cdots & M_{n2} \\ \vdots & \vdots & \cdots & \vdots \\ M_{1n} & M_{2n} & \cdots & L_n \end{pmatrix} \begin{pmatrix} i_1 \\ i_2 \\ \vdots \\ i_n \end{pmatrix} \tag{A15}$$

and the torque is therefore expressed as

$$T = \frac{1}{2} \begin{pmatrix} i_1 \\ i_2 \\ \vdots \\ i_n \end{pmatrix}^{\mathrm{t}} \frac{\partial}{\partial \theta} \left[\begin{pmatrix} L_1 & M_{21} & \cdots & M_{n1} \\ M_{12} & L_2 & \cdots & M_{n2} \\ \vdots & \vdots & \cdots & \vdots \\ M_{1n} & M_{2n} & \cdots & L_n \end{pmatrix} \right] \begin{pmatrix} i_1 \\ i_2 \\ \vdots \\ i_n \end{pmatrix} \tag{A16}$$

By classification, the torque developed is composed of the reluctance torque T_{rel}, which consists of the terms with self-inductance terms and the excitation torque T_{exc}, which consists of terms with the mutual-inductance terms, M.

$$T_{rel} = \frac{1}{2} \sum_{1}^{n} i_n^2 \frac{dL_n}{d\theta} \tag{A17}$$

$$T_{exc} = \frac{1}{2} \sum_{k=1}^{n} \sum_{m=1}^{n} i_k i_m \frac{dM_{km}}{d\theta}, k \neq m \tag{A18}$$

For the FSM under study, the topology of the stator and rotor is designed and arranged to produce torque entirely as excitation torque component.

A.4 Torque in a Wound-Field FSM with 12-Tooth Stator

The machine has 12 coils and since it is intended to operate as a three-phase machine with half the total coils being used for field excitation, the operation can be represented by the action of the first 6 coils, as in figure A3.

Designating the field winding by *f* and the armature winding by *a*, the excitation torque is the summation of the torques produced by the interaction of the armature phase coils *a*[*A*, *B*, *C*] , and the field coils *f*[*1*, *2, 3*] through their respective mutual inductances.

$$T = \sum i_f i_a \frac{dM_{fa}}{d\theta} \tag{A19}$$

where it is assumed that

$$M_{fa} = M_{af} \tag{A20}$$

As armature coils are arranged in alternate sequence with the field poles, simplification can be obtained by assuming that each field coil interacts only with each adjacent armature coil. The valid mutual inductances are as tabulated below in Table A1.

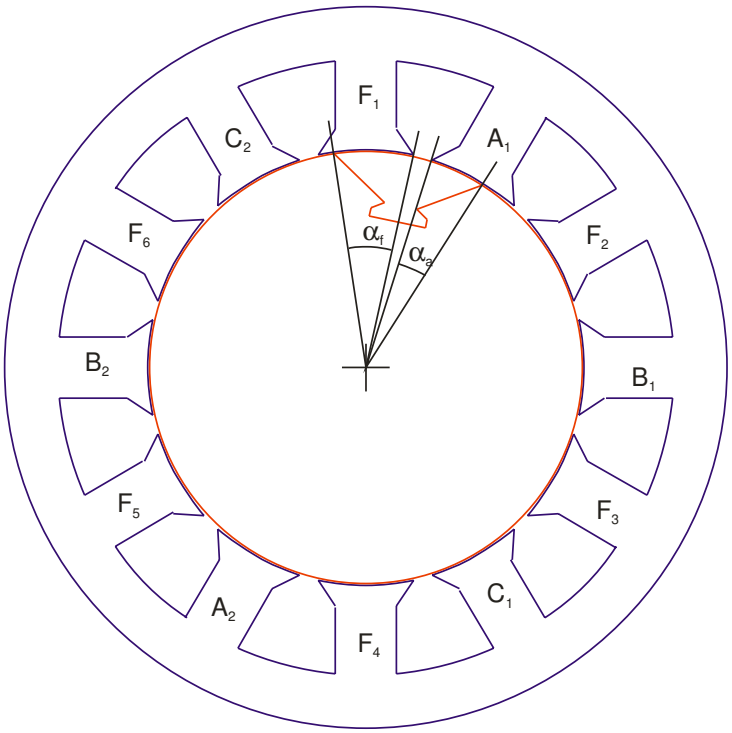

Figure A3. 12-tooth stator with a rotor segment

Table A1. Possible mutual inductances

	i_{f1}	i_{f2}	i_{f3}
i_{aA}	$M_{f1\text{-}aA}$	$M_{f2\text{-}aA}$	$M_{f3\text{-}aA}$
i_{aB}	$M_{f1\text{-}aB}$	$M_{f2\text{-}aB}$	$M_{f3\text{-}aB}$
i_{aC}	$M_{f1\text{-}aC}$	$M_{f2\text{-}aC}$	$M_{f3\text{-}aC}$

Taking into account that the six coils represent only half the machine, the total torque equation becomes

$$\begin{aligned} T = 2\left(i_{f1}i_{aA}\frac{dM_{f1-aA}}{d\theta} + i_{f1}i_{aB}\frac{dM_{f1-aB}}{d\theta} + i_{f1}i_{aC}\frac{dM_{f1-aC}}{d\theta} \right) \\ + 2\left(i_{f2}i_{aA}\frac{dM_{f2-aA}}{d\theta} + i_{f2}i_{aB}\frac{dM_{f2-aB}}{d\theta} + i_{f2}i_{aC}\frac{dM_{f2-aC}}{d\theta} \right) \\ + 2\left(i_{f3}i_{aA}\frac{dM_{f3-aA}}{d\theta} + i_{f3}i_{aB}\frac{dM_{f3-aB}}{d\theta} + i_{f3}i_{aC}\frac{dM_{f3-aC}}{d\theta} \right) \end{aligned} \tag{A21}$$

The torque expression of (A21) has 9 terms. Further simplification can be obtained by checking for void terms, on the assumption that each armature coil interacts only with the adjacent field coil. The 2nd, 6th and 7th term are revealed to be void on this basis and (A21) reduces to

$$\begin{aligned} T = 2\left(i_{f1}i_{aA}\frac{dM_{f1-aA}}{d\theta} + i_{f1}i_{aC}\frac{dM_{f1-aC}}{d\theta} \right) \\ + 2\left(i_{f2}i_{aA}\frac{dM_{f2-aA}}{d\theta} + i_{f2}i_{aB}\frac{dM_{f2-aB}}{d\theta} \right) \\ + 2\left(i_{f3}i_{aB}\frac{dM_{f3-aB}}{d\theta} + i_{f3}i_{aC}\frac{dM_{f3-aC}}{d\theta} \right) \end{aligned} \tag{A22}$$

Torque is designed to be produced when a rotor segment is in overlap with two adjacent teeth, typically a field tooth and armature tooth. If a rotor segment overlaps a field tooth by an angle α_f and an adjacent armature tooth by an angle α_a, then the mutual inductance between a field coil and an armature coil, M_{af}, can be expressed as

$$M_{af} = \frac{N_a N_f lr}{g}\left(\frac{1}{\frac{1}{\alpha_f} + \frac{1}{\alpha_a}} \right) = \frac{N_a N_f lr}{g}\left(\frac{\alpha_f \alpha_a}{\alpha_f + \alpha_a} \right) \tag{A23}$$

where l is the axial length, g is the gap length and r is the radius of the rotor plus half the gap length.

Knowing that there are positions for rotor position θ for which either α_a or α_f is zero, and other positions for which α_a is changing while α_f is not, and vice-versa, mutual inductance with respect to θ can be plotted with the help of (A23), as in Figure A4 and A5.

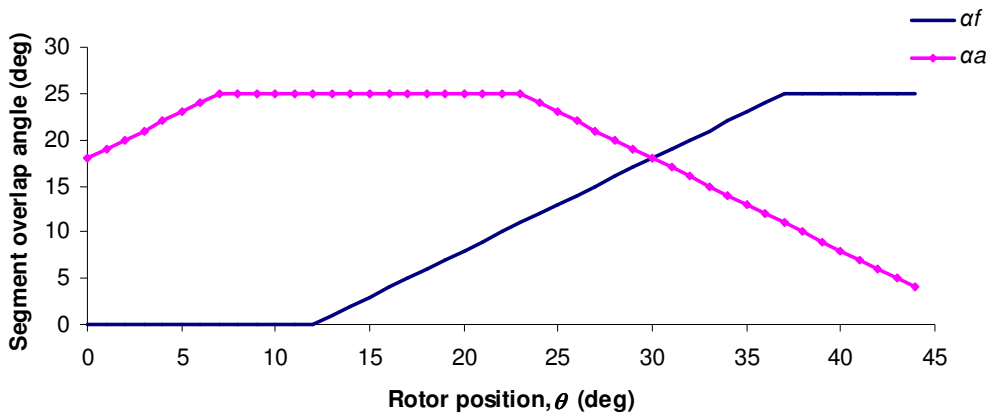

Figure A4. Variation overlap angle of segment with field and armature teeth.

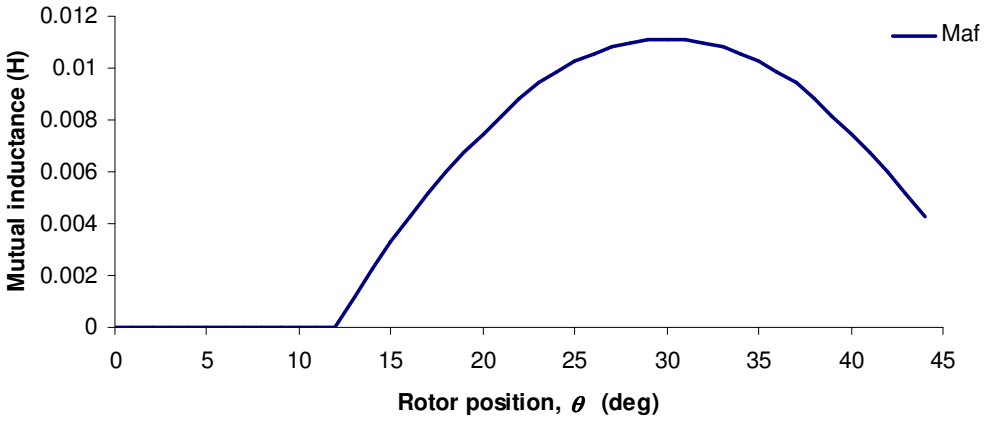

Figure A5. Variation of mutual inductance with position.

Appendix B

Determination of initial dimensions of 12-tooth stator

The initial dimensions applied on the 12-tooth stator, excluding the outside diameter, axial length, stator bore and airgap length, which are determined by specifications, may be determined by an outline design process applying linear electromagnetic principles. This appendix illustrates the process for determining the initial width of the field tooth, the armature coil turns and the magnet depth.

B.1 Initial Width of Field Tooth

The field tooth width is initially determined from the principle which ensures that the magnetic loading is nearly the same as the electric loading, which is achieved by having the span of the stator tooth being the same as the span of the stator for the size of the machine under consideration. The tooth width is calculated at a radius, r_{tg} at which the tangs on the tooth are chosen to appear (50 mm in this case). As the tooth sides have parallel sides, the width of the stator tooth, t_w for the stator with a number of teeth, N_{st} is

$$t_w = 2r_{tg}\sin\left(\frac{360^\circ}{2N_{st}}\right)$$
$$= 2\times 50\sin\left(\frac{360^\circ}{2\times 12}\right) \quad \text{(B1)}$$
$$\approx 13 \quad \text{mm}$$

A tooth field tooth of 12.5 mm has been applied in the designs of this investigation width

B.2 Coil Turns

Referring to figure B.1, and allowing subscripts *g* and *Fe* to denote airgap and steel parameters, let :

slot width	≈	stator tooth width
stator back iron depth	≈	stator tooth width
stator tooth overhang span	≈	3/2 x stator tooth width span
rotor diameter	≈	½ x stator outside diameter
airgap	=	0.3 mm
segment span	≤	2 x (stator tooth width + slot width) span

Set:

axial length l_a	=	150 mm
outside diameter D_s	=	150 mm

If saturation fux density of in steel is $B_{Fe\text{-}sat}$, and assuming infinite permeability in steel, applying Ampere's law,

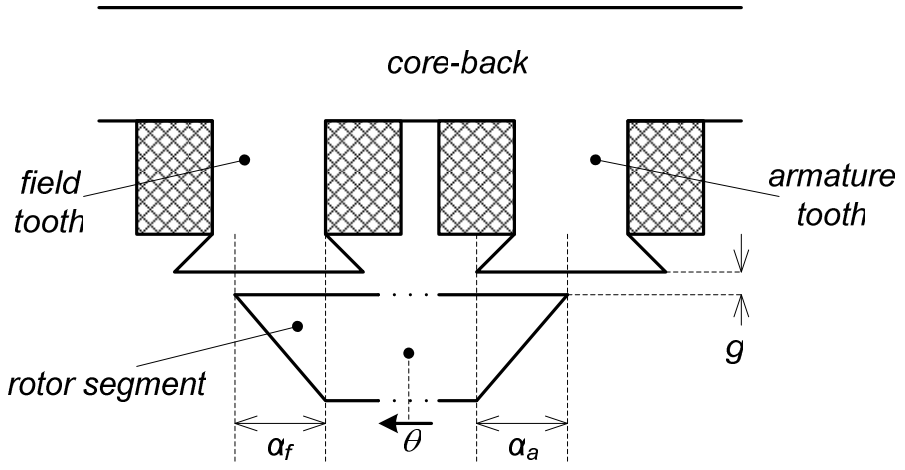

Figure B.1. Magnetic circuit scheme for FSM with segmental rotor.

$$\text{“}\int Hdl = Ni\text{”} \tag{B2}$$

The circuit of figure B.1 has flux ϕ such that

$$\phi_g = \phi_{Fe} \tag{B3}$$

or

$$B_g A_g = B_{Fe} A_{Fe} \tag{B4}$$

where B is flux density and A cross sectional area. Thus

$$A_g = A_{Fe} \tag{B5}$$

This geometry gives

$$B_g = \frac{2}{3} B_{Fe-sat} \tag{B6}$$

Then,

$$H_g .2l_g = Ni \tag{B7}$$

and

$$mmf = Ni = 2l_g \frac{B_g}{\mu_0} = \frac{4}{3} l_g \frac{B_{Fe-sat}}{\mu_0} \tag{B8}$$

Choosing steel with $B_{Fe\text{-}sat}$ = 1.5 T;

$$Ni \approx 478 \text{ A} \tag{B9}$$

If geometry allows, as in 12/5 topology $B_g = B_{Fe-sat}$, then $Ni \approx 716$ A.

Choosing to use 1.4 mm diameter conductor, and with assumed rated current density of 10 A/mm^2, the conductor can take up to 11 A and therefore *N* is about 44 turns of coil.

Allowing for $B_g = B_{Fe-sat}$, with $Ni \approx 716$ A, then *N* is about 65 turns. Ultimately, the winding skills shall determine *N*, and the cooling considerations shall determine *i*, which can be inferred from thermal tests. With this possibility, the choice of coil turns can range between 40 and 65, with the range of maximum current loading of between 10 and 15 A.

B.3 Magnet Depth

Assuming a choice of 50 turns and 14 A, then Ni = 700 A. The equivalent length of magnets in the PM excited machine to give the same flux density can be estimated as follows.

Appying (B1),

$$H_g.2l_g + H_m l_m = 0 \tag{B10}$$

or

$$B_m = B_g \tag{B11}$$

and

$$B_m = B_0 + \mu_m H_m \tag{B12}$$

Using the known values of B_g and μ_m

$$l_m = -2\lg.\frac{B_g}{\mu_0}\frac{\mu_m}{(B_g - B_0)} \tag{B13}$$

With $B_{Fe\text{-}sat}$ = 1.5 T, B_g = 0.9 T, and for neodymium-iron-boron with B_0 =1.1 T and μ_m = 1.05, l_m = 2.835 mm.

Appendix C

Evaluation of *dq* inductances from *abc* inductances

The basis of evaluating the *dq* inductances from *abc* inductances is in the application of (8.4) and (8.9) under defined conditions as in the following cases. Park's transformation matrix, $\boldsymbol{P}$ is as defined in (8.7), with θ given as

$$\theta = N_{seg}\theta_r \tag{C1}$$

where θ_r is the rotor position and N_{seg} is the number of segments.

Case 1. With i_f only and $i_a = i_b = i_c = 0$ (i.e., $i_d = i_q = 0$)

$$\boldsymbol{\psi}_{dqf} = \boldsymbol{P}\boldsymbol{\psi}_{abcf}\big|_{i_d = i_q = 0} \tag{C2}$$

$$\begin{bmatrix} \psi_d \\ \psi_q \\ \psi_{f_{d-q}} \end{bmatrix} = \begin{bmatrix} L_{fd} \\ L_{fq} \\ L_f \end{bmatrix} i_{f_{d-q}} \tag{C3}$$

gives L_f , L_{fd} and L_{fq}.

Case 2. With i_f only and $i_q = 0$ (i.e., $\beta = 0°$)

$$\boldsymbol{\psi}_{dqf} = \boldsymbol{P}\left[\boldsymbol{\psi}_{abcf}\big|_{i_q = 0} - \boldsymbol{\psi}_{abcf}\big|_{i_d = i_q = 0}\right] \tag{C4}$$

$$\begin{bmatrix} \psi_d \\ \psi_{f_{d-q}} \end{bmatrix} = \begin{bmatrix} L_d \\ L_{fd} \end{bmatrix} i_d \tag{C5}$$

gives L_d and L_{fd}

Case 3. With i_f only and $_{id} = 0$ (i.e., $\beta = 90°$)

$$\boldsymbol{\psi}_{dqf} = \boldsymbol{P}\left[\boldsymbol{\psi}_{abcf}{}_{|i_d=0} - \boldsymbol{\psi}_{abcf}{}_{|i_d=i_q=0}\right] \tag{C6}$$

$$\begin{bmatrix} \psi_q \\ \psi_{f_{d-q}} \end{bmatrix} = \begin{bmatrix} L_q \\ L_{fq} \end{bmatrix} i_q \tag{C7}$$

gives L_q and L_{fq}

Case 4. With i_f only and known $i_d = i_q = I_m/\sqrt{2}$ (i.e., $\beta = 45°$)

$$\boldsymbol{\psi}_{dqf} = \boldsymbol{P}\left[\boldsymbol{\psi}_{abcf}{}_{|i_d=i_q=I_m/\sqrt{2}} - \boldsymbol{\psi}_{abcf}{}_{|i_d=i_q=0}\right] \tag{C8}$$

$$\psi_q = L_{dq} i_d + L_q i_q \tag{C9}$$

and with known L_q from (C7), gives L_{dq}.

Appendix D

Cutting patterns for modular stator cores

The following figures show the cutting patterns that may be followed for the six degrees of modularisation for a stator of a wound-field FSM. The cutting patterns are designed to minimise wastage for modularisation applied. It is assumed that lamination sheets are supplied in a standard size of 300 mm x 600 mm, and that margins of 5-10 mm are required at the edges for handling. On each lamination sheet, the dark spaces indicate the lamination that remains as waste after the cutting process.

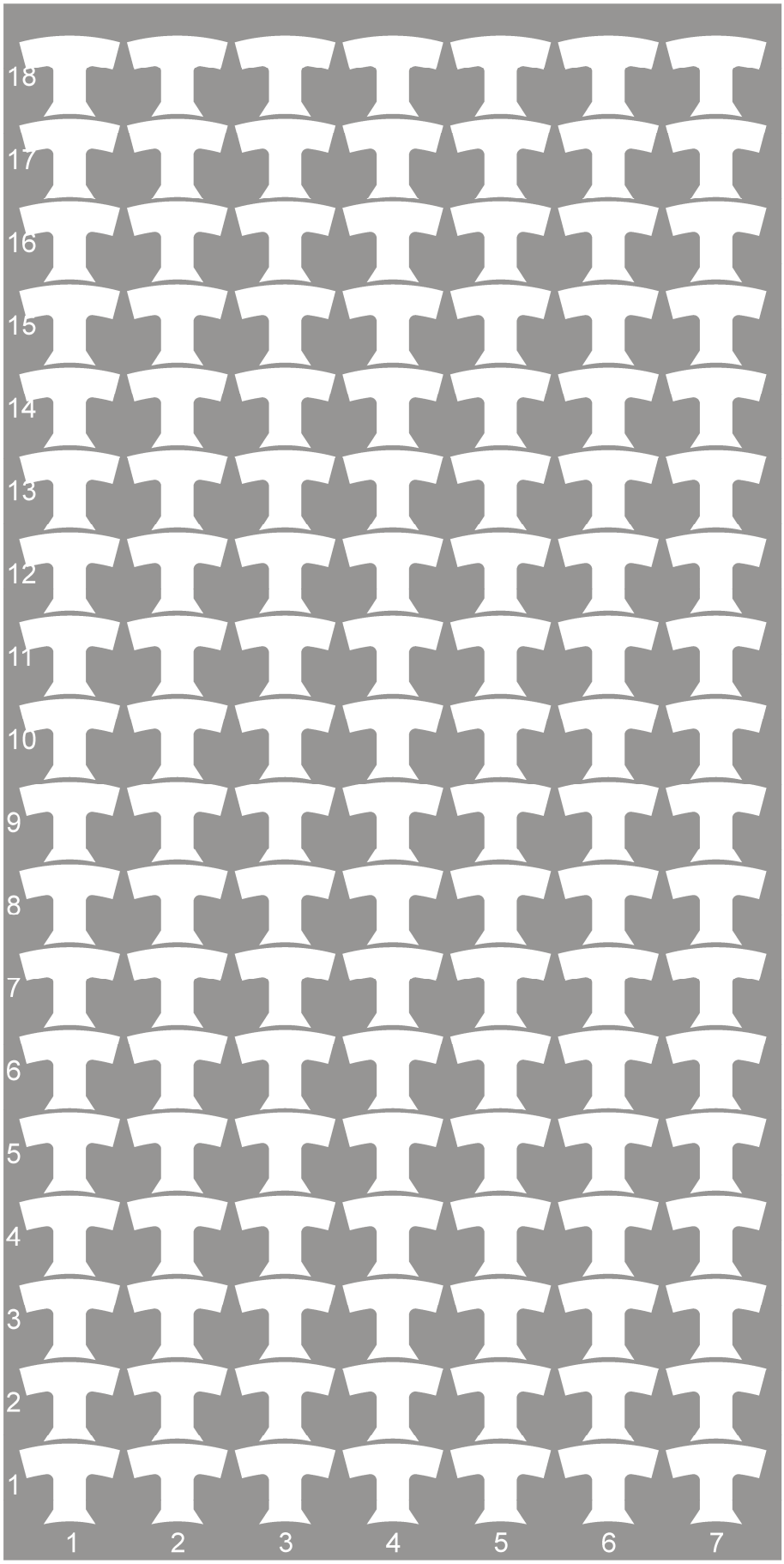

Figure D1. 30° modularisation.

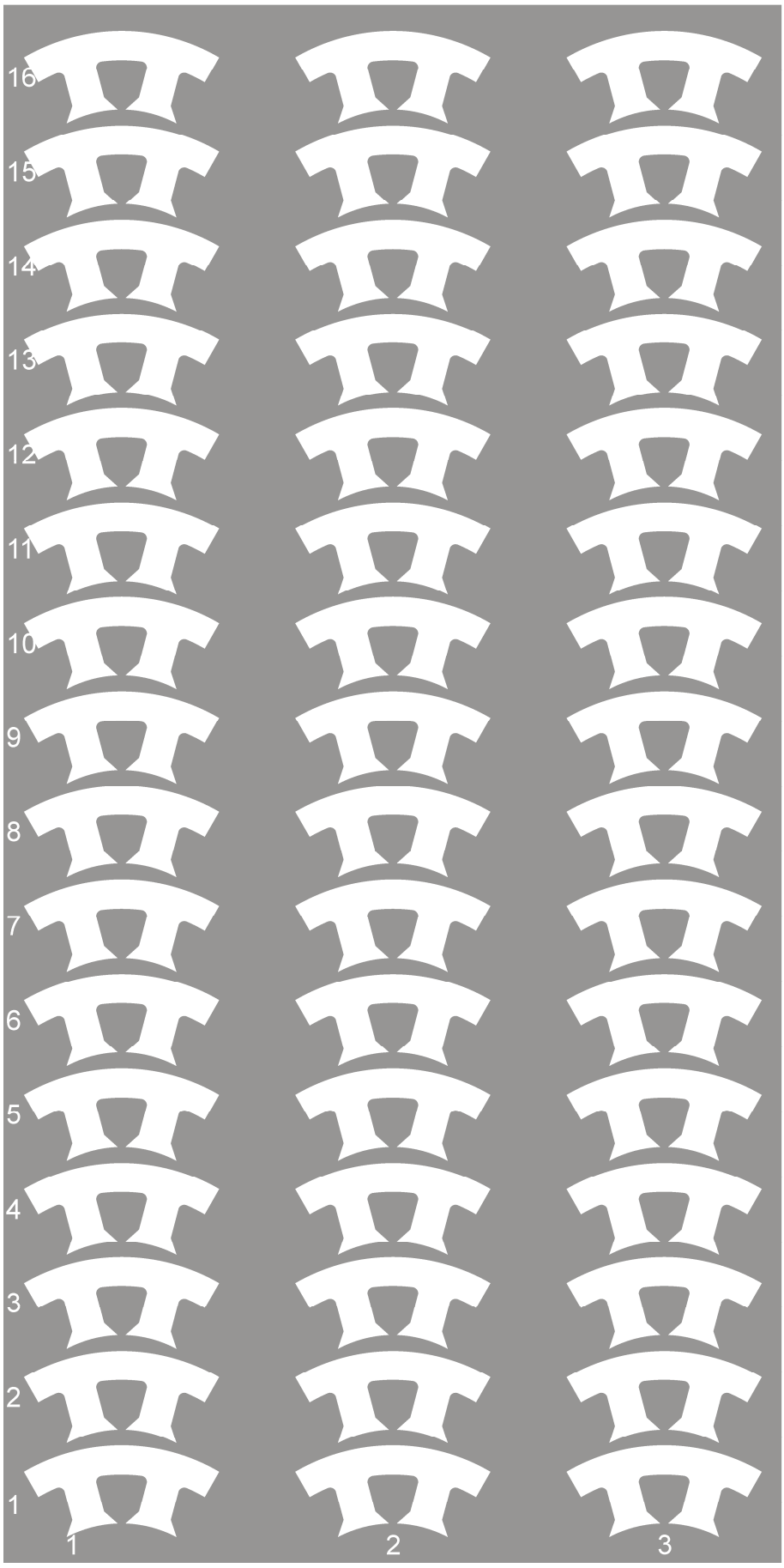

Figure D2. 60° modularisation.

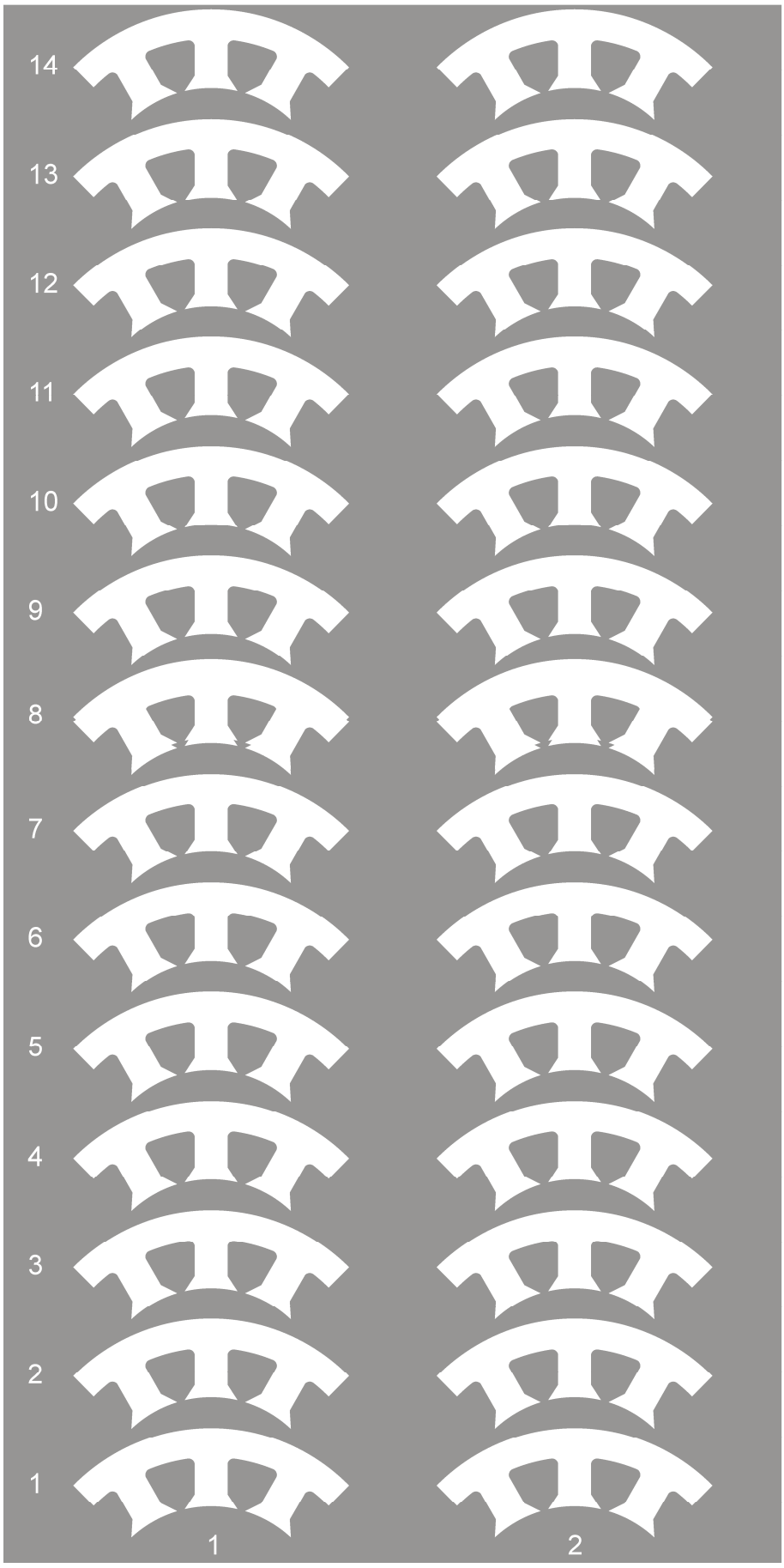

Figure D3. 90° modularisation.

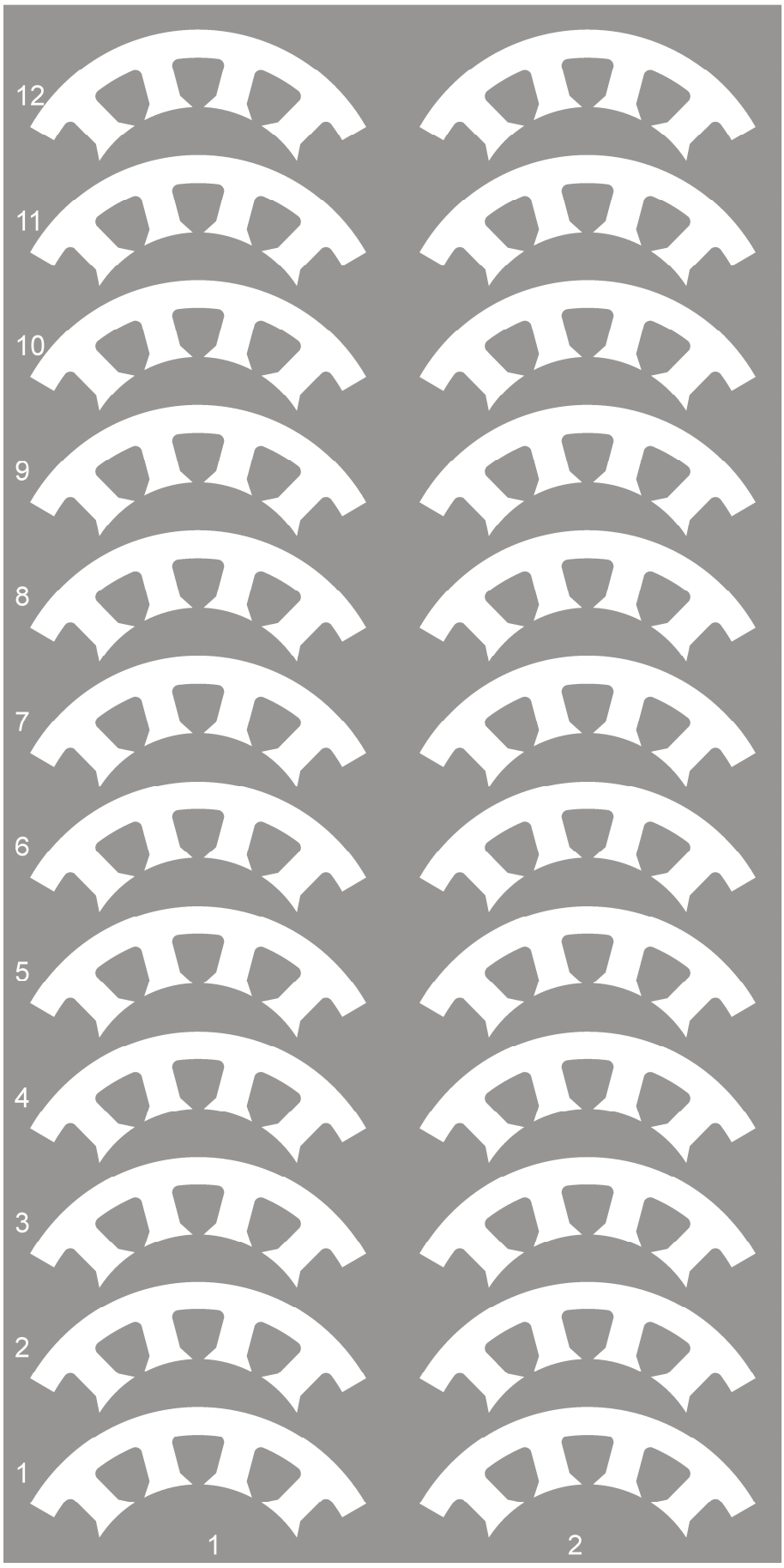

Figure D4. 120° modularisation.

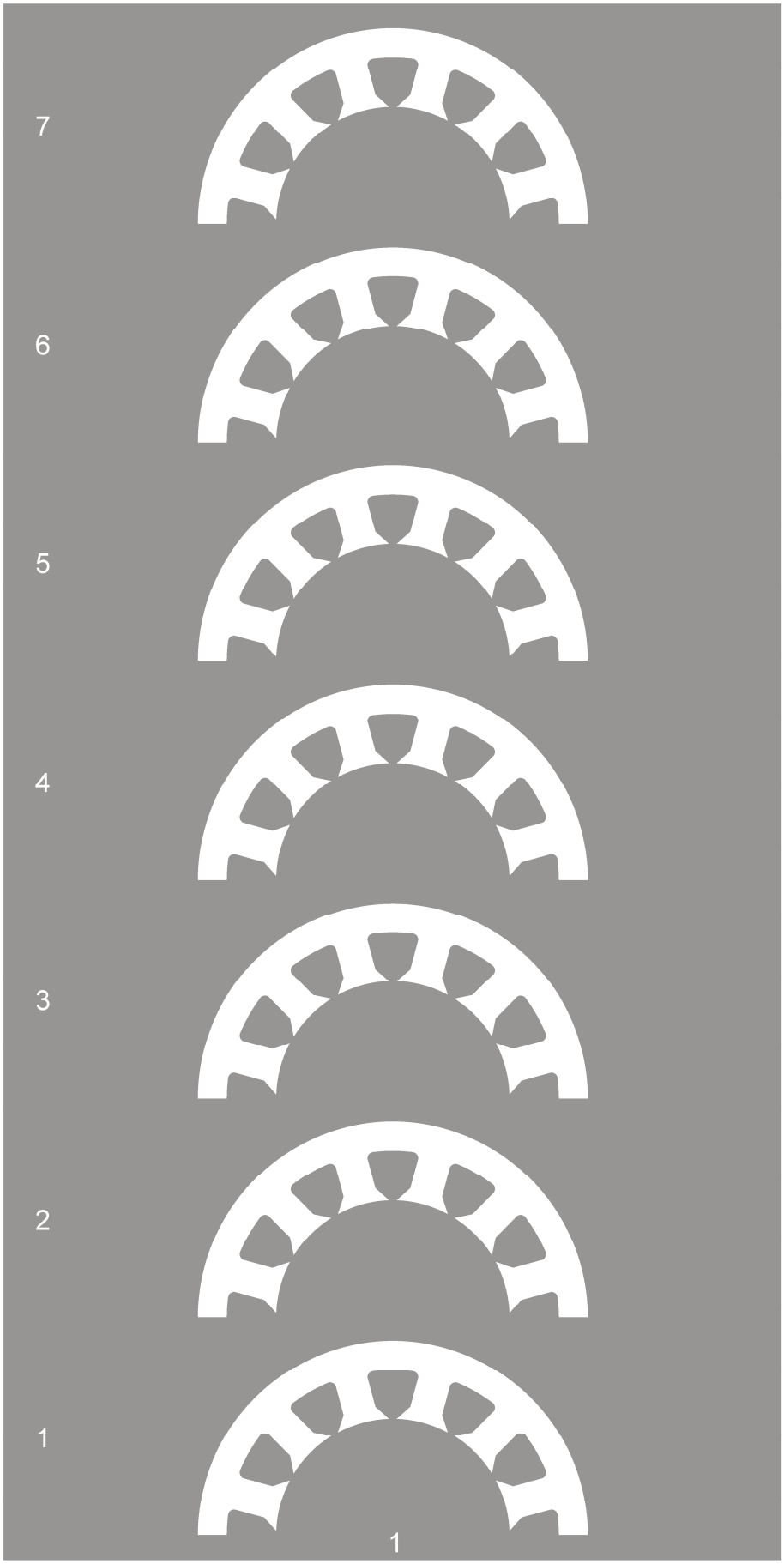

Figure D5. 180° modularisation.

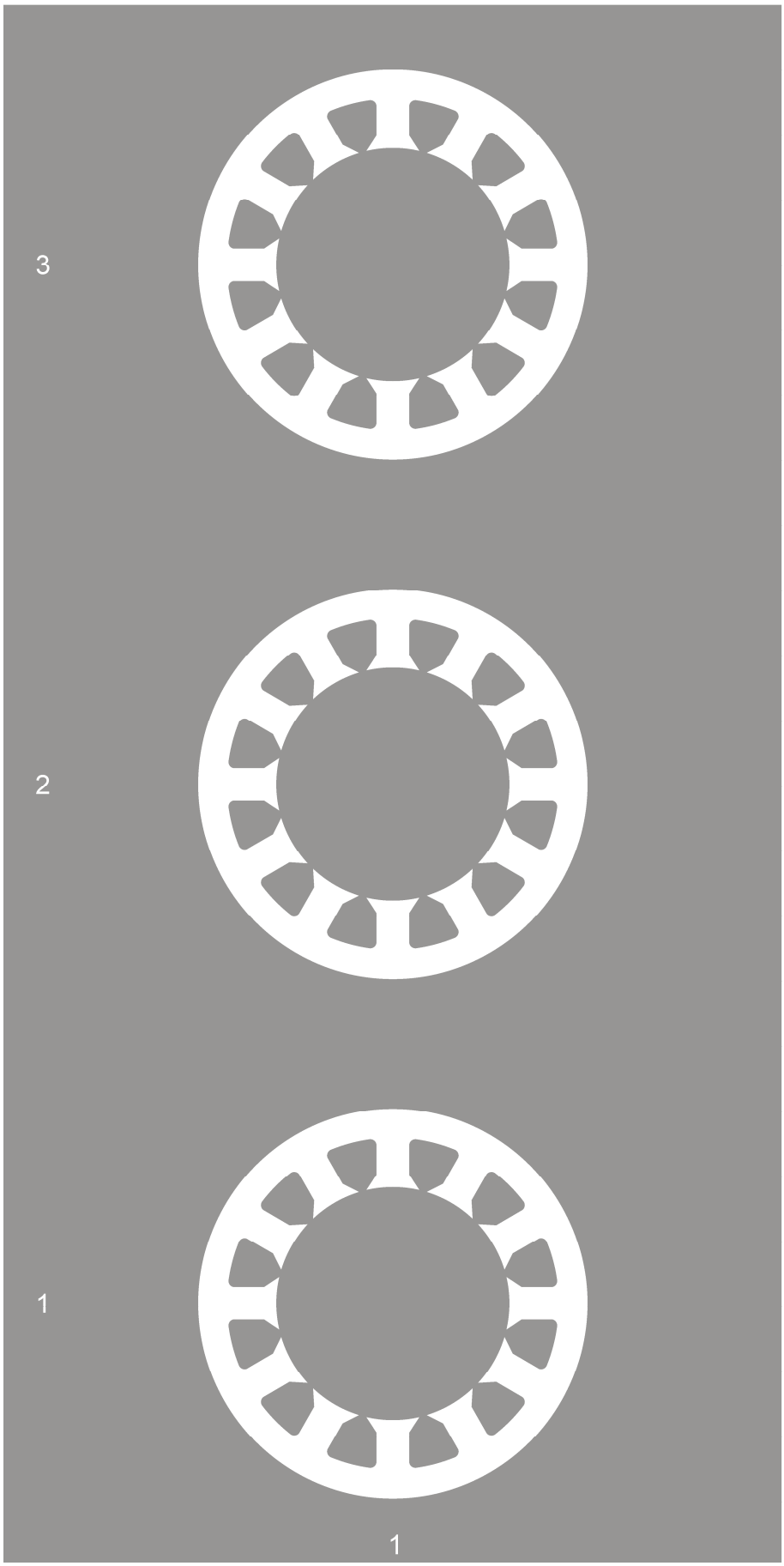

Figure D6. Complete core (360°).

Appendix E

Dimensions for elementary rectilinear cells

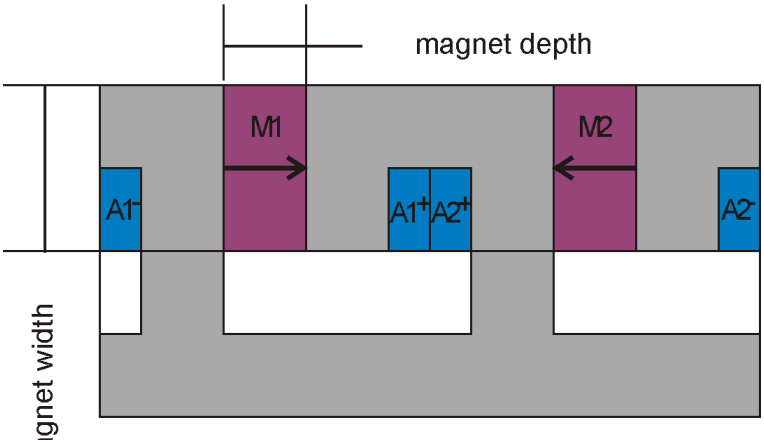

(a) toothed-rotor scheme

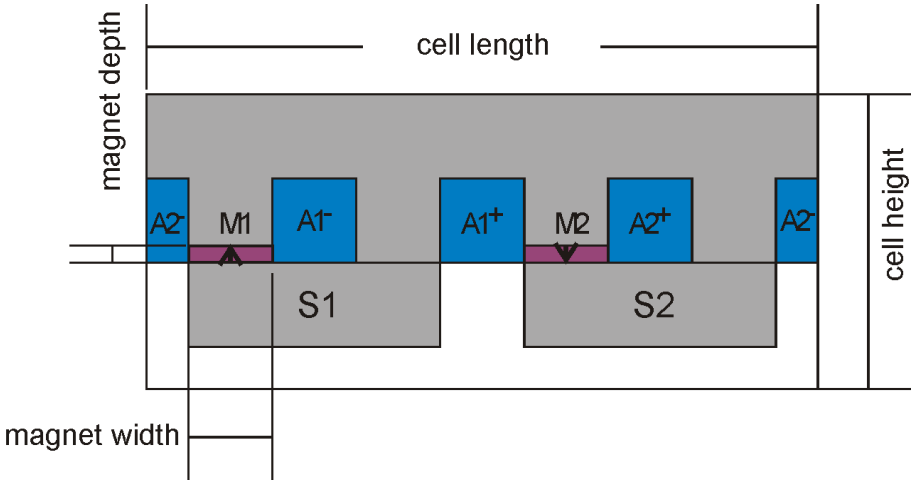

(b) segmental-rotor scheme

Figure E1. Dimension labels for elementary rectilinear cell structures.

Table E1. Dimensions for the elementary rectilinear cell structures.

	Units	Wound-field		Permanent Magnet	
		toothed	segmental	toothed	segmental
Cell axial thickness	mm	20	20	20	20
Cell length	mm	80	80	80	80
Cell height	mm	35	35	40	35
Stator tooth width	mm	10	10	10	10
Stator slot width	mm	10	10	10	10
Stator slot height	mm	10	10	10	10
Core back depth	mm	10	10	10	10
Number of stator teeth	-	4	4	4	4
Number of stator slots	-	4	4	4	4
Number of field turns/tooth	-	100	100	-	-
Number of armature turns/tooth	-	100	100	100	200
Rotor tooth width	mm	10	-	10	-
Rotor tooth height	mm	5	-	10	-
Rotor segment width (nominal)	mm	-	30	-	30
Rotor segment height	mm	-	10	-	10
Number of rotor teeth	-	2	-	2	-
Number of rotor segments	-	-	2	-	2
Airgap length	mm	0.1	0.1	0.1	0.1
Magnet width	mm	-	-	10	2
Magnet depth	mm	-	-	20	10
Field current (nominal)	A	1.6	1.6	-	-

Appendix F

Prototype machines

Table F1. Specified principal dimensions for the 12/8 FSM.

Axial length	150	mm
Stator outside diameter	150	mm
Stator yoke depth	11	mm
Stator bore	91.2	mm
Stator tooth width	12.5	mm
Stator tooth overhang span	25	^{o}
Stator slot opening span	5	^{o}
Air-gap length	0.3	mm
Number of turns per field coil	44	
Number of turns per armature coil	44	
Conductor diameter	1.4	mm
Rotor diameter	90.6	mm
Number of segments	8	
Span of each segment	41	^{o}

Table F2. Specified principal dimensions for the 12/5 FSM

Axial length	150	mm
Stator outside diameter	150	mm
Stator bore	91.2	mm
Stator tooth width	12.5	mm
Stator tooth overhang span	25	^{o}
Stator slot opening span	5	^{o}
Air-gap length	0.3	mm
Number of turns per field coil	44	
Number of turns per armature coil	44	
Conductor wire diameter	1.4	mm
Rotor diameter	90.6	mm
Number of segments	5	
Span of each segment	55	^{o}

Table F3: Specified principal dimensions for the 12/8 FSMPM

Axial length	150	mm
Stator outside diameter	150	mm
Stator yoke depth	11	mm
Stator bore	91.2	mm
Stator tooth width	12.5	mm
Stator tooth overhang span	25	^{o}
Stator slot opening span	5	^{o}
Air-gap length	0.35	mm
Number of turns per armature coil	100	
Conductor wire diameter	1.25	mm
Rotor diameter	90.5	mm
Number of segments	8	
Span of each segment	41	^{o}
Magnet depth at tangential side	2.835	mm
Magnet width span	25	^{o}

Table F4. Specified principal dimensions for the 12/5 FSMPM

Axial length	150	mm
Stator outside diameter	150	mm
Stator yoke depth	11	mm
Stator bore	91.2	mm
Stator tooth width	12.5	mm
Stator tooth overhang span	25	^{o}
Stator slot opening span	5	^{o}
Air-gap length	0.35	mm
Number of turns per armature coil	100	
Conductor wire diameter	1.25	mm
Rotor diameter	90.5	mm
Number of segments	5	
Span of each segment	55	^{o}
Magnet depth at tangential side	2.835	mm
Magnet width span	25	^{o}

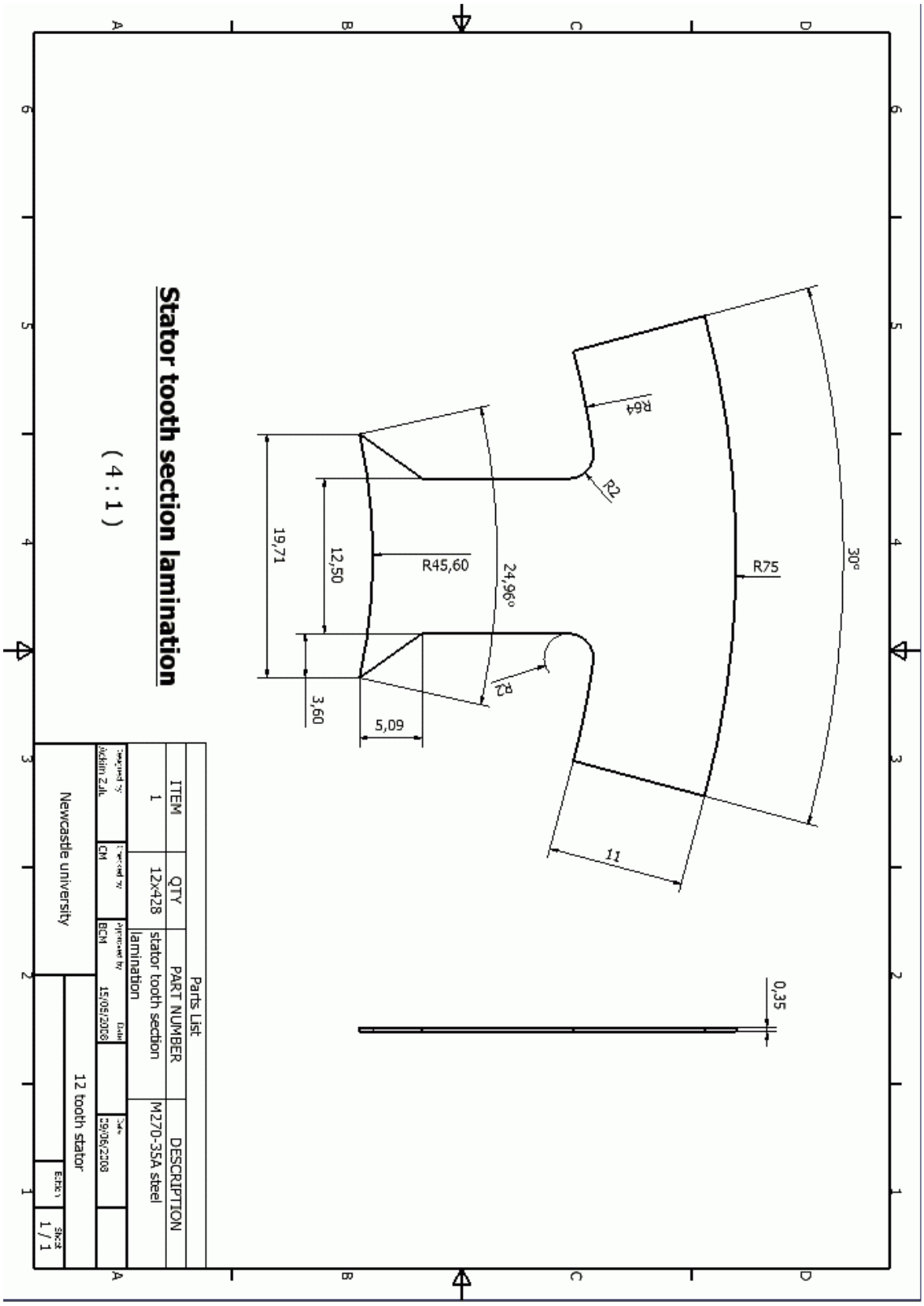

Figure F1. Wound field machines' modular stator tooth section.

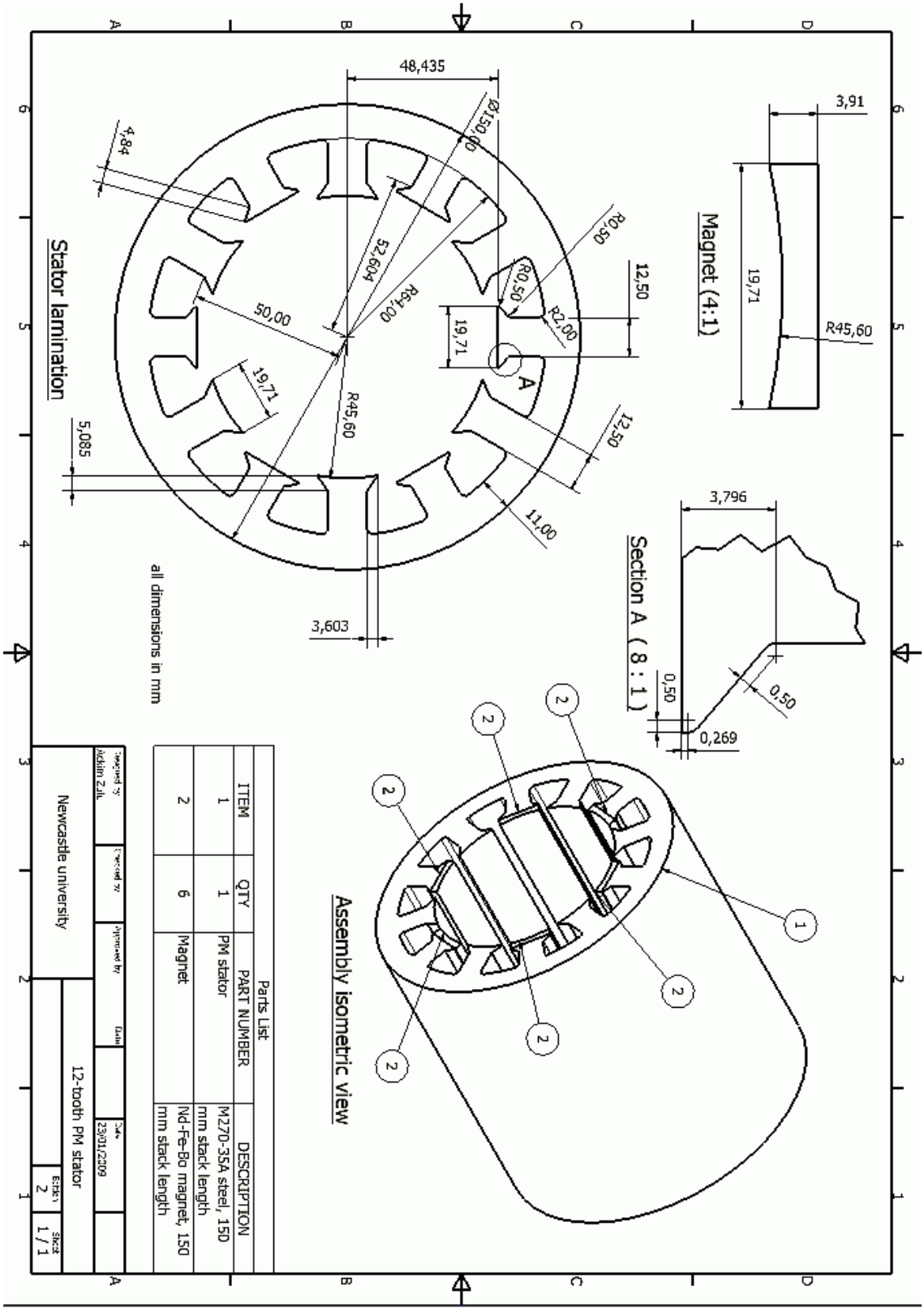

Figure F2. PM machines' complete stator.

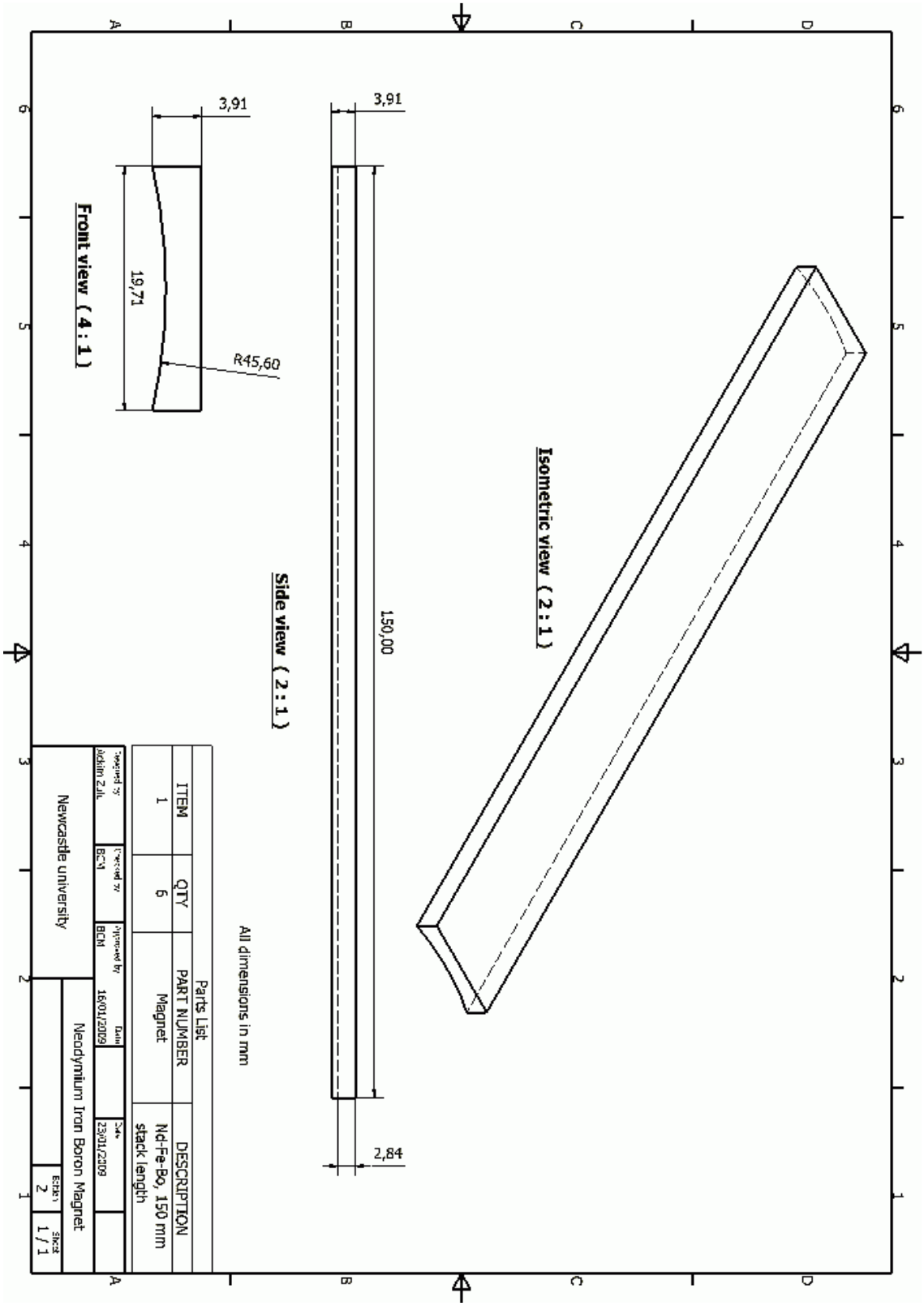

Figure F3. Permanent magnet.

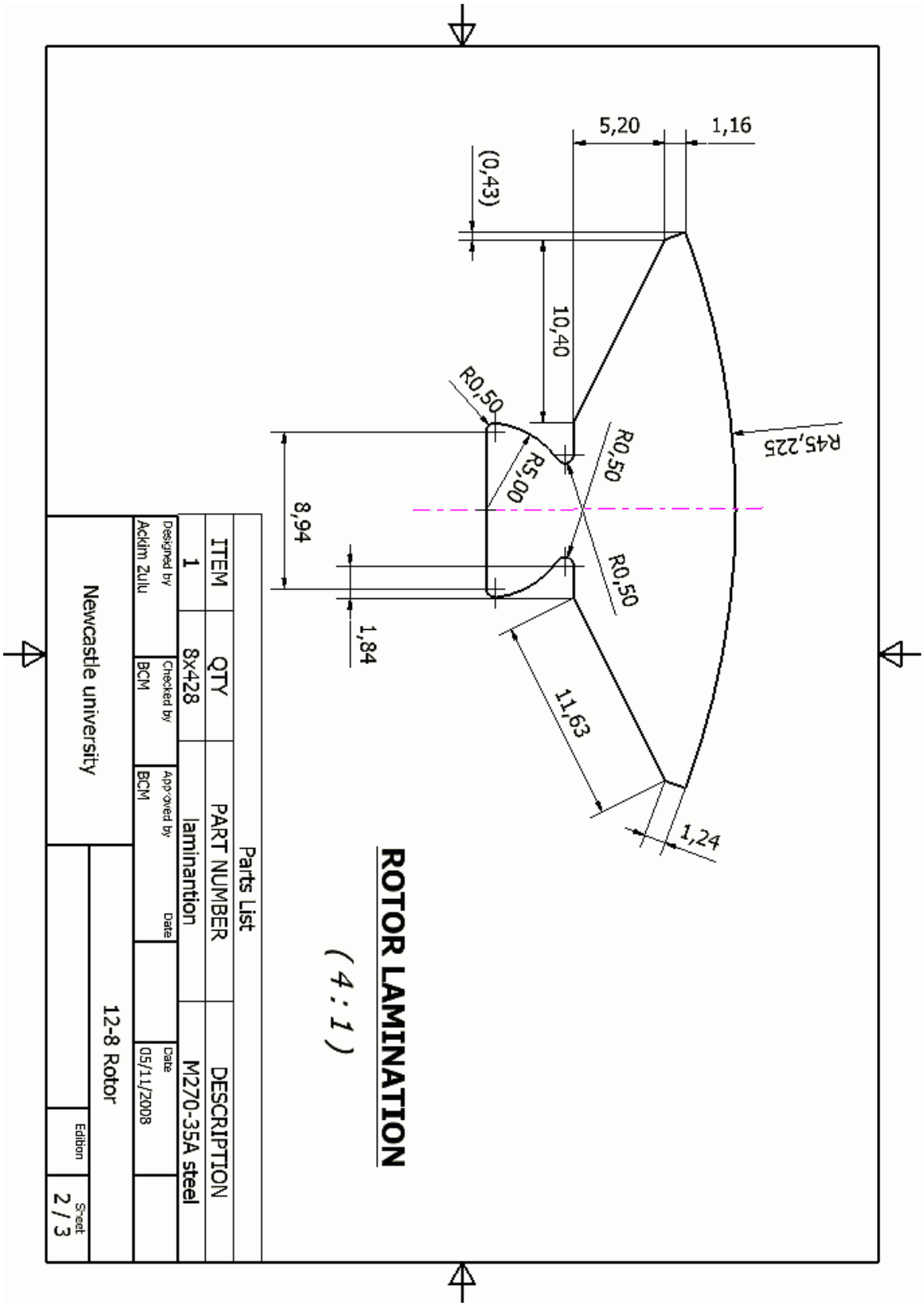

Figure F4. Rotor lamination for 8-segment rotor.

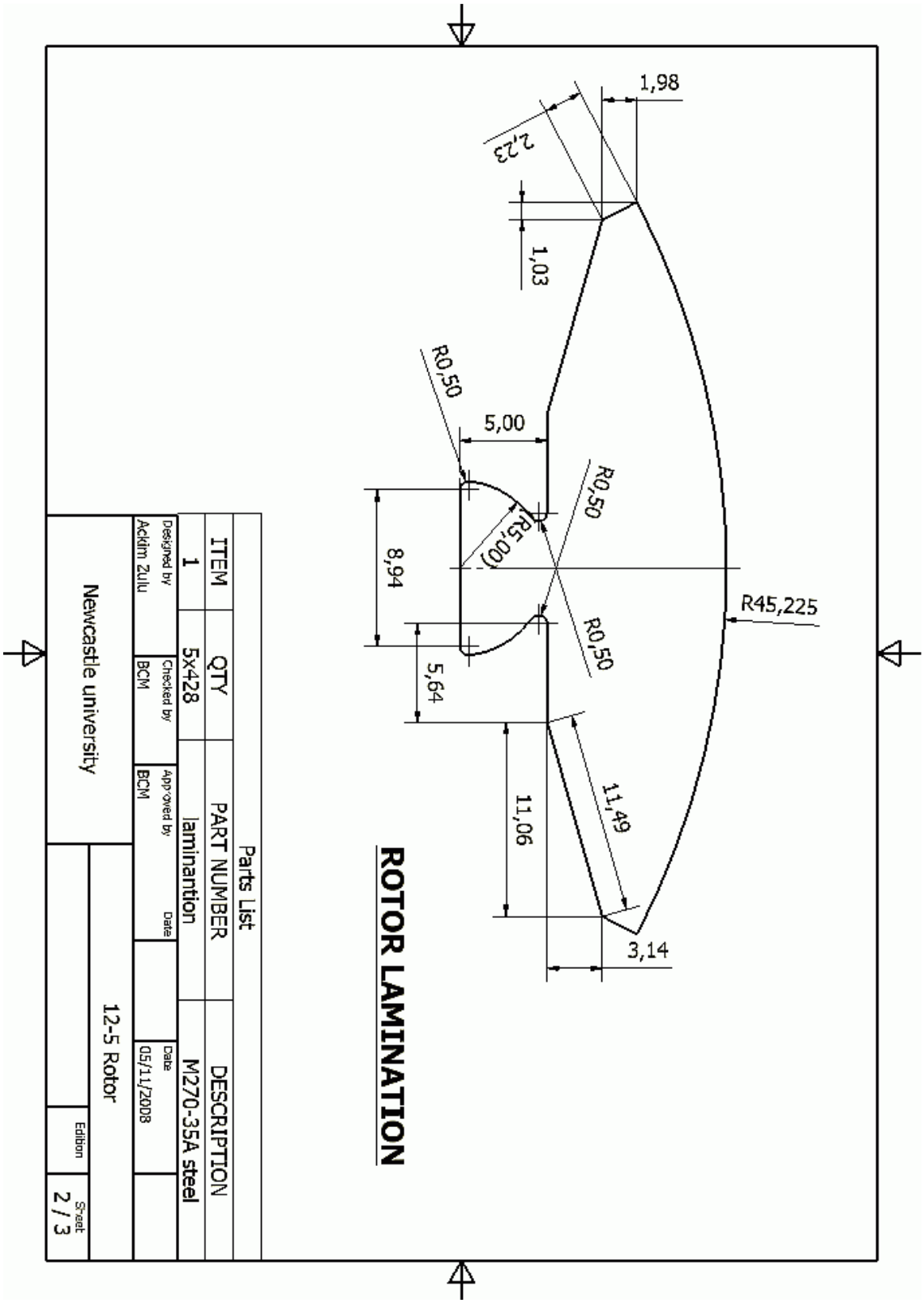

Figure F5. Rotor lamination for 5-segment rotor.

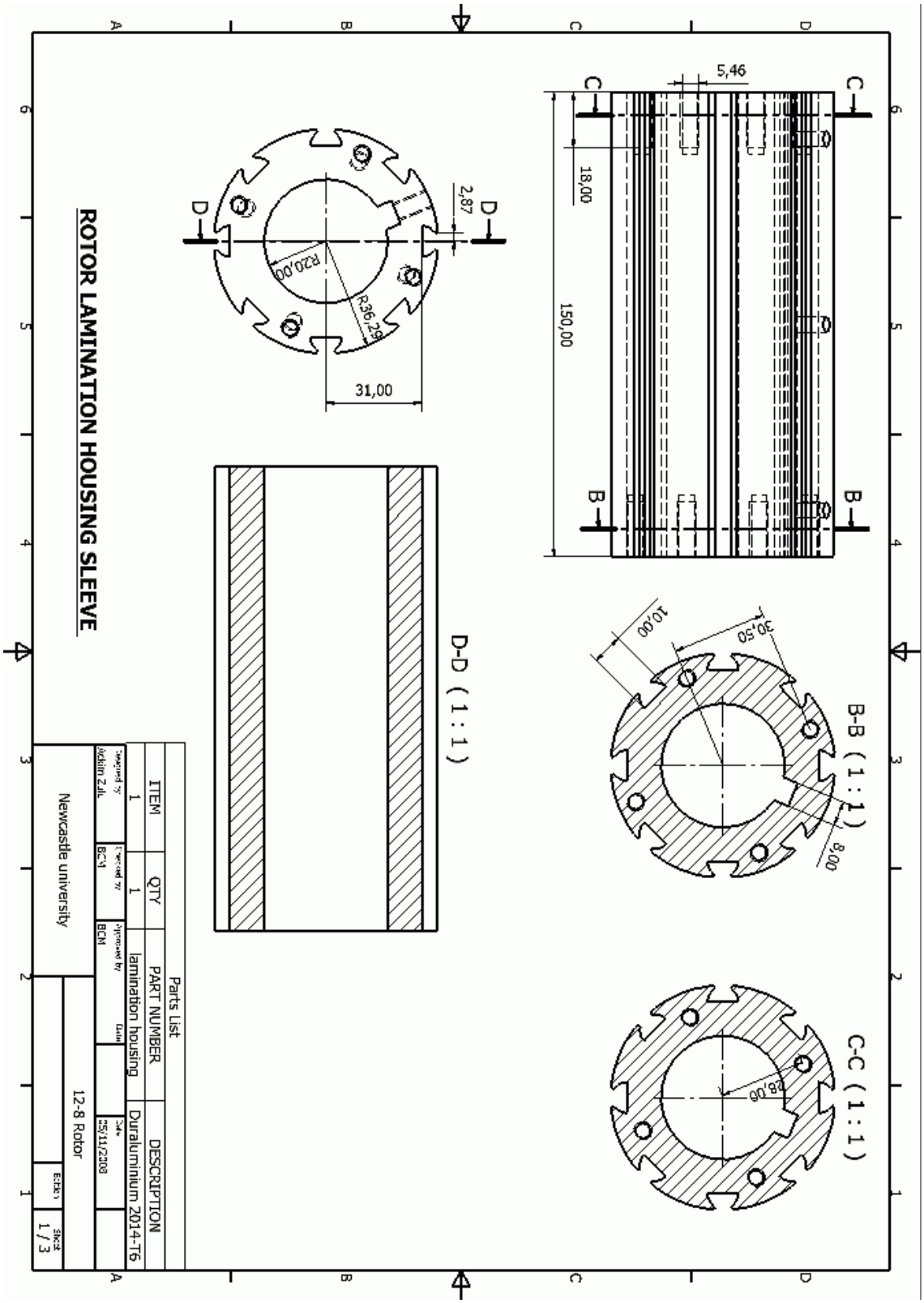

Figure F6. Rotor lamination housing for 8-segment rotor.

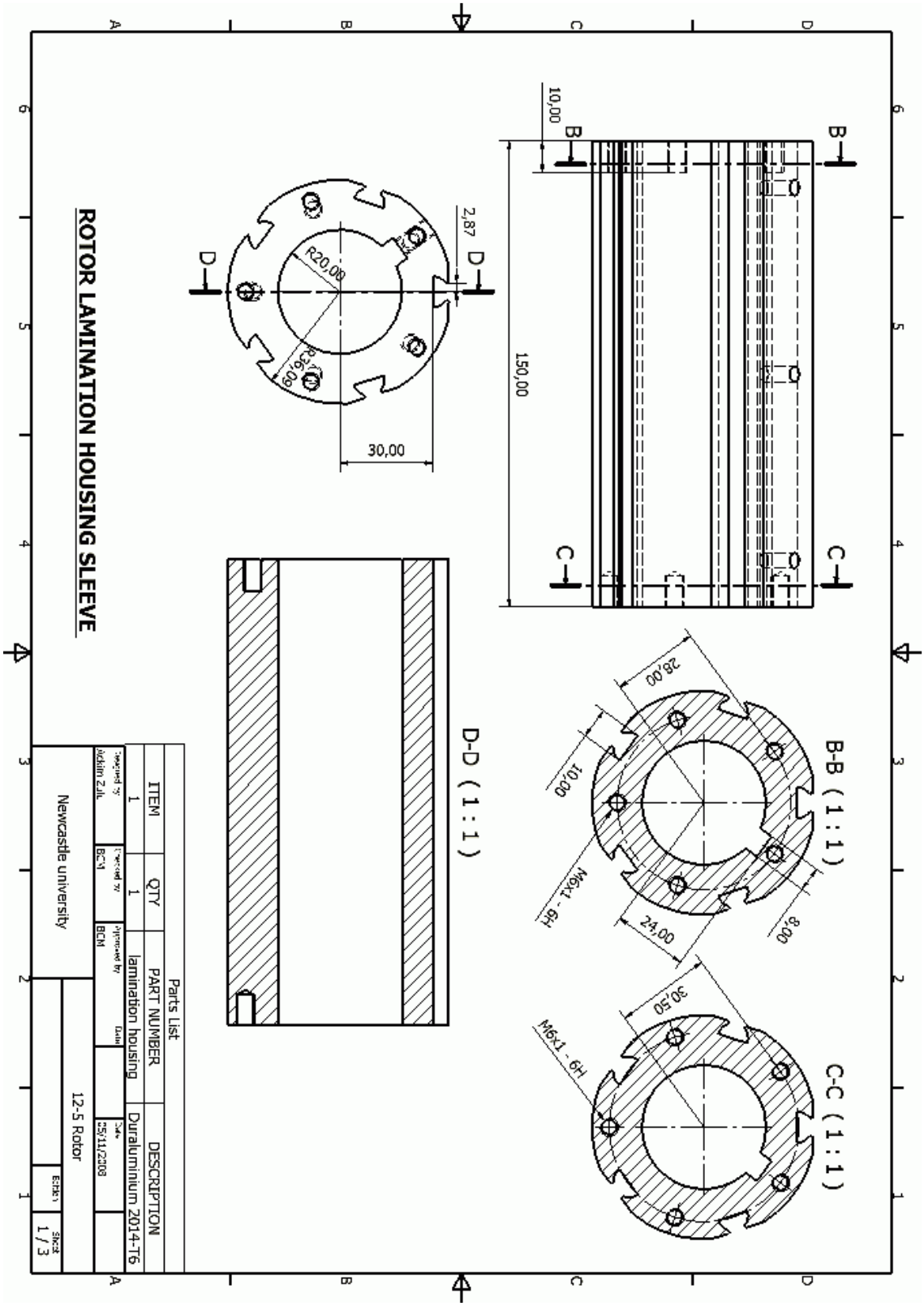

Figure F7. Rotor lamination housing for 5-segment rotor.

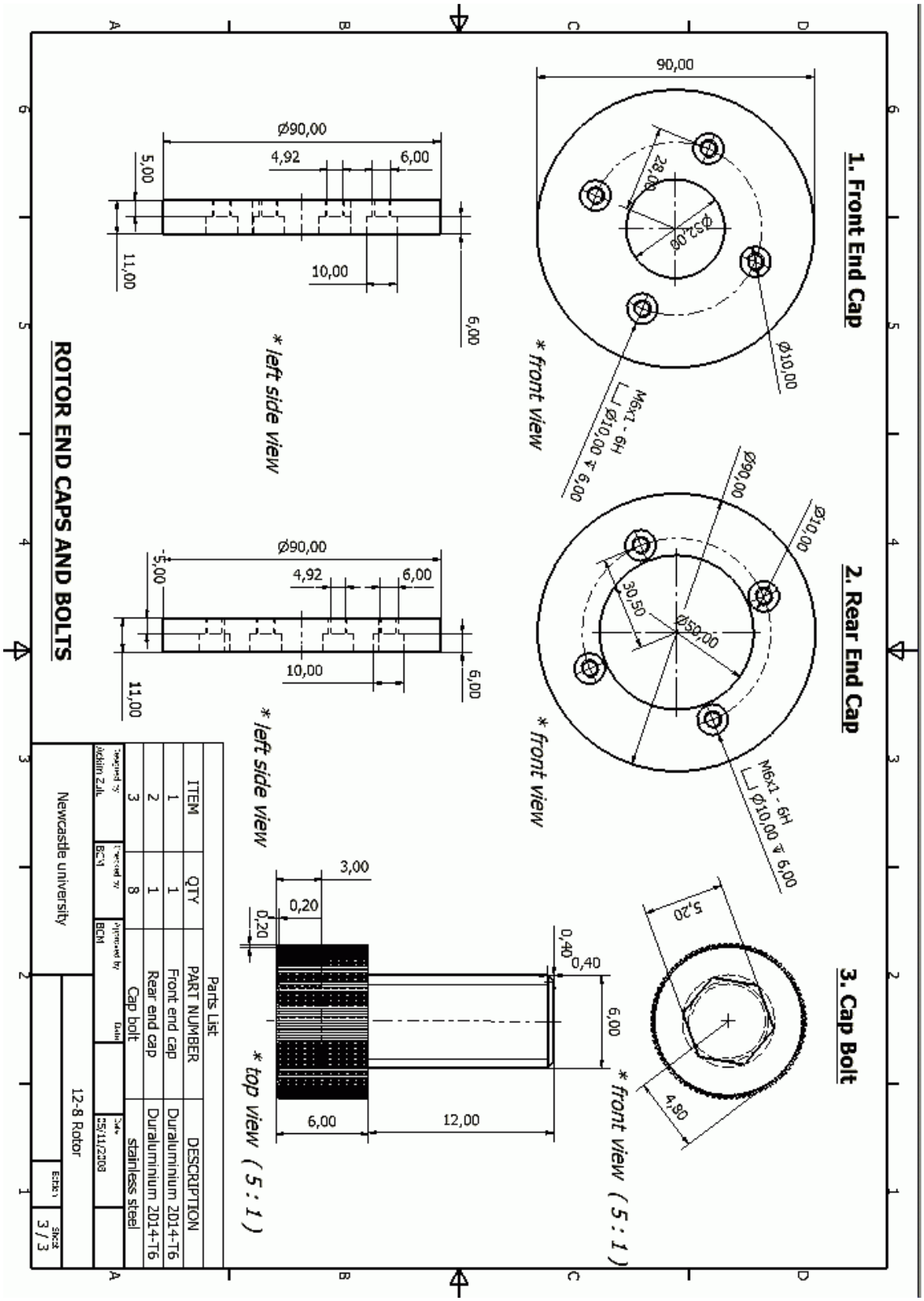

Figure F8. Rotor lamination end-cap discs for 8-segment rotor.

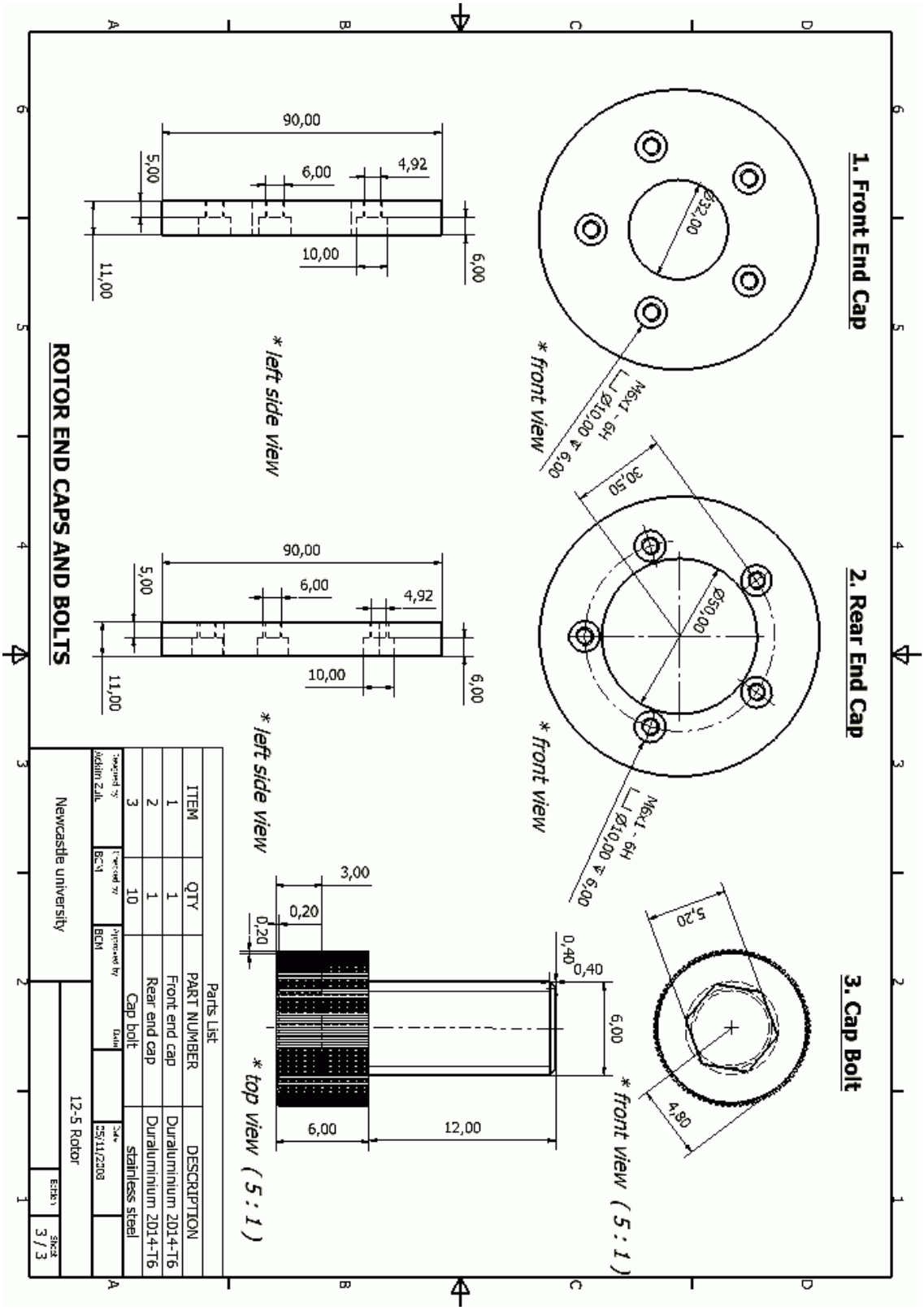

Figure F9. Rotor lamination end-cap discs for 5-segment rotor.

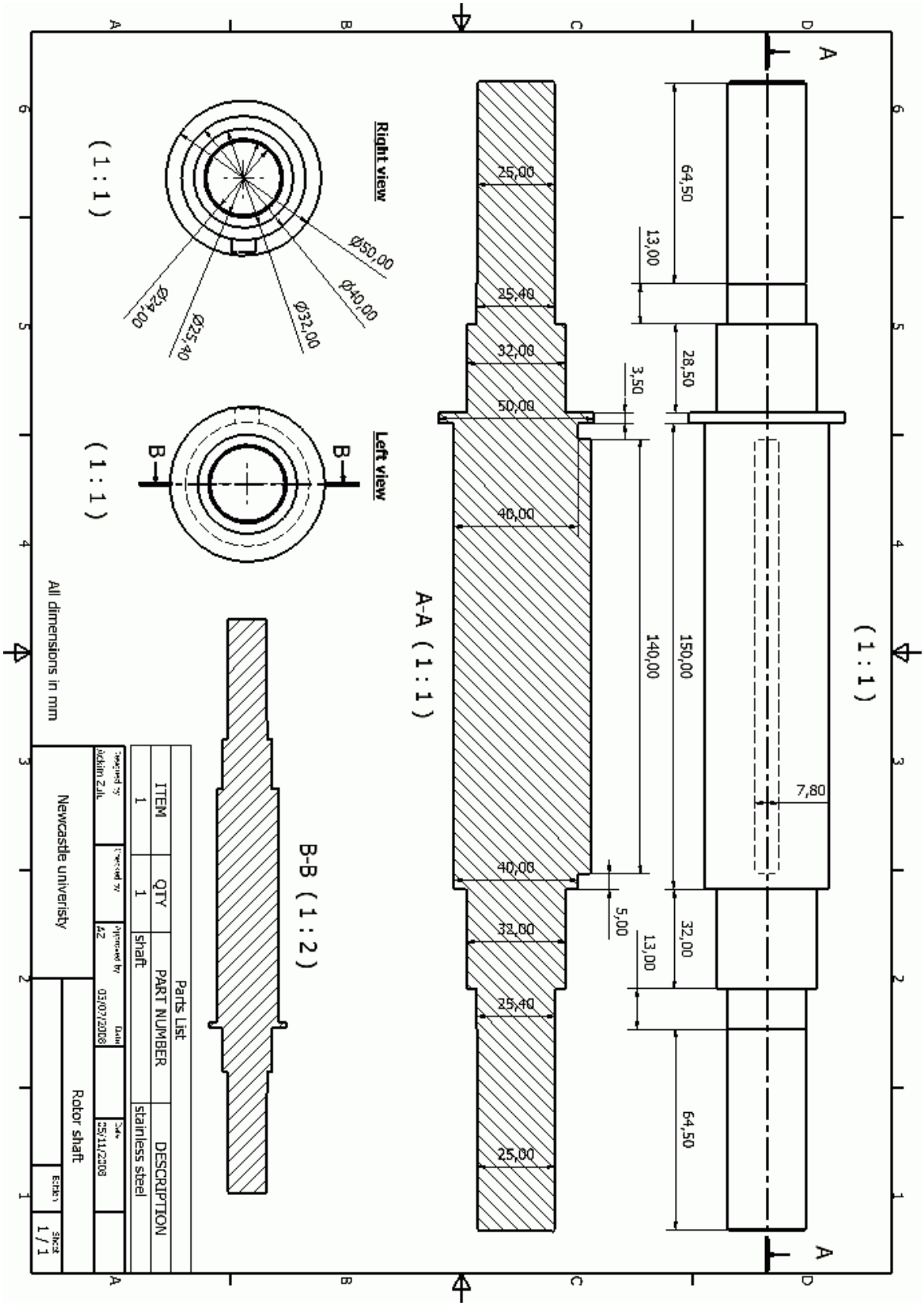

Figure F10. Rotor shaft.

Appendix G

Equipment and measuring instruments

Below is a list of the equipment and measuring instruments used in the experiments for testing the wound-field and permanent magnet demonstrator machines.

Table G1: Equipment

Item	Manufacturer	Model	Specifications
3-phase Drive for test machine	Control Techniques	SP3401 (2007)	400 V, 3-phase, 50 Hz, 50 A
3-phase Drive for load machine	Control Techniques	SP3403 (2007)	400 V, 3-phase, 50-Hz, 50 A
DC field power supply	Agilent	6684A	Input AC: 400 V, 3-phase; Output DC: 0-40 V, 0-128 A
DC armature power supply	ET Power Solutions	LAB/SM 320/AT-10/LT	Input AC: 230 V, 1-phase; Output DC: 0-20 V, 0-150 A
Load machine	Emerson	Unimotor 190U2D400VACAA515320	380/480 V, 8 poles, 4000 rpm

Table G2: Sensors and transducers

Item	Manufacturer	Model	Specifications
High voltage differential probe, 2 off	Tektronix	P5200	130/1300 V
Current probe, 2off	Tektronix	A622 AC/DC	0-70 A rms, DC – 100 kHz
Torque/speed transducer	Magtrol	TM310	0-50 Nm 0-32,000 rpm
Test motor's position/speed feedback device	Kuhnke	AC 58 SSI	12-bit, binary/gray, 5 /10-30 V output, 10,000 rpm
Thermocouple, 6 off	RS	-	J-type, PTFE, pre-wired, -50 to +250 °C

Table G3: Measuring and display meters

Item	Manufacturer	Model	Specifications
Digital oscilloscope	Tektronix	MSO 4034	350 MHz / 2.5 GS/s, 4 channels
Digital power meter	Yokogawa	WT1600, 760101-06-C2-Q	6 voltage and 6 current elements, 0-1000 V rms, 0-50 A rms, 16-bit A/D converter
Torque/speed display	Magtrol	3410	99,999 rpm Speed error : 0.01% of reading, Torque error : 0.01% of range
Temperature display	Tenma	72-2065A	3½ digit display, 1°C resolution, ±(0.5% reading +1°C) accuracy

Table G4: Software and computer packages

Type	Name	Proprietor	Version	Specifications
FEA	MagNet	Infolytica	6.24, 6.26, 6.28, 7.1	2D, 3D, static, harmonic, transient, transient with motion
CAD	Inventor	Autodesk	10	-
	Coreldraw	Corel	X4	-
Numerical analysis, graphing and visualisation	Matlab	Mathworks	7.1-7.8	-
	Excel	Microsoft	2003	-

Appendix H

Test rigs set up

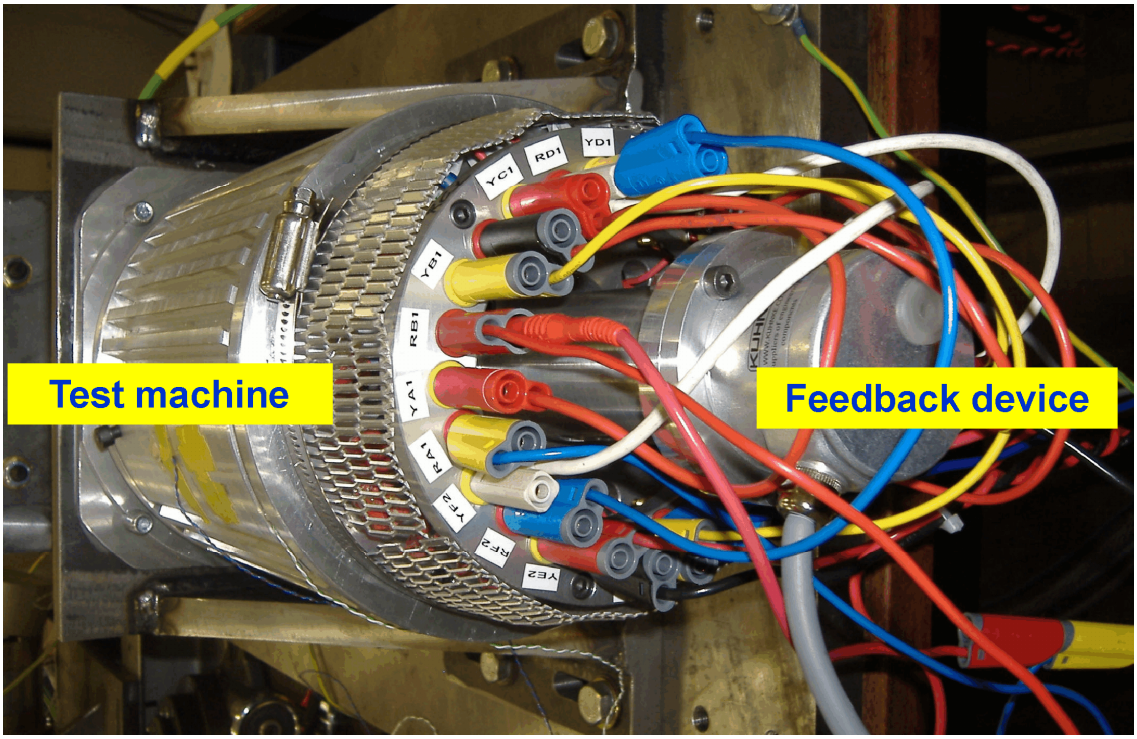

Figure H1. Field and armature wiring for wound-field 12/8 machine.

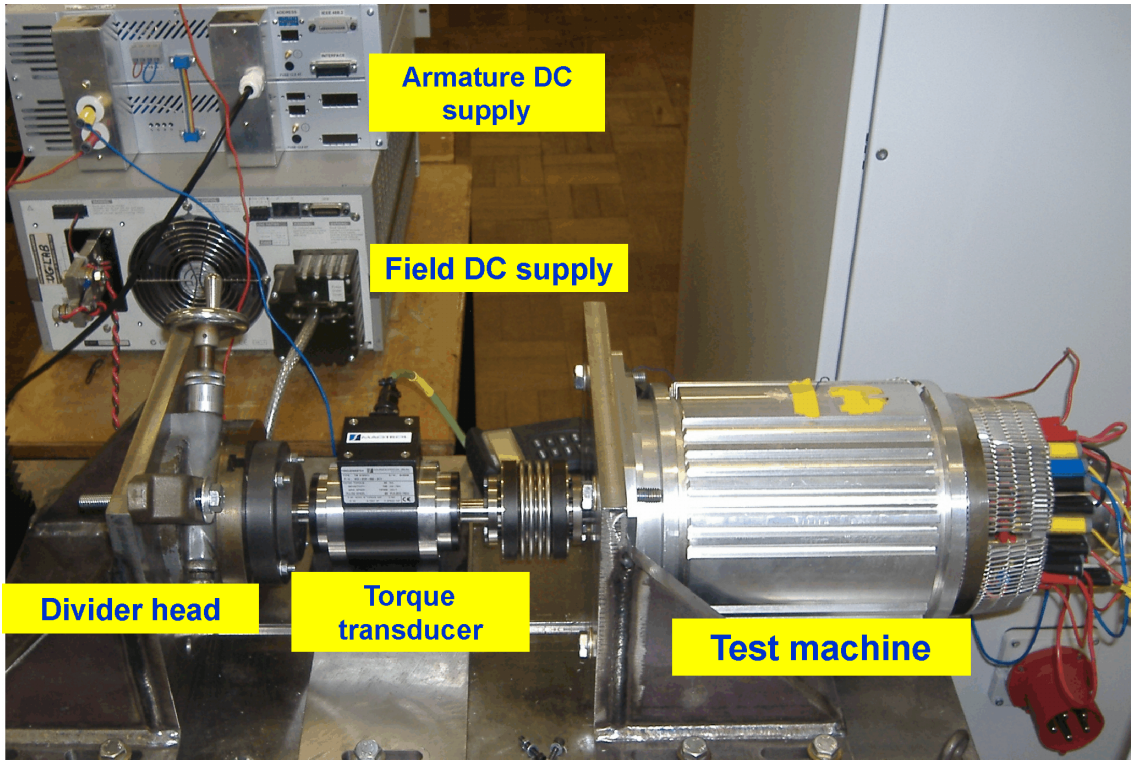

Figure H2. Static torque set up

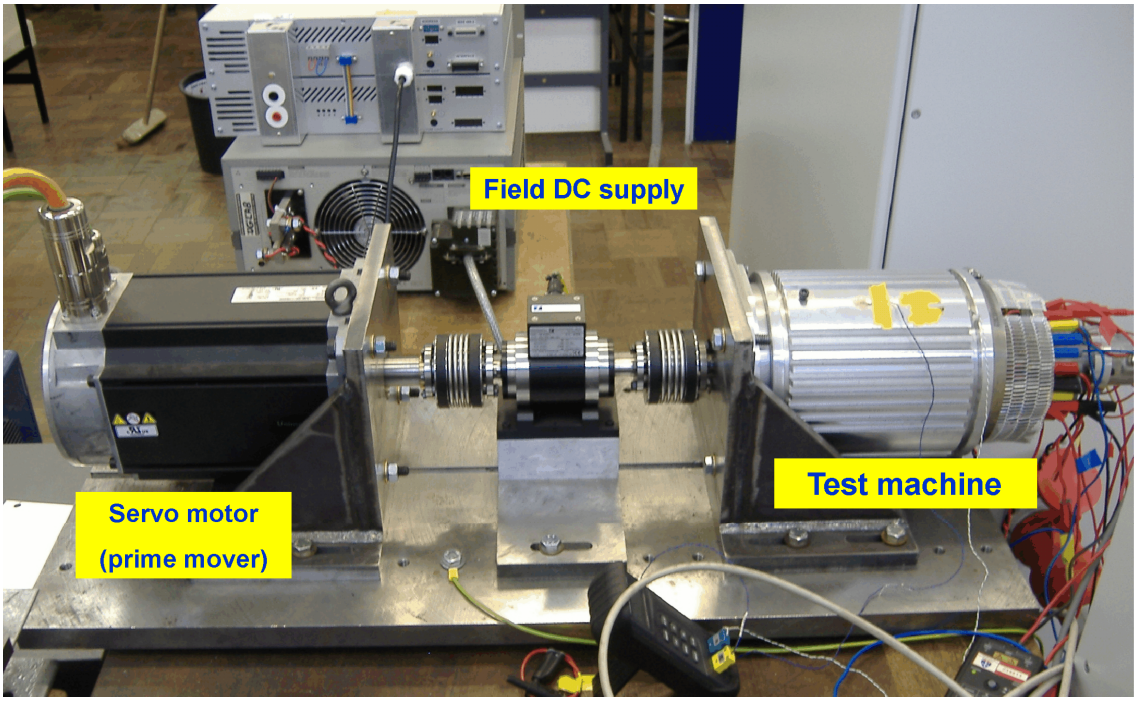

Figure H3. No-load running test

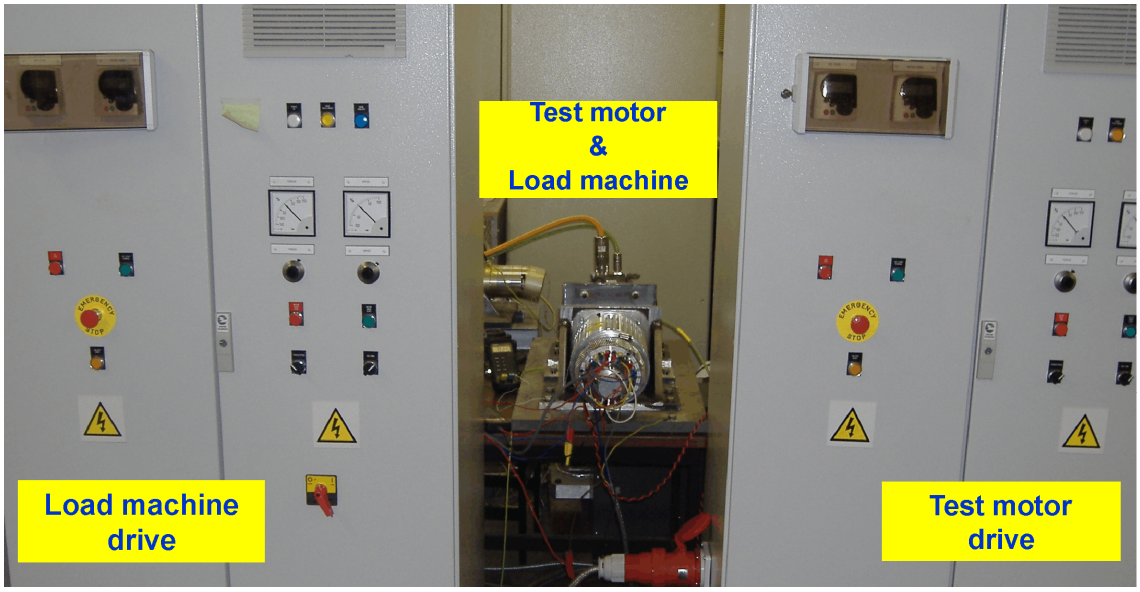

Figure H4. Running load test.

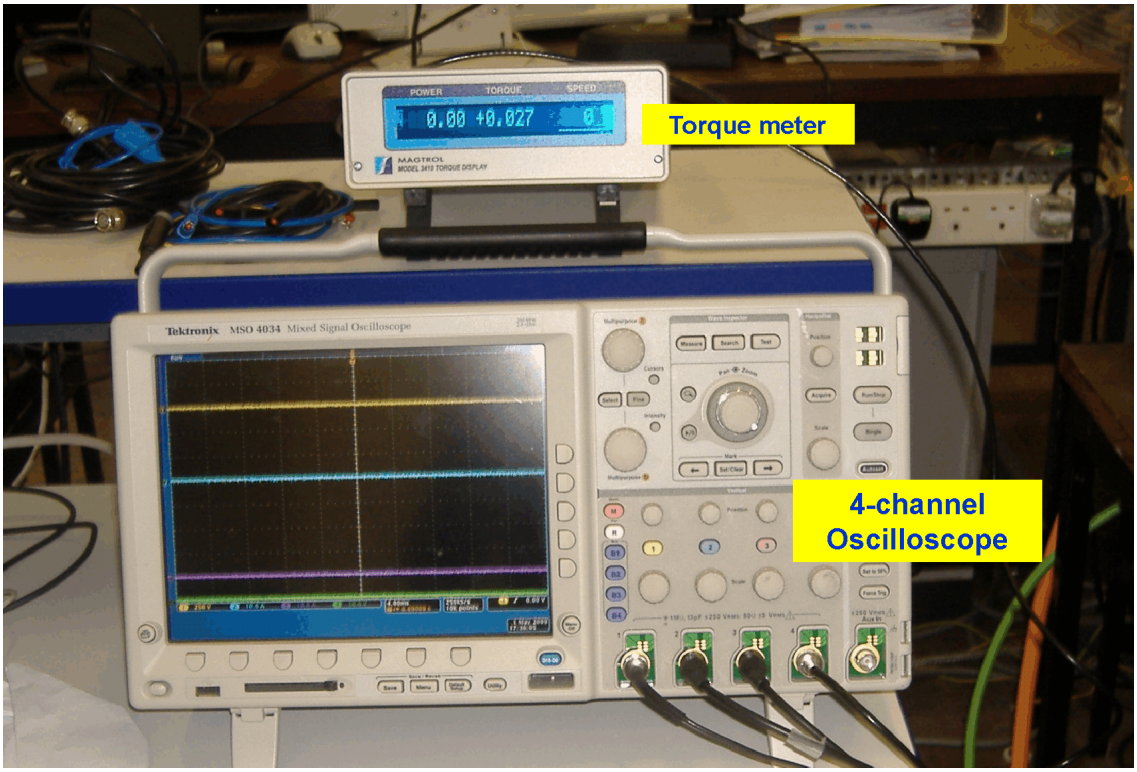

Figure H5. Instrumentation desk.